Mechanism of Self-Assembly of Small Designer Peptides and Their Potential Applications

Thesis submitted for the degree of

Doctor of Philosophy
in
Chemistry

Submitted by-

Karabi Roy

Roll No-156122021

Supervisor

Dr. Sunanda Chatterjee

Assistant Professor

Department of Chemistry

Indian Institute of Technology Guwahati

Guwahati, Assam-781039

India

August, 2020

Dedicated To My Parents, My Grandfather

and My Brother

For their endless love, support, encouragement and prayers

and

The Almighty

Declaration by the Candidate

I, Karabi Roy, present the thesis work for Ph.D. entitled "**Mechanism of Self-Assembly of Small Designer Peptides and Their Potential Applications".** The work has been carried out by me under the guidance of Dr. Sunanda Chatterjee, Assistant Professor, during the period from July 2015 to August 2020 at Department of Chemistry, IIT Guwahati, Assam. The work presented in this thesis has not been submitted for the award of any other degree or diploma at any other institution.

Though I have taken care while writing this thesis, there may still be some typographical errors or otherwise which are inadvertent on my part.

Date: August, 2020 **Karabi Roy**

Place: IIT Guwahati Roll No-156122021

Certificate by the Supervisor

Dated: 26.8.2020

This is to certify that the thesis entitled "**Mechanism of Self-Assembly of Small Designer Peptides and Their Potential Applications**" submitted by **Ms. Karabi Roy** (Roll number: **156122021**) for the award of Ph.D. degree to IIT Guwahati is absolutely based on her own research work and that neither this thesis or any part of it has been submitted for any degree/ diploma or any academic award anywhere before.

Dr. Sunanda Chatterjee

Assistant Professor

Dept. of Chemistry

Indian Institute of Technology Guwahati

Contact: +91 361 258 3310

Fax: +91 361 258 2349

Email: sunanda.c@iitg.ac.in

Acknowledgements

My first and foremost sense of profound obligation, deepest regards and utmost respect is towards my supervisor ***Dr. Sunanda Chatterjee*** *for her tireless guidance, tenacious motivations and for providing a genial ambience for working throughout my research work in the lab. It has been an immense pleasure for me to learn a lot of things by working under her supervision. I would like to deeply thank her for providing with best of the facilities which was required to carry out my research work. I deeply thank her for guiding me constantly and providing me with the best of suggestions while writing this thesis.*

I want to extend my sincere thanks to my Doctoral Committee members, ***Prof. Debapratim Das****, Professor, Department of Chemistry, IIT Guwahati,* ***Prof. Debasis Manna****, Professor, Department of Chemistry, IIT Guwahati and* ***Dr. Shirisha Nagotu****, Assistant Professor, Department of Biosciences and Bioengineering, IIT Guwahati for their unwavering guidance, support and encouragement throughout my research work.*

I want to extend my sincere thanks to ***Dr. Priyadarshi Satpati****, Assistant Professor, Department of Biosciences and Bioengineering, IIT Guwahati and his group for performing the theoretical studies which is an integral part of my thesis work. Also, I would ardently thank Sir for providing me with valuable guidance and advice during the course of my work.*

I would also thank gratefully, ***Dr. Anil P. Bidkar*** *Department of Biosciences and Bioengineering, IIT Guwahati for the biological studies that he has performed in his laboratory.*

A special thanks to ***Prof. Debapratim Das's*** *lab for providing facility to do the rheology experiments. Additionally I thank* ***Dr. Nilotpal Singha****,* ***Dr. Bapan Pramanik*** *and* ***Sumit Chowdhuri*** *of his lab for helping me with the said experiments.*

I am also thankful to ***Prof. Debapratim Das*** *and my supervisor* ***Dr. Sunanda Chatterjee*** *for the group meetings that they conducted every week for oral presentations and scientific discussions which helped me a lot in carrying out my research work, increased my scientific knowledge and also enhanced my confidence level.*

I would also like to thank ***Dr. Kalyan Raidongia*** *and his group for providing help needed to complete certain work of this thesis. Special mentions are* ***Dr. Rajkumar Gogoi****,* ***Kundan Saha*** *and* ***Jumi Deka*** *for helping me when required.*

I would like to gratefully acknowledge ***Department of Chemistry****, IIT Guwahati for providing all the instrumentation facilities for carrying out my research work. I would also like to thank the staff members' for being there when needed.; Special mentions are* ***Dr. Babulal Das****,* ***Mr. Imdadul Islam*** *and* ***Mr. Aniruddha Gogoi*** *for helping me in learning the instruments.*

Also, heartiest thanks to the ***Central Instruments Facility*** *(CIF), IIT Guwahati for providing facility for 600 MHz NMR, AFM, FESEM, PXRD and FETEM experiments.*

I would also like to thank the ***Centre for Environment*** *and* ***Department of Civil Engineering****, IIT Guwahati for providing the facility of Atomic Absorption Spectrometry.*

Words cannot express the love and synergy provided by my lab mates, ***Gopal Pandit****,* ***Swapna Debnath****,* ***Monikha Chetia*** *and* ***Tanumoy Sarkar*** *for their valuable help and support during the course of this work. They have been a constant support system for me through all the ups and downs during my Ph.D. journey. Also, thanks to all the project students who helped a lot in my research work.*

I wish to express my profound gratitude for endless encouragement, sustained support, close co-operation, unasked help from my friends throughout my journey.

I gratefully acknowledge ***Indian Institute of Technology Guwahati*** *for providing me with all the facility and financial assistantship for carrying out my work smoothly.*

Needless to mention, this thesis could not have been possibly completed successfully without the blessings of my parents and the Almighty.

I thank all for staying there with me through thick and thin.

August, 2020 ***Karabi Roy***

Abstract

The thesis "**Mechanism of Self-Assembly of Small Designer Peptides and Their Potential Applications**" describes the design of small peptides, studies on their self- and co-assembly and application of the developed materials in wastewater remediation and drug delivery. Several of the designed peptides also act as anion sensors.

Chapter 1 is an introduction to peptide self-assembly and briefly summarizes development in the field. It sets the pretext of the work undertaken in the current thesis.

Chapter 2 describes the assembly of dicyclohexylurea derivatives of amino acids into organogels and their applications in wastewater remediation. The amino acid derivatives selectively sense fluoride and hydroxide anions.

Chapter 3 involves design of two charge complementary peptides, development of self- and co-assembled hydrogels from them and their applications in wastewater remediation which involves removal of different kinds of organic dyes, metal ions including Pb^{2+} and Hg^{2+}. Peptides act as selective sensors for hydroxide (OH^-), arsenite (AsO_2^-) and arsenate (AsO_3^-) anions.

Chapter 4 describes the application of a peptide based hydrogel as drug delivery platform for topical delivery of several drugs and proteins.

Chapter 5 discusses the mechanism of self-assembly of a tryptophan rich tetrapeptide into nanospherical assemblies.

Chapter 6 contains concluding remarks, revisits lessons learnt and discusses the scope of future studies.

Contents

L-Amino Acid with Abbreviations and Single Letter Codes

Amino Acid	Abbreviation	One Letter Code
Alanine	Ala	A
Valine	Val	V
Isoleucine	Ile	I
Leucine	Leu	L
Methionine	Met	M
Phenylalanine	Phe	F
Tyrosine	Tyr	Y
Tryptophan	Trp	W
Threonine	Thr	T
Serine	Ser	S
Asparagine	Asn	N
Glutamine	Gln	Q
Cysteine	Cys	C
Glycine	Gly	G
Proline	Pro	P
Arginine	Arg	R
Lysine	Lys	K
Histidine	His	H
Aspartic acid	Asp	D
Glutamic acid	Glu	E

List of Abbreviations

UV: ultraviolet

NP: nanoparticle

DNA: deoxyribonucleic acid

PNF: peptide nanofibers

GN: graphene nanosheets

GQD: graphene quantum dots

MBHP: metal binding hairpin protein

Hyp: hydroxyproline

LMWG: low molecular weight gelator

SEM: scanning electron microscope

AFM: atomic force microscopy

FESEM: field emission scanning electron microscopy

PA: peptide amphiphile

1D: one dimension

2D: two dimension

3D: three dimension

TEM: transmission electron microscope

PNT: peptide nanotube

Boc: tert-butoxycarbonyl

Z: N-carbobenzoxy

HFIP: hexafluoro-2-propanol

Tle: tert-leucine

PGA: poly-l-glutamic acid

ELP: elastin like polypeptides

CPP: cell penetrating peptide

PEG: poly ethylene glycol

GO: graphene oxide

GSH: glutathione

BSA: bovine serum albumin

IgG: immunoglobulin G

HUVEC: human umbilical vein endothelial cells

ECM: extra cellular matrix

AMP: antimicrobial peptide

NBD: 4-nitro-2,1,3-benzoxadiazole

List of Abbreviations

FRET: fluorescence resonance energy transfer

ACQ: aggregation caused quenching

Fmoc: fluorenylmethyloxycarbonyl

PDI: pyrelenediimide

NMR: nuclear magnetic resonance

COSY: co-relation spectroscopy

NOESY: nuclear overhauser effect spectroscopy

TOCSY: total correlation spectroscopy

HSQC: heteronuclear single quantum coherence

HMBC: heteronuclear multiple bond correlation spectroscopy

HMQC: heteronuclear multiple quantum coherence

DOSY: diffusion ordered spectroscopy

MAS: magic-angle spinning

REDOR: rotational-echo double resonance

CGC: critical gelation concentration

IR: infrared

CD: circular dichroism

DLS: dynamic light scattering

ITC: isothermal calorimetry

SERS: surface enhanced raman scattering

AIE: aggregation induced quenching

ANS: 8-anilinonaphthalene-1-sulfonic acid

XRD: X-ray diffraction

PXRD: powder X-ray diffraction

SAXS: small angle X-ray scattering

AAS: atomic absorption spectrometry

AES: atomic emission spectroscopy

ICP-MS: inductively coupled plasma mass spectrometry

LOD: limit of detection

NDI: naphthalenediimide

FITC: fluorescein isothiocyanate

PET: photoinduced electron transfer

HEPES: (4-(2-hydroxyethyl)-1-piperazineethanesulfonic acid

DCU: dicyclohexylurea

List of Abbreviations

FTIR: fourier transform infrared

ESI-MS: electrospray ionization mass spectrometry

1, 2 DCB:1, 2 dichlorobenzene

DCC: N, N'-dicyclohexylcarbodiimide

TFA: trifluoroacetic acid

CV: crystal violet

RB: rhodamine B

NR: neutral red

MGC: minimum gelation concentration

Phg: phenylglycine

Gaba: γ-aminobutyric acid

RT: room temperature

F^-: fluoride

Cl^-: chloride

Br^- : bromide

I^-: iodide

HSO_4^-: hydrogensulphate

$H_2PO_4^{--}$: dihydrogenphosphate

CH_3O^- : acetate

OH^- : hydroxide

THF: tetrahydrofuran

DFT: density functional theory

TDDFT: time-dependent density function theory

PCM: polarizable continuum model

SPPS: solid phase peptide synthesis

PB: phosphate buffer

PBS: phosphate buffer saline

MO: methyl orange

HOBt: hydroxybenzotriazole

PyBOP: benzotriazole-1-yl-oxy-tris-pyrrolidino-phosphonium hexafluorophosphate

DMAP: 4-dimethylaminopyridine

DIC: N, N′-diisopropylcarbodiimide

DIPEA: N, N-diisopropylethylamine

DCM: dichloromethane

List of Abbreviations

DMF: dimethylformamide

FETEM: field emission transmission electron microscopy

CP: ciprofloxacin

5-FU: 5-fluorouracil

EtOH: ethanol

MTT: 3-(4,5-dimethylthiazol-2-yl)-2,5-diphenyl tetrazolium bromide

DMEM: dulbecco's modified eagle medium

MALDI: matrix-assisted laser desorption/ionization

CF: carboxyflorescein

EDC.HCl: N-(3-dimethylaminopropyl)-N′-ethylcarbodiimide hydrochloride

MeOH: methanol

Chapter 1

Introduction

Chapter 1
Introduction

1.1. Self-Assembly

Self-assembly is the spontaneous association of numerous individual entities into a coherent organization, generating well-defined structure.[1-6] It is ubiquitous in nature at both macroscopic and microscopic levels. For example, from the assembly of schools of fish in the ocean to flocks of birds in the sky to herds of wild animals to oil droplets in water to proteins like collagen and keratin, which forms ligaments and hair respectively, self-assembly plays the underlying role. Folded functional proteins, genetic material and the cell membrane constituted by phospholipids and proteins, which are all vital to life, are all generated due to self-assembly. During self-assembly, systems have a natural tendency of exchanging energy with their surroundings and then assuming patterns or structures of reduced free energy. Inspired by nature, several groups across the world have been engaged in the understanding and design of self-assembling systems, giving birth to an independent branch of chemistry known as supramolecular chemistry.[9] Molecular self-assembly is all about artfully designing the molecular building blocks which are able to spontaneously form assemblies *via.* the formation of numerous intermolecular/intramolecular interactions. Approach of molecules to constitute an assembly is facilitated and governed by several weak non-covalent forces like electrostatic interactions, hydrogen bonding, π-π interactions, cation-π interactions, charge transfer interactions, hydrophobic interactions, van der Waals interactions etc. (Figure 1.1).[7-9] Though each of these non-covalent forces is weak in nature, their collective effect is significant, sufficient to drive the molecules to form ordered structures. Molecules spontaneously undergo stepwise interactions to form hierarchical assemblies[3, 10-11] from nanoscale up to macroscale which generates several kinds of soft materials that find a spectrum of interesting applications. The process of self-assembly often needs to be triggered

by several parameters like appropriate building blocks, concentration, solvent, temperature, sonication, ultraviolet (UV) radiation, ionic strength, pH, chemical reactions, enzymes etc. despite of it being a spontaneous process (Figure 1.1).[12-16] Tuning of these parameters can lead to a controlled self-assembly process.

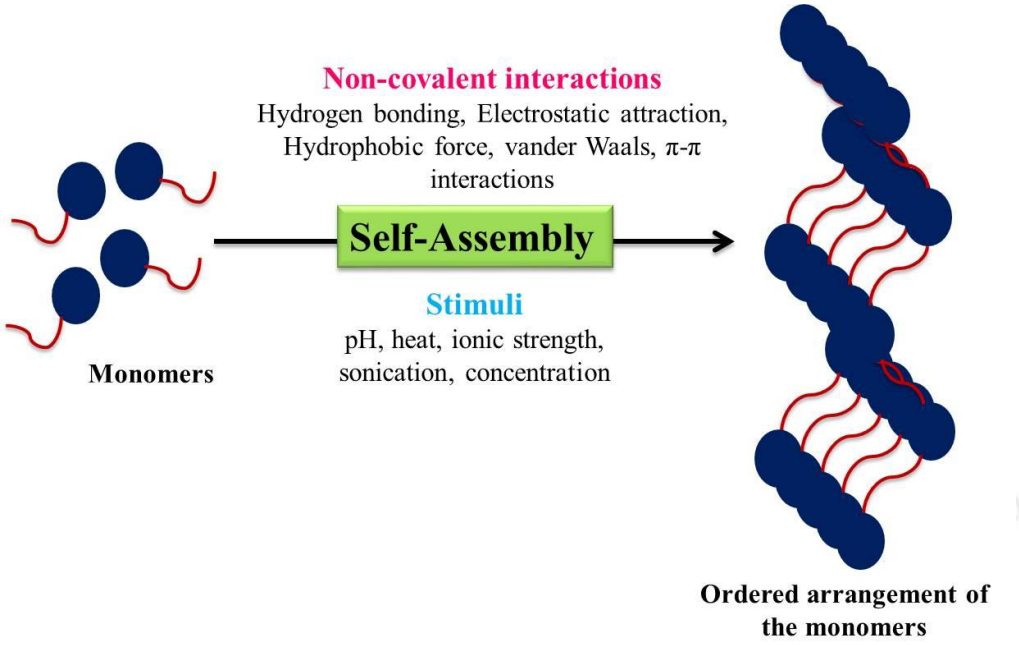

Figure 1.1: Schematic representation of molecular self-assembly driven by different non-covalent interactions and assisted by several stimuli.

Self-assembly, is a simple and competent technique for preparation of several functional nanomaterials with ordered structures. Apart from nanoparticles (NPs), polymers, and other inorganic nanoscale building blocks, there are examples of many kind of biomolecules like DNA, proteins, peptides, viruses, enzymes, and others, that have exhibited great potential to form ordered nanomaterials by controllable self-assembly.[17-24] Bio-molecules have a unique advantage over the other self-assembling nanomaterials in having biocompatibility, tuneable chemistries and unique molecular properties like recognition, immunocompatibility and favourable pharmacokinetics that make them eligible for a myriad spectrum of biological applications.[25] Nanomaterials derived from lipids, proteins, peptides, nucleic acids etc. have

been extensively utilized for applications in the fields of biomedical engineering, drug delivery, tissue engineering, biosensors, and nanotechnology.[26]

1.2. Thermodynamics and Kinetics of Self-Assembly

The term self-assembly is used to describe spontaneous thermodynamic and kinetic driven processes where nanoscale entities pack into regular arrangements in order to attain a minimum free energy through minimisation of repulsive and maximisation of attractive molecular interactions. It is an equilibrium process, *i.e.* the individual and assembled components exist in equilibrium.[27] The lower free energy conformation is usually a result of synergistic effect of various weak non-covalent intermolecular forces between the self-assembled moieties and is essentially enthalpic in nature.

The thermodynamics of the self-assembly process can be represented by a simple Gibbs free energy equation:

$$\Delta G_{SA} = \Delta H_{SA} - T\Delta S_{SA}\ ;\ SA=\text{Self-assembly}$$

Self-assembly is a spontaneous process when ΔG_{SA} is negative. ΔH_{SA} is the enthalpy change of the process and is largely determined by the potential energy/intermolecular forces between the assembling entities. ΔS_{SA} is the change in entropy associated with the formation of the ordered arrangement. In general, ΔH_{SA} is negative owing to the favourable non-covalent interactions that drive self-assembly. For the $T\Delta S_{SA}$ term to contribute to the negative ΔG_{SA}, the ΔS_{SA} term should be positive. Desolvation of the solute molecules, during the self-assembly process leads to the positive ΔS_{SA} term (Figure 1.2). The self-assembly is governed by the normal processes of nucleation and growth. Small assemblies are formed because of their increased lifetime, as the attractive interactions between the components lower the Gibbs free energy. As the assembly grows, the Gibbs free energy continues to

decrease, both from favourable enthalpic and entropic components, until the assembly becomes stable enough to last for a long period of time.

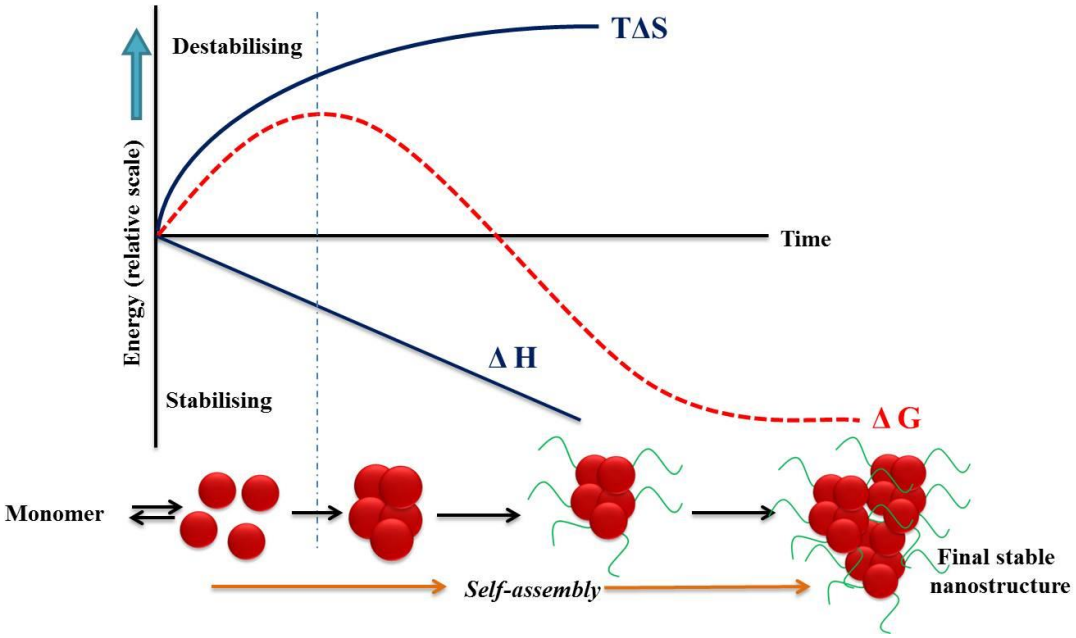

Figure 1.2: Schematic representation of thermodynamics of self-assembly

Self-assembly is formed from the synergistic effect of several non-covalent forces. The synergistic effect of these non-covalent interactions determines the thermodynamic stability and the state of minimum energy of the ultimately formed nanostructures. Although, the ultimate driving force is energy minimization of the system and the corresponding evolution towards equilibrium, not all self-assembly processes are examples of simple thermodynamics. Due to the weak nature of the non-covalent forces they can be modulated by various factors like temperature, pH, salt concentration and solvents. This can result in the assembled structures being trapped in metastable states (Figure 1.3). In the absence of any intervention from the kinetic parameters, metastable structures finally grow into the thermodynamically favourable structures. Therefore, a competitive relationship between kinetic and thermodynamic states of assembly provides the possibility of transformation of self-assembly from thermodynamic to kinetic control.[28]

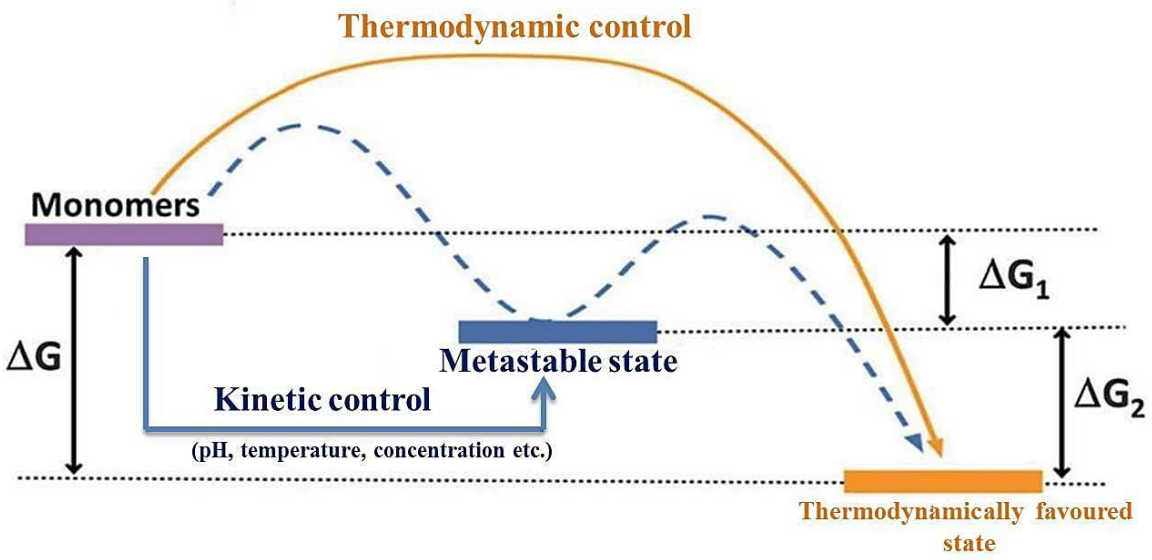

Figure 1.3: Schematic of the assembly pathways under thermodynamic and kinetic control. Under thermodynamic control, the final nanostructures are in the state of minimum free energy (orange solid line). If kinetic control (e.g. pH, temperature etc.) intervenes, the structure can be trapped in a metastable state (blue solid line). These metastable structures can further grow into the thermodynamically favoured state (blue dashed line). All structures are interconvertible under certain kinetic controls. The figure has been adapted with permission from reference 28. *Copyright 2016, Royal Society of Chemistry.*

1.3. Interactions Driving Molecular Self-Assembly

Intermolecular forces govern the interaction in between monomers in the self-assembled systems. Non-covalent interactions are of prime importance in the process of self-assembly since they set up the scenario through which monomers interact with each other to form ordered structures. They represent the machinery through which molecules approach each other and eventually pack together. An intricate balance of the multiple non-covalent forces plays a significant role in the interaction of molecules which can cause further aggregation through a cascade of dynamic structural transitions with other or similar kind of molecules. The main non-covalent interactions that control the self-assembly process includes hydrogen bonding, electrostatic interaction, hydrophobic interaction, π-π interactions, cation-π

interaction and van der Waals forces which have been discussed. Though individually, these non-covalent interactions are weak in nature, synergistic effect plays the crucial role. These interactions, alone or in combination with one another are one of the most efficient approaches to achieve stable self-assembly for the fabrication of nanostructures.

1.3.1. Hydrogen Bonding: One of the important interactions that occur between a hydrogen atom attached to an electronegative atom and another electronegative atom like oxygen or nitrogen in molecules is called hydrogen bonding (Figure 1.4a). A typical hydrogen bond (H--X) length ranges from 1.5-2.6 Å and is of the order of 4-13 kJ/mol.[29] It plays important roles in the formation of functional nanomaterials. Several kinetic factors modulate the strength of the hydrogen bond which enables structural transitions between different self-assembled structures. More importantly, the selectivity and high directionality of hydrogen bonds can convert monomers into diverse nanostructures[30, 31] There are number of reports in the literature where we can find the formation of self-assembled nanostructures mediated by hydrogen-bonding. Diphenylalanine (FF) is a popular dipeptide motif for self-assembly in water driven by hydrophobic interactions; however, other interactions are also likely play important roles. For instance, Li *et.al.* demonstrated the formation of FF microrods by hydrogen-bond based self-assembly.[32] In another instance, Yang and co-workers studied the self-assembly of an FF peptide on a graphene surface and the formation of peptide nanowires wherein they observed that the self-assembly of the FF peptide with graphene in water was ascribed to both hydrogen bonds and π–π interaction.[33] In addition to peptides, proteins, enzymes, DNA, and viruses can also be utilized to form self-assembled biological nanomaterials through hydrogen bonds. Cheng and his group developed a di-functional supramolecular polymer, ureido-cytosine-polypropylene glycol (UrCy-PPG) containing self-complementary quadruple hydrogen-bonded ureido-cytosine (UrCy) moiety, which spontaneously self-assembled to form long-range-ordered lamellar structures in the bulk

state.[34] In another study, A. K. Das and his co-workers demonstrated the involvement of hydrogen bonding and π- π stacking interactions as the driving force for the self-assembly of Amoc-capped dipeptides (Figure 1.4b).[35]

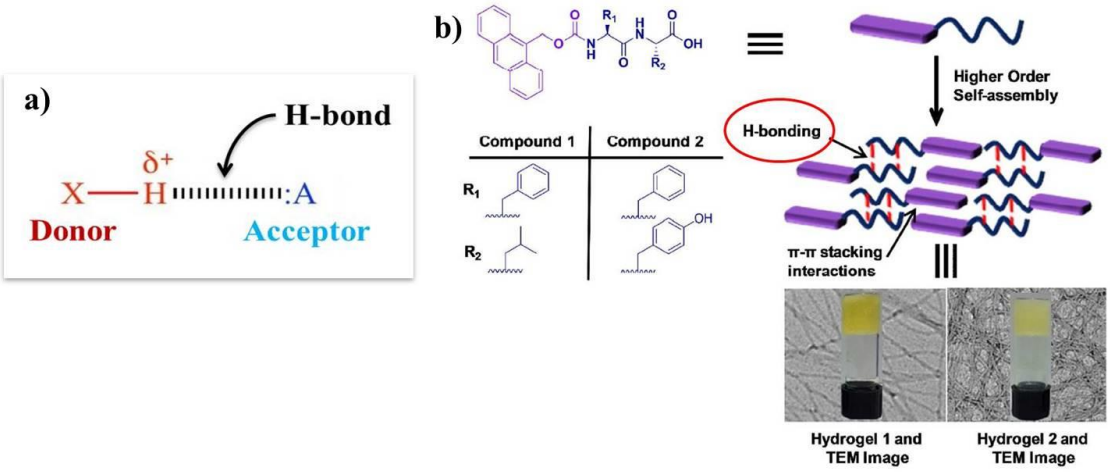

Figure 1.4: Hydrogen bonding in self-assembly: a) A typical representation of a hydrogen bond. b) Chemical structures of Amoc-capped dipeptides. Schematic representation of self-assembly leading to the formation of nanofibrillar hydrogels and evaluations of the self-supporting hydrogels. The figure has been adapted with permission from reference 35. *Copyright 2018, American Chemical Society.*

1.3.2. Electrostatic Interaction: Coulombic interactions between opposite charges in solution can lead to the formation of ion pairing. The strength of an ionic bond is dependent on the solvent (particularly its dielectric) and the presence of mobile ions. Electrostatic interaction has a significant role in the formation of nanostructures formed from peptides, proteins, DNA, enzymes and others and in stabilizing the formed nanostructures. For instance, Wang *et.al.* investigated the self-assembly of a motif-designed peptide for the formation of peptide nanofibers (PNF) and bioinspired PNF based silver nanowires (AgNWs), wherein they fabricated graphene nanosheet (GN)-PNF-AgNW nanocomposites through an electrostatic interaction between negatively charged PNF-AgNWs and a polymer-

modified with positively charged GN.[36] In another study, Deming and his group investigated the self-assembly of discrete metal complexes $[Au(CN)_2]^-$ in aqueous solution using block copolypeptide $K_{183}L_{19}$ into nanorods in which electrostatic interaction played a major role (Figure 1.5b).[37] Liu and co-workers studied the fabrication of micelle-induced protein nanowires through an electrostatic interaction when the electronegative cricoid stable protein one (SP1) assembled with positively charged core-crosslinked micelles.[38]

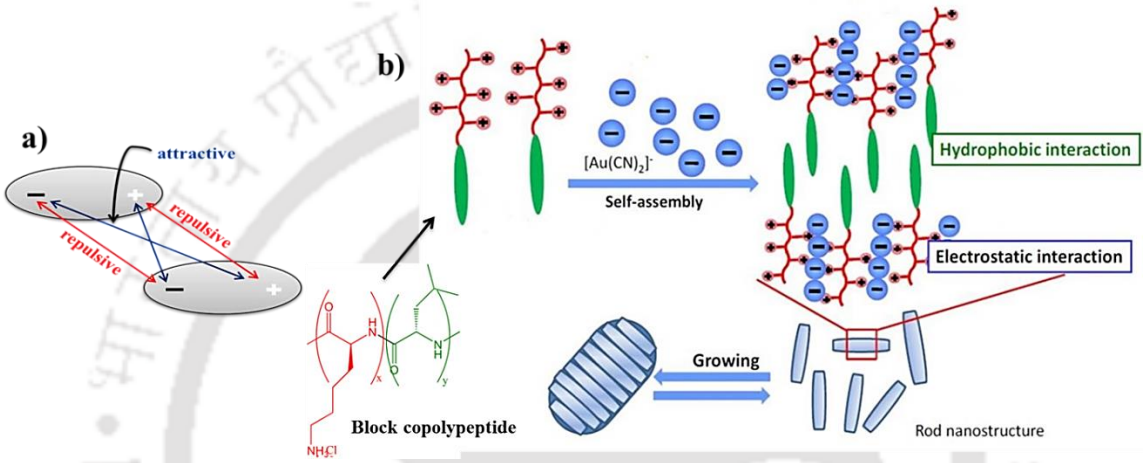

Figure 1.5: Electrostatic-interaction-mediated self-assembly: a) Schematic diagram of electrostatic interaction. b) Schematic illustration of self-assembly of co-polypeptide amphiphiles/Au complexes to develop the functional nanostructure. The figure has been adapted with permission from reference 37. *Copyright 2013, International Journal of Molecular Science. (This is an open access article distributed under the Creative Commons Attribution Licenses.)*

1.3.3. Hydrophobic Interaction: It constitutes one of the most important types of non-covalent interactions facilitating the self-assembly process. Many biomolecules, such as peptides and proteins, can form higher ordered nanostructures *via*. hydrophobic interaction due to their hydrophobicity[39] (Figure 1.6). A lot of studies on the hydrophobic-interaction induced self-assembly of proteins and peptides have been pursued till date which has given rise to a variety of functional bionanomaterials.[40] For example, Liao *et. al.* demonstrated the

formation of higher ordered nanofibers in solution *via*. hydrophobic interaction by using a small peptide amphiphile (NapFFKYp) as a model[41]. In another study, Yang and co-workers investigated the self-assembly of a model ionic-complementary peptide EAK16II (AEAEAKAKAEAEAKAK) on hydrophilic and hydrophobic substrates through electrostatic and hydrophobic interactions, respectively.[42] Conjugation of biomolecules with other nanomaterials, such as nanoparticles or graphene can lead to the formation of functional nanomaterials *via*. a hydrophobic interaction.[43,44]

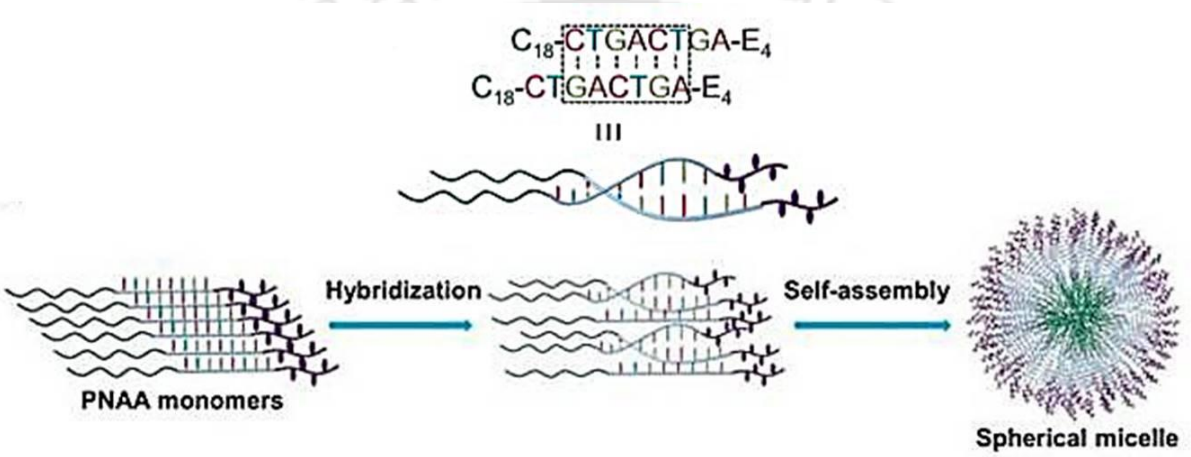

Figure 1.6: Hydrophobic interaction in self-assembly: a) Self-assembly of Peptide Nucleic Acid Amphiphles (PNAAs) C_{18}-CTGACTGA-E_4 into spherical micelles *via*. hydrophobic interaction. The figure has been adapted with permission from reference 39. *Copyright 2014, American Chemical Society.*

1.3.4. π-π Interaction: Non-covalent π-π interactions are another potential driving force to promote the self-assembly. It is the attractive non bonded interaction between planar aromatic rings which is referred to as π-π interaction or π-stacking.[45] The steric constraints associated with the formation of these ordered stacking structures have a fundamental role in self-assembly processes leading to the formation of supramolecular structures[46-51] (Figure 1.7). Some biomolecules, including peptides, proteins, DNA, enzymes, and viruses containing aromatic motifs, undergo the formation of highly ordered superstructures by π-π stacking or

functional hybrids by biomolecule–material π-π interaction. For example, Su and co-workers investigated the role of π-π interaction between a designed peptide (RGDAEAKAEAKYWYAFAEAKAEAKRGD) which formed PNFs and graphene quantum dots (GQDs) towards the formation of novel PNF–GQD nanohybrids for the simultaneous targeting and imaging of tumor cells.[52] In addition to peptides, other biomolecules, such as proteins, DNA, enzymes, and viruses, have also been widely used to conjugate with graphene to form nanomaterials *via*. this non-covalent force for various applications.[53,54] Huang *et.al.* designed a GQDs–ionic liquid–nafion (GQDs-IL-NF) composite film, which could interact with single stranded DNA through non-covalent π-π interactions to fabricate a novel biosensor platform for detecting a carcinoembryonic antigen with high sensitivity.[55]

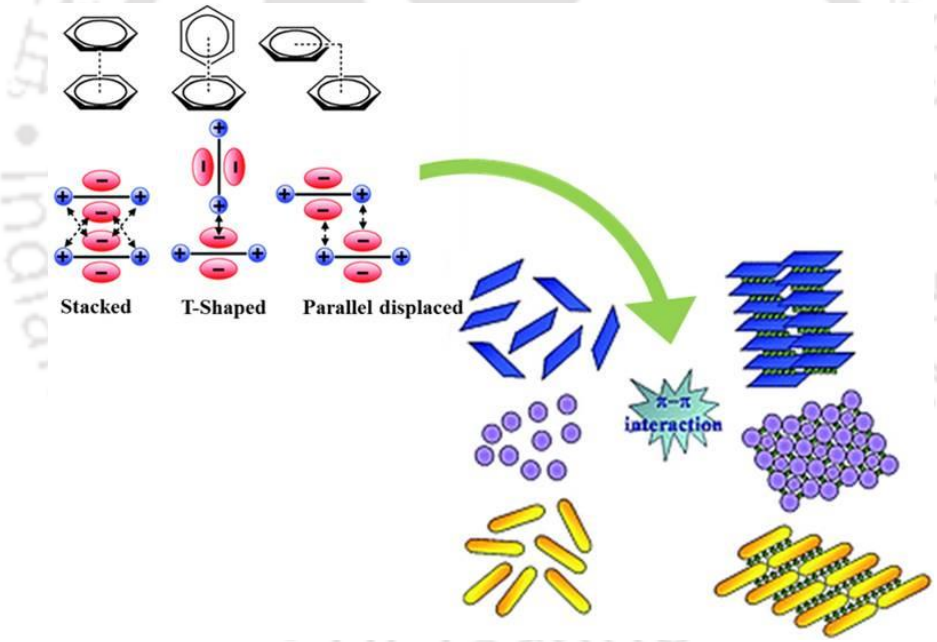

Figure 1.7: Schematic representation of π-π stacking leading to different nanostructures.

1.3.5. van der Waals Interaction: This interaction is of comparable strength to hydrogen bonding, but it is non-selective, non-directional, and non-additive.[56] The vander Waals forces, such as the interactions between aliphatic tails in peptide amphiphiles, represent the main contribution to the non-covalent interactions and are ubiquitous in peptide self-assembly.

There are however only a few examples that employ this interaction as a dominant force for the control of peptide nanostructuring.[57,58] For example, the self-assembly of oligopeptides (FKFEFKFEFKFE) occurred when solution conditions reduced intermolecular electrical double layer repulsion below the threshold of vander Waals attraction (Figure 1.8).[57]

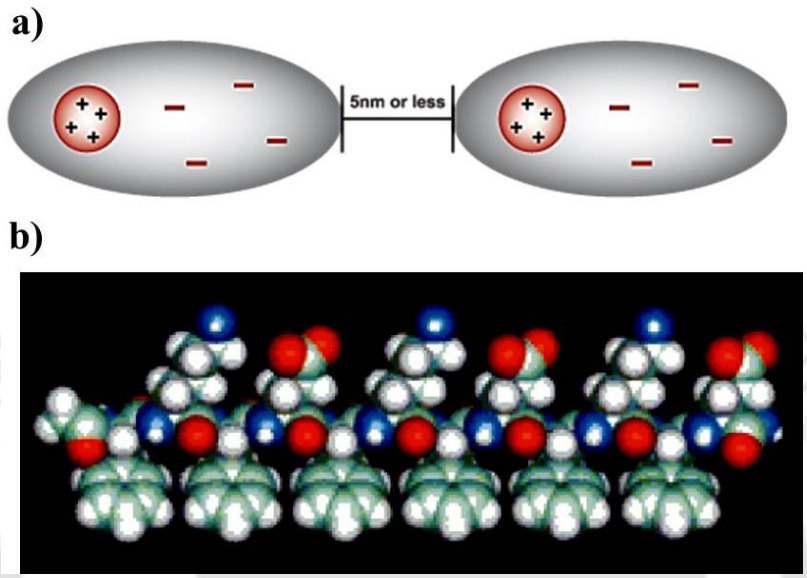

Figure 1.8: vander Waals interaction: a) Schematic representation of vander Waals force. b) Schematic molecular model of FKFEFKFEFKFE (KFE12) wherein the vander Waals force plays a guiding role in the self-assembly of the peptide; Carbon atoms are pale green, Oxygen atoms are red, Nitrogen atoms are blue, and Hydrogen atoms are white. The figure has been reproduced with permission from reference 57. *Copyright 2000, American Chemical Society*.

1.3.6. Cation-π Interactions: It is a non-covalent molecular interaction between the face of an electron-rich π system and an adjacent cation (Figure 1.9a). It is regarded as an electrostatic attraction between a positive charge and the quadrupole moment of the aromatic ring.[59] π-systems are important building blocks. Cation-π interactions are widely used in supramolecular assembly,[60-63] molecular recognition[64] and the stability of protein structures.[65] For instance, Horng and his group studied the self-assembly of collagen-related peptide, $RG(POG)_{10}F$ in which one Arg is attached to the N-terminus of Pro-Hyp-Gly triplets

and one Phe is attached to the C-terminus of the peptide into fibrils facilitated by cation-π interactions (Figure 1.9b).[60] In another case, Lee and co-workers demonstrated progressive assembly for polydopamine coating in which Dopamine is first sequentially oxidized into its various heterogeneous derivatives *via.* covalent bonds. The covalently bonded oligomers then self-assembled, physically grown and chemically gained new functions progressively over the time in which cation-π played an important role.[62]

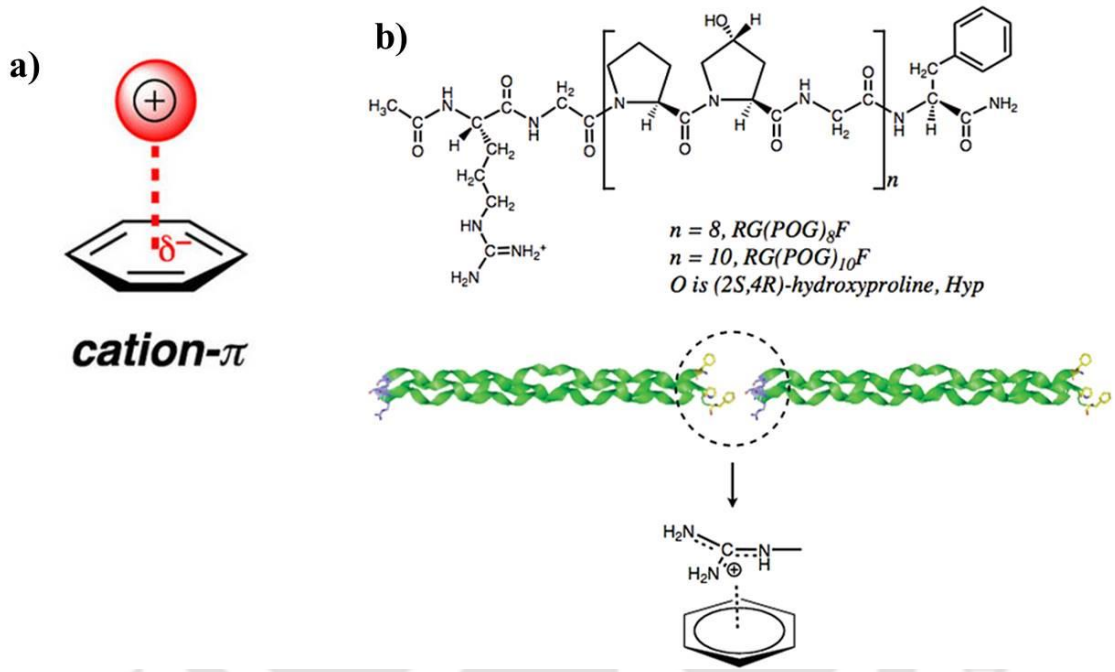

Figure 1.9: a) Cation-π interaction. b) Head-to-tail self- assembly of collagen-related peptides RG(POG)$_{10}$F *via*. cation-π interactions. The figure has been adapted with permission from reference 60. *Copyright 2011, American Chemical Society.*

1.4. Effect of External Factors Towards Molecular Self-Assembly

Though the self-assembly is a thermodynamically favourable process, multiple stimulating factors might play a crucial role in overcoming the activation barrier involved in the process. Such factors include solvents, solution environment, including the pH, sonication, temperature, ion concentration, photo stimulation or chemical reactions (Figure 1.10). Such factors in some instances help in obliterating the existing intramolecular interactions, so that

the molecules can undergo intermolecular associations. In the other instances, the molecule may need a pre-adjustment in its structure to be able to undergo effective self-assembly. In other cases, tuning the solubility of the monomers by changing the solvent, temperature etc. might help in formation of effective self-assembly. The following section briefly discusses the commonly used stimuli for generating supramolecular nanostructures.

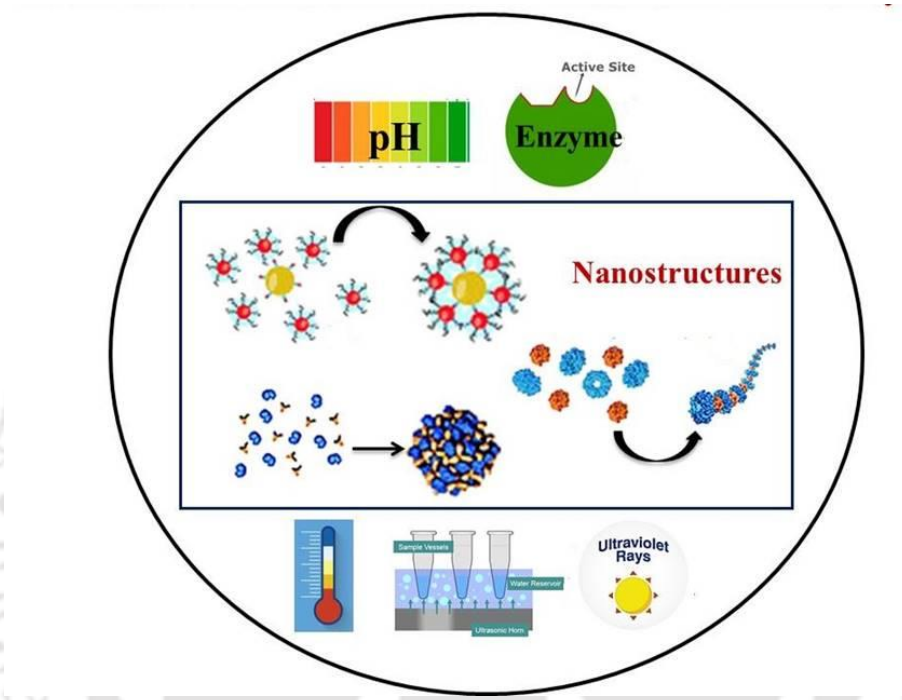

Figure 1.10: External factors/stimuli that can be used to control molecular self-assembly.

1.4.1. pH: One of the most effective and simplest method to trigger self-assembly is the change in pH. Addition of a small amount of acid or base can easily and rapidly lead to a large pH shift *via.* a diffusion-limited process which might ultimately lead to the growth of nanostructures. Change in pH may affect the solute-solvent interactions and help molecules to grow from a homogeneous solution to a fibrillar structure in solution *via*. non-covalent forces, including aromatic−aromatic interactions, hydrogen bonding, and hydrophobic interactions. Literature encompasses the formation of varied structures by alteration of pH.[66-70] For instance, it is well known that the peptide sequence KLVFFAE from the Aβ (16–22)

peptide of Alzheimer's disease is very sensitive to the environmental pH. Hsieh and co-workers demonstrated that the Aβ (16–22) peptide (KLVFFAE) could self-assemble in neutral and acidic conditions to different nanostructures.[66] Under a neutral condition, the peptide assembled into nanofibers, however, under an acidic pH condition, the peptide formed nanotubes. In another example, Ghosh *et. al.* developed a strategy for precisely tuning the self-assembly behaviour of peptide amphiphiles by adjusting the solution pH where they found that the peptide amphiphiles could self-assemble into nanofibers under pH 4 and spherical nano-micelles at pH 10.[67] The self-assembly of DNA molecules into ordered nanostructures can also be mediated by the pH-responsive formation of a triplex/tetraplex.[68-70] For example, Willner and his group reported the pH-stimulated reconfiguration and structural isomerization of a DNA origami dimer and trimer by designing pH-sensitive origami dimers and trimers.[70]

1.4.2. Temperature: It is well-known that temperature is another important factor that affects the conformation, disrupts local intramolecular interactions and promotes/disrupts intermolecular interactions such as hydrophobic interactions and/or hydrogen bonding of molecules during self-assembly. Hamley's group reported that a peptide amphiphile C_{16}-KKFFVLK self-assembled into nanotubes and helical ribbons in aqueous solution at room temperature. However, on heating, remarkable unwinding transition occured which led to the formation of twisted tapes. The nanotubes and ribbons re-formed on cooling.[71] Further, Huang *et.al.* designed a "rod-coil" graft copolymer containing a polyphenylene backbone linked with poly(ethylene oxide) sidechains,[72] which could form nano ribbons and multilayer sheets at different temperatures.

1.4.3. Sonication: It is routinely used in inducing self-assembly. The force of ultrasound readily rearranges the aggregation of molecules by cleaving the self-locked intramolecular hydrogen bonds or π-stacking to form the interlocked structures through intermolecular

association.[73,74] Ultrasound may reshape the morphologies of the peptides and convert them into more elongated fibres that give rise to hydrogels, due to sono-crystallization.[75] Gu *et. al.* reported that ultrasound not only accelerates the gelation process but also induces the formation of fibrils that entangle to form 3D networks.[76]

1.4.4. Salt Concentration: Learning from nature that metal ions can impart stabilization and function to proteins,[77, 78] peptides have been designed to take advantage of the same for self-assembling.[79] Scheneider *et.al*. has reported a 20 residue β-hairpin peptide where a negatively charged non-natural amino acid residue has been incorporated to induce metal binding property to the peptide. The peptide adopted a random coil conformation in water but self-assembled into β-sheet rich fibrillary hydrogels in the presence of Zn^{2+} ions.[80] Another 20 residue β-hairpin peptide, metal binding hairpin (MBHP) also showed responsive hydrogelation in the presence of heavy metals like Zn^{2+}, Pb^{2+}, Hg^{2+} etc.[81] Near infrared light induced leakage of Ca^{2+} ions into a solution of β-sheet forming peptides, triggered the self-assembly of the peptide into a hydrogel.[82]

1.4.5. Photo-Stimulation: Light is another form of stimuli which might direct self-assembly. Various nanostructures can be obtained by the photo-induced self-assembly of molecules.[83-87] In the photo-triggered assembly process, the photo-responsive groups act as photo switching units to mediate the structure and functions of the formed nanostructures. For example, Muraoka *et.al.* synthesized photo-responsive peptide amphiphiles with a palmitoyl tail, the 2-nitrobenzyl group, and an oligopeptide motif ($GV_3A_3E_3$), which were capable of self-assembling into supramolecular quadruple nanofibers.[84] Sugiyama and co-workers presented the fabrication of predesigned multi orientational patterns by photo-induced self-assembly of DNA origami nanostructures.[88] Schneider *et.al.* developed a photocaged peptide which remains unfolded and unable to self-assemble when being dissolved in an aqueous medium, however, the irradiation ($260\ nm < \lambda < 360\ nm$) of the solution triggered the peptide folding

to produce amphiphilic β-hairpins that self-assembled to generate viscoelastic hydrogels.[89] Sophisticated supramolecular assemblies can be achieved by controlling assembly and disassembly using light. Stilbene derivatives are well-known molecular entities which show the photoinduced isomerization; They are isomerized from trans to cis form and from cis form to trans form under irradiation with UV and visible light, respectively.[90] Harada *et.al.* illustrated the switching between supramolecular dimer and non-threaded supramolecular self-assembly consisting of 3-stilbene-α-cyclodextrin with photoirradiation.[91] Zhang and co-workers integrated photo sensitive spiropyran with the peptide ^{D}Ala-^{D}Ala and demonstrated that irradiation of light induced self-assembly in the system. Upon irradiation of light, the non-planer spiropyran moiety got converted into planer merocyanin unit that readily stacked and underwent self-assembly.[92] Light induced cis-trans isomerization of azobenzene has also been used as an optical trigger in many photo induced systems.[93]

1.4.6. Enzymes: Involvement of enzymes is another way of directing the self-assembly process in achieving unexpected successes in the generation and applications of supramolecular nanostructures. Enzymes influence the self-assembly process significantly as they may catalyse the formation of biological materials, capable of self-assembling. Based on their functions and types, enzymes can promote or inhibit the aggregation and self-assembly of biomolecules through different strategies.[94] Despite the diversity of enzymes, only a handful of them have been used for catalysing self-assembly. While enzymes like phosphatase[95-98] β- lactamase,[99] esterase,[100] matrix metalloproteinase-9,[101, 102] α-chymotrypsin,[103] thrombin, chymotrypsin,[104] and β-galactosidase,[105] catalyze bond cleavage reactions, others like lipase,[106] microbial transglutaminase[107] and thermolysin[108] catalyze bond forming reactions. Other examples of enzymes are glucose oxidase,[109]peroxidase[110] and tyrosinase.[111] Regardless of the enzymes or the reactions they catalyse, the essential feature involves the conversion of a precursor molecule to the hydrogelator. In the very first example

of its kind, alkaline phosphatase was used to dephosphorylate Fmoc-tyrosine phosphate under alkaline conditions to form the hydrogelator which forms supramolecular hydrogel.[112] Ulijn *et.al.* triggered the peptide self-assembly to form hydrogels by the use of thermolysin to catalytically promote the formation of peptide bond in between two amino acids to form the hydrogelator.[108] Amir *et.al.* introduced an enzyme-triggered strategy to mediate the self-assembly of a block coplymer into nanoparticles under physiological conditions.[113] Xu's group designed a series of structural precursors based on the GNNQQNY peptide sequence of the yeast prion Sup35, which self-assembled to form supramolecular hydrogels induced by alkaline phosphatase in water.[114] Qi and co-workers developed a novel hydrogel from the enzyme-induced supramolecular self-assembly of a synthetic glycopeptide to mimic the glycosylated microenvironment of the extracellular matrix.[115]

1.4.7. Covalent Bond Formation: Disulphide bond formation is an important technique that is used to induce self-assembly. Bowerman and co-workers adopted this strategy to linearize a cyclic peptide by the reduction of the disulphide bond.[116] Cyclization induced conformational constraint in the peptide prevented it from forming self-assembly. Linearization of the peptide led to the formation of β-sheets, which led to fibriller morphology that eventually formed hydrogels.[116] Yang *et.al.* designed a precursor hydrogelator peptide containing a disulphide bond. Addition of reducing agent to the precursor peptide led to the clevage of the disulphide bond, the release of the hydrogelator and the subsequent self-assembly that eventually led to hydrogelation.[117] Das *et.al.* used native ligation to generate a peptide that forms dimer upon oxidation in the presence of O_2. The dimer acted as the gelator in mixed solvent systems of methanol/water.[118] Besides redox reactions, hydrolysis has been utilized in the formation of supramolecular assemblies. Xu *et. al.* reported a small amino acid ester molecule that upon alkaline hydrolysis gave rise to an acid with diminished solubility that formed supramolecular hydrogel that was kinetically

stable over a large range of pH.[119]

1.4.8. Tailoring Molecular Structure: Molecular structure is important for guiding the self-assembly of molecules (especially for peptide and DNA molecules) into well-ordered superstructures.[120, 121] For instance, by designing peptide sequences with multiple functions, such as recognition, binding, signal acceptor and self-assembly motifs, it is easy to create 1D, 2D, and 3D peptide superstructures with desired functions.[122] Dai *et.al.* used an amyloid peptide sequence KLVFFAK to self-assemble 2D peptide nanosheets by adjusting the molecular structure.[123] Also, in case of DNA, it is possible to synthesize superstructures by designing and modifying DNA sequences and other complex DNA building blocks.[121]

1.5. Peptide Self-Assembly

The first protein capable of self-assembly was discovered in 1980, when a DNA binding protein zuotin was isolated from Type I fimbriae of *E. coli*. This protein that was involved in the attachment of the bacteria to the eukaryotes, assembled into right handed helix and could be reassembled post denaturation.[124] A repeat of a 16 residue long peptide sequence within the protein was responsible for its self-assembling behaviour. The peptide (EAK16-II, AEAEAKAKAEAEAKAK) was characterized by Alanine (Ala) residues alternating with positively and negatively charged amino acid residues. Another seminal advancement in the field came from the identification of the short peptide sequence in the amyloid β peptide, responsible for the aggregation of the amyloid fibrils that causes the Alzeimers disease.[125] Since this revelation, the dipeptide FF, which is the core aggregating motif of the pentapeptide KLVFF, has been thoroughly exploited to yield various nanostructures with novel applications by Gazit and co-workers and other groups. This in turn opened up a new horizon for the small peptide based gelator molecules to obtain materials with diverse applications in various fields. The first report on nanostructures built from amino acids was obtained in 1990's. In one of the early on studies, Ghadiri and co-workers reported

antiparallel stacking of cyclic peptide *cyclo*[-D-Ala-Glu-D-Gln)$_2$-] to give rise to open ended tubular assemblies.[126] One of the earliest example of amino acid based hydrogelator was reported by Gortner and Hoffman almost a century ago,[127] though it was only in the 1990's that Menger *et.al.* demonstrated that π-π stacking and hydrogen bonding were the driving forces for this self-assembly process.[128, 129]

Out of the wide range of biomolecules that can potentially self-assemble, peptides, composed of a diverse variety of amino acids, both natural and unnatural, form a class of versatile biologically-inspired building blocks, which have attracted increasing attention with respect to the creation of advanced materials and applications in nanotechnology and biomedicine. Peptides have a unique ability to adopt secondary, tertiary and quaternary structures which is absent in the other class of self-assembling molecules.[130] This gives peptides a unique advantage over the others for design of unique nanomaterials which is not possible with the other types of organic molecules. Peptides have facile modes of synthesis (solution and solid phase), are relatively cost effective, are easy to handle and biocompatible. They are composed of twenty natural amino acids and can be further tuned by incorporation of unnatural amino acids with diverse side chains. Owing to this variation in the peptide composition, they have variable chemistries and physico-chemical properties. The side chains of the amino acids are decorated with various functional groups making peptides easily functionalizable with different groups such as fatty acids, antibodies or fluorescent molecules. Such variable and tunable chemistry helps in generation of building blocks of choice from the peptides. Additionally peptides have better immunocompatibility and favourable pharmacokinetics.[131,132] Non-covalent interactions play very important roles in the peptide self-assembly processes. Electrostatic interaction, hydrophobic interaction, hydrogen bonding, and π-π stacking are the key contributors of peptide self-assembly.[133, 134] Non-polar amino acids, such as aromatic and aliphatic amino acids, are mainly responsible

for hydrophobic aggregation through π-π stacking and hydrophobic interactions. Polar amino acids result in either electrostatic interactions or hydrogen bonding depending on whether they have uncharged or charged residues.[135, 136] Besides individual amino acids, the peptide backbone itself also provides considerable stability through hydrogen bonds. As these non-covalent interactions are easily affected by the external stimuli like pH values, temperature and solvent polarity, peptide self-assembly like others can also be triggered, manipulated and controlled using them.

1.5.1. Self-Assembling Peptides:

Peptides comprising of short amino acid sequences or repeated amino acid sequences have high tendency of assembling to form nanostructures. There is also a vast amount of literature where simple amino acid derivatives have been shown to self-assemble. A number of peptide-based building blocks, including dipeptides, cyclic peptides, amphiphilic peptides, surfactant-like oligopeptides and aromatic dipeptides, have been designed and developed for the creation of functional supramolecular architectures and the exploration of their possible applications in biology, nanotechnology and several other applications.

1.5.1.1. Amino Acid Derivatives: Not only peptides, but single amino acid derivatives are also very prone to undergo self-assembly (Figure 1.11). Most amino acid derivatives containing an alkyl chain act as conventional amphiphiles. These contain a polar head group and one or more hydrophibic tails.[137-139] In another strategy, aryl motifs like ferrocenyl, fluorenyl, napthyl and pyrenyl that undergo π-π stacking to promote self-assembly are appended to amino acids. Such molecules have been shown to form hydrogels.[140-142] Xu *et.al.* reported the first case of using Fmoc amino acids (Fmoc-Tyr phosphate/ Fmoc-Lys with Fmoc-Lys (bonded through the γ-amino group) to form multicomponent supramolecular hydrogels.[112. 143, 144] Though alkyl chains and aromatic groups promote self-assembly through hydrophobic interactions and π-π stacking interactions, these groups severely compromise

the solubility of the molecules in aqueous medium. One of the simplest strategies adopted to improve the solubility is to introduce charge into the molecules. Suzuki *et.al.* reported the synthesis of a L-Lys alkali metal salt which self-assembled into nanofibers and formed 3D network that generated a hydrogel.[145] In another study, pyridinium salt of L-Lys formed a hydrogel in a large range of pH.[146] Similarly ammonium and pyridinium salts of Phe have been demonstrated to form hydrogelators.[147-149]

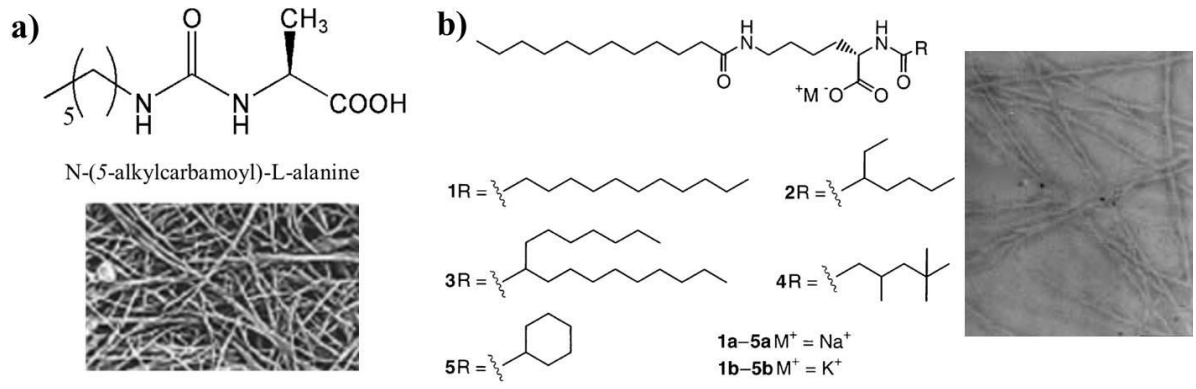

Figure 1.11: Amino acid derivatives as self-assembling materials. a) Chemical structure of N-(5-alkylcarbamoyl)-L-alanine and the corresponding FESEM image of the air dried gels formed from it in p-xylene. The figure has been adapted with permission from reference 139. *Copyright 2011, American Chemical Society*. b) Chemical structures of L-Lys derivatives and corresponding TEM image of 1a in water. The figure has been adapted with permission from reference 145. *Copyright 2004 Verlag Helvetica Chimica Acta AG, Zürich.*

1.5.1.2. Dipeptides: The simplest peptide building blocks are dipeptides that can self-assemble into a vast range of nanostructures (Figure 1.12). A classic example of dipeptide self-assembly is the L-Phe-L-Phe (FF) peptide, which forms the core recognition motif of the Alzheimer's β-amyloid peptide. Reches and Gazit first reported the self-assembly of FF into nanotubes by π-π stacking and β-sheet secondary structure formation.[150] These nanotubes were used to cast silver nanowires which enabled its application in the bioelectrical field. FF nanotubes have been shown to have unique optical properties, like emitting blue fluorescence

and manifesting second order non-linear optical response which make them invaluable for nanophotonics. FF nanotubes have piezoelectric and ferroelectric properties while cationic FF nanotubes could pass through cell membranes and have been employed as drug delivery vehicles. FF could also self-assemble into nanospheres, while Fmoc-FF could form nanocylinders which gave rise to hydrogels. Many studies have indicated that the peptide FF and its derivatives could self-assemble into highly ordered nanostructures which included nanotubes,[150] nanospheres,[151] nanofibrils,[152] nanowires[153] and ordered molecular chains.[154]

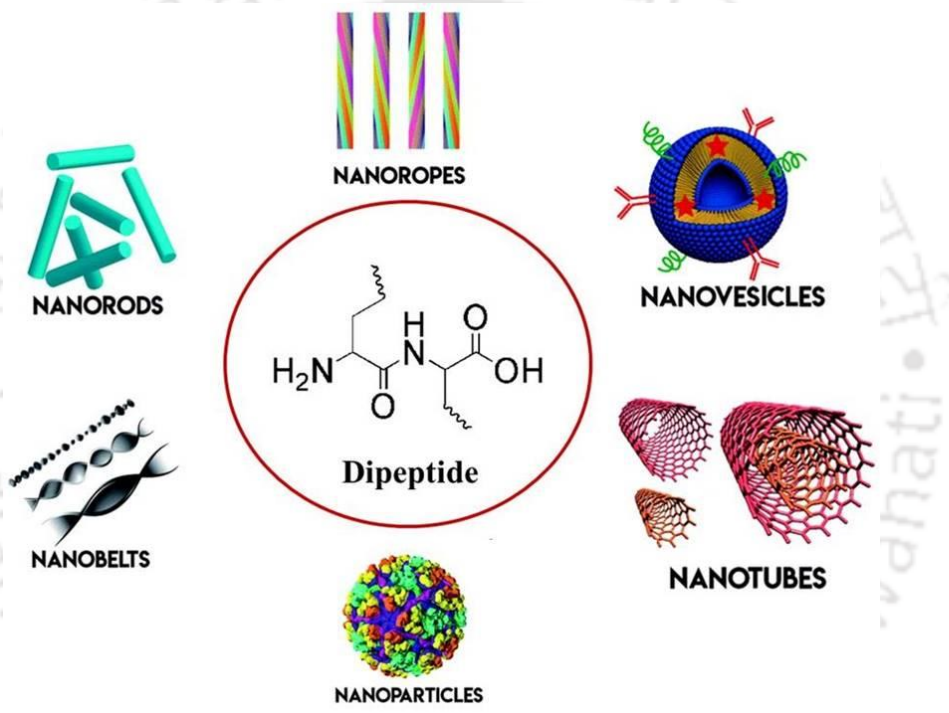

Figure 1.12: Different nanostructures formed by dipeptides.

Besides diphenylalanine, reports are also there for hydrophobic dipeptides such as LL, LI, and LF, self-assembling into nanotubes through hydrogen bonding.[155,156] Dipeptide nanoparticles formed from peptide WF have been exploited for bioimaging applications.[157] Other nanostructures were also reported to be formed by N-terminally modified diphenylalanine to a non-charged FF analog, such as Boc–F–F–COOH, Z-F–F–COOH and Fmoc–F–F–COOH. While the Boc-F–F-COOH peptide formed highly ordered tubular

structures, the Fmoc-F–F-COOH and the Z-F–F-COOH peptides self-assembled into fibrillar structures[158]

1.5.1.3. Peptide Amphiphiles (PAs) With an Alkyl Group: These are the molecules which have a hydrophobic tail group, usually an alkyl chain, which leads to hydrophobic interactions, a peptide sequence that is able to form intermolecular hydrogen bonds, which determines the interfacial curvature of self-assembly, a section of charged amino acids to promote solubility.[160] Self-assembly of peptide amphiphiles has been widely studied due to their potential to assemble into a large range of novel nanostructures which are of interest commercially and biomedically. This peptide self-assembled structure can largely be controlled by amino acid sequence, length of sequence and lipidation. When the alkyl chain combined with a peptide block is exposed to aqueous environment, the hydrophobic tail of the peptide adopts a 3D structure and usually results in the formation of nanofibers, micelles or vesicles.[160, 161] For example, Hartgerink *et.al.* reported a mineralized self-assembling peptide, including an alkyl tail and phosphorylated serine residues, to interact with calcium (Figure 1.13).[162] A C_{16} alkyl tail with a VVVAAAEEE ($V_3A_3E_3$) peptide was reported to form a gel under pressure or through electrostatic interaction with divalent cations .[163]

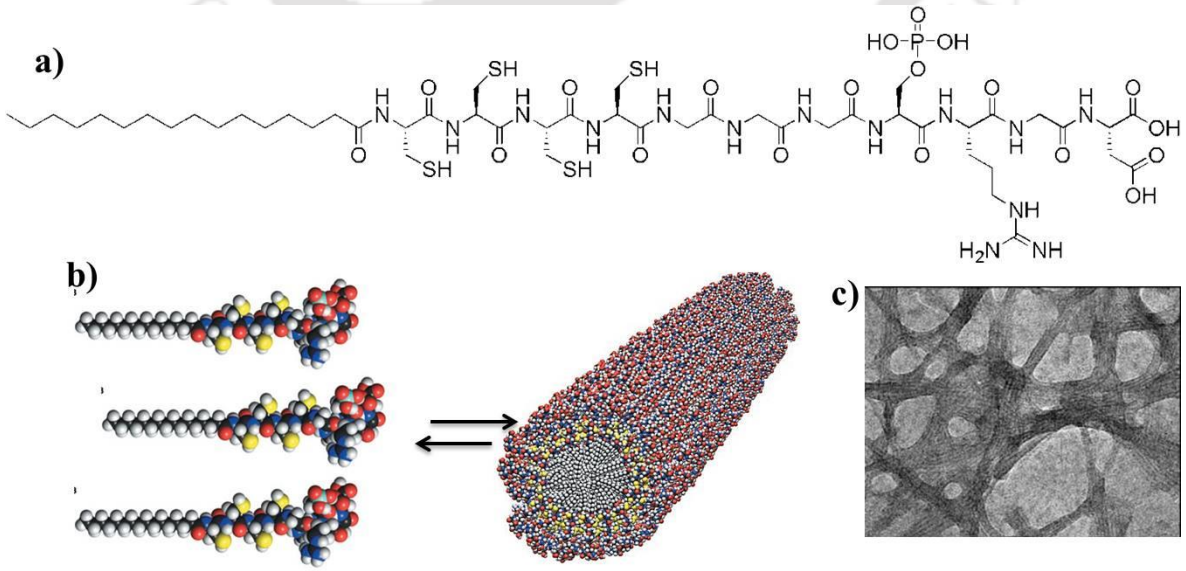

Figure 1.13: a) Chemical structure of the Hartgerink's peptide amphiphile. b) Schematic showing the self-assembly of PA molecules into a cylindrical micelle. c) TEM of the self-assembled nanofibers formed from the PA. The figure has been adopted with permission from reference 162. *Copyright 2001, The American Association for the Advancement of Science.*

1.5.1.4. Peptides with Aromatic Groups: Aromatic π-π interactions play an important role in the self-assembly process. Some amino acids like Phe and Trp contain aromatic side chains that promotes self-assembly. Exploiting this concept further, peptides functionalized at the N-terminus with large aromatic moieties have been thoroughly investigated. As a matter of fact this class of peptides form potential hydrogelators. Fmoc,[164-167] Napthalene,[168-170] Pyrene[171] are some of the aromatic moieties that have been often appended to the N-terminus of the peptides to yield self-assembling peptides (Figure 1.14). Ladouceur *et.al.* synthesized hydrogelators containing an electroactive aromatic group, anthraquinone. The system exploited a well-known redox couple anthraquinone/anthradehydroquinone as the hydrophobic part of a series of hydrogelators.[172]

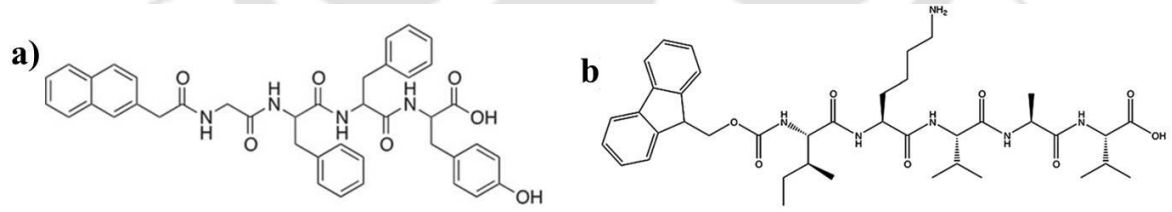

Figure 1.14: Chemical structures of aromatic self-assembling peptides: a) 2-Nap-GFFY peptide[165] and b) Fmoc-IKVAV peptide. [166]

1.5.1.5. Surfactant-Like Peptides: These peptides have been designed using natural lipids as a guide.[173] It has been found that, often, surfactant-like peptides include a hydrophilic head group with one or two charged amino acids such as Asp, Glu, Lys or Arg, and a lipophilic tail made of hydrophobic amino acids such as Ala , Val, or Leu (Figure 1.15); the

N-terminus has no charge.[174, 175] When dissolved in water, these surfactant-like peptides tend to self-assemble to shield the hydrophobic tail from contact with water. Like lipids and fatty acids, the supramolecular structure is characterized by the formation of a polar interface that isolates the hydrophobic tail from water. Vauthey *et.al.*,[173] Zhao,[174] and Wang *et.al.*,[176] suggested that, this class of peptides form nanotubes or nanovesicles as their main structures and can function in a manner similar to lipid detergent micelles or the lipid bilayer of cells.

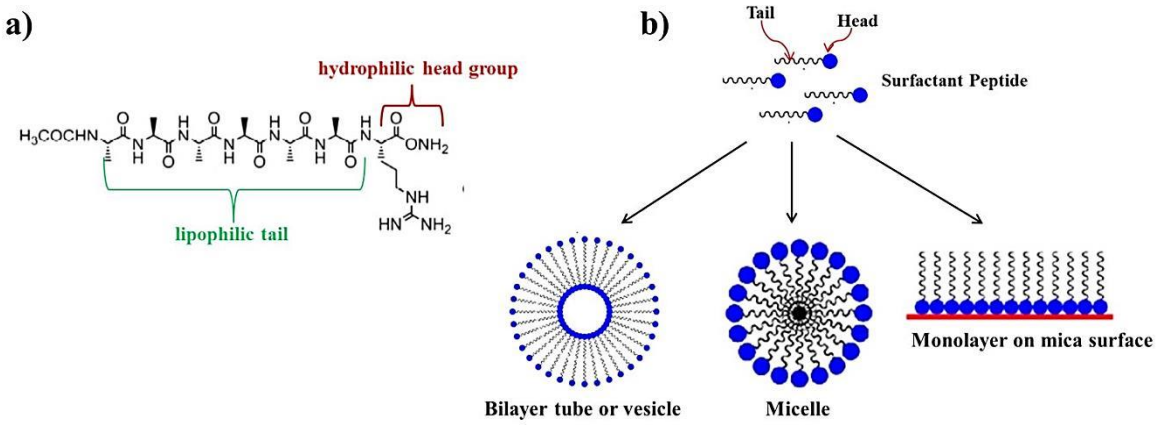

Figure 1.15: a) Chemical structure of a typical surfactant like peptide Ac-A_6R-NH_2.[175] b) The self-assembling models of typical surfactant-like peptides.

1.5.1.6. Ionic-Complementary Self-Assembling Peptides: These peptides are characterized by an alternating arrangement of negatively and positively charged residues (Figure 1.16a). According to their charge distribution, the following three types of charge distribution are the most widely studied among ionic-complementary peptides: type I, - +; type II, --++; type IV, ----++++.[177] The ionic-complementary peptides can be combined and modified in order to design other peptide blocks. For example, RADA16 is an ionic-complementary self-assembling peptide.[178] RADA 16-I (RADARADARADARADA) has the charge distribution pattern of +-+-+-+-, whereas RADA16-II (RARADADARARADADA) has the charge distribution pattern of ++--, but both form β-sheets after assembly. Two types of peptides, AEAEAKAKAEAEAKAK (EAK16-II) and AEAEAEAEAKAKAKAK (EAK16-IV) were

investigated. EAK16-II has a charge sequence of --++--++ at neutral pH, whereas, EAK16-IV has a charge sequence of ----++++. EAK16-II forms fibrillar assemblies (Figure 1.16c), whereas EAK16-IV forms globular assemblies.[179-181]

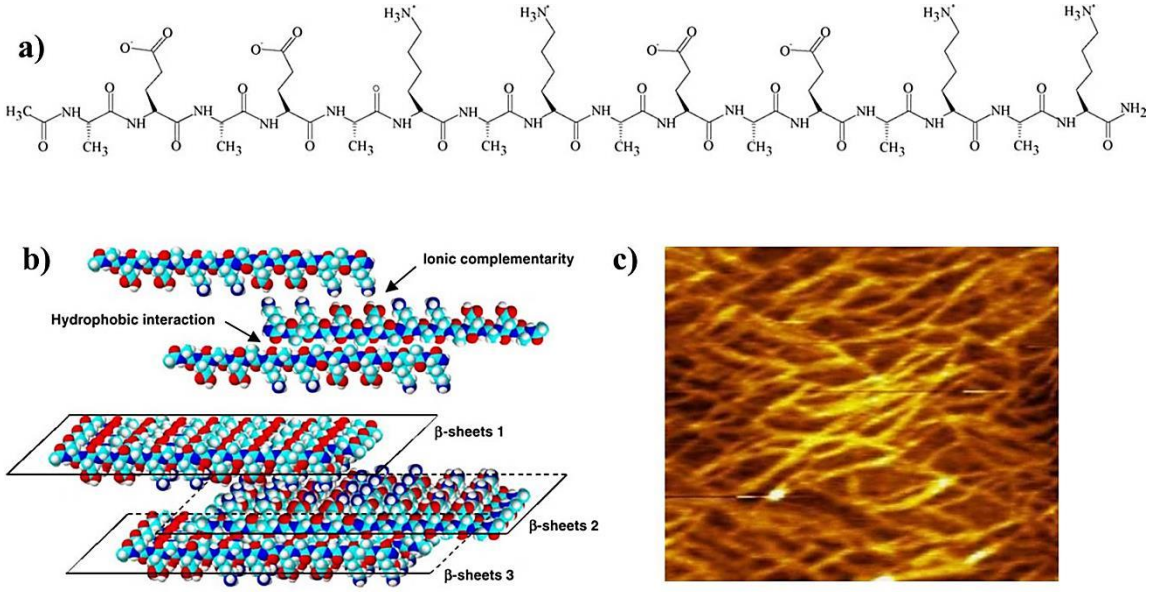

Figure 1.16: a) Chemical structure of an ionic-complementary self-assembling peptide—EAK16-II. b) A scheme of EAK16-II self-assembly through hydrophobic interaction and ionic-complementarity into β-sheet-based aggregates. c) AFM images of EAK16-II formed nanostructures. The figure has been adapted with permission from reference 177. *Copyright 2005 Published by Elsevier B.V.*

1.5.1.7. Cyclic Peptides: Cyclic peptides are polypeptide chains adopting cyclic ring structure. The ring structure can be formed by linking one end of the peptide and the other with an amide bond, or other chemically stable bonds such as lactone, ether, thioether or disulphide. The N-to-C (or head-to-tail) cyclization is amide bond formation between amino and carboxyl termini, and many biologically active cyclic peptides are formed this way.[182] The first self-assembled nanotube using cyclo-(L-Gln-D-Ala-L-Glu-D-Ala)$_2$ cyclic peptides was achieved in 1993.[126] Also, there are examples of cyclic peptides, self-assembled into

nanotubes, stabilized by hydrogen bonding between amide groups[183] wherein, due to the alternating D type and L type amino acids, the peptide side chains could be positioned on the outside of the ring that can create a nanotube structure. There are many cyclic peptide sequences that can be used for the self-assembly, including alternating D type and L type α-amino acids, alternating α- and β-amino acids, β-amino acids[185] (Figure 1.17), and δ-amino acids.[184-186]

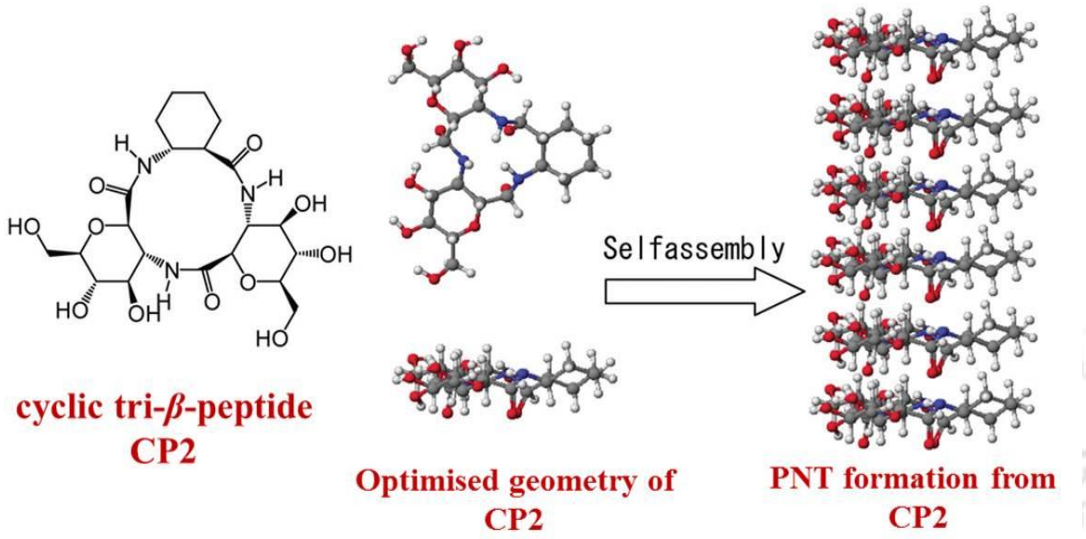

Figure 1.17: Cyclic Self-assembling peptides: Schematic illustration of PNT formation from cyclic tri-β-peptide. The figure has been adapted with permission from reference 185. *Copyright 2010 European Peptide Society and John Wiley & Sons, Ltd.*

1.5.1.8. Bolaamphiphilic Peptides: Another well studied class of self-assembling peptides are called bolaamphiphiles. In these peptides, two hydrophilic heads are connected by a hydrophobic region that is generally composed of alkyls (Figure 1.18a).[187, 188] Presence of versatile functional groups on peptides such as carboxyl, amine, thiol, hydroxyl and the hydrophobic groups enables peptide bolaamphiphiles to exhibit diverse self-assembling behaviors in response to the various environments (Figure 1.18b).[189] Das *et.al.* developed a library of bolaamphiphiles that contain various polar amino acids as the head group and reported their pH dependent self-assembly. Methylation of the phenols or the esterification of

the acids led to a stark change in the morphology of this class of peptide bolaamphiphiles.[190] Another class of U-shaped peptide bolaamphiphiles contain dibenzofuran template and two peptide strands made up of hydrophilic and hydrophobic amino acid residues with a blocked carboxy terminus.[191] These molecules afforded wide nanofibers with cross β-sheet structure in water *via.* intermolecular hydrogen bonding and hydrophobic interactions. In another design strategy, Tovar and co-workers introduced π conjugated nanostructures into peptide based bolaamphiphiles to replace the alkyl chain. This class of bolamphiphiles contained a polar part for solubility, a β-sheet containing part for self-assembly and a core oligothiophene moiety for conductivity.[192, 193] Self-assembly of these molecules resulted in a hydrogel.

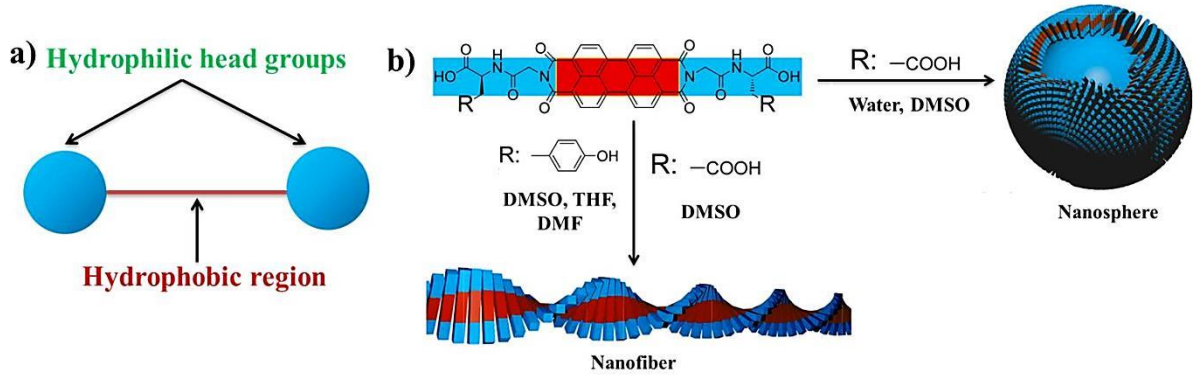

Figure 1.18: Bolaamphiphilic self-assembling peptides: a) Schematic representation of a bolaamphiphile. b) Self-assembly of a bolaamphiphilic peptide conjugate to fibrous and spherical structures in different polar solvents. The figure has been adapted with permission from reference 189. *Copyright 2014, American Chemical Society.*

1.5.1.9. Peptide Dendrimers: Woolfson *et.al.* proposed an approach that utilizes non-linear or dendritic peptides to direct the self-assembly of two complementary peptides. The two complementary peptides combine to exclusively form linear fibres. The dendrimer formed from the linear peptides gives rise to specific structures as hyperbranched networks, polygonal matrixes and regularly segmented and terminated fibres.[194] Liu *et.al.* reported an amphiphilic dendron containing three dendrite Glu unit and a long alkyl chain which formed

hydrogels over a large range of pH (Figure 1.19).[195] Lee *et. al.* designed a dendritic peptide with repeating hydrophobic and hydrophilic residues and Lys terminals, that self-assembles to give uniform toroid structures. He demonstrated that decreasing the electrostatic component or increasing the hydrophobic interactions of this peptide formed β-sheets that led to generation of 1D nanostructure. [196]

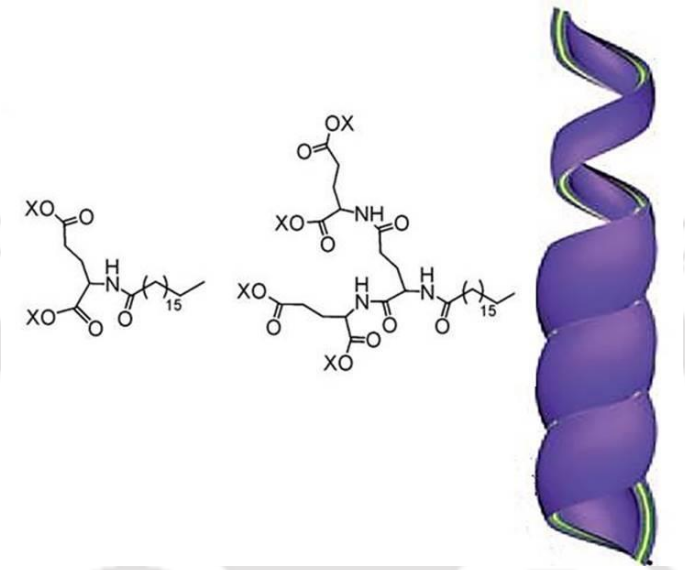

Figure 1.19: Dendritic peptides: Chemical structure of an amphiphilic dendron containing three dendrite Glu units and a long alkyl chain which can self-assemble to nanotubular structures at pH 2–9. The figure has been adapted with permission from reference 195. *Copyright 2011 WILEY-VCH Verlag GmbH & Co. KGaA, Weinheim*

1.5.1.10. Peptides Containing Photo Responsive Group: Peptides containing photo responsive group are an interesting class of molecules for studying self-assembly. The self-assembling behavior of the peptides can be controlled by irradiation of UV or visible light that may bring about change in the geometry or conformation of the photo responsive group.[197] A variety of photo responsive groups have been used as the photochemical module in these peptides. A classic example is spiropyran whose geometry can be switched in between the nonplanar spiropyran and the planer merocyanin upon the irradiation of UV and

visible light.[92] While the planer merocyanin form undergoes π-π stacking that favours self-assembly, the non-planer spiropyran form disfavors π-π stacking. Zhang *et. al.* reported spiropyran appended dipeptides forming hydrogels upon being irradiated with UV light in its planer merocyanin form.[92] Azobenzene group containing peptides are another class of photo responsive gelators (Figure 1.20).[93,199,200] The reversible photoregulated cis-trans isomerization influences the intermolecular interactions that leads to the sol-gel conversion. Huang *et.al*. reported dipeptide amphiphile containing azobenzene, which forms nanoribbons that gave rise to a macroscopic gel. Upon irradiation with the UV light, there was a stark change in viscosity with the conversion of the nanoribbons to the short fibers as revealed by the electron microscopic studies.[200]

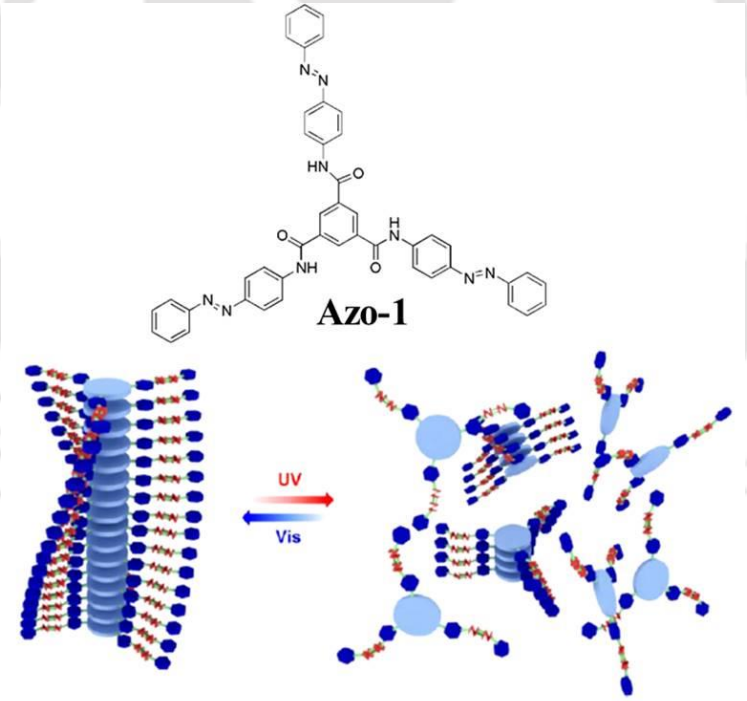

Figure 1.20: Photo responsive group containing peptides: Schematic representation of photo induced reversible phase transition of Azo-1 supramolecules. The figure has been adapted with permission from reference 199. *Copyright 2013, American Chemical Society.*

1.5.1.11. α-Helical Peptides: α-helical peptides form nanostructures that are present in the cytoskeleton and in the extracellular matrix[201] of biological systems. α-helical peptides which

are 25-30 residues long give rise to filamentous nanostructures.[202] α-helical peptides, 2-6 helices long can also aggregate around each other to form coiled coil structure that eventually gives rise to form fibers.[203, 204] Helix oligomerization occurs through hydrophobic collapse of the hydrophobic residues and electrostatic interactions or dipole-dipole interactions in between the charged or polar residues. Nano fibrous structures could also be formed by ionic interactions in between peptides containing Glu residues at the middle of the sequence and Lys residues at the termini of the sequence (Figure 1.21).[205]

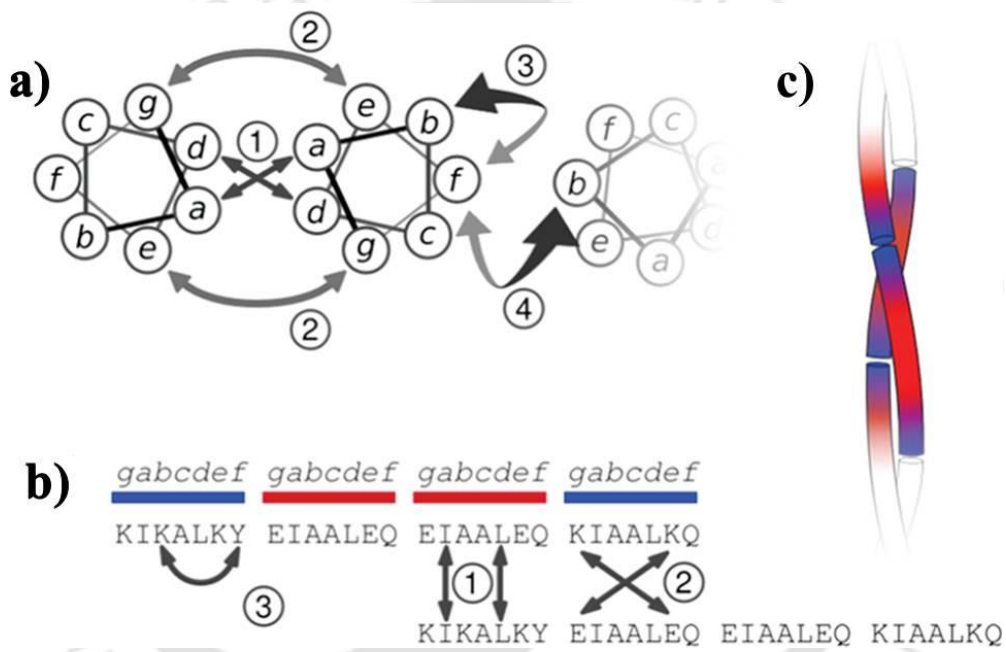

Figure 1.21: Illustration of the MW1 peptide: a) Helical-wheel representations for two α-helices showing various coiled-coil interactions: 1, hydrophobic packing; 2, charge-charge interactions; 3, intra-helical and 4, inter-helical cation-π interactions; b) Amino acid sequence with interactions 1-3 from (a) and c) Coiled-coil structure for MW1 illustrating fiber assembly. The figure has been adapted with permission from reference 205. *Copyright 2008, American Chemical Society.*

Hydrogels were reported from helical peptides with triblock motifs that have coiled coil blocks. Tuning the length and structure of the coiled coil units led to tuning of the hydrogel

properties.[206] Repeated hydrophobic and charged amino acid residues could give rise to coiled coil structures from α-helices.[207]

1.5.1.12. β-Sheet Peptides: β-sheet peptides have been used extensively for the formation of self-assembled structures (Figure 1.22). β-sheet peptides containing alternate hydrophilic and hydrophobic amino acid residues in the sequence attain amphipathicity that drives the self-assembly of the β-sheets.[208] They self-assemble to form structures like nanorods, monolayers, bilayers, nanofibers etc.[150, 209, 210]

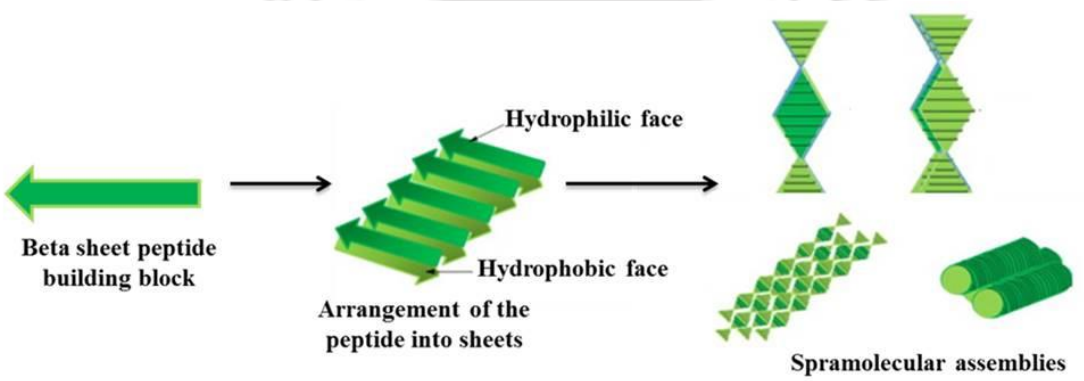

Figure 1.22: Schematic diagram showing the formation of supramolecular architectures by a β-sheet peptide building block containing hydrophobic and hydrophilic residues.

β-sheet peptide QQRFEWEFEQQ self-assembled into a pH responsive hydrogel using the ionizable side chains of Glu and Arg amino acids .[211] At neutral pH the peptide was soluble while at a lower pH it formed a hydrogel. This was due to the formation of antiparallel β-sheets in acidic conditions that self-assembled to form the nanofibrils and gave rise to the hydrogel. β-hairpin peptides were also found to self-assemble into nanostructures at the air and the water interface.[212] β-hairpin is another secondary structure adopted by the peptide where two antiparallel peptide strands are connected through a tight turn. A β-hairpin peptide with the sequence of VKVKVKVKVDPPTKVKVKV was utilized to form responsive (pH, salt concentration) hydrogels by Schneider *et.al*.[213] Patrick and his group investigated hydrogel formation by the self-assembly of two complementary β-sheet forming decapeptides

forming twisted fibres.[214]

Using all these different kinds of peptides as building blocks, it is possible to create nanoscale architectures ranging from few nanometers to hundreds of nanometer through a bottom-up methodology which makes peptide self-assembly a hierarchical process.[8]

1.5.2. Hierarchical Peptide Self-Assembly:

Molecules spontaneously undergo stepwise interaction in nature to form hierarchical assemblies from nanoscale to macroscale. Nature is therefore an obvious source of inspiration for the design of nanoscale materials using the bottom up approach. Inspired by nature, the hierarchical self-assembly of molecules occurs across different length and time scales. This is driven by multiple non-covalent interactions leading to a ubiquitous fabrication strategy to create various architectures from the microscopic to macroscopic scale, especially for biomolecules.[215, 216] A ‘‘bottom-up’’ approach provides a route for the development of nanoscale objects and devices.

Peptide self-assembly is also hierarchical in nature (Figure 1.23). This hierarchical self-assembly process occurs across a wide range of time and length scales from the microscale to the macroscale *via.* different interactions such as hydrophobic interaction, π-π stacking, hydrogen bonding, electrostatic interactions which have distinct roles at various steps at different scales. As peptides are composed of amino acids, proper sequencing of these amino acids in a peptide molecule is the first step to establish self-assembly in a hierarchical order. In solution, the primary structure of peptide molecules adopt a specific secondary conformation, which in the presence of proper stimuli or favourable physical conditions self-assemble to form different architectures of nanoscale order. Further assembly/elongation of these nanoscale structures lead to the formation of higher ordered functional materials which can range upto microscale. For example, peptide secondary structures like α-helices or β-sheets can self-assemble to form fibers. Assembly of many such fibers leads to the bundles of

fibers which are stronger and thicker in nature. Elongation of these fibers in three-dimensional space leads a 3D fibrillar network which ultimately might result into self-supporting hydrogels which is a form of higher ordered architecture that can be visualised even with the naked eye.[217] Peptides thus undergo this process of hierarchical self-assembly which generates several kinds of soft materials that give rise to a wide spectrum of applications.

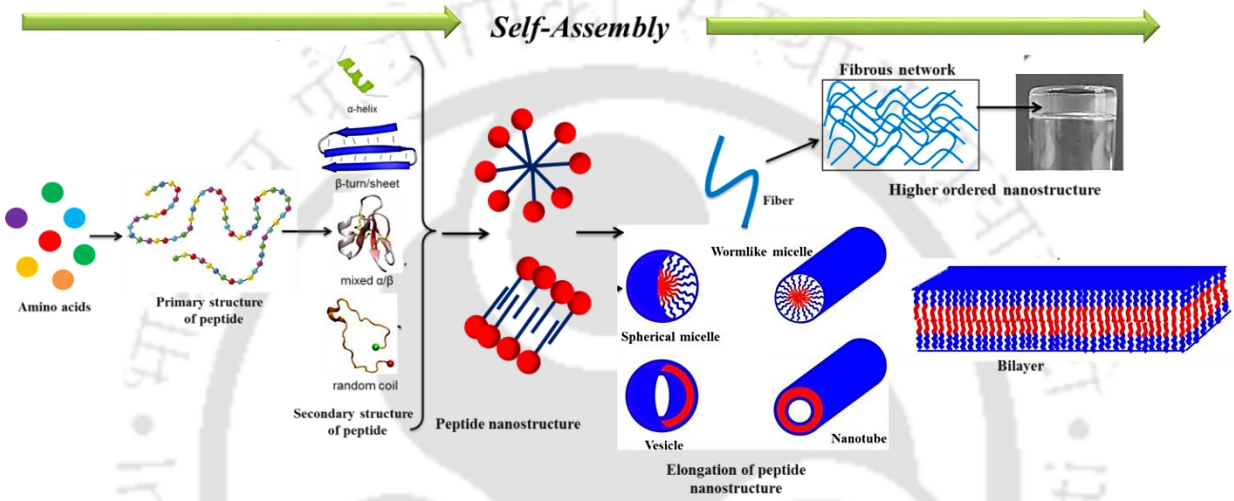

Figure 1.23: Schematic illustration of hierarchical peptide self-assembly.

1.5.3. Serendipity vs. Directed Design:

The phenomenon of self-assembly was serendipitously discovered at the beginning. The process and the materials which resulted from this caught the attention of the scientists and opened up an extremely active area of research. Now, about a couple of decades down, as the the sequence-structure relationship of the proteins are being better understood, the ability of designing self-assembling proteins/peptides have considerably advanced. Understanding the underlying mechanisms of self-assembly, the non-covalent forces that play an important role in the process facilitate the rational design of the self-assembling systems. Understanding the secondary structural motifs and their hierarchical assembly process opens up the possibilities to design and modulate the self-assembly properties of the peptides with the proper use of the

various stimuli. Thus peptide self-assembly is no more a merely serendipitous observation but can be designed and tuned to a fair extent. Though the success to failure ratios in such exercises is not extremely high, yet the field has come a long way since its inception.

1.5.4. Peptide Nanostructures:

Peptides, based on their design and also on the environmental conditions, can assemble into different kinds of supramolecular architectures such as fibers, vesicles, spherical structures and nanotubular structures.

1.5.4.1. Tubular Nanostructures: Nanotubes are nanometer-sized tube-like elongated hollow structures with a definite inner hole. Nanotubes are particularly attractive because of their potential applications in biology, chemistry, and physics, such as chemotherapy, drug delivery, catalysis, molecular separation, optics, and electronics.[218] Gazit and his co-workers investigated the simplest peptide block, L-Phe- L-Phe, FF, which formed a tubular structure in HFIP (hexafluoroisopropanol) with a diameter in the range of 100–150 nm. The self-assembly was mediated through hydrogen bonding as well as π–π stacking of aromatic residues.[150] Modification of the termini of FF was done to form cationic dipeptide, NH_3^+-FF-NH_2·HCl which self-assembled into nanotubes at physiological pH (Figure 1.24).[219] The peptide NH_2-Phe-ΔPhe-COOH where ΔPhe denotes the non-coded and non-chiral α, β dehydrophenylalanine residue also formed nanotubes.[220] There are reports of nanotubes formed from other dipeptide motifs; for instance, dipeptides containing β-alanine (β-Ala-Xa, with Xa=V, I or F) were found to form crystalline nanotubes, onto which gold nanoparticles could be templated .[221] A. Bonetti reported dipeptides composed of unnatural fluorine-substituted β- 2, 3-diarylamino acid and Ala which self-assembled into proteolytically stable nanotubes.[222]

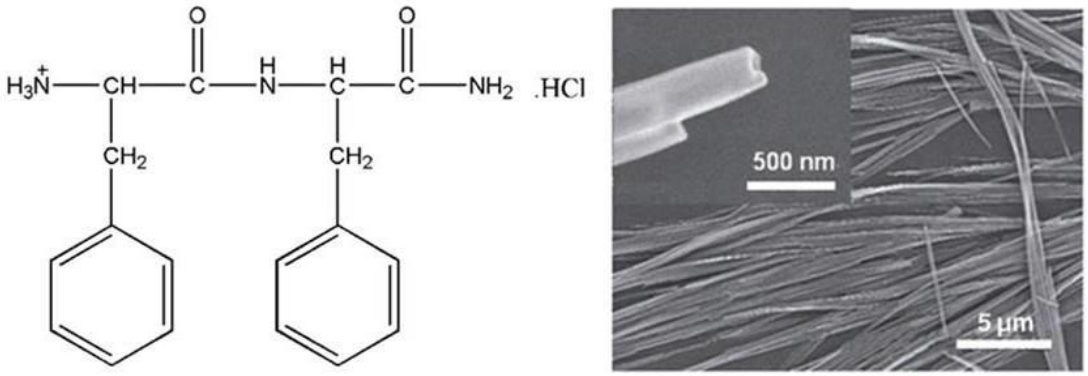

Figure 1.24: SEM image of the cationic dipeptide nanotubes formed from FF (inset: a hollow nanotube at greater magnification). The figure has been reprinted with permission from reference 219. *Copyright 2007 John Wiley and Sons.*

Apart from dipeptides, the most commonly used materials for nanotubes are cyclic peptides as has been discussed in an earlier section (Figure 1.17) (Section 1.5.1.7). A cyclic peptide that was reported to self-assemble into nanotubes of viral capsid-like dimension was the Lanreotide octapeptide, NH_2-(D)Naph-Cys-Tyr-(D)Trp-Lys-Val-Cys-Thr-$CONH_2$ which was synthesized as a growth hormone inhibitor.[223] Nanotube formation at low concentration was also observed for enantiomeric mixtures of cyclic peptides such as cyclo-[(D- Gln-L-Tle-D-Glu-L-Tle)$_2$] (Tle: tert-leucine). The nanotubes formed were stabilized by close antiparallel hydrogen bonds.[224] Amphiphilic and surfactant-like peptides also form nanotubes by self-assembly.[173] For example, S. Zhang and his group investigated the formation of nanotubular structures of 2Ds, one of 40–80 nm and another in the order of 100–200 nm with Gly rich amphiphilic peptide G_nD_2-OH (where n = 4, 6, 8, 10).[225] Also, nanotubular structures with diameter of 25–30 nm were found in the self-assembly of TFA salt of A_6K.[226]

1.5.4.2. Nanofibers: These are defined as fibers with a diameter of less than 100 nanometers. Basically, the difference between nanofibers and nanotubes is that the nanotubes are hollow structures unlike nanofibers. PAs with an alkyl group are the most renowned self-assembling peptides that form nanofibers that self-assemble into ordered structures in water through

hydrophobic interactions. In presence of specific solution environment, such as temperature, pH and ionic strength, these molecules generally assemble in water into nanofibers. Also, it has been cited that stable nanofibers can be formed by mixing two oppositely charged PA molecules (C_{16}VVVAAAKKK and C_{16}VVVAAAEEE) to support favourable ionic interactions.[227] Stupp and his co-workers investigated the formation of nanofiber networks by the aggregation of the amphiphilic peptide IKVAV (Figure 1.25).[228]

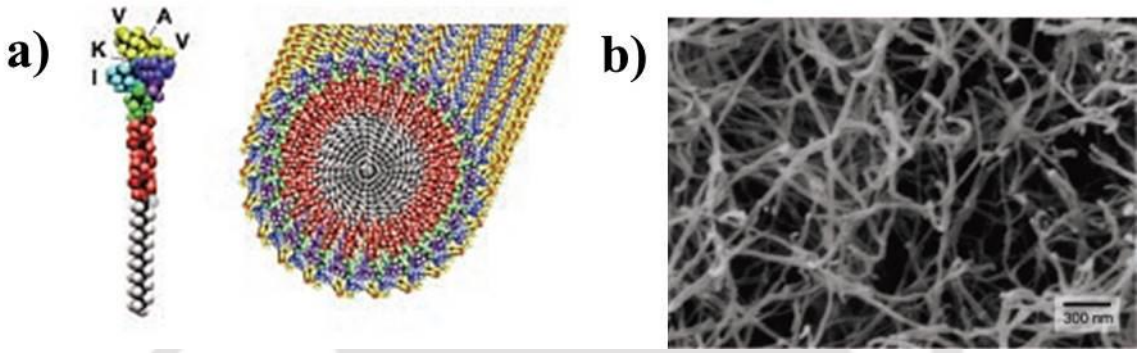

Figure 1.25: (a) Molecular graphics illustration of an IKVAV-containing peptide amphiphile molecule and its self-assembly into nanofibers and (b) SEM image of an IKVAV nanofiber network. The figure has been adapted with permission from reference 228. *Copyright 2004, American Association for the Advancement of Science*.

They also reported a helical fiber formed by a photoresponsive peptide amphiphile containing a palmitoyl tail, a 2-nitrobenzyl group and an oligopeptide segment $GV_3A_3E_3$ which converted into single fibers upon photochemical cleavage of the 2-nitrobenzyl group present in the former peptide.[84] Short peptide FKFEFKFE having an alternating pattern of hydrophobic and hydrophilic amino acids was shown to form self-assembled nanofiber structures.[229]

1.5.4.3. Vesicle or Spherical Structures: Amphiphilic peptides with distinct hydrophobic and hydrophilic parts self-assemble into vesicles or spherical structures which have a hollow core and can encapsulate hydrophilic molecules as shown by Van-Hell *et.al.*[230] Proline rich peptides, co-polypeptides and cyclic peptides are the other classes of peptide molecules which give rise to vesicular nanostructures. For example aqueous assembly of oppositely charged poly(L-Lys)-b-poly(L-Leu) and poly(Glu)-b-poly(L-Leu) block co-polypeptides gave rise to unilamellar vesicles.[231, 232] The driving force of the aggregation was the formation of α-helices by the hydrophobic poly(L-Leu) part. Polyarginine coated vesicles showed potential intracellular delivery of the entrapped hydrophilic molecules. Rodriguez Hernandez *et.al.* reported formation of pH sensitive vesicles from zwitterionic diblock co-polypeptides containing poly-L-Glu-b-poly-L-Lys (PGA-b-PLys) (Figure 1.26).[233] Charged co-polypeptides changed from random coil conformation into α-helical structures upon neutralization. At acidic pH, PGA block was neutralized, which formed the core while the Lys formed the shell, in contrast to the basic pH where the Lys was neutralized and formed the core while the PGA part formed the shell.[233] Dreher *et.al.* developed thermo-responsive elastin-like polypeptides (ELP) of linear AB diblock architecture that assembled into spherical micelles with a slight increase in temperature from 37 to 42 °C. Size of the micelles were controlled by the length of the copolymer and the hydrophobic to hydrophilic ratio.[234] Lee and co-workers designed a block copolymer of Pro and Arg $P_{10}R_3$, where the peptide showed polyproline II like rigid conformation and self-assembled into vesicles.[235, 236] Another Pro rich peptide P_{10}Tat also self-assembled into vesicles. Both of these peptides were used for the intracellular delivery of hydrophilic drugs. Cyclic peptides also produce vesicle-forming nanostructures. In a study, Parang and his group designed a number of cyclic peptides, among which the designed peptides, $[WR]_n$ (n = 3-5) generated vesicle-like nanostructures at room temperature.[237]

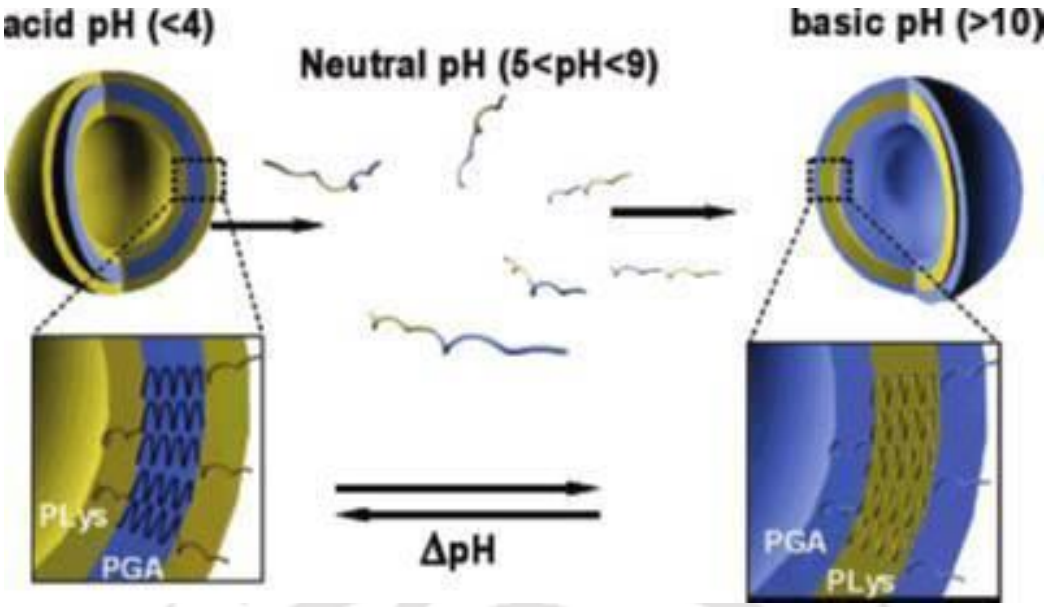

Figure 1.26: Schematic representation of the self-assembly into vesicles by the diblock copolymer PGA_{15}-*b*-$PLys_{15}$. The figure has been reproduced with permission from reference 233. *Copyright 2005, American Chemical Society*.

1.5.4.4. Amyloid Nanofibrils: The self-assembly of peptides and proteins into fibrillar structure is a very common phenomenon in biological systems. Amyloid fibrils are key examples of protein self-assembly into nano-fibrillar structures.[238] Amyloid fibrils have β-sheet conformation generated by polypeptides of 30–40 amino acids or longer. It has been shown by Gazit in a study that short peptide fragments, for example, tetra- to hexapeptides, form a fibrillar structure with similar biophysical and structural properties of amyloid fibrils.[239] Thus, they can be used as a model system for studying amyloid fibrils formation and biological self-assembly processes. NFGAIL and FGAIL are very good examples of short peptides which can self-assemble into fibrillar structures.[240] It was found that aromatic residues played critical roles in the process of amyloid formation. Diphenylalanine (FF) is the core recognition motif of the Alzheimer's β-amyloid polypeptide as mentioned earlier. Fmoc-FF self-assembled into nano-fibrils in aqueous solution, which led to a hydrogel formation.[152]

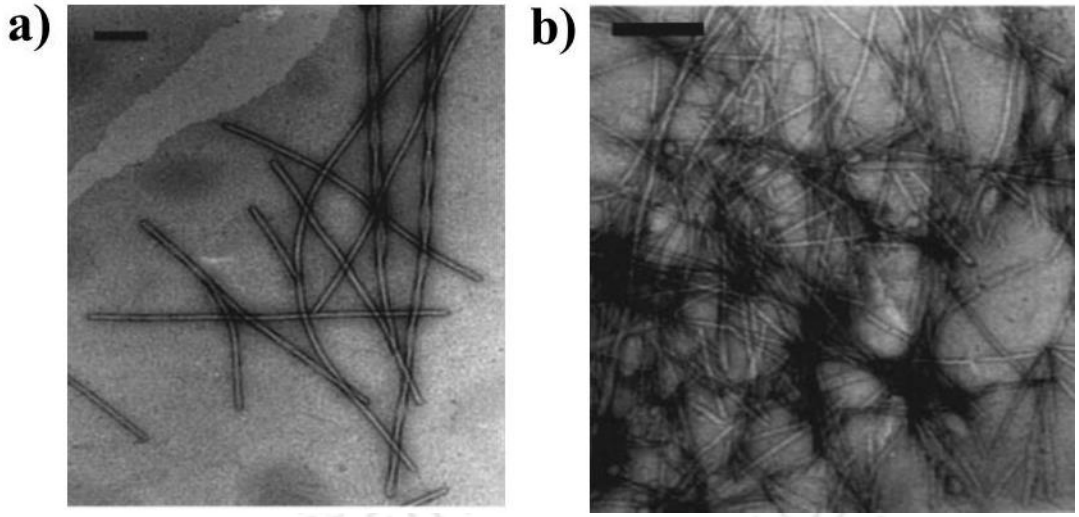

Figure 1.27: Amyloid fibrils. Electron micrograph of insoluble aggregates formed in an aged peptide solution in phosphate buffer (pH 7.4) of a) hIAPP (22-27) (NFGAIL), b) hIAPP (20-27) (SNNFGAIL). The figure has been adapted with permission from reference 240, *Copyright 2000, with permission from Elsevier*.

1.5.4.5. Rod-Coil/Coiled Coil Nanostructures: These peptides have alternating blocks with rod like stiffness and coil like flexibility. Like other building blocks these molecules can be used to construct distinct nanostructures of controlled shape and size. Lomander *et.al.* reported a hierarchical assembly into a coiled coil from a 31 residue long peptide containing alternate hydrophobic and hydrophilic amino acid residues. The coiled coil structure was stabilized by the disulphide bond formed in between the cysteine residues of different coils (Figure 1.28).[241] Ryadnov *et. al.* designed a nano-reactor with multiple cavities by assembling supramolecular dendrimers called supradendrimers in two steps. The monomeric peptide SD1 (QEIARLEQEIARLEYEIARLE) formed a dimeric coiled coil structure also known as the Leu zipper. These dimers gave rise to the rigid rods which hierarchically formed hollow dendrimer cells through tight non-covalent packing. In the second step, a complementary peptide SD2 (Ac-(K(KIEALKOKIEALKYKIEALK-εAhx))$_3$) was used to form compartment in the dendrimeric cavities. Co-assembly of the two peptides resulted in dimer

SD1, 2 which had encapsulation ability and acted as nano reactors where Ag nano particles, of the same size as the nano cavities were synthesized by the reduction of silver nitrate by sodium citrate.[242]

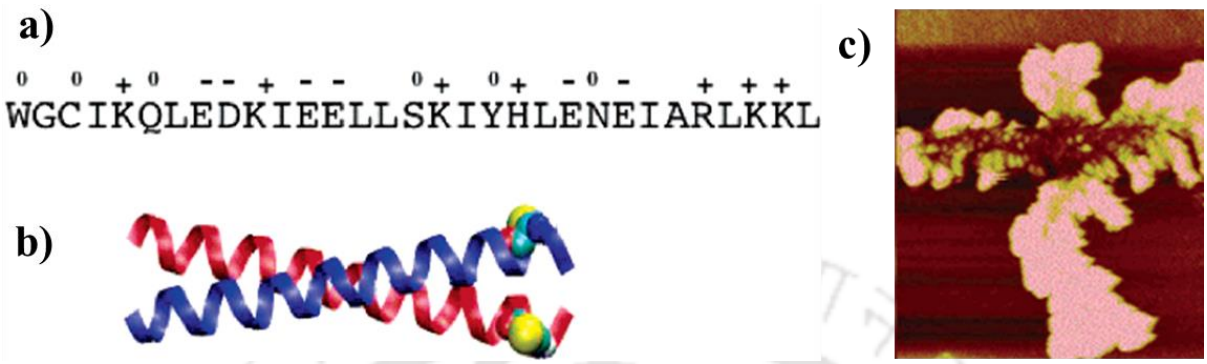

Figure 1.28: a) Peptide sequence of the 31 residue peptide. Charged amino acids are labelled with (+) or (-) and polar amino acids are labelled with (0) b) Model of a coiled-coil. c) Morphology of coiled-coil assembly of the peptide at pH 2. The figure has been adapted with permission from reference 241. *Copyright 2005, American Chemical Society.*

1.5.4.6. Gels-Hydrogel/Organogel: Peptide self-assembly often forms a class of soft materials called gels which loses their flow property, in spite of holding large amounts of water/organic solvents. Hydrogels are three dimensional network of mesh like structures formed from the assembly of peptide molecules that entraps large amounts of water while organogels entrap large amounts of organic solvents. Gels are formed by different classes of molecules and can be classified into two types: a) Physical gels, which are formed from the supramolecular self-assembly of molecules driven by the non-covalent forces discussed earlier and b) Chemical gels, which are formed by covalent crosslinking in between the molecules (Figure 1.29). In physical gels, the molecular property of the constituents is retained while in the chemical gels, the molecular property is completely lost, due to formation of covalent bonds.

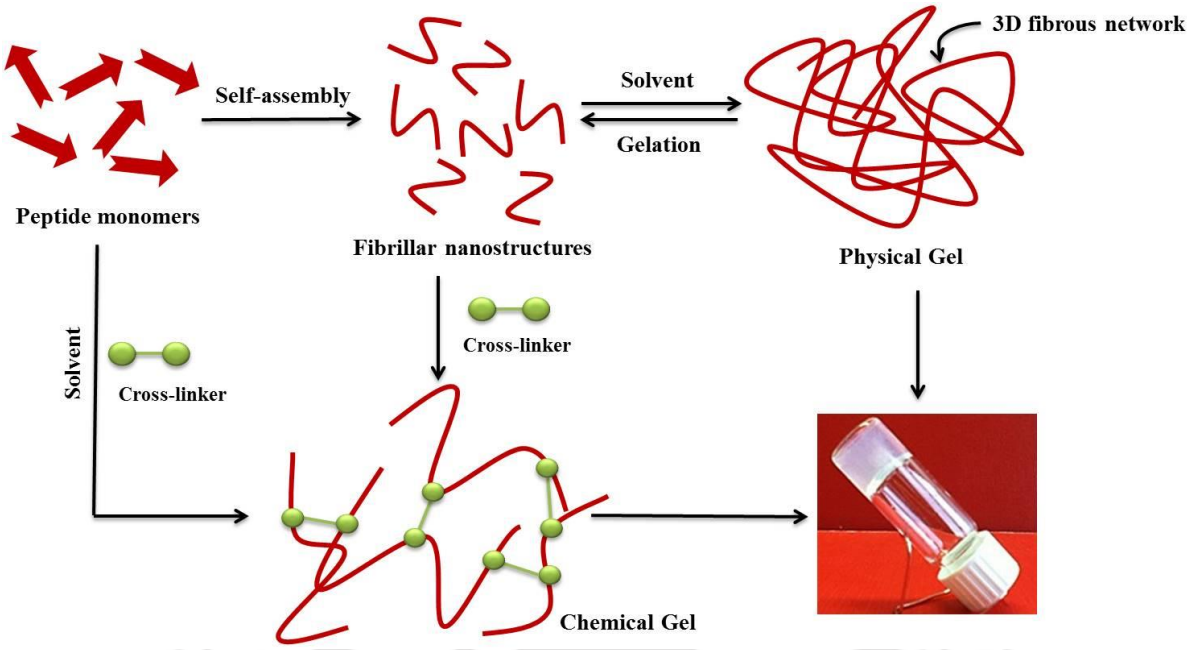

Figure 1.29: Schematic representation of peptide gels formed by physical association of the fibrillar nanostructures or chemical crosslinking using a crosslinker in presence of a solvent.

Peptide-based hydrogels are known to be highly biocompatible and biodegradable. Fmoc-FF was found to form hydrogels comprising of nanofibril networks in aqueous solutions.[243] Hydrogel formation is not limited to simple block structures. For instance, A. Saiani explored the use of graphene oxide (GO) as nano-filler for the reinforcement of FEFKFEFK, a β-sheet forming self-assembling peptide into hydrogels.[244] In another study, Hiew and his group studied the formation of a hydrogel in water by an eight residue peptide, Ac-GLYGGYGVNH$_2$ without any cross-linking agent or chemical modification.[245] Xu and co-workers reported a new class of hydrogelators, based on the Fmoc-^{D}Ala-^{D}Ala dipeptide which efficiently formed hydrogels that responded to ligand–receptor interaction stimuli. A transition occurred upon the binding of the dipeptide to its ligand, vancomycin.[246] An ultrashort peptide containing α, β-dehydrophenylalanine, LeuΔPhe was developed by V. S. Chauhan and his group which spontaneously formed strong and stable injectable hydrogel under physiological conditions. The gel was capable of entrapping and releasing

mitoxantrone, an anticancer drug that significantly controlled tumor growth.[247] Apart from hydrogels; there are also reports of organogels which are equally important and useful.

Organogels have been used as potential materials to clean oil spillage in the oceans due to their phase selective gelation abilities. Poddar and co-workers studied a series of tripeptide based low molecular weight organogelators in different saturated hydrocarbons, crude oil, and aromatic solvents.[248] Chatterjee and co-workers have studied the organogelation of low molecular weight gelator (LMWG) dipeptides containing para amino benzoic wherein the dipeptides formed phase selective, thermoreversible, rigid gels in a large range of organic solvents and fuels such as petrol, diesel, and kerosene.[249] Banerjee and his co-workers investigated the role of protecting groups in the formation of organogels by keeping the ideal peptide sequence but modifying the terminal ends of the peptide. They used the peptide sequence P–Ala–Val–Ala–Q, where P=Boc/Piv/Cbz/Ac and Q=methyl ester/ethyl ester/ n-propyl ester/isopropyl ester/benzyl ester.[250] In his another work, an N-terminally pyrene-attached tripeptide, namely, Py-Phe-Phe-Ala-OMe was developed which formed stable transparent fluorescent thermoreversible organogels in various organic solvents and showed strong blue-emitting fluorescence. This fluorescent organogel was found to be an excellent host for the incorporation of graphene.[251]

1.5.5. Applications of Peptide Based Self-Assembled Nanomaterials:

Self-assembled peptide nanostructures have been considered as potential biomaterials and are used for biomedical applications such as drug delivery, tissue engineering etc. and also in non-biomedical applications which includes wastewater treatment, nano-electronics, nano-reactors, template for nanofabrication and many more.

1.5.5.1. Biomedical Applications: Nanostructures formed by peptides have been widely utilised in biomedical applications such as delivery platforms, tissue engineering, 3D cell culture, cell adhesion, antimicrobial agents and biosensors which are discussed briefly in the following section.

1.5.5.1.1. Delivery Systems: Peptide self-assembled nano architectures are more suitable as delivery systems due to their intrinsic physical and biological properties compared to other organic materials. They are widely used in the diagnosis and treatment of human diseases. Out of the known peptide nanostructures, hydrogels are widely used in delivering protein/peptide drugs. For drug loading and release, the nanocarriers should encapsulate molecules effectively, protect them from dilution and degradation, and release them in a controlled and sustained manner. Additionally, drug delivery systems need to be non-cytotoxic, capable of site specific in delivery, and should be easily biodegradable.

1.5.5.1.1.1. Drug Delivery: It has been found that, the conventional administration of hydrophobic drugs suffers several disadvantages, including low water solubility, poor oral availability, quick biodegradation, nonspecific delivery, and serious side effects.[252,253] Therefore, drug delivery systems could be used to encapsulate these therapeutic agents to increase drug efficacy.[254] PAs often self-assemble into vesicles or nanotubes which can encapsulate the hydrophobic drug, while the surface can be modified to achieve target specific delivery. For example, Stupp and his co-workers conjugated the anti-inflammatory drug dexamethasone with the PA (C_{16}-$V_2A_2E_2$) *via.* a hydrazine linkage to achieve long-term drug release in both *in vitro* and *in vivo* tests.[255] In another study, Zhang *et.al.* used the Tat CPP as a molecular building unit to construct well defined nanofibers that could encapsulate hydrophobic drug paclitaxel and facilitate its delivery efficiently.[256] KLD based peptide hydrogel[257] with injectable properties could also be used to directly come into contact with the tumor sites to enhance the efficacy and safety of tumor therapy. Peptide self-assembled

microtubes, such as that formed from L-diPhe also could be utilized for cancer therapy through conjugation with doxorubicin in high efficiency.[258] The nanofiber structures which self-assembled from the EAK peptides have been demonstrated to deliver anticancer drug ellipticine through encapsulation method.[259] Dendrimer peptide GFLG self-assembled into compact nanoparticles with negative charges on the surface after conjugation with the PEG and anticancer drug doxorubicin.[260] The nano-carrier was capable of 9.62 wt % of drug loading and release accompanied by enzyme responsive drug delivery applications. This formulation had greater efficacy and lower cytotoxicity compared to the free drug with non-detectable side effects. Peptide based hybrid nanostructures were fabricated from PLA and V_6K_2 peptides. The self-assembled nanoparticles were conjugated with doxorubicin and paclitaxel. These nano-assemblies had higher toxicity towards the cancer cells and were less toxic to the healthy cells compared to the free drugs.[261, 262]

Targeted Drug Delivery: Chemotherapy which is one of the most widely practised form of treatment for cancer has the biggest disadvantage of being non-specific in its action. Apart from affecting the cancerous cells, it also affects other normal healthy cells involved in active division and proliferation. Peptide nanomaterials show important roles by recognizing cancer-specific receptors and delivering anticancer drugs to cancerous cells and tissues. Peptides designed as hydrogels target cancer cell surfaces and the tumor vasculature to minimize the side effects of chemotherapy.[263] Peptide RGD that originates from the cell surface glycoprotein binds to integrins, which are expressed on the cell surface. Hence RGD peptides are tethered to several self-assembling peptides to improve the targeting.[264] Cyclic RGD further improves the binding to the integrins and is used to target drugs to the cancer cells. It has been tethered to the anticancer drugs like doxorubicin. Murphy *et.al.* demonstrated cyclic RGDfK tethered doxorubicin targeting supressed growth of primary tumor and prevented metastasis.[265] Peptide Lyp-1, -CGNKRTRGC- a nine-amino acid cyclic

peptide is known to recognize lymphatic metastatic tumors. Lyp-1 conjugated PEG-PLGA nanoparticles showed 4-8 fold increased cellular uptake both *in vitro* and *in vivo*. The peptide showed good targeting efficacy but exerts cytotoxic activity.[266] Peptide based dual-functional liposomes have been used in the targeted drug delivery in cancer treatment. Hyaluronic acid coated R_6H_4 peptides were screened for pH responsive anticancer drug delivery. This module was demonstrated to have very high *in vitro* and *in vivo* efficacy of tumor targeted drug delivery.[267]

***Stimuli Responsive Drug Delivery*:** Peptide assembled nanostructures, especially hydrogels have acted as an important class of drug delivery vehicle. They can encapsulate the drug whose release can be controlled with the help of various stimuli such as pH, temperature etc.[268] For example, a curcumin containing hydrogelator system was developed from the curcumin-FFE-ss-ERGD monomers. The FFE peptide and the disulphide moiety helped in the self-assembly of the system while ERGD motif guided the assembly to the cancer cells. The self-assembled nanostructures were responsive to pH change that they encountered after endocytosis and then disassembled into monomers.[269] Wu and his co-workers designed a pH and redox dual stimuli-responsive polyAsp derivative as a controlled drug release system. The polyethylene glycol (PEG) chain was grafted onto the polyaspartamide backbone *via.* redox responsive disulfide linkage, providing a shedable shell for the polymeric micelles in a reductive environment. Doxorubicin was encapsulated into the core of micelles. The doxorubicin-loaded polymeric micelles exhibited accelerated drug release behavior in the acidic and reductive environment of glutathione (GSH).[270]

1.5.5.1.1.2. Protein/Gene Delivery: Peptide nanostructures have also been utilised in protein and gene delivery or gene therapy. For example, Zhang *et.al.* conducted pioneering work in this field wherein they used the RADA16-I peptide to self-assemble into a hydrogel which encapsulated four proteins, lysozyme, trypsin inhibitor, bovine serum albumin (BSA), and

immunoglobulin G (IgG). This self-assembled peptide hydrogel scaffold had enhanced effects on sustained-release.[271] Shea *et.al.* observed that the self-assembled cationic peptides modified with lipoplex had enhanced gene delivery efficiency, having higher transfection efficiency, higher internalization, enhanced nuclear accumulation and a lower percentage of lysosomal DNA compared to lipoplexes.[272] Also, Zhang *et.al.* designed and synthesized two types of biocompatible bola-like amphiphilic peptides with dual ligands comprising of a tumor-targeting moiety of RGD sequence and a cell-penetrating moiety of R8 sequence which acted as gene vectors.[273] Targeting peptide GE11 with branched structures has been developed and assembled with other components for gene delivery.[274,275]

1.5.5.1.2. Tissue Engineering: Tissue engineering is an important field of regenerative medicine for tissue repair and has become a hot topic in the recent past. Besides application as delivery systems, the self-assembled peptide-based nanomaterials also have shown to be potent candidates for tissue engineering. Self-assembling peptides like RADA16 I and II have been found to promote extensive neuron outgrowth.[276] The IKVAV pentapeptide combined with Glu and A_4G_3 alkyl residues is another example of self-assembling peptides that promoted neuronal growth.[228] Peptide fragments SKPPGTSS, PFSSTKT, and RGD combined with the RADA16-1 peptide increased the levels of nestin, β-tubulin, and other neuronal markers.[277, 278] The nanofibrous scaffolds of self-assembling peptide SAPNF, have been used to regenerate tissues such as nerve, cartilage and bone.[279] Self-assembled peptides with nanotubular or nanofiber structures could mimic the natural extracellular matrix of many tissues and localize drug release at the desired site making them useful for tissue regeneration.[280] Grodzinsky *et.al*. reported KLD-12 hydrogel as a promising peptide scaffold for cartilage tissue repair.[281]

1.5.5.1.3. 3D Cell Culture: Peptide nanomaterials have also been used in 3D cell culture. The 3D culture could mimic the *in vivo* structure environment and enhance biological activity.[282]

The groups of Ulijn and Gazit, first applied hydrogels of Fmoc-FF in 3D cell culture.[283, 284] Besides the Fmoc, even the Napthalene and the Cbz ((benzyloxy)carbonyl) derivatives of the di-Phe were studied for their cell culture applications. All the di-Phe hydrogels could support proliferation and cell culture of chondrocytes in both 2D and 3D for up to 10 days.[152] Zhang *et.al.* did 3D cell culture with different cells, such as stem cells, neural cells, venous endothelial cells, hepatocytes and chondrocytes. They synthesized hydrogels by the self-assembly of RAD16 peptides and other linear peptides which have been used in 3D cell culture.[285] Multicomponent hydrogels were generated that had improved properties than the single component ones. RADA16 was co-assembled with the RGDA 16 peptide. The mixture scaffold was shown to promote better cell attachment and proliferation of the MC3T3-E1 cells compared to the RADA scaffold.[286] Collier *et.al.* designed multicomponent hydrogels using RGDS-Q11 and IKVAV-Q11, which contained a self-assembling fiber forming part Q11 tethered to a ligand for integrins RGDS or the IKVAV segment. Such a design allowed the ligand to be pointed on the surface of the nanofibers and specifically increased Human Umbilical Vein Endothelial Cells (HUVEC) attachment, spreading and growth over the Q11 peptide.[287] The Q11 derived peptides were very less immunogenic and hence were potential candidates for *in vivo* use.

1.5.5.1.4. Cell Adhesion: For use in biological studies, epitopes that promote cell adhesion are frequently incorporated into peptide amphiphiles. It is known that cells adhere to the Extra Cellular Matrix (ECM) through the formation of a focal adhesion complex between cell membrane integrins and ECM proteins.[288,289] The incorporation of such cell adhesion sequences into assembled networks of peptide amphiphiles allows for both structural and functional mimicry of native ECM. Peptide RGD is one such common ligand present on several ECM proteins,[290, 291] which is sufficient for triggering cell adhesion. Stupp *et.al.* linked cyclic RGD peptide at the side chain of a PA to construct a branched architecture in

the monomer. This gave rise to the cylindrical nanofibers. By controlling the branching of the monomers the density of the RGD epitopes on the nanofibres could be precisely controlled which in turn improved the signalling for cell adhesion, spreading and migration of the 3T3 fibroblast cells in the 2D and the MDA 231 cells in the 3D migration.[292]

1.5.5.1.5. Antimicrobial Agents: Antimicrobial peptides (AMPs) are a class of peptides which have the ability to kill microbes *via.* a rapid membrane disruptive mechanism with very low resistance development against them. Compared to natural AMP sequences, designed AMPs have their sequences optimized, with lesser cytotoxicities, better protease resistance and are easier to synthesize and scale up. Most designed AMPs are cationic and amphiphilic. Self-assembled peptide nanostructures are found to have significant antimicrobial activity in spite of their relatively weak membrane disrupting power in the monomeric form.[293-295] Schnaider *et.al.* showed a higher bactericidal activity of the nanofibers self-assembled from FF dipeptides than the non-assembled GG peptide.[295] In another study, Veiga *et.al.* synthesized Arg rich antibacterial peptide hydrogels with different Arg contents (two, four, six, or eight Arg residues in the sequence).[296] Chu-Kung *et.al.* studied the effect of the length of fatty acids of peptides on their antimicrobial properties where the peptides YGAAKKAAKAAKKAAKAA (AKK) and LKKLLKLLKLLKL (LKK) were conjugated with fatty acids, and the results indicated that the increased length of the fatty tails conjugated to AKK peptides enhanced interactions between the peptides and membranes, which consequently increased their antibacterial activity.[297, 298]

1.5.5.1.6. Biosensors: Wang *et.al.* constructed a thrombin responsive hydrogel by functionalizing the hydrogelator with both the aptamer and its complementary sequence as the physical crosslinking points. Upon exposure to the human thrombin solution, the aptamer binds with the thrombin instead of its complementary sequence, leading to the swelling of the hydrogel due to loss of crosslinking.[299] Park *et.al*. employed a Fmoc -FF hydrogel as a bio

sensing platform by encapsulating enzymes (e.g. Glucose oxidase or horse radish peroxidase) and fluorescent reporters like CdTe or CdSe quantum dots into the hydrogel simply by addition to the peptide. These systems successfully detected analytes (glucose or phenolic compounds) on the basis of photoluminescence quenching of the hybridized quantum dots.[300] Yang *et.al.* demonstrated self-assembling peptide conjugates with the vancomycin (Van), NBD–FFYEGK(Van) and NBD–FFYEEGK(Van) for the detection of bacteria. This antibiotic tethered derivative exhibited more effective antimicrobial activities against *E. faecalis* than the parent Van molecule.[301] Yang *et.al.* synthesized compounds dabcyl-GF_nG_{3-n}DEVDGK- (FITC/rhodamine) (n = 0-3) with and without F- substitution on the 4-position of the benzyl ring of Phe as the self-assembling probes for caspase-3.[302] They demonstrated that one or two units of Phe or 4-fluoro Phe greatly lowered the background fluorescent intensities of the conventional quenched probes with quenchers dabcyl by the synergistic effect of Fluorescence resonance energy transfer (FRET) and aggregation caused quenching (ACQ). These probes could detect caspase 3 in complex environments such as apoptotic cells. Matsui *et.al.* showed several types of architectures of biosensors based on functionalized peptide nanotubes allowing for the detection of viruses and heavy metallic ions and their use as probes for bacteria and other microorganism sensing.[303]

1.5.5.2. Non-Biomedical Applications: Apart from usage in biomedical applications, peptide based nanostructures have also found their utility in applications which are non-biomedical. Few of them are discussed below.

1.5.5.2.1. Wastewater Treatment: The 3D network of the hydrogels is capable of immobilizing several metal ions, organic dyes and other small molecules which are responsible for water pollution. For instance, amino acid and peptide based gels have been gaining popularity in wastewater remediation. Water pollution is an increasing area of concern due to the negative impacts and consequences for human and ecosystem health due

to toxic organic dyes and heavy metals from industrial waste. In response to this issue, supramolecular peptide gels present a fascinating counter measure due to their waste sensitivity, reusability, and proper biodegradability. Literature encompasses a number of reports on waste water remediation by peptide nanostructures, especially peptides hydrogels/organogels. Banerjee and co-workers have reported a tripeptide-based self-shrinking hydrogel capable of removing toxic dyes and heavy metal ions such as Pb^{2+} from wastewater.[304] This tripeptide-based gelator demonstrated self-shrinking properties, allowing for easy removal of water pollutants through instant syneresis. Also in another work, Banerjee *et.al*. studied the formation of the pH responsive transition metal-ion-induced thermoreversible hydrogels using a bolaamphiphile containing Phe residues which was used for adsorbing different types of dyes from water.[305] A low molecular weight peptide-based ambidextrous gelator was designed to produce soft materials (gels) with dual function; removal of toxic organic dyes in waste water treatment and oil spill recovery.[306]

1.5.5.2.2. Chemosensing: The network of supramolecular hydrogels can reversibly entrap a variety of molecules which can develop different readouts like fluorescence enhancement or quenching, FRET, change of colour etc. depending on the nature of the gels. Das and co-workers designed a pyridine containing molecule with a pyrelenediimide (PDI) core which self-assembled in the presence of Pd^{2+} ions. This led to the quenching of the fluorescence and detection of the Pd^{2+} ion. Upon addition of cyanide ions (CN^-) to the self -assembly, the Pd^{2+} are pulled out of the assembly which fell apart and the fluorescence increased again. The detection limit was found to be 0.55 ppb (for Pd^{2+}) and 0.26 ppb (for CN^-).[307] Ko and his group developed a biodegradable colorimetric chemosensor for Cu^{2+} ions detection in aqueous water using a poly(Asp) nanofibrous hydrogel. This hydrogel sensor exhibited high sensitivity and selectivity toward Cu^{2+} ions over other competing ions with a detection limit of 0.01 mg/L.[308]

1.5.5.2.3. Templates for Nanofabrication: Apart from usage in wastewater remediation, peptide nanostructures have been used as template for nanofabrication. Gazit's group demonstrated the use of nanoscale fibers or tubes as templates for the formation of metal nano-wires with an aromatic system. They used the di-Phe tube to template a silver nanowire inside it. The peptide was then removed using proteinase K to give a fine nanowire 20 nm in diameter.[150] Guler and his co-workers have developed an amyloid inspired short peptide sequence (Ac-KFFAAK-Am) which formed 1D nanofibers. This fibrous network was used as template to mineralize SiO_2 and TiO_2. After calcination of the organic part, micron-long nanotubes of SiO_2 and TiO_2 were formed.[309] Other examples of self-assembled peptide templates include I_3K, phage-displayed P7A peptides[310] and aniline–GGAAKLVFF[311] to synthesize Pt nanoparticles for different applications. I_3K assembled nanofibers have been used to template Pt nanoparticles while phage-displayed P_7A peptides were utilized to tune morphologies of Pt nanoparticles. I_3K assembled nanofiber decorated Pt nanostructures were used for electrochemical oxidation of hydrogen and methanol while aniline– GGAAKLVFF supported Pt nanoparticles were used as an electrocatalyst to improve oxygen-reduction reaction.

So far, we have discussed several promising applications of self-assembled peptide nanomaterials in drug/gene delivery, tissue engineering, antibacterial therapy, and biosensor devices, waste water treatment and nanofabrication. Besides all these, there are many more applications found in literature which are derived from peptide architectures. Extensive discussion on all the topics is beyond the scope of our thesis.

1.5.6. Characterisation Techniques Used for Self-Assembled Peptide Nanostructure:

So far we have found that peptides are a very popular class of building blocks and the nanomaterials derived therefrom are endowed with various applications from regenerative medicine to nanofabrication. Characterization of the self-assembled nanoscale architectures

using sophisticated techniques is important to understand the mechanism of self- assembly. This will enable improved design of molecules to control the self-assembly process and achieve custom-made applications. Various experimental techniques that are used for characterization purposes can be broadly classified into spectroscopic, X-ray and powdered crystallographic, microscopic, rheometric and biophysical tools which are discussed below (Figure 1.30). These experimental techniques have been used extensively in all the studies entailed in this thesis.

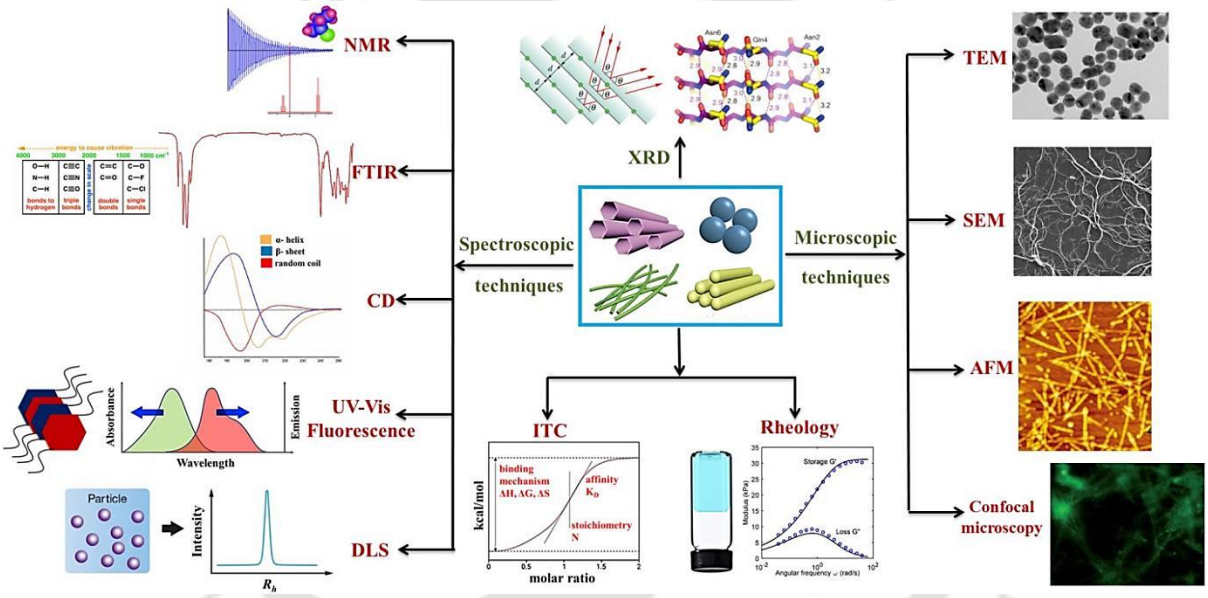

Figure 1.30: Schematic representation of the characterisation techniques used for self-assembled peptide nanostructures.

1.5.6.1. Spectroscopic Analysis: Spectroscopic techniques, in general, employ light to interact with matter and thus probe certain features of a sample to learn about its consistency or structure. In order to have an understanding about the chemical and physical characteristics of nanoscale peptide organizations, such as their bond properties, vibrational modes and covalent and non-covalent interactions, spectroscopic methods are useful. The common spectroscopic techniques such as nuclear magnetic resonance (NMR), Fourier transform

infrared (FTIR) spectroscopy, Raman, CD spectroscopy, Dynamic light scattering (DLS) and UV-Vis/Fluorescence spectroscopy have been widely used for the analysis of different self-assembled peptide nanostructures designed for various applications.

1.5.6.1.1. NMR Spectroscopy: It is a key method for studying the structure and dynamics of peptide-based architectures in both liquid and solid conditions.[312] NMR experiments primarily involves 1D NMR of active nuclei like ^{1}H(Proton), ^{13}C(Carbon) ^{19}F(Fluorine), ^{31}P(Phosphorous) etc. and 2D NMR spectroscopy wherein multipulse sequences are employed to provide additional information not obtainable from 1D spectra. The most useful and commonly used forms of 2D NMR spectroscopy provide correlations between proton and other NMR-active nuclei signals based on some interaction between them. 2D NMR includes COSY (co-relation Spectroscopy), NOESY (nuclear overhauser effect spectroscopy), TOCSY (total correlation spectroscopy) and heteronuclear correlation experiments, such as HSQC, HMQC, and HMBC. Literature encompasses a number of reports on the usage of these NMR spectroscopic experiments in elucidating the self-assembly pattern as well as structural pattern of peptide nanostructures. For example, the self-assembly mechanism of Fmoc-protected peptide networks have been studied by 1D proton and 2D NOESY in liquid and sol–gel transition states, and it was found that hydrophobic and intermolecular interactions were the key forces for nanostructure formation.[313] Diffusion ordered NMR (DOSY) spectroscopy, is used to measure the diffusion coefficient of the species in the solution. As with the progress in the self-assembly, the size of the assemblies increase and diffusion coefficient diminishes, DOSY is a good experimental technique for studying the process.[314] It was used to investigate the transient supramolecular configuration and assembly of the peptide nanostructures due to the biocatalytic activity and hydrolysis of the assemblies in a liquid environment.[315] The molecular conformation of peptide fragment 105–115 of transthyretin, TTR (105–115) in the fibrillar state was probed by 1D and 2D magic-

angle spinning solid-state NMR (MAS ssNMR).[316] ^{13}C and ^{15}N linewidth measurements indicated that the peptide formed highly ordered fibrils in which there was a single unique environment for each residue. The packing of self-assembled palmitoyl PA (GANPNAAG) nanostructures and their supramolecular organization into fibers have been identified by the analysis of the data derived from ssNMR and rotational-echo double resonance (REDOR) NMR analysis measuring the distances between ^{13}C and ^{15}N isotopically labelled PA molecules.[317] Also, the structural model of RADA16-I nanofibers, based on solid state NMR measurements on samples with different schemes for ^{13}C isotopic labelling was identified, where NMR peak positions and line widths indicated that the nanofibers were composed of two stacked β-sheets stabilized by a hydrophobic core formed Ala side chains.[318] In another study, solution-state NMR spectroscopy was employed to measure the surface chemical properties of the fibres in a range of hydrogels formed from N-functionalised dipeptides.[319] The evidence of the presence of β-hairpin conformation within the nanofiber structure of the self-assembled peptide MAX8 was reported from ssNMR spectroscopy.[320] Information about the presence of intermolecular forces driving self-assembly like hydrogen bonding, hydrophobic interactions or aromatic π-π stacking interactions, the critical aggregation concentration (CGC) of the peptides etc. can also be obtained from specialized experiments like solvent titrations,[321] deuterium exchange,[322] temperature dependent NMR ,[323, 324] concentration dependent NMR[325] etc. NOESY NMR gives an idea about the spatial distance in between protons and is an invaluable technique for studying the self-assembly process.[326, 327]

1.5.6.1.2. Infrared (IR) Spectroscopy: IR spectroscopy deals with the electromagnetic spectrum change of peptides due to molecular vibrations and conformational changes within amide A (~3200–3300 cm^{-1}), amide I (~1600–1700 cm^{-1}), amide II (~1480–1580 cm^{-1}) and amide III (~1200–1300 cm^{-1}) bands in the mid-infrared region.[328-330] The shifts in these

bands are analysed to monitor the structural changes as a result of the peptide self-assembly. For example, the structural changes which occur as a result of peptide self-assembly triggered by various factors such as UV radiation, ultrasonication or pH were investigated by the shifts in the amide I band.[331-333] Also, the peaks in the amide I region which correlate to the C=O stretching of the self-assembled peptide nanostructures gives an indication about the presence of parallel or antiparallel β-sheet secondary structure organization of the peptide assemblies.[334, 335] Presence of hydrogen bonding can be established by monitoring the NH stretching bands in the 3200-3600 cm^{-1} range. While the non-hydrogen bonded NH's appear towards the 3400 cm^{-1}, the hydrogen bonded NH stretching shifts more towards lower wavenumber of about 3200 cm^{-1}.[336, 337]

1.5.6.1.3. Raman Spectroscopy: Similar to the vibrational IR techniques, Raman spectroscopy is used to provide a structural fingerprint by which molecules can be identified. In peptide self-assembly, Raman scattering helps in the analysis of the structural properties in the assigned modes of molecular bonds found in the peptide architectures.[338] However, lack of spatial resolution at dilute conditions makes detailed characterization of the peptide nanostructures a strenuous task using conventional Raman spectroscopy. Different approaches have been developed to improve the scattering intensities for the analysis, for example, the relatively low Raman signal of the peptide assemblies was increased *via.* surface-enhanced Raman scattering (SERS) using the localized surface plasmon resonances of the metallic clusters in liquid or solid environments.[339, 340]

1.5.6.1.4. Circular Dichroism (CD) Spectroscopy: It is an absorption spectroscopy which uses circularly polarized light to investigate structural aspects of optically active chiral media. CD spectroscopy functions at the near and far UV regions (180–320 nm) and provides information on the secondary structure of peptide assemblies.[341] Changes in the conformation of the self-assembling peptides which may occur because of pH change,[342] chirality of

supramolecular architectures[343] and interactions in between different molecules or metal ions[344, 345] can be investigated by CD analysis. A shift in the CD spectra gives an insight into the conformational differences, such as twisting or disordering of β-sheets in the assemblies due to the π–π* transitions within the peptide backbone.[342, 346] In addition to secondary structure analysis, π–π interactions between aromatic peptide assemblies can also be monitored by CD.[347, 348]

1.5.6.1.5. Dynamic Light Scattering (DLS): It is a spectroscopic method used to determine the size distribution of particles (polymers, proteins, colloids, etc.) in solution. It relies on fluctuations in the scattered light due to the internal mobility of the structures within 1–1000 nm size range in the solution.[349, 350] DLS helps in gaining information about the peptide assembly mechanisms. Various supramolecular peptide nanostructures and peptide polymer conjugates[351-353] have been analysed *via*. DLS, and the size distribution, hydrodynamic radii,[236, 354] polydispersity index and zeta potential of the assemblies were reported in conjunction with other characterization techniques.

1.5.6.1.6. UV-Visible and Fluorescence Spectroscopy: UV-Vis and fluorescence spectroscopy are inevitable tools for elucidating the aggregation kinetics and self-assembly mechanisms of chromophore conjugated peptides. They measure the changes in the wavelength of light absorbed or emitted, that result from the energy absorptions between electronic levels, which are in turn controlled by the intramolecular/intermolecular interactions. UV-Visible deals with the absorption of light in the region of 100-700 nm while fluorescence spectroscopy deals with the decay of the electronic excited states of the molecule. The shift in the absorption or emission wavelengths, quenching (ACQ), or enhancement of fluorescence (Aggregation induced emission, AIE) signal, appearance of additional peaks in the UV/fluorescence spectra (excimer/exciplex bands) helps in the in-depth understanding of the peptide self-assembly. The time dependent self-assembly

properties of chromophore-conjugated peptides were studied by using fluorescence technique.[355] The contribution of π–π stacking in the self-assembly of aromatic peptides[356, 357] and β-sheet peptide fibrils[358] have been studied by monitoring the fluorescence emission signal. Additionally, the investigation of the self-assembly process of peptides into different nanostructures driven by π-π stacking molecular interactions in the chiral tether constrained cyclic peptides,[359] peptide-tetrathiophene-peptide conjugates[360] and cyclic pentapeptides Ac-$CAAAS_5(X)$-NH_2, , where X = methyl, phenyl, or naphthyl[361] was carried out using UV–Vis spectroscopy and fluorescence spectrophotometry. For being able to use fluorescence spectroscopy in studying the self-assembly processes, either fluorophores are linked to the self-assembling peptide monomers or fluorophore dyes such as congo red, ANS, ThT etc. are added into the peptide solution. Valuable information about the self-assembled system like the packing fashion of the aromatic moieties (J or H aggregates), increasing hydrophobicity due to the progression of self-assembly can be obtained from the UV spectroscopy. It is quite a common practise to incorporate chromophores in the monomeric units as a probe to monitor the self-assembly of the system using the UV-Vis/ fluorescence spectroscopic techniques.

1.5.6.2. Microscopic Techniques: Microscopic characterization at nanoscale is critical to understand the processes directing peptide molecules to self-assemble and identify structure–function relationship of the nanostructures. Fundamental microscopic techniques such as TEM, SEM, AFM, fluorescence microscopy provide a detailed insight into the peptide architectures.

TEM allows imaging of size and morphology of self-assembled peptide nanomaterials with high resolution and magnification at a scale of a few nanometers or even below. TEM not only involves structural characterization but also identification of elemental composition and chemical bonding. It is based on transmission of electrons through the specimen, which should be thin, to get good quality images. A variety of TEM images of the self-assembled

peptide aggregates including nanofibers, nanospheres, nanobundles, nanotubes, helices, etc. have been reported.[362-367]

Unlike TEM, SEM gives information only about surface of the specimen at nanoscale. When specimen is too thick for TEM imaging, using SEM is a more appropriate choice to get high resolution images. Unlike TEM, SEM uses electrons reflected from surface of sample as signals for image generation. The morphologies of different peptide nanostructures using SEM are found in literature.[368-373]

AFM is a highly sophisticated technique, which can not only generate high resolution 3D topography of the surface, but also mechanical properties of peptide nanomaterials. It facilitates *in situ* visualization of the self-assembly process of a variety of peptide building blocks into supramolecular nanostructures with nanoscale resolutions. For instance, by time-lapse AFM, the growth, directionality, and changes in morphology of individual amylin fibrils on mica surface was observed over several hours[374]. Also, AFM imaging has been used to observe the formation of right-twisted helical ribbons and their conversion to micro-crystals in an amyloid derived peptide fragment, ILQINS hexapeptide.[375] Investigation of a dual-mode self-assembling peptide NH_2-VGGAVVAGVFF-$CONH_2$ into nanofilaments was performed using the *in situ* liquid-phase atomic force microscopy.[376]

Apart from the above imaging techniques, direct visualization of peptide self-assembly is also possible using fluorescence imaging techniques like fluorescence microscopy and confocal microscopy[377] either *via*. covalent conjugation of fluorescence probes to the peptides or by using the intrinsic fluorescence properties of the peptide nanostructures without any probe conjugation.[377-379]

1.5.6.3. X-Ray Diffraction (XRD) Techniques: It is a technique which uses the interactions (reflection, diffraction or scattering) of high energy electromagnetic radiations with the self-

assembled peptide nanostructures to provide valuable information for the determination of size, shape and structural orientation. XRD patterns of self-assembled peptide nanostructures were used to determine packing parameters and molecular organization focusing on the non-covalent interactions between the building blocks. A very few studies have succeeded in obtaining single crystal XRD patterns from small amyloid peptide fragments.[380-382] For example, fiber XRD pattern from a peptide YYKLVFFC containing a key aggregation sequence (KLVFF) from the amyloid β-peptide was obtained from a dried stalk of the amyloid peptide.[383] Unlike single-crystal XRD, powder XRD (PXRD) looks at a large sample of polycrystalline material and therefore is considered a bulk characterization technique. The powder pattern is considered a "fingerprint" for a given material; it provides information about the phase (polymorph) and crystallinity of the material. The PXRD pattern provides information associated with the hydrogen bonding, π–π stacking and β-sheet secondary structural organization of the peptide assemblies. For instance, the interplanar spacing (d) of about 4.7 Å is the distance between the peptide chains within a β-sheet, while the d spacing of about 9.0 Å can be characterized as the distance between two stacked β-sheets.[384, 385] Another peak at around d = 3.8 Å signifies the π–π interaction between the aromatic groups of the molecules.[386] In addition to PXRD, another X-ray technique involve small-angle X-ray scattering (SAXS), which is performed using lower angle X-ray scatterings at a range of 1° to 10°.[387,388] SAXS can be a highly complementary tool to microscopy as it allows the investigation of the samples in their wet-state without the need for any sample preparation. SAXS is in particular well suited to the study of the proteins and peptides self-assembly as it allows the investigation of objects and features in the 10 to 500 nm scale.[388]

1.5.6.4. Mechanical Characterization Technique-Rheology: There is also a need to characterize certain peptide nanostructures using nanomechanical characterization techniques. The most important one is rheology which measures the viscoelastic behaviour of

different peptide assemblies especially peptide gels. The mechanical properties of peptide gels can be determined using oscillatory rheology or micro rheology techniques, which highlight the sol–gel transition of the peptide architectures due to the external or internal stimulus.[214, 389-392] Rheometric experiments such as oscillatory time sweep, frequency sweep and strain sweep measurements are carried out using common bench-top rheometers. In a common oscillatory rheological measurement, the storage modulus, G′, and loss modulus, G″, are the most common parameters that are measured for a gel system. G′ (Pa) and G″ (Pa) are usually monitored as a function of time, applied angular frequency, and applied oscillatory strain. In a viscous sol state, G″ is greater than G′. Therefore, for a solid, physical gel the storage modulus is greater than the loss modulus (G′ ≫ G″) and is the key requirement for such systems.[393] Inter-crossing of the G′ and G″ denotes the point of sol-gel conversion.

1.5.6.5. Isothermal Calorimetry (ITC): It is a physical technique used to determine the thermodynamic parameters of interactions in solution. ITC can measure the amount of heat released or absorbed upon molecular interactions, at constant temperature and pressure. The thermodynamics of self-assembly provides an insight towards predicting the type of supramolecular structure that will eventually form through aggregation of molecules which can fundamentally contribute to the rational design of self-assembling peptides, leading to development of structures with specific and desired functions.[394] One of the earliest reports on the application of ITC in the study of peptide/protein self-assembly published by Lakshminarayanan *et.al.* showed that the ITC dilution experiments proved the thermodynamic driving force for micellar self-assembly of an eggshell matrix protein to be entropic in nature.[395] In another study, ITC was used to gain a quantitative understanding of the formation of supramolecular nanoparticles as a result of dendrimer-dye self-assembly.[396]

ITC experiments also indicated an enthalpic advantage for rippled β-sheet co-assembly compared to self-sorted β-sheet assembly of the enantiomeric peptides L- and D-$(FKFE)_2$.[397]

1.5.6.6. Surface Tension Measurements: Surface tension is a solution property and based on the molecular adsorption at the interface, affecting the surface free energy. The adsorption process involves three steps: i) diffusion of the molecules from the bulk to the sub-interface; ii) transfer of the molecules from the sub interface to the interface; iii) rearrangement of the molecules at the interface.[398] Considering diffusion to be the rate limiting step, small molecules are expected to rapidly accumulate at the interface due to their faster diffusion rate than large ones. Thus, in the self-assembling peptide systems, the surface tension may reflect predominantly the properties of peptide monomers and small peptide assemblies, rather than those of the large peptide aggregates.[399] Surface tension measurements can give useful insights on the hydrophobicity of peptide self-assembly in solution. It is expected that increased hydrophobicity would lead to increased surface activity at the air-water interface, resulting in decreased surface tension.[179] This information on hydrophobicity makes it possible to speculate the conformation of the assemblies of peptide. For instance, the surface tension results show that EAK16-IV (AEAEAEAEAKAKAKAK) in pure water has a lower surface tension than EAK16-II (AEAEAKAKAEAEAKAK), indicating that EAK16-IV assemblies are likely more hydrophobic.[179] Also, in another study surface tension measurements for the peptide EAK16-I (AEAKAEAKAEAKAEAK) revealed a critical self-assembly concentration of 0.3 mg peptide/mL water, below which the surface tension decreased rapidly with increasing peptide concentration, and above which the surface tension remained at a constant. There were two structural transitions observed with increasing peptide concentration: the first was from globular nanostructures to fibrils, and the second from the fibrils to relatively thick fibers. The second structural transition occurred at the critical self-assembly concentration as determined by the surface tension measurements.[400]

1.6. Chemosensors

1.6.1. What are Chemosensors?

Sensor is a system that on stimulation by any form of energy undergoes change in its own state and thus one or more of its characteristics.[401] This change is used to analyse the stimulant both qualitatively and quantitatively. Considerable research efforts have been invested in developing efficient sensors for different target analytes. According to the definition proposed by IUPAC "***a chemical sensor is a device that transforms chemical information, ranging from the concentration of a specific sample component to total composition analysis, into an analytically useful signal***".[402] However strictly speaking, a chemosensor is not a sensor, as it is not a device, rather it can be the active part of the device. In simple words, a chemosensor is a molecule that teams up with an analyte to relay a noticeable change in the form of a signal which can either be related to the concentration of the analyte[402] or provide a binary "on" or "off" signal.[403] Design of the chemosensors consist of three components as shown in Figure 1.31; a chemical receptor capable of recognizing the guest of interest usually with high selectivity; a transducer or signalling unit which converts that binding event into a measureable physical change and finally a method of measuring this change and converting it to useful information.

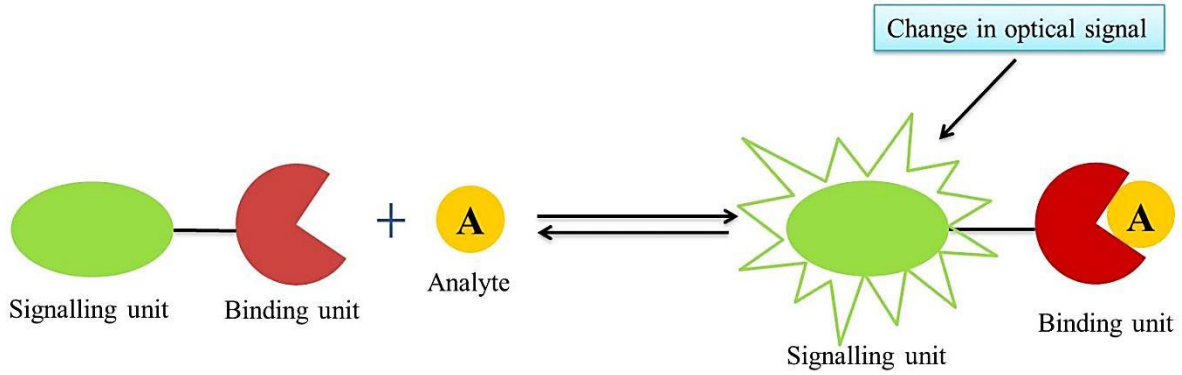

Figure 1.31: Schematic diagram showing binding of an analyte A (guest) by a chemosensor (host), producing a complex with altered optical properties.

1.6.2. Classification of Chemosensors:

Depending on the type of signals produced or the spectral changes created by the binding event, chemosensors may be classified as follows:

1.6.2.1. Electrochemical: These types of sensors can be created by the attachment of redox active group to a receptor and produce signals in the form of changes in the electrochemical properties which can be measured by methods like voltammetry and potentiometry.

1.6.2.2. Electrical: These are based on measurements, where no electrochemical processes take place, but the signal arises from the change of electrical properties caused by the interaction with the analyte.

1.6.2.3. Thermometric: These are based on the measurement of the heat effects of a specific chemical reaction or adsorption which involves the analyte.

1.6.2.4. Optical: In these types of chemosensors, the coordination site binds the guest in such a way that signalling unit brings changes in the optical properties. Depending on the changes in the spectroscopic properties of sensors, upon interaction with analytes, these can be divided into two categories:

1.6.2.4.1. Chromogenic Chemosensors: These are the molecular systems in which physical and chemical properties change when interacting with an analyte, so that a change in colour which might be visible by naked eye, accompanied by a corresponding change in absorbance wavelength (recorded using ultraviolet–visible spectroscopy) or change in chirality (using CD spectroscopy) is produced.

1.6.2.4.2. Fluorogenic Chemosensors: In fluorogenic chemosensors, the interaction between the coordination site and the guest moiety shows the changes in fluorescence behavior of the signalling unit.

A number of analytical techniques are being used to monitor and measure metal ions/anions which include atomic absorption spectroscopy (AAS), atomic emission spectroscopy (AES), inductively coupled plasma mass spectrometry (ICP-MS), electrochemical techniques, anodic stripping voltammetry, colorimetry and spectrophotometric methods like UV-Vis spectrophotometry and fluorimetry. Among these methods naked eye detection (colorimetry), UV-Vis spectrophotometry and fluorimetry are preferable due to their operational simplicity and cost effectiveness in contrast to other methods, all of which involve high cost of analytical instrumentation and are operationally critical. The development of colorimetric sensors is increasingly appreciated since naked eye detection can offer qualitative and quantitative information without resort to any spectroscopic instrumentation. The fluorescence measurement on the other hand is usually very sensitive, versatile and offer sub-micromolar estimation of guest species. A wide variety of optical chemosensors have been reported for the cation, anion and neutral molecules.

1.6.3. Need for Chemosensors:

The development of chemosensors for metal ions and anions has received significant attention in the recent years. Metals are present everywhere around us, in living or non-living species. Chemosensors are of great importance for the detection of chemical species in a variety of fields including physiology, medical diagnostics, catalysis and environmental chemistry. As cations and anions are prevalent in both industry and in farming and as such in the environment, chemosensors are beginning to find extensive applications in these fields. Heavy metals like Hg^{2+} and Pb^{2+} are known to cause severe environmental pollution and is detrimental to health of human beings.[404, 405] A wide variety of symptoms are observed upon exposure including digestive, kidney and especially neurological diseases. Cobalt is an essential element, required for the coenzyme vitamin B_{12} but is also believed to be cardiotoxic and may cause lung damage if present in excessiveness.[406, 407] Likewise, other

metal ions such as magnesium, zinc, iron have an impact industrially, biologically and environmentally.[408-411] Moreover, Arsenic, being a teratogenic and carcinogenic toxic element, causes serious skin problems, neurodegenerative disorders and cardiovascular diseases etc.[412, 413] Similarly in case of anions, few examples may include fluoride, chloride, and cyanide sensing which is now being used for environmental monitoring. Sensing these anions can aid the monitoring of landfills for leaks, tracing the movement of pollutants within a natural water body and detection of salt water intrusion into drinkable ground or surface waters.[414-416]Moreover, the excess of fluoride can lead to fluorosis which is fluoride toxicity and results in increase in bone density which makes its detection really important.[417]

From the above it is clear that proper detection of the ions at trace level is very important as many industrial and agricultural processes can lead to the release of ions to the environment. If left unchecked, these can have devastating effects. Moreover, certain ions, if not detected at proper time can lead to serious health hazards. Therefore, designing new selective ion sensor systems is an important goal for detection of ionic species selectively at lower concentrations.

Limit of Detection: The limit of detection (LOD) is an important figure of merit in analytical chemistry. It is defined as the lowest concentration that can be measured or detected with statistical significance by means of a given analytical procedure. Several ways of determining (estimating) the limit of detection are present: visual estimation, calculation based on the numerical value of the signal/noise ratio, calculation based on determinations for blank samples, graphical method, calculation based on the standard deviation of signals and the slope of the calibration curve. The choice of an appropriate method for LOD determination depends on the method's purpose as well as the requirements of a given analytical procedure.[418]

1.6.4. Examples of Chemosensors:

As discussed in the above section, design and synthesis of chemosensors for using in sensing of metal ions and anions is of significant importance. Literature encompasses a number of chemosensors for detecting metal ions/anions. Some of the representative examples are mentioned in this section. Nam *et.al.* reported a urea derivative of naphthalene which showed colour change with fluoride ion.[419] Sokkalingam and Lee developed another coumarin-based probe to quantitatively determine fluoride ion concentrations in both acetonitrile and water solutions. The sensor operated through "turn-on" chromogenic and fluorogenic dual modes that were triggered by fluoride-promoted cleavage of the Si-O bond.[420] Bozdemir *et.al.* fabricated two BODIPY derivatives containing silyl-protected phenolic groups that served as sensors for fluoride in solution and a poly- (methylmethacrylate) matrix.[421] H. Sayahi *et.al.* reported a ratiometric, colorimetric and ''turn-on'' fluorescent chemosensor based on phenol–bisthiazolopyridine hybrid for cyanide ion.[422] Li *et.al.* reported a azobenzene based ratiometric colorimetric chemosensor which was highly selective for cyanide ion.[423] Jiang *et. al.* reported a novel iminocumarin based turn off chemosensor for acetate ion.[424] Vilar and co-workers synthesised compounds containing thiourea group linked to an azophenyl group to produce a cyanide sensor.[425] Likewise, Saha and Guha have described the fluoride sensing *via.* anion–π interaction and charge/electron transfer by a π-electron deficient naphthalenediimide (NDI).[426] A pyrene based probe was synthesized as a 'turn-on' fluorescent chemosensor for the detection of Fe^{2+} and Fe^{3+} ions in acetonitrile/water solvent mixture.[427] Carbon nanodots based iron sensors were also reported which could detect iron in human serum and living cells.[428] Arene based fluorescent probes could detect iron selectively.[429] A salicylaldehyde appended rhodamine hydrazine derivative has been reported for the selective determination of Cu^{2+} at photophysical condition without interference from other cations.[430] Fluorophore of tetramethyl substituted bis(difluoroboron- 1,2-bis[(1H-

pyrrol-2-yl)methylene] hydrazine has been reported as an ideal turn-on fluorescent sensor for Cd^{2+} ion.[431] Yang *et.al.* prepared benzo[α]-phenoxazinium based chemosensor for selective detection of Zn^{2+}.[432] Likewise, a pyrene based derivative bearing an azadine group was designed and synthesized as ratiometric and turn off-on chemosensor for selective detection of Hg^{2+} in aqueous solution by Zhou *et.al*.[433] Huang and co-workers reported a rhodamine based chemosensor that was capable of sensing Hg^{2+} ions in aqueous buffer solution.[434] In addition to the examples cited here, there are many other well reported chemosensors which are useful in the detection and sensing of a wide variety of metal ions and anions. Reporting them extensively is beyond the scope of the current discussion. Out of the various sensors studied, amino acids and peptides are also known to bind to ions, in some cases very strongly, which makes them as potent candidates as chemosensors.

1.6.5. Peptides as Chemosensors:

The development of peptide based chemosensors for the detection and quantification of metal ions and anions in biological or environmental samples is the subject of considerable research. The majority of this research involves the design, synthesis and testing of amino acids or peptide motifs with a high degree of selectivity for a target ion. Few such examples of peptide based chemosensors are discussed below.

The amino terminal Cu(II)- and Ni(II)-binding (ATCUN) motif which has been studied for more than 35 years is a structural feature which is present in a protein or peptide. It has a (1) a free NH_2-terminus, (2) a histidine residue in the third position, and (3) two intervening peptide nitrogens and is known to bind Cu (II) and Ni (II) specifically.[435] A novel peptide-based fluorescent chemosensor (Dansyl-His-Pro-Gly-His-Trp-Gly-NH_2) containing both Trp and a dansyl fluorophore has been designed to serve as a promising analytical tool for detecting Zn^{2+} in 100% aqueous solution and living cells.[436] Another example includes a new fluorescence chemosensor based only on a tripeptide conjugated with FITC group (FITC-

Ahx-GCA-NH_2), as a promising analytical tool for simultaneous detection of Cu^{2+}, Ag^{+} and S^{2-} in aqueous solutions (Figure 1.32).[437]

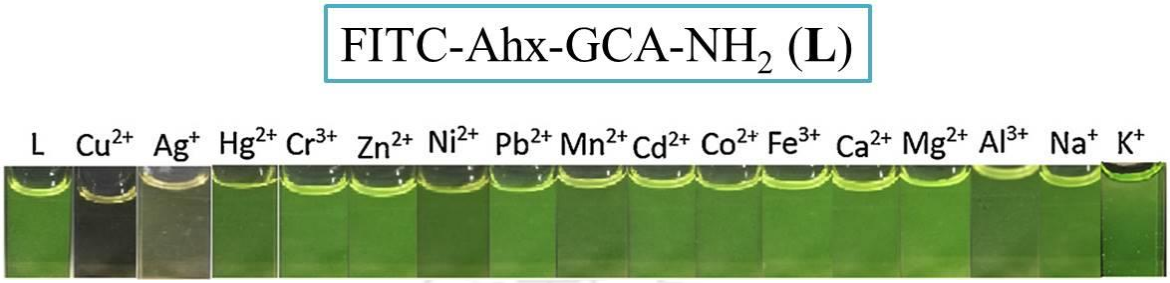

Figure 1.32: Fluorescence emission colour changes of L under UV lamp (365 nm) in the presence of metal ions. The figure has been adapted from reference 437. *Copyright 2018 Elsevier B.V.*

Similarly, another fluorescence chemosensor based on tetra–peptide conjugated with dansyl groups (Dansyl–Ser–Pro–Gly–His–NH_2) was developed as a promising analytical tool for detecting Cu^{2+} and S^{2-} in 100% aqueous solutions, which exhibited excellent cell biotoxicity and intracellular biosensing ability. The chemosensor displayed "on–off–on" response type fluorescence change upon subsequent additions of Cu^{2+} and S^{2-} to the aqueous media and living cells.[438] In another study, a fluorescent peptide sensor based on pentapeptide dansyl-Gly-His-Gly-Gly- Trp-COOH was designed which had selective and sensitive responses to Hg^{2+} and Cu^{2+} (Figure 1.33).[439] The peptide probe differentiated Hg^{2+} and Cu^{2+} ions by a 'turn-on' response to Hg^{2+} and a 'turn-off' response to Cu^{2+}. Another study involved the detection of Cd^{2+} using a fluorescent "turn-on" peptide chemosensor DSC (Dan-Ser-Cys-NH_2) based on photoinduced electron transfer (PET).[440] Another example of Cd^{2+} detection involved the study of fluorescent chemosensor with a Lys backbone and both –NH_2 sites conjugated with cysteine and dansyl group (H_2L).[441]

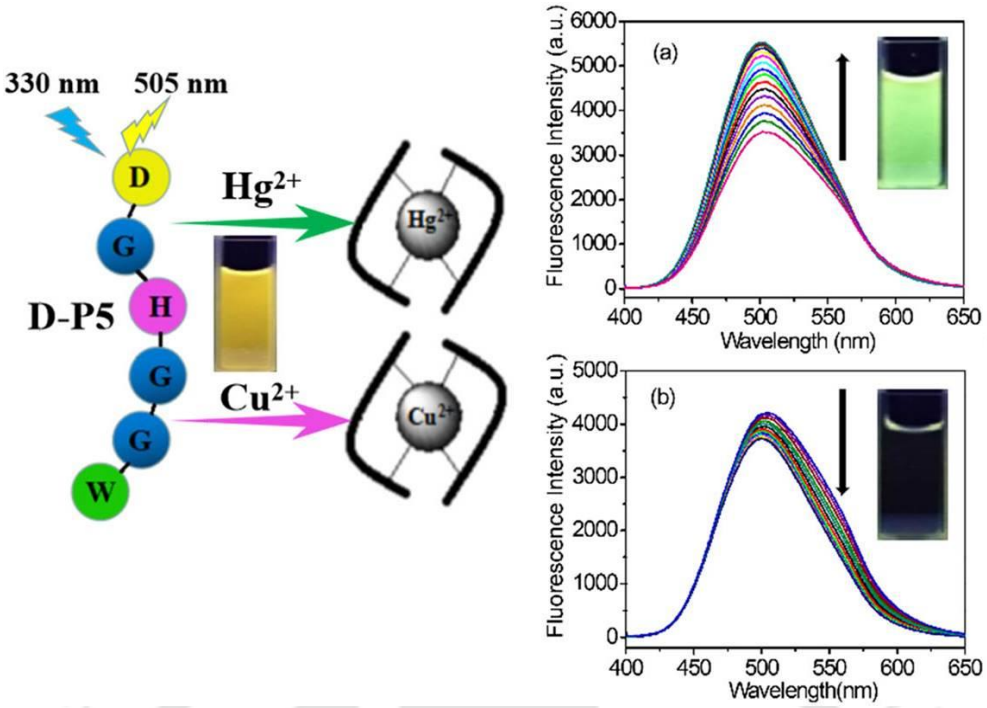

Figure 1.33: Proposed fluorescence detection mode of dansyl- Gly-His-Gly-Gly-Trp-COOH for Cu^{2}, Hg^{2+}. The figure has been adapted with permission from reference 439. *Copyright 2019, John Wiley & Sons, Ltd.*

In an interesting example of a chemosensor based on Trp for monitoring Pb(II) and Hg(II) in aqueous solutions, Trp displayed the unique function as a ligand for the metal ions as well as a quencher of fluorescence upon the metal binding event (Figure 1.34).[442] A colorimetric visualization of arsenic using unmodified gold nanoparticles (AuNPs) and a phytochelatin-like peptide $(\gamma\text{-Glu-Cys})_3$-Gly-Arg (denoted as PC_3R) was developed in which arsenic prevented the peptide from attaching to the surface of AuNPs by coordinating to all the three cysteine residues of PC_3R, thus preventing the PC_3R-triggered AuNPs aggregation and color change.[443]

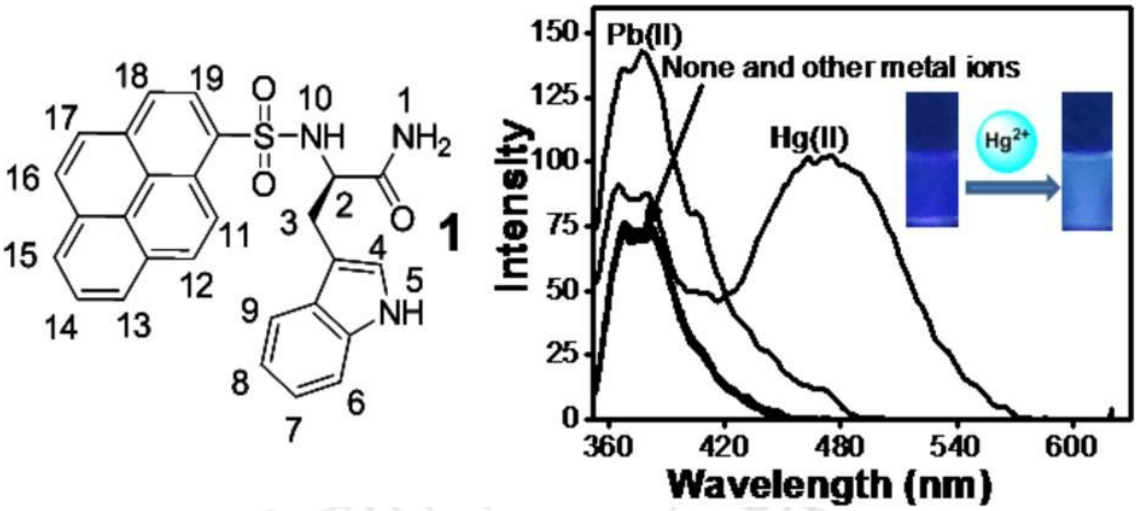

Figure 1.34: Structure and fluorescence emission spectra of a Trp based chemosensor in the presence of metal ions in HEPES buffer solution at pH 7.4 displaying the response towards Hg^{2+}. The figure has been reproduced from reference 442. *Copyright 2013, American Chemical Society.*

Selective anion sensing can often be controlled by a judicious arrangement of recognition moieties around an anion of interest and as such peptides have proven to be highly efficient and selective anion receptors using a small number of amino acid building blocks placed in a precise arrangement. For instance, a cyclic tetrapeptide composed of alternating Gly and 8-amino-4-iso-butoxyquinoline-2-carboxylic acid showed a high binding affinity for fluoride ion.[444] In another study, a coumarine-attached peptoid based fluorescence probe was developed as an efficient CN^- sensor which exhibited significant Turn-ON fluorescence upon the addition of CN^-.[445]

Although amino acids and peptides are known to bind to ions and in some cases very strongly, making them useful as chemical sensors, but there are only a few instances of exploiting this binding in sensing. However, during the last few years, there has been an increase in the design, synthesis, and detection of ions using peptide based sensors. Much of the sensing work is focused on utilising spectroscopic response of the materials towards ions

in solutions. There has been a push to develop and utilise other analytical methods that are simple, fast, and reliable to detect ions in the field, however, optical spectroscopy, out of all, is of particular interest as it provides the basis for sensitive and inexpensive methods of detection.

1.7. Aim of the Thesis

In the present thesis, we have designed small peptide based self-assembling systems. We have explored the mechanism of the assembly process in molecular details and employed the materials developed for various applications, specifically in drug delivery and wastewater remediation. Some of these small peptides also manifest a potential for detection of anions like fluoride and arsenite. This body of work involves several experimental techniques like UV, fluorescence, NMR, PXRD, FTIR, FESEM, FETEM, AFM Rheology, CD etc. and theoretical analysis using DFT studies.

Chapter 1: The present chapter talks about development in the field of peptide self-assembly by summarizing the literature and introduces the pretext of the present work undertaken in the current thesis.

Chapter 2: Dicycloyhexylurea derivatives of amino acids have been designed to form organogels that can efficiently remove organic dyes from wastewater. The organogelator molecules can efficiently and selectively detect fluoride and hydroxide anions.

Chapter 3: Two charge complementary peptide hydrogelators have been prepared and their self-assembly and co-assembly have been studied in details. The self- and co-assembled gels efficiently remove organic dyes, divalent metal ions like Ni^{2+} and Co^{2+} and heavy metals like Pb^{2+} and Hg^{2+} from water. Peptides can act as selective sensors for cation Fe^{3+} and anions like arsenite, arsenate and hydroxide.

Chapter 4: Hydrogel formed by the positively charged peptide from Chapter 3 was exploited to act as a universal drug and protein delivery platform. Antibiotic drug ciprofloxacin (CP), anticancer drug 5 fluorouracil (5-FU) and proteins like BSA and lysozyme were co-assembled/loaded into the hydrogel and released sustainably with the retention of activity in the case of the drugs and the retention of secondary structure in the case of the proteins respectively.

Chapter 5: The self-assembly mechanism of a small tryptophan based tetrapeptide was studied and explained explicitly with the help of fluorescent drug and dye molecules such as curcumin and carboxyfluorescein respectively.

Chapter 6: The concluding remarks and overall summary of the work of the thesis is explained in this chapter along with the discussion of the scope of future studies.

Chapter 2

Dicyclohexylurea Derivatives of Amino Acids as Dye Absorbent Organogels and Anion Sensors

Chapter 2
Dicyclohexylurea Derivatives of Amino Acids as Dye Absorbent Organogels and Anion Sensors

2.1. Peptide Organogels

Organogelators are a family of low molecular weight organic molecules that can form gels in organic solvents at low concentrations. Amino acid or peptide based organogels are versatile in biological and nano-technological applications. These are assemblies of gelators in organic liquids to produce viscoelastic semisolid materials that exhibit no flow property at the steady-state. During the gelation process, small molecular gelators self-assemble into one-dimensional aggregates which further entangle to form three-dimensional networks that entrap and immobilize a large amount of organic solvents. Self-organization of the monomeric species to higher-order structures in a hierarchical fashion gives rise to several nanostructures such as fibrous, tubular, or helical.[446,447] As discussed in the introduction, the process of gelation is driven by several non-covalent intermolecular interactions, commonly electrostatic, van der Waals, π-π stacking, hydrophobic and hydrogen bonding (Figure 2.1). Hydrophilic-lipophilic balance[448-452] plays an important role in the gelation event. Several external factors such as heat, solvent, light and ions[453-456] facilitate gelation and can be used to control the process. Junbai Li and his group reported that the single dipeptide molecule (L-Phe- L-Phe, FF) self-assembled into long nanofibrils in organic solvents, HFIP/chloroform and entangled further to form gels. The obtained FF gels were responsive to temperature. The formation of FF organogels was found to be driven by the hydrogen bond of peptide main chains and the π-π interactions between aromatic residues of the peptide.[456]

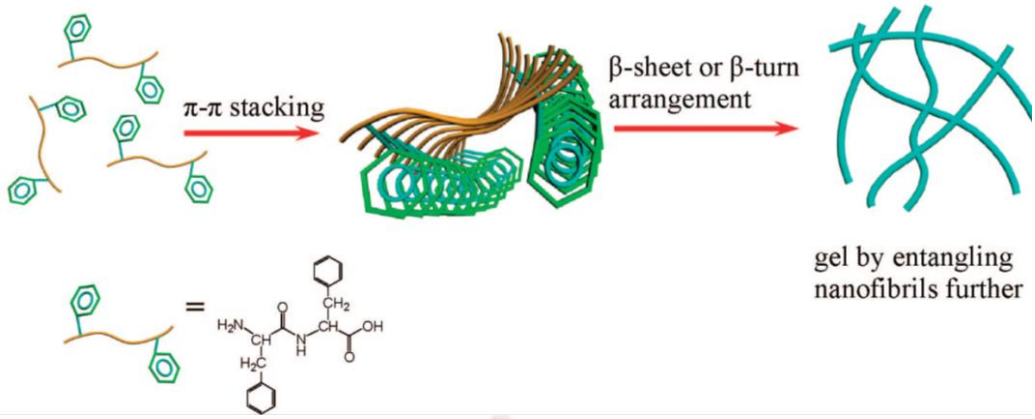

Figure 2.1: Schematic depiction of the proposed self-assembly mechanism of the dipeptide FF where phenyl groups stack through π-π interactions, and the resulting molecular stacks further assemble to form nanofibrils. Such nanofibrils may entangle to form the peptide organogel. The figure has been reproduced with permission from reference 456. *Copyright 2008, American Chemical Society*.

Yan and his group have found that the properties of a trace amount of hydrogen bond forming solvent such as ethanol have an impact on the formation of FF organogels in DCM when the ethanol content was increased to 3% v/v (Figure 2.2).[457]

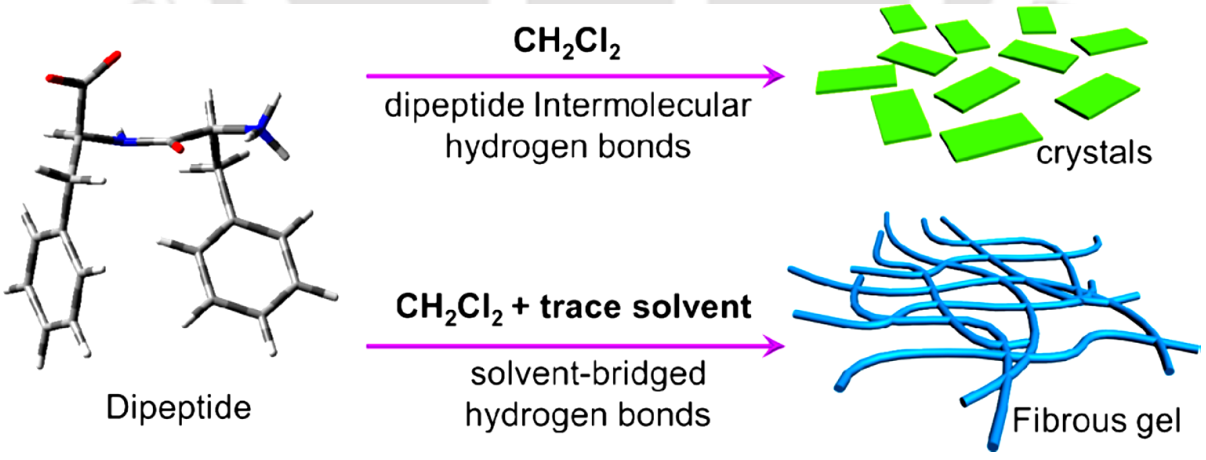

Figure 2.2: Schematic depiction of gelation of FF dipeptide in presence of trace amounts of solvent (ethanol) in DCM. The figure has been reproduced with permission from reference 457. *Copyright © 2016, American Chemical Society*.

In another study Ulijn and Bai *et.al.* developed an *in situ* ultrasonic method to obtain organogels assembled by FF-based tripeptide ^{D}FFD in methanol.[332]

The physical properties of an organogel like the transition temperature (T_{gel}), viscosity, and elasticity change with the change in the nature of the network which is responsible for gel formation. Gels with a long-range and cross-linked aggregation among gelator molecules result in a robust network compared to a short-range and unidirectional packing forming a transient gel.[458, 459] The formation of a gel is treated as a kinetically trapped structure[28] and so, they can be rationally designed and regulated by external stimuli like solvent,[457] pH,[460] temperature[248] etc. Although intense effort has been devoted to establish a structure– property relationship for the development of LMWGs it is still difficult to predict the gelation ability of a compound unambiguously. Thus, a major challenge in this field is the rational design of gelator molecules together with the proper understanding of the gelation mechanism.

2.2. Applications of Peptide Organogels

Different from hydrogels, organogels have 3D networks that are capable of capturing a large amount of organic solvent molecules. Because of the toxicity of organic solvent, organogels are limited in their applications in drug delivery and biological tissue engineering.[461-463] However, despite of this fact, peptide based organogels continue to evoke intense interest because of their wide-ranging applications in other fields such as nanofabrication, templated materials, sensors, phase selective gelation and waste water remediation by dye and metal ion adsorption/absorption.[251,306,464-470] Few examples are discussed here. Peptide based fluorescent organogels have been found as important organic functional materials. For example, the thermo-responsive organogel formed from FF in chloroform (or toluene) was used as candidate to entrap lipophilic nanocrystals, such as quantum dots (QDs). The achieved hybrid gels not only remain the photoluminescence of QDs, but also improve the

stability of the QDs, and protect QDs from oxidation.[456] In another study, an N-terminally pyrene-conjugated oligopeptide, Py-Phe-Phe-Ala-OMe, formed blue-emitting transparent fluorescent organogels in various solvents such as toluene, xylene, and ethanol. The organogel was used as an excellent host to embed graphene nanosheets to form a stable hybrid organogel with thermoreversibility and shear-thinning properties.[251] Apart from being used as templates to prepare nanomaterials *in situ*, organogels can also be used as stabilizing agents to stabilise gold and silver nanoparticles.[464] The treatment of wastewater requires urgent attention in environmental science and in this regard amino acid/peptide based organogels have turned out to be potential materials. Out of all the applications, we are going to emphasize those in which of peptide based organogels were used in waste water treatment.

2.2.1. Wastewater Treatment-Dye Absorption: Water pollution is a matter of grave concern in the modern day society. The treatment of wastewater demands utmost attention to sustain human civilization. Dyes used in textile, paper, leather, cosmetics, pharmaceutical and food industry are major sources of water pollution.[471] Manufacture and use of synthetic dyes have become a huge industry in the recent past.[472] The toxic synthetic dyes upon reaching water bodies have adverse effect on all forms of life and on ecosystem as a whole.[473] The dye effluents have a negative impact on the immune system and reproductive system. Moreover, they exhibit potential geno-toxicity and cardio-toxicity.[474] Dye effluents undergo degradation to form products which are highly toxic and carcinogenic.[475-477] It is of grave environmental concern and treatment of waste water is of primary importance. Conventional methods of treating dye effluents like incineration, biological treatment, and absorption upon solid matrices like activated carbon, chemical precipitation, electrochemical techniques, ion exchange, and others, have their own limitations due to their low sensitivity, incomplete removal, high-energy requirements, and production of toxic sludge.[478] Amino acid/ peptide based organogels offer an appealing alternative for removal of dyes from contaminated water

due to their high water permeability, large surface area for adsorption and simplicity in use along with reusability and proper biodegradability. There are several works on these organogels found in the literature, whereby they are employed in wastewater management. For instance, S. Guchhait and S. Roy studied two peptide based LMWGs, [11-(2-tert-Butoxycarbonylamino-3-methyl-butyrylamino) undecanoylamino]-acetic acid (TBMBUA) and [11-(2-tert Butoxycarbonylamino-3-methyl-pentanoylamino)-undecanoylamino]-acetic acid (TBMPUA) which were able to entrap toxic dyes like rhodamine B (RB), crystal violet (CV) and methylene blue from aqueous dye solution (Figure 2.3).[469] Chen and Yin *et. al.* studied a series of monopyrrolotetrathia-fulvalene (MPTTF) containing tripeptide organogels formed in aromatic solvents, such as toluene and xylene which could adsorb RB and CV dyes from water, indicating a potential application in environmental remediation.[479]

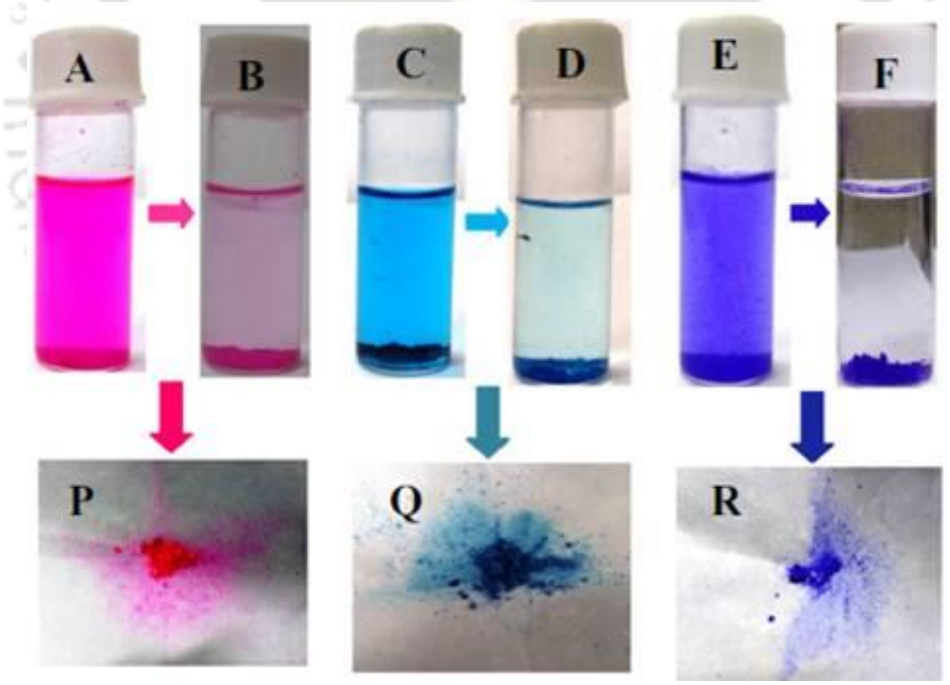

Figure 2.3: Absorption of A, B) RB, C, D) Methylene blue and D,E) CV by the amphiphile TBMPUA. P, Q and R are the Rhodamine B, Methylene blue and Crystal violet dye entrapped amphiphile, respectively. The figure has been adapted with permission from reference 469. *Copyright 2018, Springer Nature*.

2.2.2 Oil Spill Recovery: Oil spills have been regrettably common environmental havoc around the world despite of the technological control and the continuously improved preventive measures. They often originate in oil platforms, refineries, or oil tankers that have an accident or that 'clean' their tanks in the ocean. Different ecosystems such as open and protected sandy beaches, estuaries, and rocky shores are affected to a great extent due to the oil reaching the coast. Also, the spilled oil remains in the water to be finally deposited on the sea bottom in deep or shallow waters creating a serious threat to the marine life and marine ecosystem.[480, 481] Phase-selective organogelators (PSOGs) which are capable of gelling organic solvents in the presence of a second, immiscible liquid phase, which is typically water, can be a useful solution to this.[482-485] The PSOGs can selectively gel the oil layer from the oil-water biphasic mixture, thus controlling the spreading of the oil spill. The gelled oil can then be efficiently separated from the water phase by mechanical methods such as filtration.[482, 486, 487] For example, Das and his group studied dipeptide based organogelators which underwent phase selective gelation in variety of aromatic solvents in presence of water (Figure 2.4a).[468] Additionally, these dipeptides also possessed dye adsorption quality which made them useful in water purification.[468] Another example is of a terminally protected peptide based gelator Boc-cis-ACHC-Aib-Phe-OMe (cis-ACHC=cis-2 aminocyclohexanecarboxylic acid), that can entrap various organic solvents and oils, leading to the formation of self-supporting gels which made it useful for oil-spill recovery (Figure 2.4b).[470] We can find a large number of works done in this field of dye absorption by various groups in the literature. Citing of all the work is beyond the scope in this thesis.

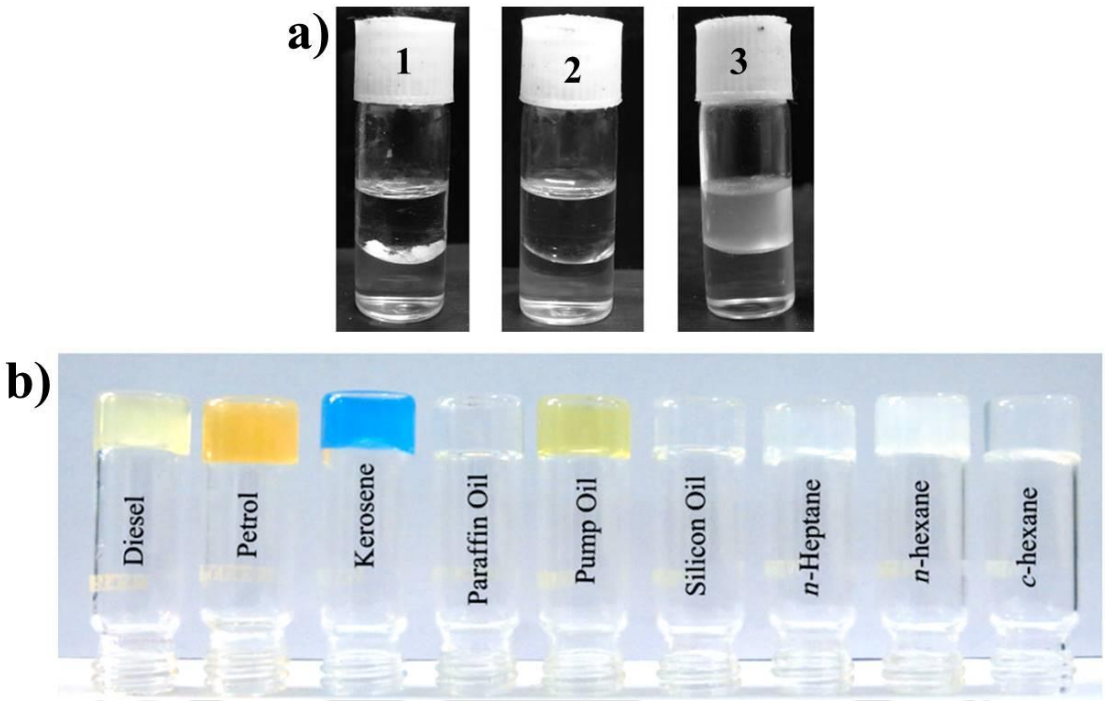

Figure 2.4: a) Phase selective gelation of the gelator $C_{15}H_{31}$-FG-$C_{16}H_{33}$. (1) 10 mg of the gelator in 1 mL toluene and 1 mL water, (2) Gelator was dissolved upon heating. (3) Selective gelation of toluene layer by gelator at RT. The figure has been adapted with permission from reference 468. *Copyright 2008 WILEY-VCH Verlag GmbH & Co. KGaA, Weinheim*. b) Photographs of gels of peptide Boc-cis-ACHC-Aib-Phe-OMe in various oils and organic solvents. The figure has been reproduced with permission from reference 470. *Copyright 2014 WILEY-VCH Verlag GmbH & Co. KGaA, Weinheim*.

2.3. Anion Sensing: Fluoride Detection

Anions play a vital role in a broad range of environmental, technological, and physiological processes, making their detection and quantification valuable. Because of their biological, technological, and environmental relevance, an ability to selectively detect anions is of paramount interest for many applications. While cation recognition and sensing has been relatively well established for some decades[488, 489], anion binding and sensing remains notably more challenging, mainly due to the more complex geometries of anions, pH dependence,

and their inherently strong hydration.[490-492] Among these anions, fluoride, having the smallest ionic radius, highest charge density, and a hard Lewis basic nature, has evolved as an attractive target for sensor designs owing to its association with a diverse array of biological, medical, and technological processes. This makes the sensing and recognition of fluoride ion a highly popular topic of interest. Fluoride is extremely important for dental care and osteoporosis, while chronic exposure to high levels of fluoride anion can lead to dental or skeletal fluorosis.[493] This anion is present in several chemical weapons like sarin, soman and chemical warfare agent.[494, 495] This makes anion detection, and hence design, synthesis and development of new sensors of immense importance.[496-498] Of the various responses generated upon ion sensing, optical sensors where the interaction with an anion leads to a change in the absorbance (color) or fluorescence properties of the receptor are the most popular being highly sensitive.[499] Urea moiety is a well-known anion binder.[500] There are several experimental[501-503] and computational[504, 505] studies on urea based fluoride sensors. For instance, a unique supramolecular sensing system for fluoride ion was constructed from new bispyrenyl thioureas formed by poly(ethylene glycol) (PEG) chains linked to methoxy benzene pyrene thiourea which had a detection limit as low as 46.2 μg/L towards F^-.[506] Another example consisted of a thiacalix[4]arene-based fluorescence sensor bearing two naphthylthiourea groups.[507] In this probe, intermolecular binding interactions between F^- ions and the NH protons of thiourea moieties trigger intramolecular π-π interactions of naphthyl groups, which led to excimer formation and emission. This sensor displayed a high selectivity for F^- with a detection limit of 2.6 × 10−7 M. Development of anion, especially fluoride responsive low molecular weight organogels have also picked up momentum in the recent years. In such systems detection of anion is accompanied by dramatic fluorescence changes and sol-gel phase transitions.[508, 509]

2.4. Present Study

Although, there have been several reports on gelation of small peptides and single amino acid derivatives,[510, 511] there are no reports of dicyclohexylurea (DCU) derivatives of single amino acids forming organogels. In this work, we have designed three single amino acid derivatives of DCU namely, Fmoc-Phe-DCU (M1), Fmoc-Phg-DCU (M2) and Fmoc-Gaba-DCU (M3) and for the first time reported their organogelation. We have also tried to understand their mechanism of self-assembly and looked at their potential applications. These molecules act as phase selective thermoreversible organogelators which can be used as dye absorbents. Additionally, molecules M1-M3 can act as sensors of selective anions like fluoride, acetate and hydroxide (Figure 2.5). Anion sensing abilities of the molecules have been studied using spectroscopic techniques like UV absorption, fluorescence and NMR on one hand and DFT studies on the other. Such simple, economically viable yet multifunctional small molecules are of immense relevance in the recent times.

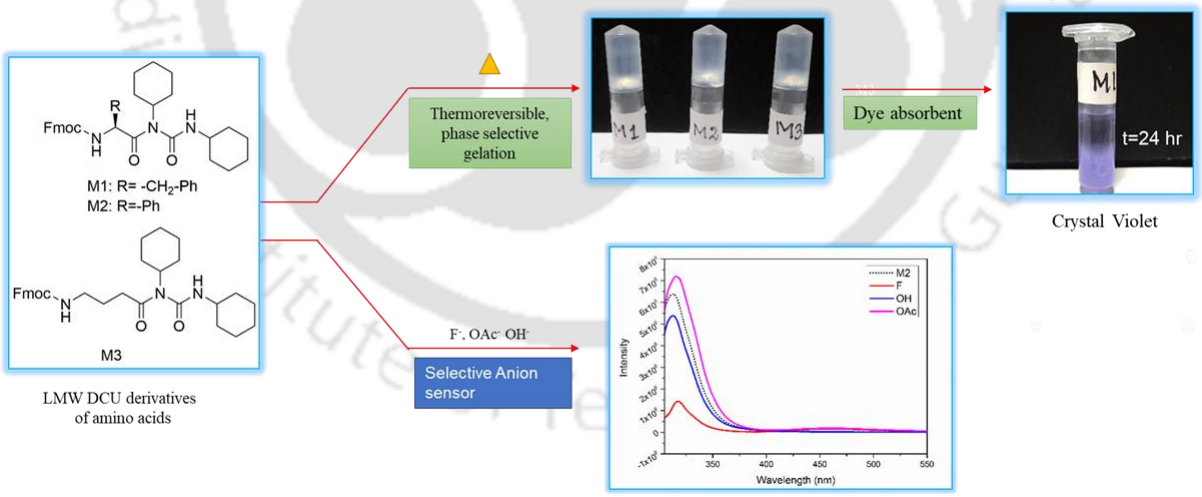

Figure 2.5: Schematic illustration of the work done in this chapter.

2.5. Experimental Details

2.5.1. General Procedure for Synthesis of the DCU Derivatives:

Amino acid based DCU derivatives were synthesized by solution phase methodology. The N-termini of the amino acids were protected by Fmoc group using Fmoc-OSu while the C-termini were protected by N,N′-dicyclohexylcarbodiimide (DCC). All the compounds were purified using column chromatography using silica gel (100-200 mesh size) as stationary phase and hexane and ethyl acetate as eluent. Finally, compounds were characterized by analytical HPLC, ^{1}H NMR (400MHz), and mass spectrometry.

2.5.1.1. Synthesis of Fmoc-Protected Amino Acids: The amino acid (5mmol, 1eq) (L-Phe, L-Phg and GABA) was dissolved in water and sodium bicarbonate (10 mmol, 2 eq) was added with stirring. The resulting solution was cooled to 5°C and Fmoc-OSu (7.5 mmol, 1.5 eq) was added slowly as a solution in 1, 4-dioxane (also cooled). The resulting mixture was stirred at 0 °C for 1 h and allowed to warm to RT overnight. Dioxane was evaporated and water was added to the residue. The aqueous layer was extracted three times with ethyl acetate. The aqueous layer was then acidified to pH 1 with 10% HCl and extracted three times with ethyl acetate. The combined organic layers were dried over sodium sulphate and concentrated *in vacuo* to obtain the product (Fmoc-AA-OH) which was then purified by column chromatography using hexane and ethyl acetate as the eluent.

Yield: Fmoc γ-Abu-OH, 4.32 mmol, 86.4%; Fmoc- Phe-OH, 3.98 mmol, 79.6% and Fmoc-Phg-OH, 4.10 mmol, 82%.

2.5.1.2. Synthesis of Fmoc-AA-Dicyclohexylurea Carbamate: To a solution of Fmoc-AA-OH, (1 eq) in dichloromethane (DCM, 15 mL), DCC (2 eq.) was added and the mixture was stirred for 48 h at RT. 50 mL of ethyl acetate was added to the reaction mixture and DCU was filtered off. The organic layer was washed three times with 1 M sodium carbonate (50 mL)

and two times with brine (50 mL), dried over anhydrous sodium sulfate and evaporated *in vacuo* followed by purification using column chromatography to obtain a solid product.

2.5.1.3. Synthesis of Boc-4-Aminobutyric Acid Dicyclohexylurea (M4): M4 was synthesised according to the protocol mentioned in reference 513.

Yield: M1: 2.10 mmol, 52.7 %; M2, 2.97 mmol, 72.5% and M3: 2.75 mmol, 63.6%.

M1-M4 were characterized using analytical HPLC (Appendix A, Figure A1a-d, Page I), ESI-MS (Appendix A, Figure A2a-d, Page I, II), and ^{1}H NMR (Appendix A, Figure A3 a,b, A4 a,b, Page II, III).

^{1}H NMR: M1 (Figure A3a): ^{1}H NMR (400 MHz, $CDCl_3$) δ 7.76 (d, **2H**, aromatic ring Hs), 7.54 (dt, **2H**, aromatic ring Hs), 7.43 – 7.27 (m, **7H**, aromatic ring Hs), 7.22 – 7.18 (m, **2H**, aromatic ring Hs), 5.37 (d,**1H**, NH-CH), 4.73 (m, **1H**, NH-CH, cyclohexyl), 4.31 (d, **2H**, -CH_2-CH- of Fmoc-), 4.21 – 4.05 (m, **2H**, -CH_2-CH- of Fmoc and –CH-, αH of Phe),), 3.71 – 3.59 (m, **1H**, cyclohexyl CH-NH), 3.02 (ddd, **2H**, CH_2, β H of Phe), 1.93-1.05 (m, **21**H, cyclohexyl Hs).

M2 (Figure A3b): ^{1}H NMR (400 MHz, $CDCl_3$) δ 7.76 (d, **2H**, aromatic ring Hs), 7.61 – 7.55 (m, **2H**, aromatic ring Hs), 7.39 (dt, **7H**, aromatic ring Hs), 7.30 (ttd, **2H**, aromatic ring Hs), 5.94 – 5.87 (m, **1H**, NH-CH), 5.66 (d, **1H**, NH-CH, cyclohexyl), 4.44 – 4.30 (m, **2H**, -CH_2-CH- of Fmoc-), 4.21 (t, **1H**, -CH_2-CH- of Fmoc), 4.04 (d, *J* = 14.3 Hz, **1H**, -CH-NH, αH of Phg), 3.67 (dtd, **1H**, cyclohexyl CH-NH), 2.00-1.04 (m, **21**H, cyclohexyl Hs).

M3 (Figure A4a): ^{1}H NMR (600 MHz, $CDCl_3$) δ 7.77 (d, **2H**, aromatic ring Hs of Fmoc-), 7.59 (d, **2H**, aromatic ring Hs of Fmoc-), 7.40 (t, **2H**, aromatic ring Hs of Fmoc-), 7.32 (td, **2H**, aromatic ring Hs of Fmoc-), 5.16 (s, **1H**, NH-CH_2), 4.33 (d, **2H**, -CH_2-CH- of Fmoc-), 4.20 (t, **1H**, -CH_2-CH- of Fmoc), 3.96 (s, **1H**, NH-CH, cyclohexyl), 3.72 – 3.63 (m, **1H**, cyclohexyl CH-NH), 3.28 (m, **2H**, -CH_2-CH_2-CH_2-CO), 3.15 (m, **2H**, -CH_2-CH_2-CO), 2.48 (t, **2H**, -CH_2-CH_2-CO), 1.96-1.05 (m, **21**H, cyclohexyl Hs);

M4 (Figure A4b): ^{1}H NMR (400 MHz, $CDCl_3$) δ 1.42 {s, **9H**, -$(CH_3)_2$ of Boc group}, 4.77 (s, **1H**, NH-CH), 4.15 (s, **1H**, NH-CH, cyclohexyl), 3.93 (m, **2H**, -CH_2-CH_2-CH_2-CO), 3.71 – 3.61 (m, **1H**, cyclohexyl CH-NH), 3.15 (m, **2H**, -CH_2-CH_2-CO), 2.44 (t, **2H**, -CH_2-CH_2-CO), 2.00 – 1.04 (m, **21**H, cyclohexyl Hs).

2.5.2. Gelation Experiment:

To check the ability of the gelator molecules to form gel in different solvents, weighed amounts of the synthesized compounds (M1-M3) were taken in vials and 500 µL of different solvents were added to them. Samples were heated in a heating block at temperatures ranging from 60- 100 ℃ and subsequently cooled to RT. Gel was formed within 15 minutes which was stable to inversion of the glass vials.

2.5.3. Determination of the Gel-to-Sol Transition Temperature:

The gel-to-sol transition temperature (T_{gel}) was determined by placing the gel containing vial in an oil bath and slowly raising the temperature of the bath at the rate of 1°C per minute. The temperature was monitored using a thermometer. The T_{gel} was defined as the temperature at which the gel melted and started to flow.

2.5.4. Rheology:

The viscoelastic properties of organogels were determined by rheology at 25 °C at a concentration of 2.0 w/v% in 1, 2 DCB. A strain sweep test was performed over a range from 0.1-10% strain at a fixed oscillatory frequency of 1 rad/s. Furthermore the mechanical strength of the organogels was determined from the oscillatory test, i.e. frequency sweep, which was carried out under an appropriate strain of 0.1% with the frequency ranging from 1-100 rad/s. Rheological experiments measure two parameters; storage modulus (G′) and loss modulus. A defining measure of gelation process is having a higher value of G′ than G″which are essentially independent of frequency.

2.5.5. FESEM:

FESEM images of the synthesised molecules M1-M3 were obtained by casting a drop of the solution of the gelator molecules in 1, 2-DCB on a silicon wafer which was allowed to dry for a few hours under vacuum before imaging. For the morphology of the organogel, it was casted on the silicon wafer and allowed to dry under vacuum before imaging.

2.5.6. Fluorescence Spectroscopy:

To gain an insight into the self-assembly behaviour of M1-M3, fluorescence experiments were performed by monitoring the fluorescence of the Fmoc moiety. Samples of different concentrations were prepared in 1,2-DCB and their fluorescence emission was monitored keeping the fluorescence excitation wavelength fixed at 301 nm.

2.5.7. FT-IR Spectroscopy:

FT-IR spectroscopy measurements were recorded using KBr pellets. Measurements were performed on powdered samples and on the xerogel obtained for M1-M3 and the two were compared with each other.

2.5.8. NMR Experiments:

^{1}H NMR experiments were performed for routine characterization of the molecule. Concentration dependent ^{1}H NMR (0.25 mM, 0.5 mM, 1 mM, 2 mM, 3.44 mM (MGC) and 5 mM) was recorded for the molecule M2 in $CDCl_3$ at ambient temperature. DMSO titration was performed at 5 mM concentration of M2 and 0.5% to 15% DMSO concentrations in $CDCl_3$ at ambient temperature. ^{1}H NMR experiments were conducted at different concentrations of fluoride ions to understand the mode of interaction between the molecules and fluoride ions for its anion sensing functions.

2.5.9. PXRD:

Wide angle X-ray diffraction analysis was done for both the powdered samples and the xerogels obtained from drying the organogels of M1-M3 obtained from 1, 2 DCB.

2.5.10. Dye Absorption Studies:

First, 2 mg of the gelator molecule was dissolved in 500 µL of 1, 2 DCB. Into it 500 µL of the aqueous solution of dye (CV, RB, Neutral Red (NR)) was added and the mixture was heated at around 100 ^{0}C for 10 minutes. Upon cooling the mixture, the bottom layer i.e. the organic solvent 1, 2-DCB with the gelator formed the gel while the aqueous phase formed a supernatant over the gel. This was allowed to stand for 24 h at RT, after which the amount of unabsorbed dye was checked by monitoring the UV of the supernatant aqueous solution and calculating the concentration from a standard calibration curve of the dye (Appendix A, Figure A10a-c, Page VI). The amount of dye loaded in the gel and the dye loading efficiency were then calculated as follows:

Dye loaded = (Initial dye-Unabsorbed dye)

Loading efficiency: Dye loaded/Initial dye X 100

2.5.11. Recycling of the Gel in Dye Absorption/Release:

M1 organogel was used for showing the recycleable nature of the organogels. CV dye was first loaded onto M1 organogel and the loading in each cycle was calculated as described above. To the dye loaded gel, 500 µL of diethyl ether was added as the release medium. Diethyl ether layer was then taken out after 1 h and kept in a vial (V1), 500 µL of fresh di ethyl ether was added to the gel for release which was subsequently taken out after 3 h (V2). This was repeated for another three times at time gaps of 6, 10 and 16 h (V3, V4 and V5 respectively). Each time the diethyl ether where the dye was released was taken out and kept in vials (V1-V5) for evaporation. After complete evaporation of ether, 500 µL of water was added to V1 and its absorbance was monitored. Then the contents of V1 were added to V2 for

monitoring the UV. In this way the contents of each vial was added to the next one for UV monitoring at time intervals of 1, 3, 6, 10 and 16 h. From the UV data, amount of dye released at these different time points could be easily calculated using a standard curve for the dye. Percentage of the amount of dye released in cycle 1 was calculated with respect to the dye loaded.

Dye release efficiency was calculated as follows:

Release Efficiency: Dye released in a cycle/ Dye loaded in the cycle X 100

For the second cycle, 500 µL, 40 µM dye solution was added to the gel again for dye loading studies. The rest of the experiment was done as already described above. Amount of dye loaded and released in each cycle was calculated. The gel could be reused effectively for three cycles after which the quality of the gel degraded.

2.5.12. Anion Sensing:

1 mM stock solutions of the gelator molecules in acetonitrile were prepared. Stock solutions of 10 mM tetrabutylammonium salts of F^-, Cl^-, Br^-, I^-, $H_2PO_4^-$, OH^-, AcO^- and HSO_4^- were prepared in acetonitrile. Then, 0.2 mM solutions of the gelator molecules were prepared from the stock solutions by dilution. Also, 0.2 mM solutions of all the anions were prepared from the 10 mM stock solution. For monitoring UV and fluorescence spectra 500 µL of 0.2 mM of the gelator solution was taken and 500 µL of 0.2 mM anion solution was added into it so that the final concentration of the gelator and the anion solution became 0.1 mM. The UV and fluorescence was monitored for all the anions with the three gelators. Anion sensing was studied with Fmoc-Phe-OH as control. For the control experiment, 500 µL of 0.2 mM of the solution of Fmoc-Phe-OH was taken and into it 500 µL of 0.2 mM anion solution was added so that the final concentration of the molecule and the anion in solution became 0.1mM.

2.5.13. Titration of the Gelator Molecules with Specific Anions:

500 µL of 0.2 mM of gelator solution was taken in different 1 mL volumetric flasks and into them 500 µL of different concentration of the anion solutions were added so that the final concentration of the gelator solution became 0.1 mM. The fluorescence of these solutions was then monitored as described above. The fluorescence emission was monitored for excitation wavelength of 301 nm.

2.5.14. Computational Details:

DFT/TDDFT calculations were performed by the Gaussian 09 program package[514] using **6-31+G*** basis set. Geometry optimizations of DCU derivative (M2) in its free and anion bound state were performed without symmetry constraints. Normal mode analysis was performed for ensuring true local minimum geometry. Polarizable continuum model (PCM)[515] with acetonitrile as solvent was used to include the solvent effects in all the calculations. A dielectric constant (ε) of 36.64 (acetonitrile) was used for including solvent effect. Gas-phase optimized geometries were subjected to further optimization in acetonitrile solvent. Based on optimized geometries of the ground states, the absorption spectra of free M2, and its complexes M2:X^- (X=F, Cl, Br, I, AcO, OH) were calculated by the TDDFT methods, at the same level of theory. Several possible geometries of free M2 and anion bound M2:X^- were studied.

2.6. Results and Discussions

2.6.1. Gelation Studies:

The gelation ability of the three amino acid based molecules was studied in a variety of aromatic and aliphatic solvents by ‘stable to inversion of vial’ test upon heating and subsequent cooling. Figure 2.6 shows the chemical structure of the synthesised molecules and the organogels formed from M1, M2 and M3 in 1, 2 DCB.

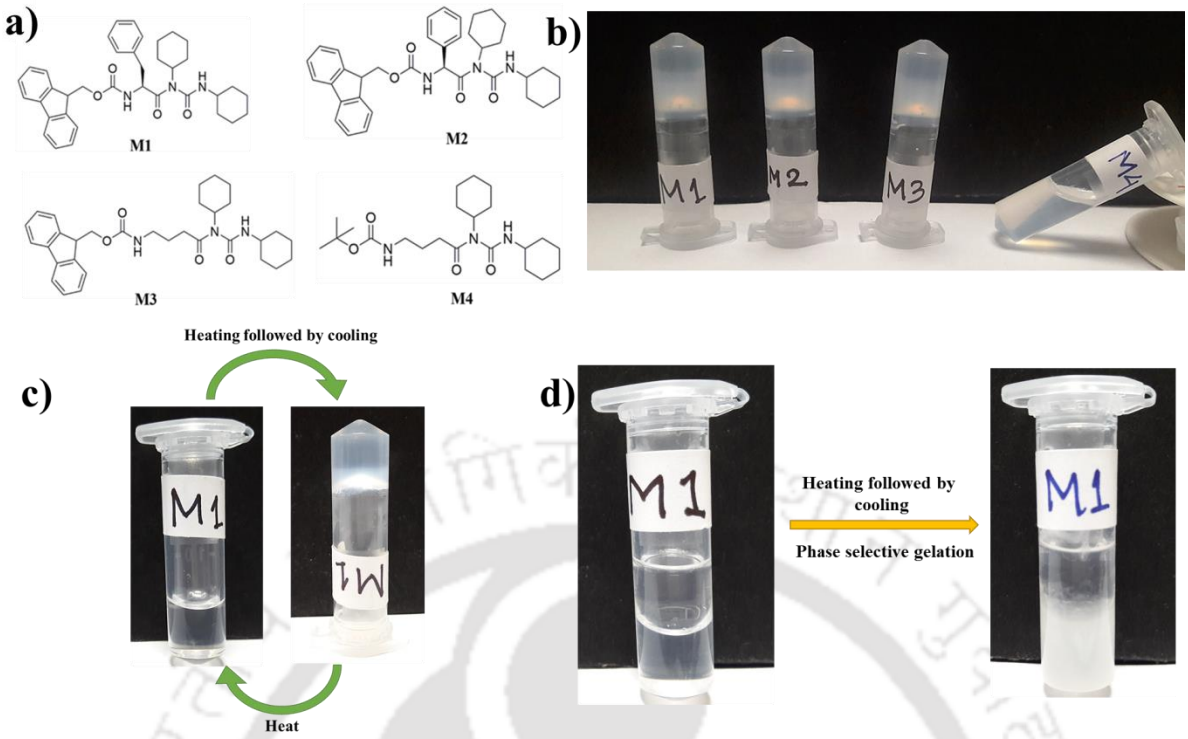

Figure 2.6: a) Chemical structures of M1-M4. b) Gels formed from M1-M3 in 1, 2 DCB. M4 does not form gel. c) Thermo-reversibility of the organogels. d) Phase selective gelation behaviour of the organogels.

We have observed that, aromatic amino acid Phe derivative Fmoc-Phe-DCU (M1), formed gel in various organic solvents like benzene, chlorobenzene, 1,2 DCB, THF, toluene, chloroform, DCM and 3-xylene upon being heated and subsequently cooled. M1 does not form any gel in aliphatic organic solvents. This is a subtle hint that the gelation process may be facilitated by aromatic interactions. M1 contains aromatic side chains of the amino acid residue Phe and an aromatic N terminal protecting group Fmoc. To investigate which if any of these groups were involved in gelation, we replaced the Phe residue with two other amino acid residues, a) aromatic Phenylglycine (Phg) to form Fmoc-Phg-DCU (M2) and b) non aromatic γ-aminoisobutyric acid (Gaba) to generate Fmoc-Gaba-DCU (M3). Both M2 and M3 formed gels like M1 and their gelation properties were same as that of M1 (Table 2.1, Figure 2.6b). This observation indicates that the aromatic side chain of the amino acid residue

may not be a necessary factor in the gelation process. The aromatic moiety Fmoc most probably plays an important role in the gelation process. To investigate the role of Fmoc group in the gelation process we have synthesised and studied the control molecule Boc-Gaba-DCU (M4). This molecule did not form gel under the experimental conditions (Figure 2.6b) suggesting that the π-π stacking of the Fmoc moieties is one of the main drivers for the gelation process. Minimum gelation concentration (MGC) of most gels for the three gelators in different solvents lies within 0.2 to 0.45 (w/v %) (Table 2.1). All the molecules M1-M3 have a very low MGC in 1, 2 DCB. Thus most of the experiments to study the morphology of the organogels have been done in 1, 2 DCB. The thermal stability of the gel has been studied in different organic solvents by monitoring the gel melting temperature (T_{gel}) at the MGC. The T_{gel} values of the gels formed from various solvents have been found to be ranging from 32° to 96° C (Table 2.1). The gels formed by M1-M3 are of thermo reversible nature, *i.e*. the gels are reversibly converted into sols upon heating. On cooling the sols, gels are formed once again (Figure 2.6c). M1–M3 act as phase selective gelators which can selectively gel the organic part from a mixture of water-organic solvent as shown in the Figure 2.6d.

2.6.2. Morphological Studies:

Morphological features of the gel formed by M1-M3 in 1, 2 DCB at MGC have been studied by FESEM (Figure 2.7 a-c). M1 forms aggregated morphology which is distinctly different from M2 and M3. M2 adopts a fibre-like morphology while M3 forms nano-tape like morphology. The morphology of M1-M3 in solution at 10 mM concentration in 1,2 DCB is distinctly different from that in the gel state as shown in Figure 2.8.

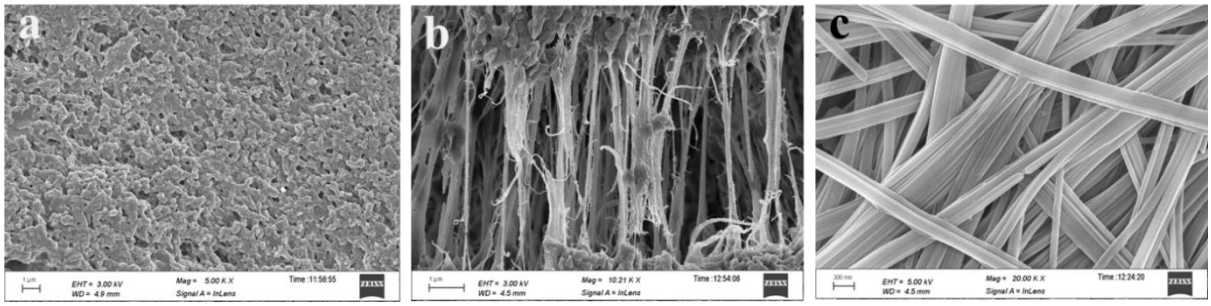

Figure 2.7: a-c) FESEM images of the organogels formed from M1-M3 in 1, 2 DCB at their MGC (~0.21 % wt/v)

Table 2.1: Table showing the gelation properties, physical state, MGC and sol-gel conversion temperature (T_{gel}) of M1-M3 in various solvents. (TNS: Translucent, OG: Opaque Gel, P: Precipitate, S: Solution)

Solvents	M1 State/MGC(%w/v)/T_{gel}(°C)	M2 State/MGC(%w/v)/T_{gel}(°C)	M3 State/MGC(%w/v)/T_{gel}(°C)
Chloroform	OG/0.30/72	OG/0.30/70	OG/0.20/76
1,2 DCB	TNS/0.21/88	TNS/0.20/86	TNS/0.21/92
Toluene	OG/0.25/102	OG/0.25/96	OG/0.25/96
Benzene	OG/0.30/76	OG/0.30/72	OG/0.32/78
DCM	OG/0.42/30	OG/0.42/32	OG/0.40/32
THF	OG/0.35/62	OG/0.35/64	OG/0.35/68
3-xylene	TNS/0.45/86	TNS/0.45/86	TNS/0.45/90
Chlorobenzene	TNS/0.35/84	TNS/0.35/88	TNS/0.35/90
Hexane	P	P	P
Cyclohexane	P	P	P
Acetonitrile	S	S	S
Methanol	S	S	S
Diethyl ether	P	P	P
Isopropanol	S	S	S
DMSO	S	S	S
DMF	S	S	S

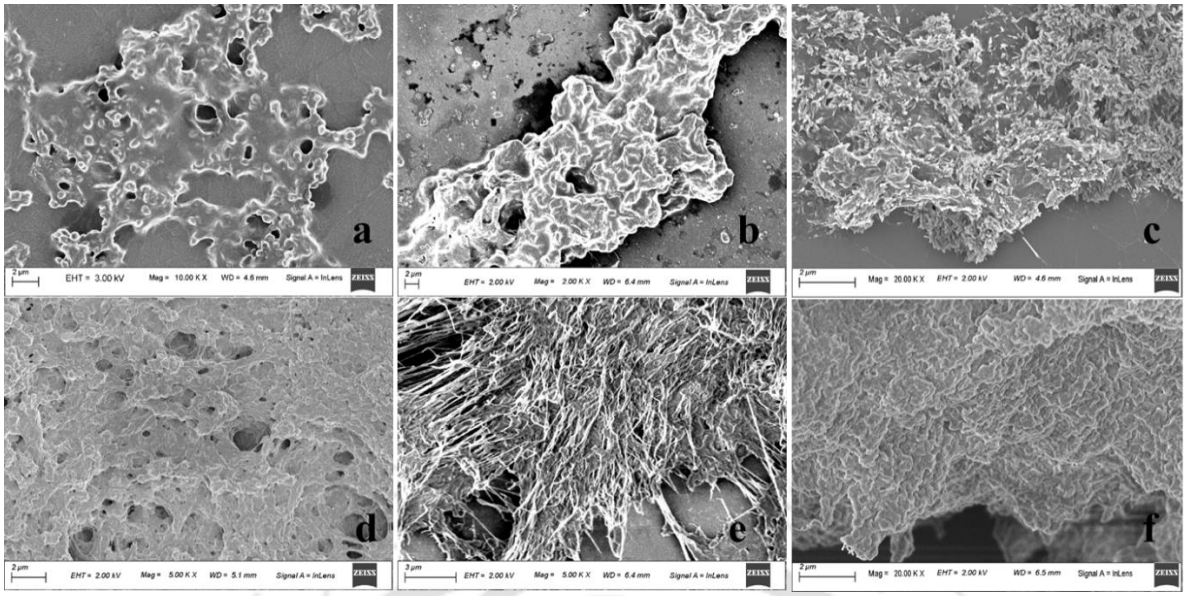

Figure 2.8: FESEM images of a-c) M1-M3 at 10 mM concentration in 1,2 DCB in solution state and in d-f) gel state respectively.

2.6.3. Viscoelasticity of the Organogels:

The mechanical strength of the gel is revealed from the viscoelastic properties, which has been studied using rheology (Figure 2.9 a-f). For rheological studies the gels have been formed from M1-M3 in 1, 2 DCB at 2% w/v concentration. An angular frequency sweep experiment was performed and the storage modulus (G′) and the loss modulus (G″) were plotted against the angular frequency sweep at a constant strain (Figure 2.9a-c). For M1, the storage modulus was greater than the loss modulus till about 100 rad/s angular frequency sweep. This observation suggested that the gel material has considerable strength and could sustain external forces. The storage modulus of the gel was of the order of 10^4 Pa which indicated a considerable mechanical strength of the organogel. In another typical experiment, the storage modulus and the loss modulus have been plotted as a function of % strain (Figure 2.9 d-f). The storage modulus was higher than the loss modulus in the experiment till a particular strain beyond which the two crossed each other. The same trend was observed for the gels prepared from M2 and M3.

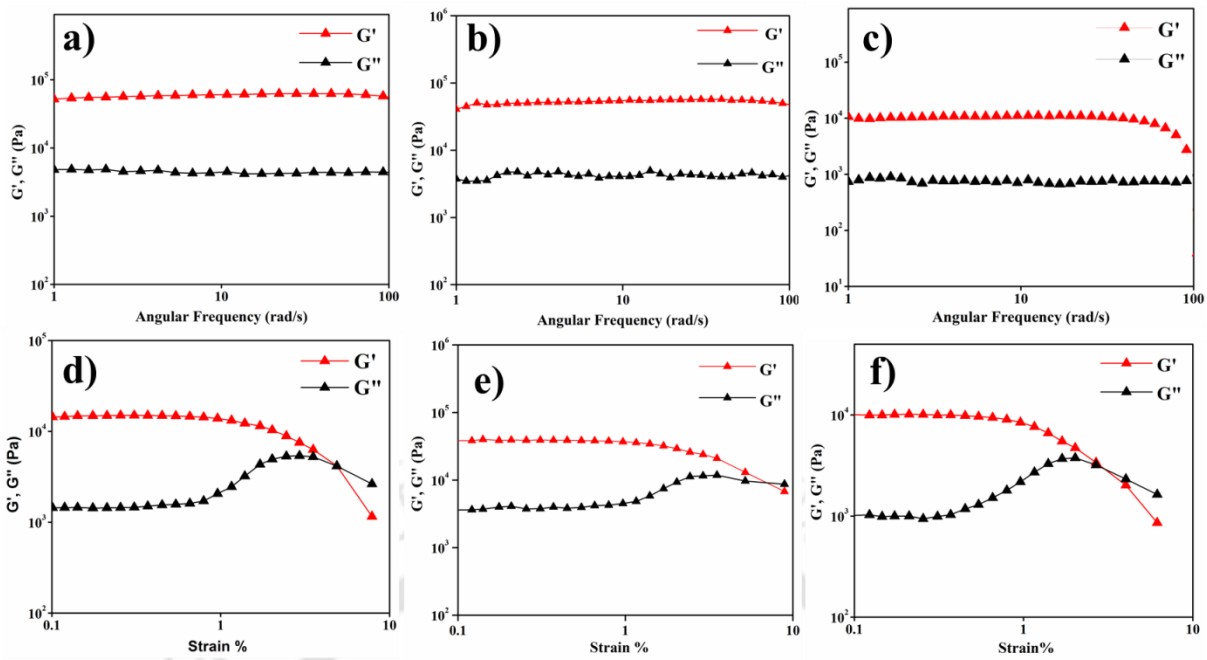

Figure 2.9: Rheology profile of the organogels M1-M3 in 1, 2-DCB respectively at 2% w/v as a function of a-c) frequency and d-f) % Strain

2.6.4. Mechanism of Self-Assembly:

The molecules designed have the following features: a) Fmoc moiety at the N terminus, b) DCU moiety at the C terminus and c) An intervening amino acid residue which is hydrophobic in nature. Amino acids Phe and Phg have aromatic side chains. Hence, the organogels formed by these molecules hence have a high chance of being stabilized by the a) π-π interactions in between the N terminal Fmoc groups and/or the side chains of the aromatic residues, b) intermolecular hydrogen bonding in between the NH and CO of the urea groups and amino acids and c) the vander Waals interaction in between the hydrophobic amino acid residues. However formation of organogel by M3 which contains the non-aromatic amino acid residue Gaba indicates that aromatic side chains are not necessary for the gelation process. On the contrary, inability of M4 (Boc-Gaba-DCU) to form organogel under similar experimental conditions is a direct proof that π-π stacking of the N terminal Fmoc moieties is of immense importance in formation of gels. In order to probe the role of

the Fmoc groups in the self-assembly process, we studied the concentration dependent fluorescence emission of the Fmoc group. Concentration dependent NMR and DMSO solvent titration were performed to study the role of hydrogen bonding in the gelation process. FTIR of powdered and xerogel samples were compared.

2.6.4.1. Fluorescence Studies:

The fluorescence emission spectra for M1-M3 in 1, 2 DCB with varying concentrations is shown in Figure 2.10a-c. The characteristic fluorescence emission peak for monomeric Fmoc group appeared at around 350 nm at lower concentrations for all the three compounds. With increase in the concentration, the peak at 350 nm was blue shifted to about 346 nm for all the compounds (Figure 2.10). Blue shifting of the emission maxima with increasing concentration, was an indication of the increasing hydrophobic environment, which is a predictable consequence of increasing self-assembly. This was accompanied by the quenching of the peak intensity (Figure 2.10) which may be attributed to ACQ upon self-assembly. Thus fluorescence experiments indicate that self-assembly occurs in all the systems M1-M3 progressively with increasing concentration. In the fluorescence spectra of M3, upon increasing the concentration, additional broad peaks appeared at 415 nm and 450 nm, which might be attributed to the excimer peaks. Absence of side chains in Gaba used in M3, might lead to closer packing of the molecules leading to appearance of excimer peaks (Figure 2.10c). This proves that the self-assembly proceeds *via.* stacking of the Fmoc groups. Thus aromatic interactions in between the Fmoc groups is an important driving force for the self-assembly of these systems.

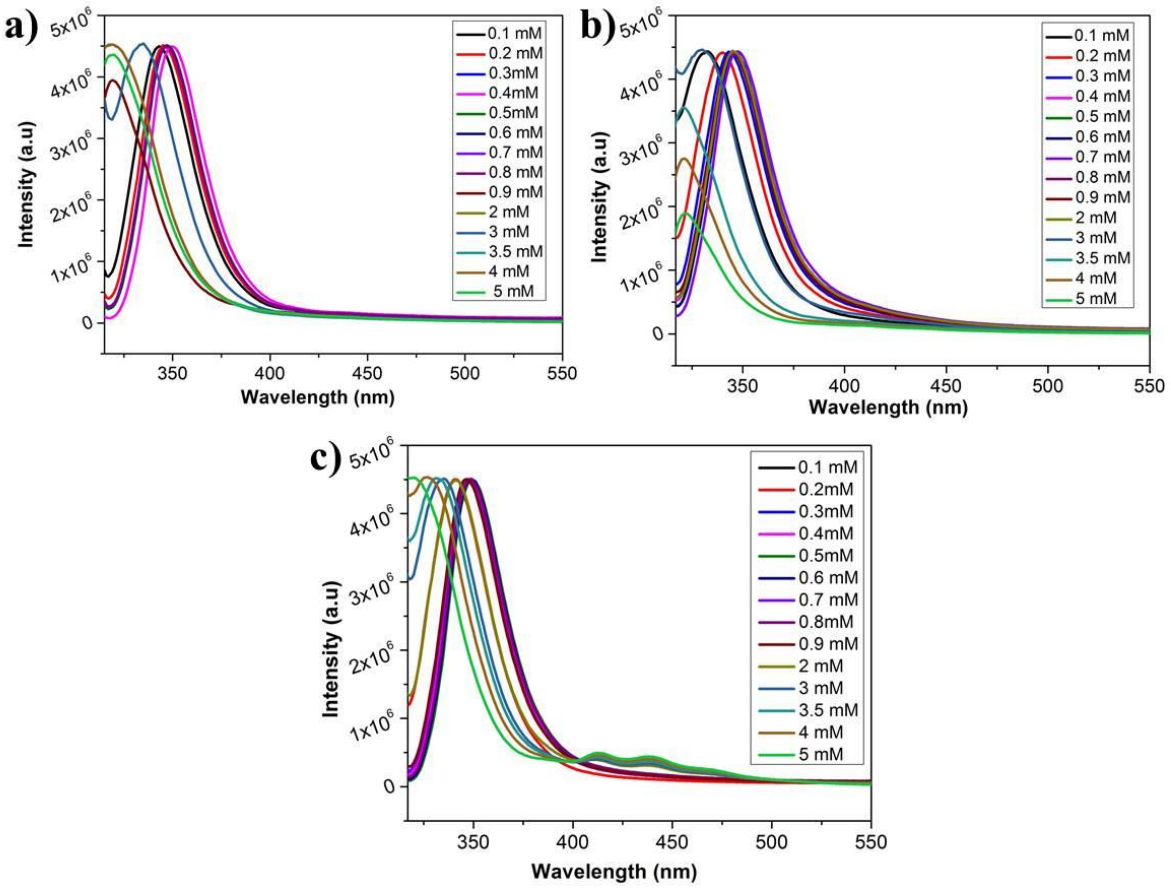

Figure 2.10: a-c) Concentration dependent fluorescence spectra of M1-M3 in 1, 2 DCB.

2.6.4.2. FT-IR Studies:

FTIR studies were performed on the powdered as synthesized gelators and the xerogels. Xerogels are dried gels obtained from the freeze-drying of the organogels. It is assumed that the self-assembled network of molecules formed from the intermolecular interactions is held intact even in the xerogel state. The superimpositions of FTIR spectra of M1-M3 respectively, from the powdered sample and the xerogels obtained from 1, 2 DCB are shown in Figure 2.11a-c. The molecules contain two NH protons and two carbonyl moieties. Peaks for NH protons in molecules M1-M3 in the powdered state appear at 3416/3319 cm^{-1}, 3405/3321 cm^{-1} and 3358/3315 cm^{-1} respectively. These peaks get significantly broadened in the xerogel state for all the compounds. Similarly the Fmoc carbamate carbonyl, the amino acid carbonyl and the urea amide carbonyls which give distinct peaks in the region of 1706-

1650 cm^{-1}in the molecules M1-M3 in the powdered state are notably diminished in the xerogel state.

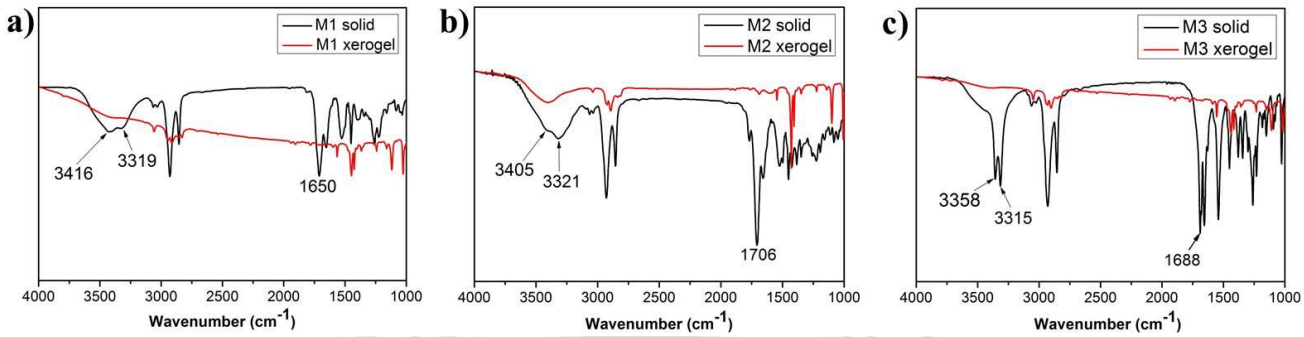

Figure 2.11: a-c) Comparison of the IR spectra of M1-M3 in powdered (black) and xerogel (red) state.

2.6.4.3. Molecular Packing:

X-ray diffraction studies have been carried out to obtain information about molecular packing of M1-M3 in gel state. XRD pattern of the xerogels obtained from 1, 2 DCB in the wide angle regions for M1-M3 is shown in Figure 2.12a-c (Table 2.2). The wide angle XRD patterns of all the xerogels show periodic diffraction patterns unlike the powdered samples and this indicates presence of ordered structures in their xerogel form. Powder XRD pattern for xerogels of all the three molecules M1-M3 looks identical suggesting that very similar packing pattern is present in all of them. The peak at 2θ = 21.88° (d = 4.08 Å), 21.78° (d = 4.08 Å) and 21.9° (d = 4.06 Å) for M1-M3 might correspond to the π-π stacking distance in between the aromatic moieties of the gelator molecules. The peak at 2θ =18.56° (d = 4.78 Å), 18.90° (d = 4.69 Å) and 18.94° (d = 4.68 Å) for M1-M3 might correspond to the distance in between the C-terminal ends of the gelator molecules.[512]

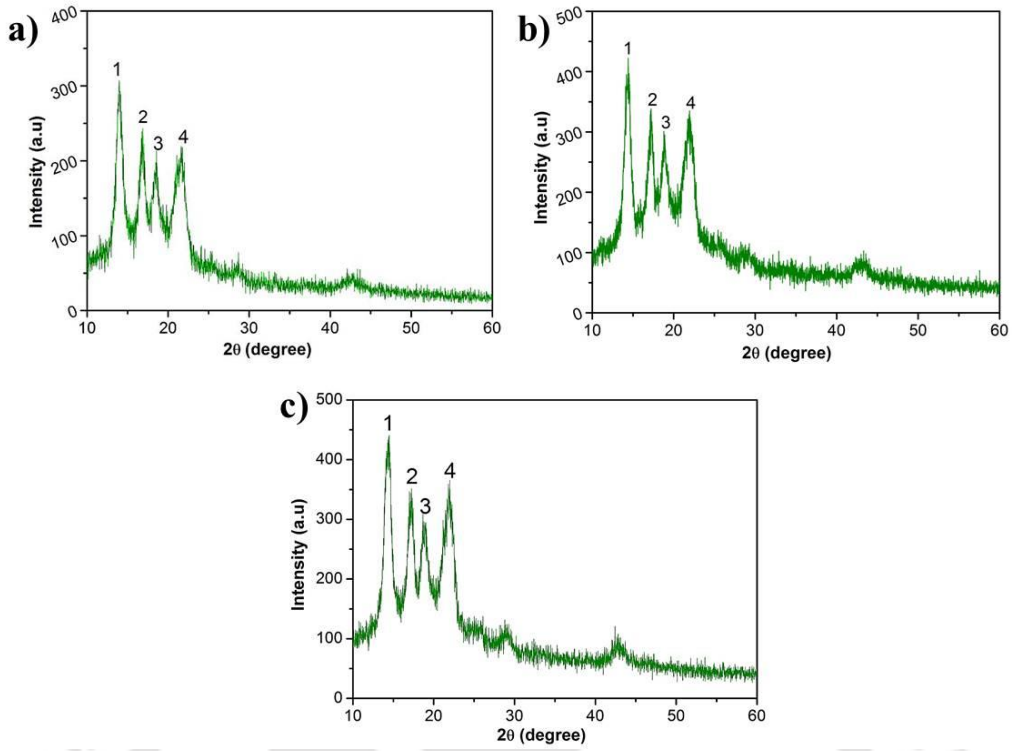

Figure 2.12: a-c) PXRD of M1-M3 xerogels.

Table 2.2: Parameters (2θ and interplaner distance (d)) obtained from PXRD experiment on the xerogels obtained from M1-M3.

Xerogel	Peak 1		Peak 2		Peak 3		Peak 4	
	2θ (degree)	d(Å)	2θ (degree)	d(Å)	2θ (degree)	d(Å)	2θ (degree)	d(Å)
M1	13.961	6.33	16.761	5.29	18.561	4.78	21.781	4.08
M2	14.521	6.11	17.221	5.16	18.901	4.69	21.881	4.07
M3	14.341	6.18	17.121	5.18	18.941	4.68	21.901	4.06

2.6.4.4. Role of Hydrogen Bonding:

The role of intermolecular hydrogen bonds in formation of the self-assembly of the peptides is probed by performing concentration dependent ^{1}H NMR experiment and monitoring the change in chemical shifts of the NH groups present in the molecules. Figure 2.13a shows the

overlay of the NH regions of the ^{1}H NMR spectra obtained for M2 at different concentrations (0.125 mM, 0.25 mM, 0.5 mM, 1 mM, 2 mM, 3.44 mM (MGC) and 5 mM) in $CDCl_3$. Concentrations less than MGC, MGC and higher than MGC were selected. There was no visible change in the chemical shifts of the two amide protons of M2 across the entire concentration range (0.125 mM - 5 mM) indicating that there was no change in the electron density about the amide protons or in other words there was no change in the hydrogen bonding status of the two amides in this concentration range. To find out the hydrogen bonding status of the amide protons, we performed a DMSO titration experiment (Figure 2.13b). Amide proton of urea (N-H_a) did not show any change in its chemical shift while the amide proton of the amino acid Phg (N-H_b) showed a considerable downfield shift ($\Delta\delta$ =0.85 ppm) indicating that the N-H_a was already hydrogen bonded unlike the Phg amide proton.

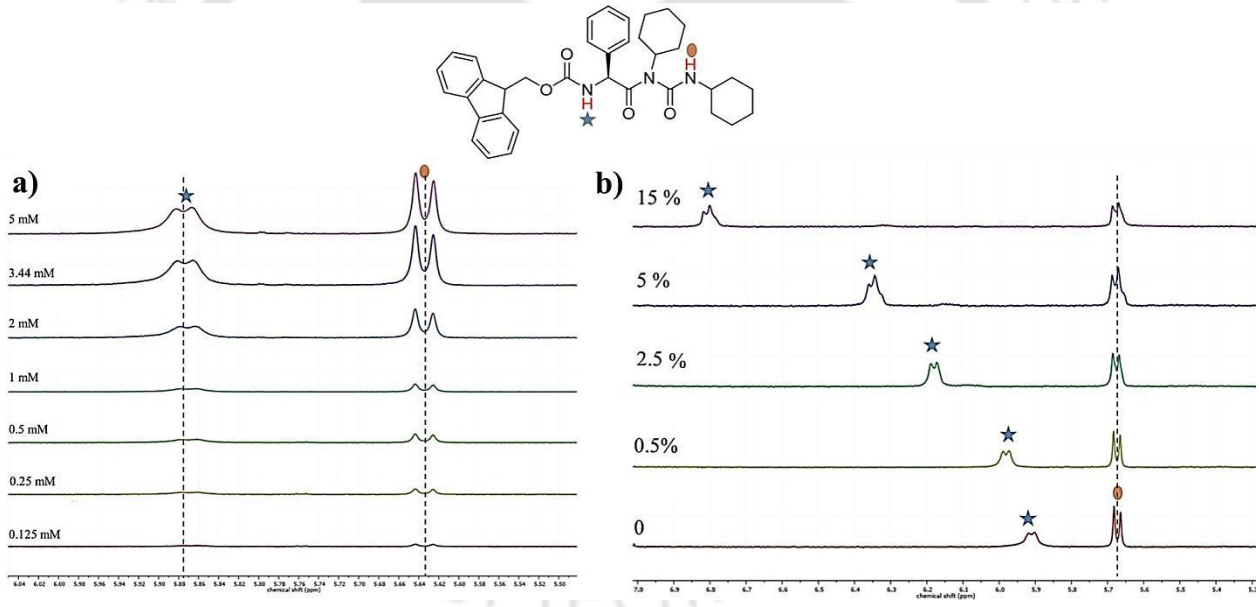

Figure 2.13: NH region of the stacked ^{1}H NMR spectra of M2 in $CDCl_3$ a) at different concentrations and b) at 5 mM concentration upon addition of different amounts of DMSO-d_6.

2.6.5 Application of the Organogels in Dye Absorption:

The organogels formed by the molecules M1-M3 were subjected to the dye absorption studies with the aim to employ these organogels for purifying water contaminated with toxic dyes. We checked the dye absorption by the gels with three dyes, namely CV, NR and RB. When the mixture of the organic solution of LMWG and aqueous solution of dye was heated and subsequently cooled, the organic phase with the LMWG molecule selectively formed gel and absorbed the dye from the aqueous solution within some time. The fading of the color of the aqueous phase, containing the dye was visually monitored as shown in Figure 2.14. The quantification of the amount of dye absorbed by the organogels was performed by monitoring UV of the aqueous phase (Figure 2.15a-i). All the organogels acted as very efficient dye adsorbents with about 90% efficiency for all the dyes (Figure 2.16, Table 2.3).

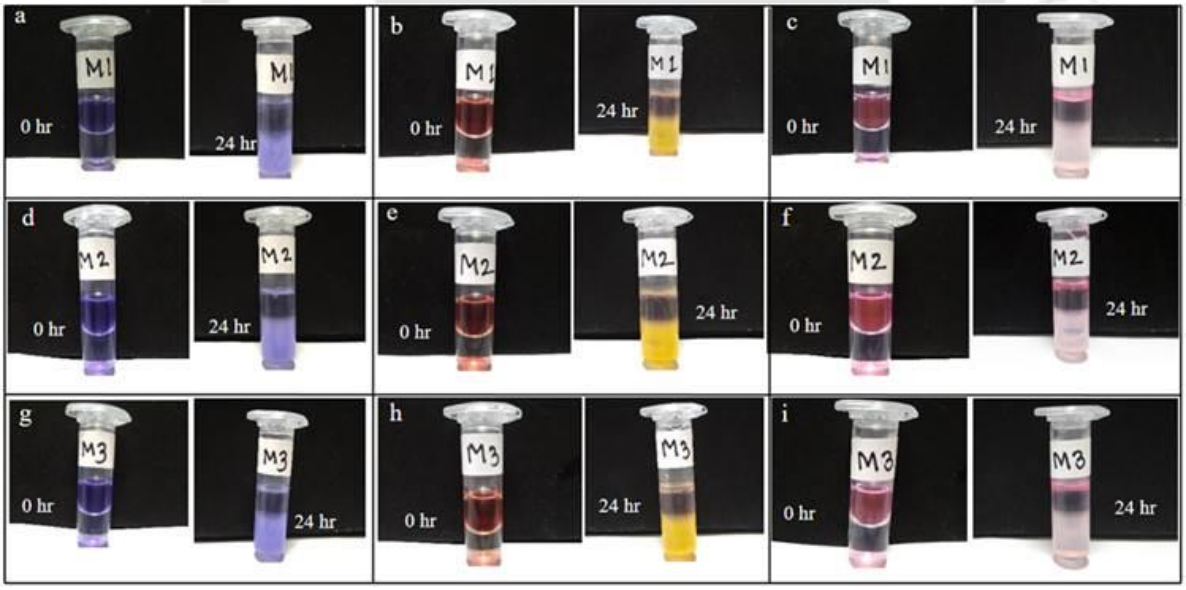

Figure 2.14: Absorption of dyes CV (a, d, g), RB (b, e, h), NR (c, f, i) by the organogels M1, M2 and M3 respectively, in 1,2 DCB at time t = 0 and t = 24 h. LMWG in 1, 2 DCB (colourless) was mixed with aqueous solution of dye, mixture was heated and cooled subsequently at t = 0 h. After t = 24 h, the gels turned coloured due to dye absorption.

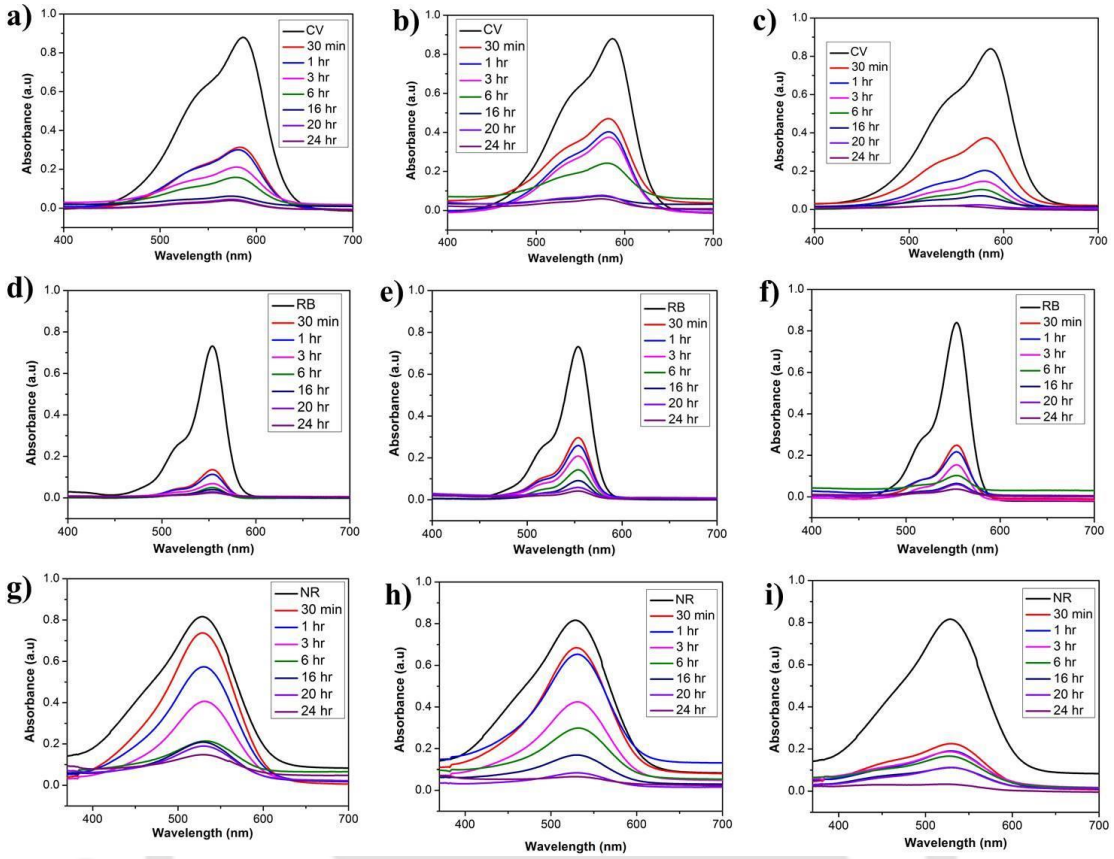

Figure 2.15: UV-Vis spectra showing absorption of dyes CV, RB and NR by organogels formed from a, d, g) M1; b, e, h) M2 and c, f, i) M3 in 1, 2 DCB.

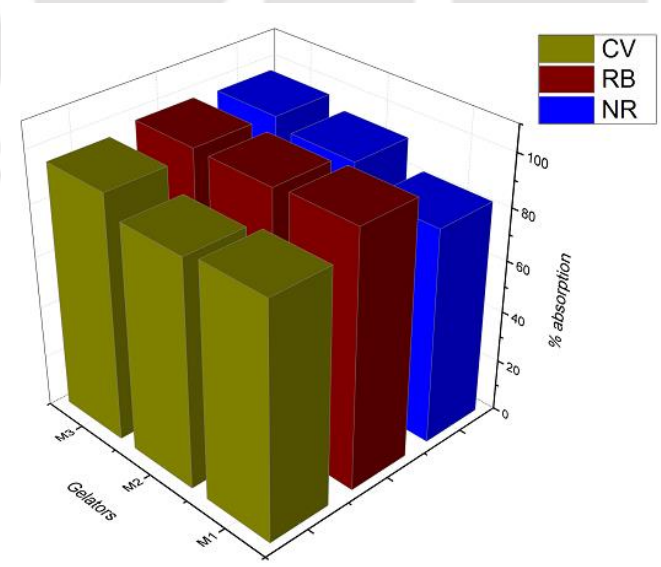

Figure 2.16 Quantitative summary of the loading efficiency of organogels formed by M1-M3 for dyes CV, RB and NR.

Table 2.3: Absorption/Loading efficiency of different dyes in organogels formed from M1-M3.

Gelators	CV (%)	RB (%)	NR (%)
M1	90.03	98.46	83.00
M2	87.70	97.24	92.84
M3	95.03	97.54	96.69

2.6.6. Reusability of the Organogel:

In order to be efficiently used as a material for water purification, the material should be economic and hence, recyclable. The organogels from M1-M3 could be reused over three cycles for subsequent loading and release of the dye, after which the quality of the gelator degraded (Figure 2.17).

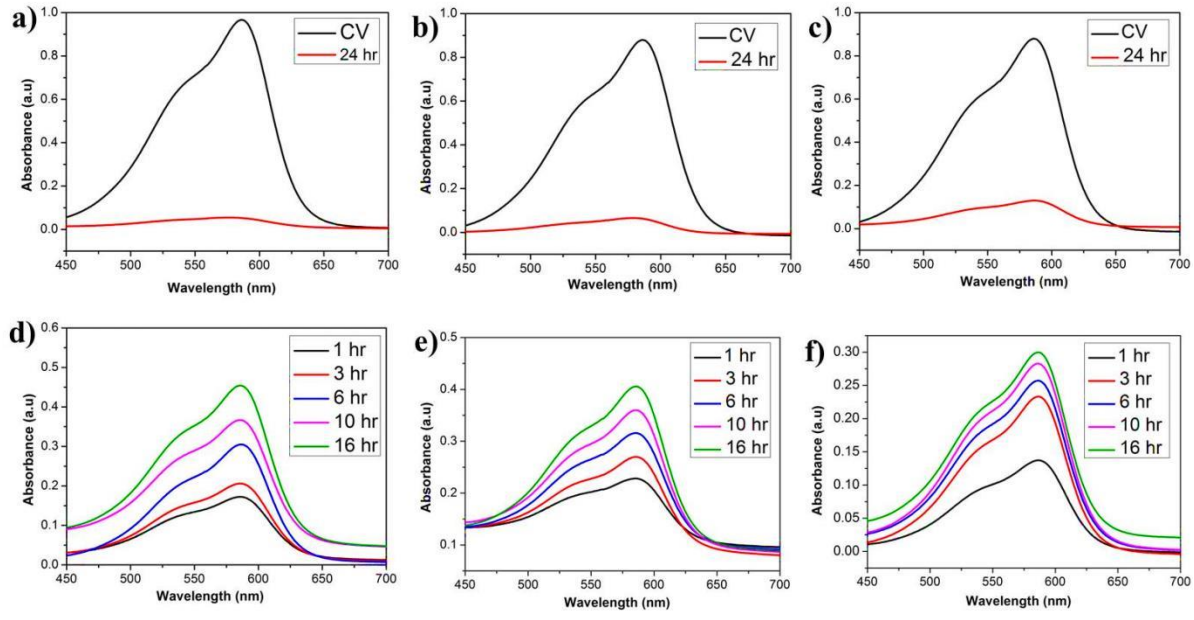

Figure 2.17: Reusability of organogels in dye absorption. a-c) UV-Vis graph showing CV (40 µM) loading after 24 h in cycles 1-3 in the organogel formed from M1 in 1,2 DCB. d-f)

UV-Vis graph showing time dependent CV release from the M1 organogel in the three subsequent cycles.

Figure 2.17a-c shows the percentage efficiency of CV uptake in 24 hours in the three subsequent cycles and Figure 2.17d-f indicates percentage release of CV after 16 hours in the three subsequent cycles from M1 organogel. Figure 2.18 compares the diminishing loading and release efficiencies of M1 organogel in the three subsequent cycles.

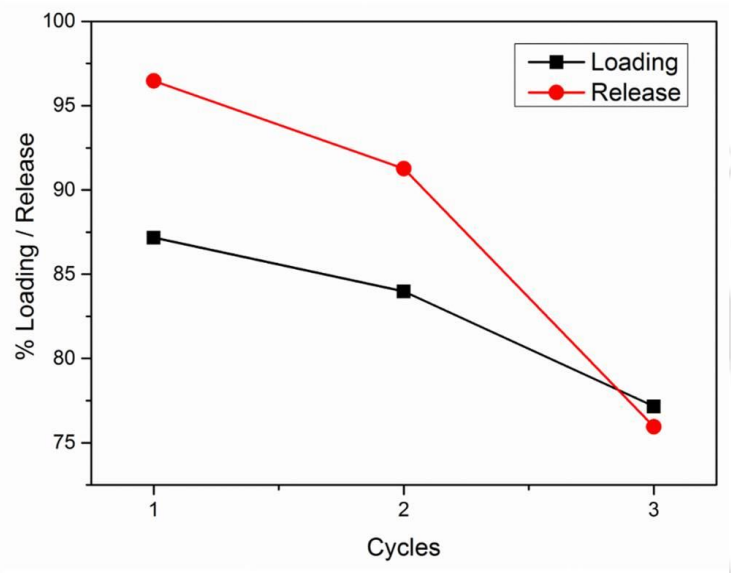

Figure 2.18: Plot of the % loading and release efficiency in three successive cycles for CV.

Table 2.4 shows the amount of dye that could be loaded and subsequently released in the three cycles.

Table 2.4: Loading/Release efficiency of organogel formed from M1 with dye CV

Cycle `1		**Cycle `2**		**Cycle `3**	
Load (%)	Release (%)	Load (%)	Release (%)	Load (%)	Release (%)
87.17	96.47	83.98	91.27	77.16	75.95

2.6.7. Ion Sensing Studies:

As our molecules contain urea moiety which is known widely as a fluoride ion sensor, we looked into anion sensing abilities of M1-M3. We first decided to look at the UV-Vis absorption and fluorescence behaviour of M1-M3 in the absence and the presence of various anions like F^-, Cl^-, Br^- , I^-, HSO_4^-, $H_2PO_4^-$, CH_3O^- and OH^- (as their Bu_4N^+salts). The spectroscopic studies were performed in acetonitrile as the molecules did not form gel in this solvent. Secondly, acetonitrile was inert and did not have any absorption in the range of 200-600 nm. UV absorption of M1-M3 was only sensitive to fluoride, acetate and hydroxide (Figure 2.19 a-c). In the absence of anions, M1 and M2 (Figure 2.19 a-b) contained peaks at 265 nm, 289 nm and 299 nm. Shoulders were observed at 255 nm and 272 nm. Upon addition of fluoride, acetate and hydroxide, the shoulder at 255 nm developed into a peak with appearance of another new peak at 245 nm. The peak at 289 nm disappeared. Peaks at 265 and 299 nm remained unchanged (Figure 2.19a-c). In the presence of other anions (Cl^-, Br^-, I^-, HSO_4^-, $H_2PO_4^-$), there was no change in peak positions and minor changes in peak intensities were observed (Figure 2.19a-c). M3 had similar UV absorptions as M1 and M2, which did not change appreciably upon addition of any anions (Figure 2.19c).

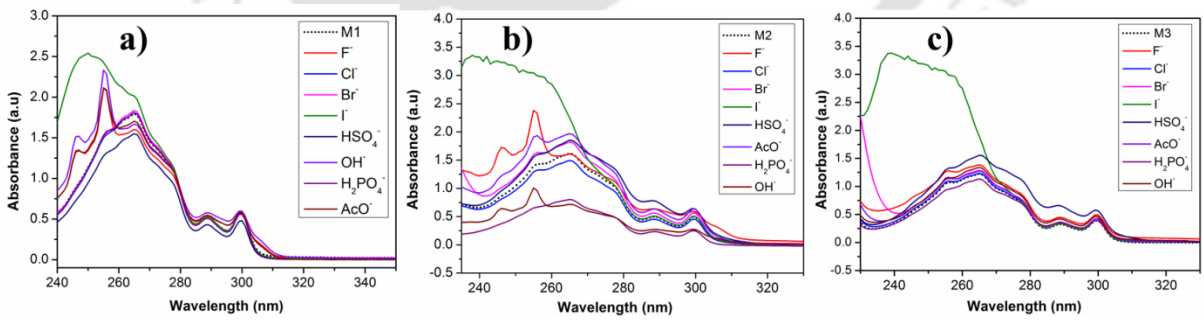

Figure 2.19: a-c) UV-Vis spectra showing anion sensing ability of M1-M3 in acetonitrile (0.1 mM) for different anions (0.1 mM).

In order to look at the effect of the anions on the excited state of the molecules, change of the fluorescence emission signal in the presence of anions was studied (Figure 2.20a-c). In the absence of anions, upon being excited at 301 nm, the fluorescence emission maxima for M1-M3 was at 332 nm. Upon addition of 0.1 mM fluoride, acetate and hydroxide, the peak at 332 nm was slightly blue shifted (for M1 and M3) (Figure 2.20a, c) and quenched (predominantly for M2) (Figure 2.20b). A prominent new peak appeared at 459 nm for all the three molecules M1-M3. There was negligible effect on the fluorescence spectra of M1-M3 in the presence of other anions (Figure 2.20a-c). Thus it was concluded that molecules M1-M3 selectively sensed fluoride, acetate and hydroxide anions.

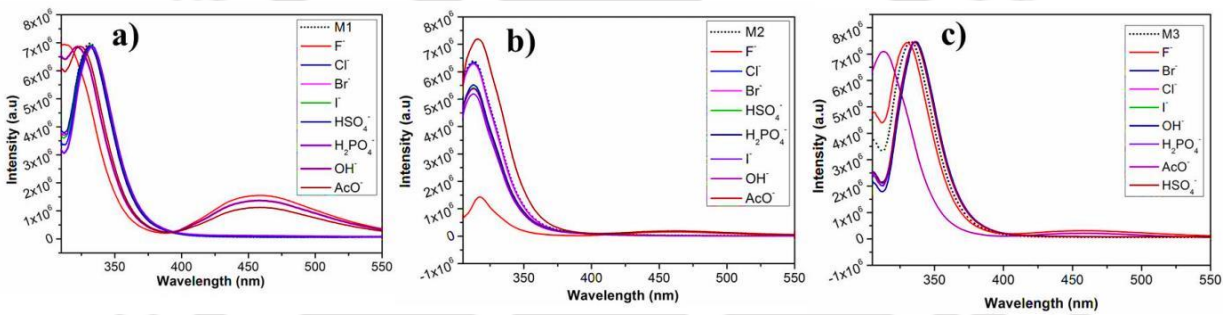

Figure 2.20: a-c) Fluorescence spectra showing anion sensing ability of M1-M3 in acetonitrile (0.1 mM) for different anions (0.1 mM).

To find out the sensitivity of anion detection, the fluorescence response was monitored as a function of anion (F^-, OAc^- and OH^-) concentration for a fixed concentration of M1-M3 (Figure 2.21, 2.22 and 2.23). For all the three molecules, anions could be detected at a minimum concentration level of about 0.02 mM. With increase in the concentration of the anion, the intensity of the peak at 459 nm steadily increased.

In order to understand the interaction in between fluoride anion and M1-M3 in greater detail, ^1H NMR titration experiment was carried out with M2 in the presence of fluoride ions (Figure 2.24). With increasing concentration of F^-, the urea NH ($N\text{-}H_a$) shows no change in

its chemical shift value while the NH proton of the amino acid Phg (N-H_b) disappears quickly with a downfield shift ($\Delta\delta$ = 0.24 ppm). This observation indicates that strong interaction *via.* hydrogen bonds exists between the amino acid NH (N-H_b) and the fluoride in the anion complexed form. The urea NH does not seem to form any hydrogen bonds with the anions as it is already intramolecularly hydrogen bonded as seen from the DMSO titration of M2 earlier (Figure 2.13b).

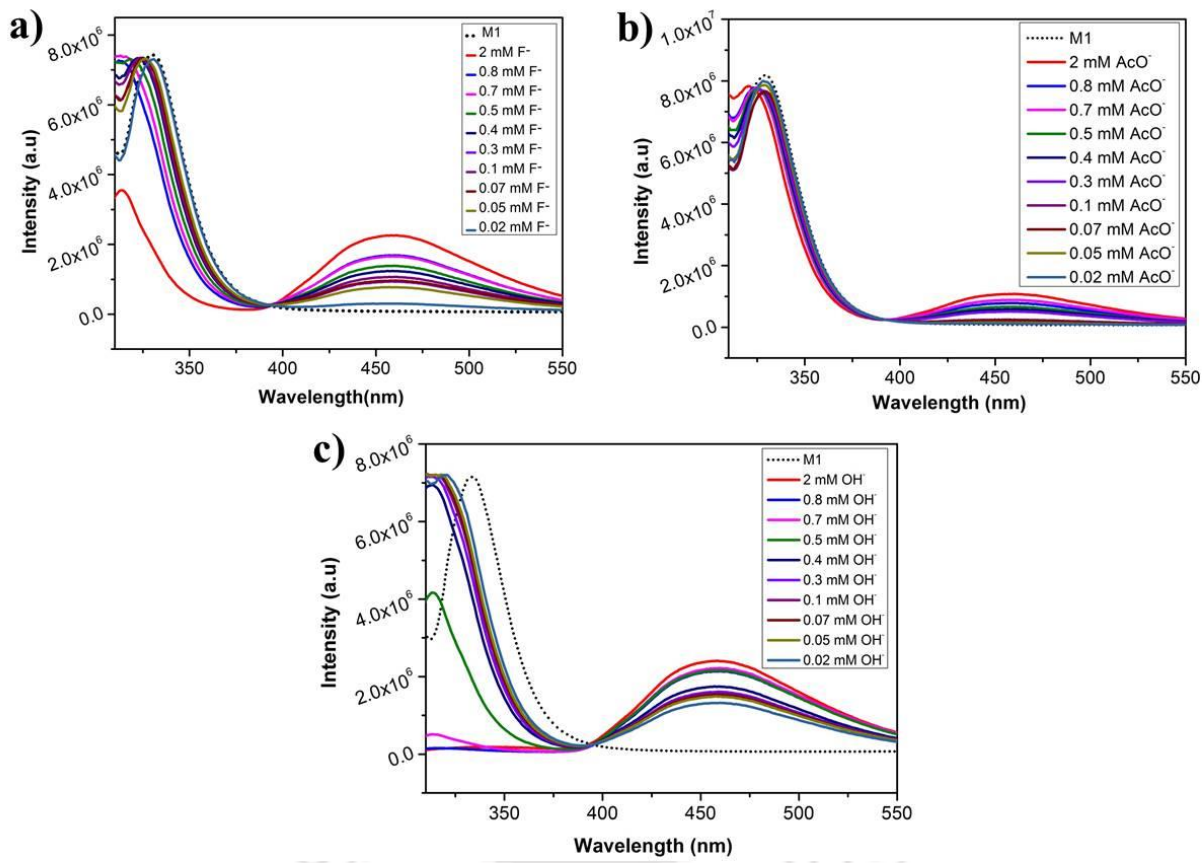

Figure 2.21: a-c) Fluorescence spectra of M1 in acetonitrile at various concentrations of anions fluoride, acetate and hydroxide.

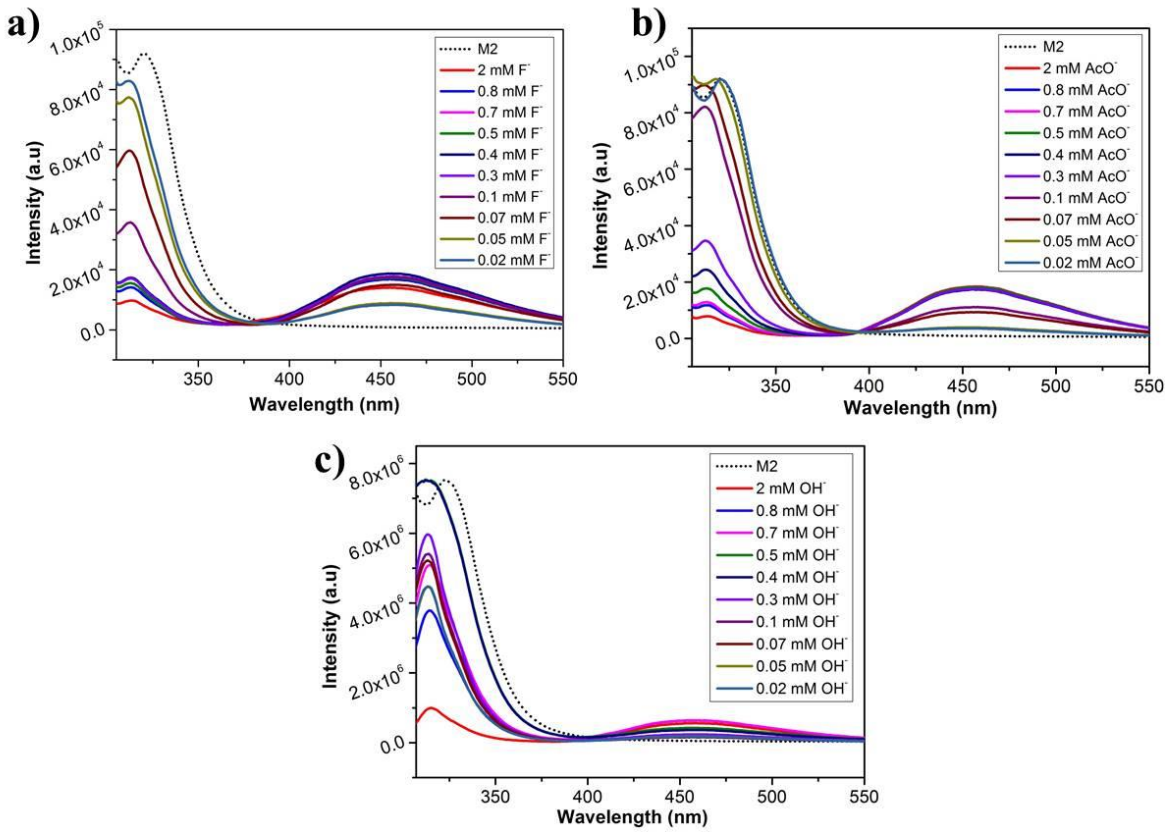

Figure 2.22: a-c) Fluorescence spectra of M2 in acetonitrile at various concentrations of anions fluoride, acetate and hydroxide.

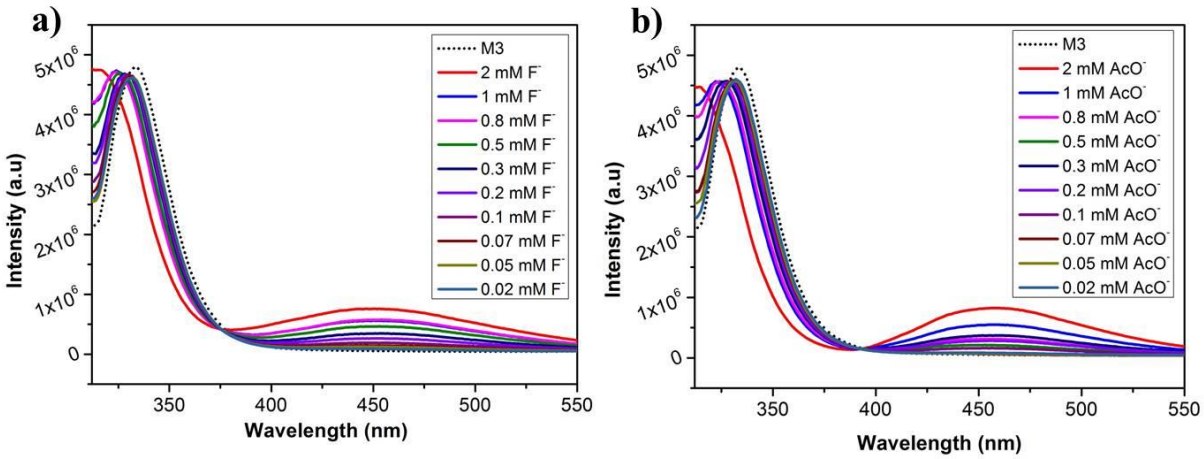

Figure 2.23: a-c) Fluorescence spectra of M3 in acetonitrile at various concentrations of anions fluoride and acetate.

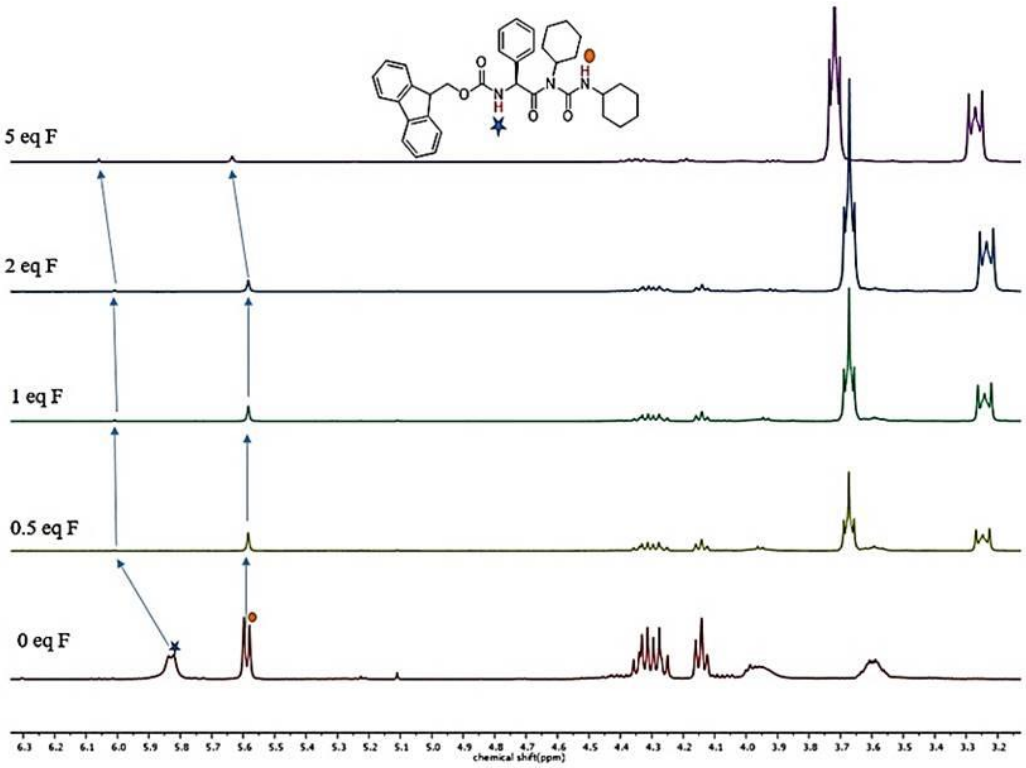

Figure 2.24: ^{1}H NMR titration of M2 with fluoride anion in $CDCl_3$ at room temperature.

2.6.8. Theoretical Studies:

We performed DFT studies for understanding the mode of binding of fluoride to the M2 molecule at the atomic level. The optimized ground state structures of M2 monomer and its fluoride bound M2:F^- complex are shown in Figure 2.25. N-H_a (DCU) and N-H_b (amino acid backbone) bond lengths are almost identical, former being slightly elongated for free M2 monomer (Figure 2.25a). Intramolecular hydrogen bond between N-H_a of DCU and carbonyl of amino acid backbone in the six-membered ring is a characteristic feature of M2. The angle N-H_a…O is 132.5^0 and H_a…O distance is 1.81Å respectively. This feature is supported by the ^{1}H NMR DMSO titration experiment discussed earlier (Figure 2.13b) in which N-H_a was shown to be intramolecularly hydrogen bonded. Calculations suggest two possible fluoride binding modes which are isoenergetic; single (M2:F^-_S1, Figure 2.25b) and double (M2:F^-_S2, Figure 2.25c) intermolecular hydrogen bonds between F^- and M2. Fluoride binding to the amino acid backbone N-H_b leads to elongation of the N-H_b bond length from 1.01Å to

1.09Å (M2:F$^-$_S1, Figure 2.25b). F$^-$…H_b distance is 1.43Å and the orientation of the six-membered ring relative to N-H_b is altered upon fluoride binding (Figure 2.25b). Double hydrogen bonded M2:F$^-$_S2 geometry suggests disruption of intramolecular hydrogen bond which is energetically compensated by the formation of second hydrogen bond in between the M2 and F$^-$, making it isoenergetic to M2:F$^-$_S1. N-H_b, F-…H_b distances in the double hydrogen bonded M2: F$^-$_S2 is 1.06Å and 1.51-1.54 Å respectively. The shorter F$^-$…H_b and larger N-H_b in M2:F$^-$_S1 with respect to M2:F$^-$_S2 makes N-H_b of the former more susceptible towards fluoride induced deprotonation. This observation is in lines with the ^{1}H NMR titration experiment discussed above (Figure 2.24).

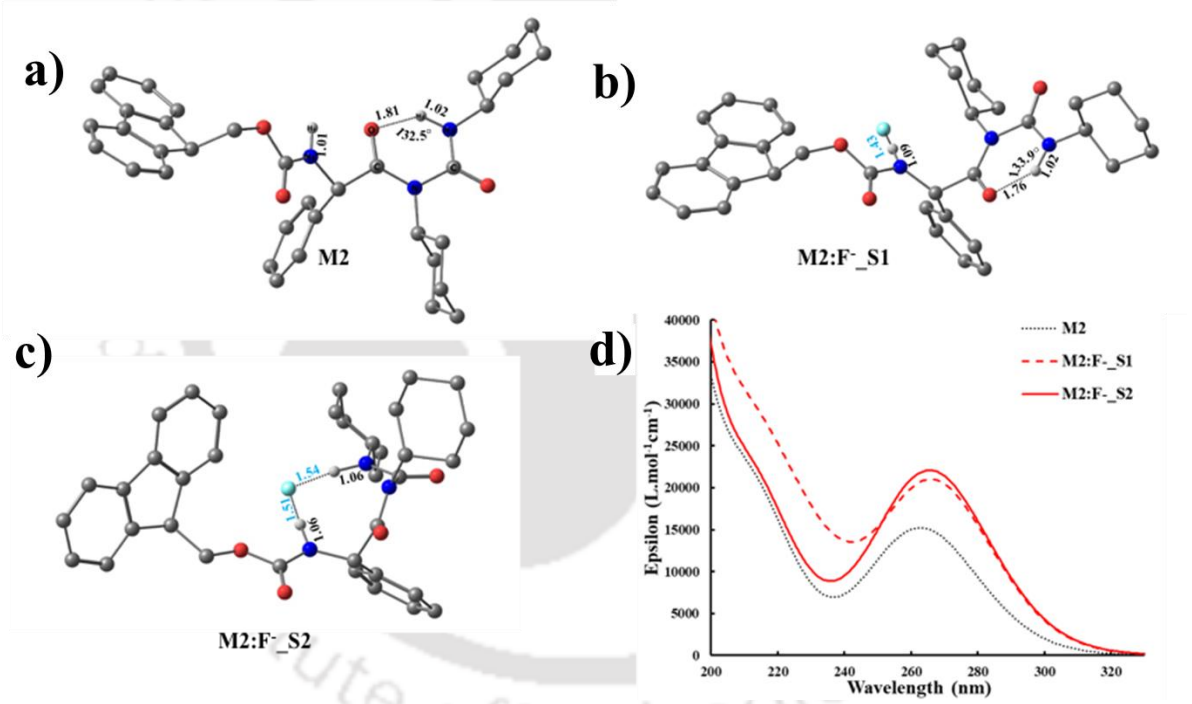

Figure 2.25: Optimized structures of dicyclohexyl urea derivative (a) M2 (b) Single coordinated fluoride bound complex, M2:F$^-$_S1 (c) Doubly coordinated fluoride bound complex, M2:F$^-$_S2. (d) Computed absorption spectra in acetonitrile for M2 (dotted black line), M2:F$^-$_S1(dashed red line) and M2:F$^-$_S2 (solid red line).

However, fully deprotonated form (M2$^-$:HF) was not observed upon geometry optimization starting with different geometries with varying F$^-$…H_b and N-H_b distances in single

intermolecular binding mode. Optimization with different initial geometries always gave M2:F^-_S1 (Figure 2.25b). Calculated normal model frequencies of all the optimized geometries indicate that all the reported structures were true minima on the potential energy hyper surface. The calculated absorption spectra of M2 and M2:F^- are shown in Figure 2.25d and calculated absorption peaks are listed in Table 2.5. For M2 monomer, the first calculated absorption peak located at 265.64 nm, is in excellent agreement with the experiment (Figure 2.19b). This absorption is primarily assigned to the highest occupied molecular orbital (HOMO) to lowest unoccupied molecular orbital (LUMO) transition. The optimized geometries of M2:X^- (X = Cl, Br, I, OH, OAc) are given in Figure 2.26. Characteristic absorption peaks of fluoride bound M2:F^- at 255 nm and 246 nm were also reproduced by theoretical calculations (Table 2.5). The molecular orbitals relevant to the absorption peaks are shown in Figure 2.27.

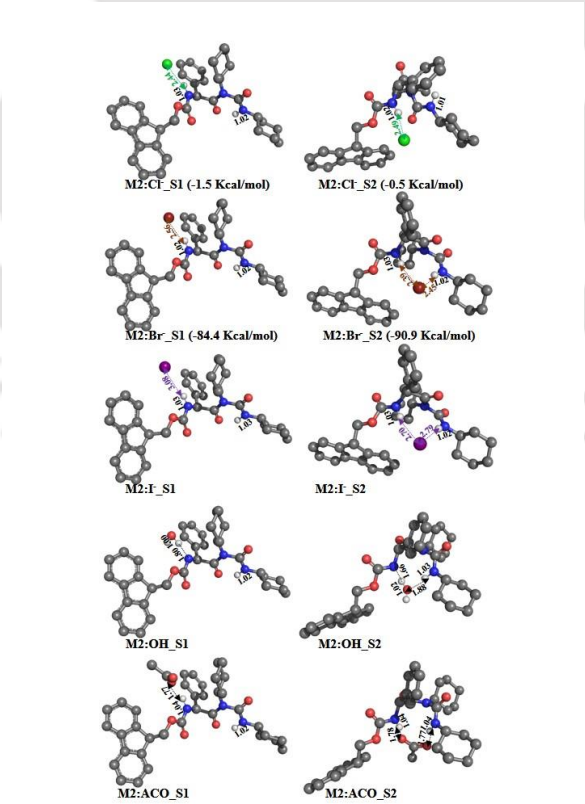

Figure 2.26: The optimized geometries of M2:X^- (X = Cl, Br, I, OH, OAc)

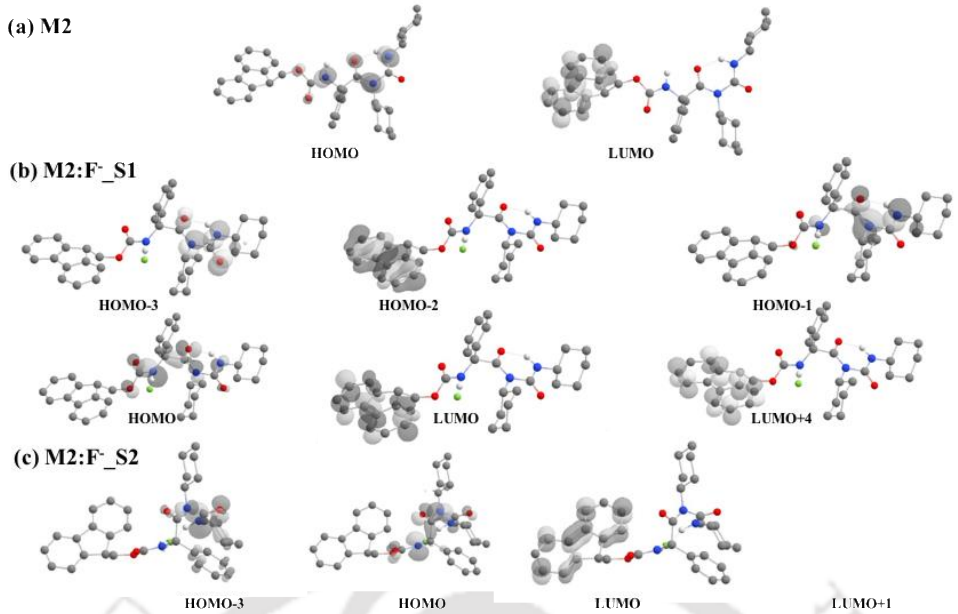

Figure 2.27: Molecular orbitals (MO) involved in characteristic UV-Vis absorption peaks (a) M2 (b) M2:F⁻_S1 (c) M2:F⁻_S2.

Table 2.5: The calculated absorption spectra, oscillator strengths (f) and assignments for M2, M2:F⁻_S1, and M2:F⁻_S2, along with experimental data.

	f value	**Assignments**	**λ_{cal} (nm)**	**λ_{exp} (nm)**
M2	0.2072	HOMO > LUMO	265.6	265
M2:F⁻_ S1	0.4088	HOMO > LUMO	268.2	265
	0.0219	HOMO-2 > LUMO	254.4	255
	0.0019	HOMO-1 > LUMO	245.5	246
M2:F⁻_S2	0.4343	HOMO > LUMO	267.9	265
	0.0006	HOMO > LUMO+1	255.3	255
	0.0704	HOMO-3 > LUMO+1	245.9	246

2.6.9. Effect of Anions on the Formation and Disruption of Organogels:

To study the effect of the anions on the ability of formation and the disruption (gel-sol transition) of organogels, the anions were added a) to the organic solvent containing M1-M3, heated together and cooled subsequently (Figure 2.28a-c, 2.29a-c, 2.30a-c) and b) to the preformed gel (Figure 2.28d-f, 2.29d-f, 2.30d-f). This study was performed only with those anions which had a fluorescence response. Fluoride prevented gel formation in all of the

LMWG molecules, while hydroxide prevented gel formation only in M2 and M3. Gel formation was not prevented by acetate for any of the molecules M1-M3. None of the anions could disrupt preformed gels formed by M1 to M3 (Figure 2.28d-f, 2.29d-f, 2.30d-f). This indicated that once the assembly was formed, the part of the molecule responsible for the anion binding was shielded from the solvent or approach of the ions was prevented due to the assembly formation. Hence the anions have no effect on preformed gels. On the other hand, interaction in between the molecules and the anions causes certain changes in its backbone conformation that prevents the assembly of the molecules thereafter. Thus the assembly formation was prevented in the presence of anions. The varying response towards the anions might be associated with the varying strength of self-assembly of different gels, which in turn arises from the subtle changes in the structures of these molecules.

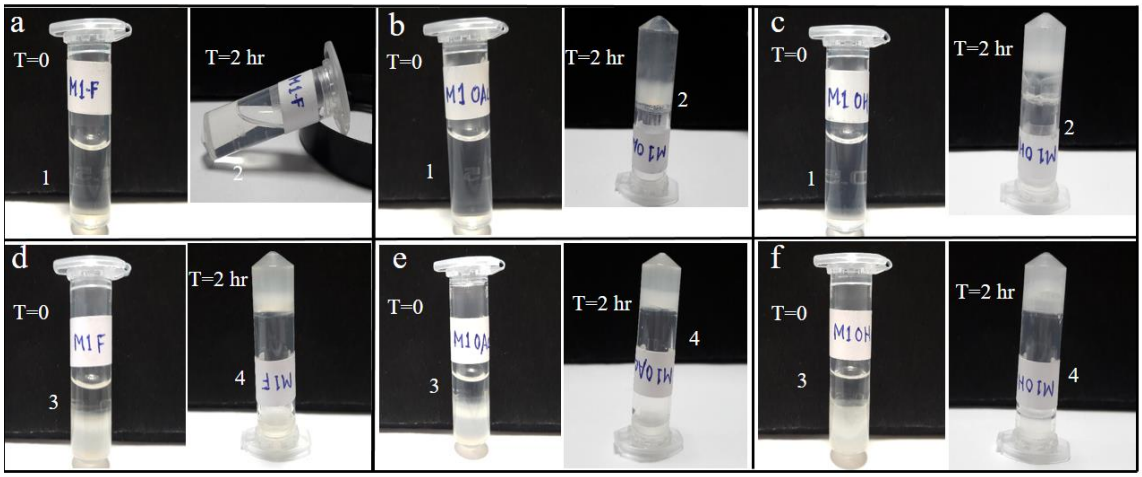

Figure 2.28: Effect of fluoride, acetate and hydroxide ions on the (a-c) formation and (d-f) disruption of organogels formed from M1. Only fluoride prevents formation of organogel, while none of the anions cause gel to disrupt.

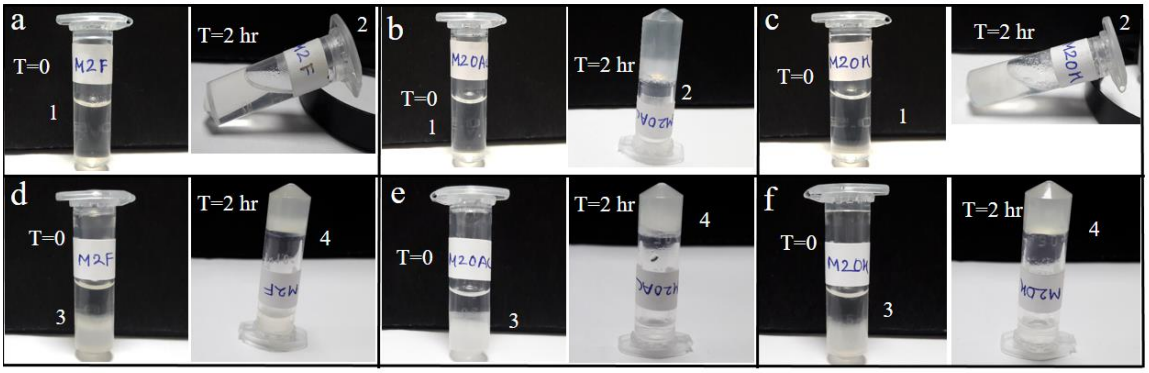

Figure 2.29: Effect of fluoride, acetate and hydroxide ions on the (a-c) formation and (d-f) disruption of organogels formed from M2. Fluoride and hydroxide prevents formation of organogel, while none of the anions cause gel to disrupt.

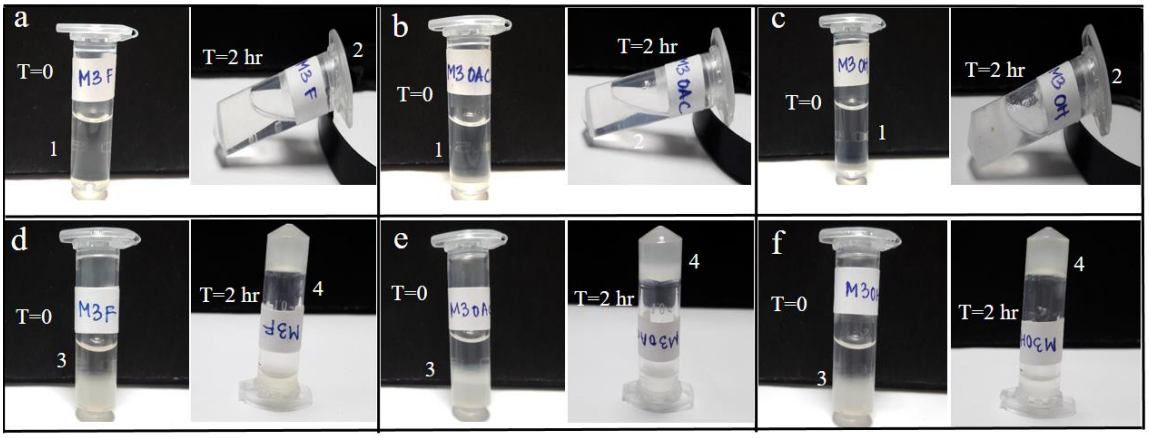

Figure 2.30: Effect of fluoride, acetate and hydroxide ions on the (a-c) formation and (d-f) disruption of organogels formed from M3. All the three anions prevent formation of organogel, while none of the anions cause gel to disrupt.

2.6.10. Importance of DCU Moiety in Ion Sensing:

Having understood now that the urea NH (N-H_a) is actually not involved in the fluoride binding event we asked the question if the DCU moiety is important at all in the ion sensing abilities of M1-M3. To probe this we considered the control molecule Fmoc-Phe-OH and studied its ion sensing abilities. There was no UV absorption or fluorescence response in the presence of any of the anions that were tested (Figure 2.31). This is crucial evidence which

indicates that the DCU moiety of the M1-M3 plays a significant role in their ion sensing. This might be due to the role of DCU moiety in modulating the molecular orbitals in a specific manner that leads to fluorescence response in the ion detection.

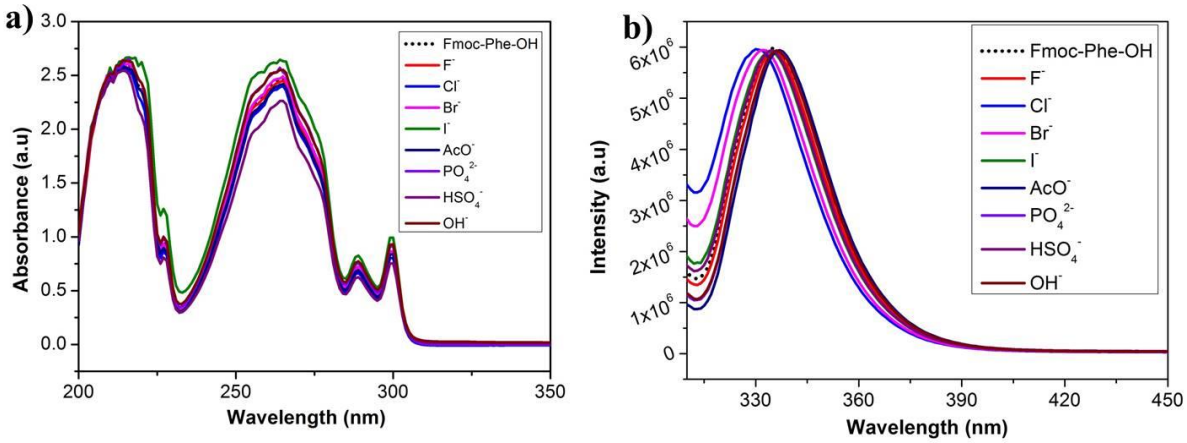

Figure 2.31: Anion sensing abilities of Fmoc-Phe-OH.

2.6.11. Self-Assembly Model and the Anion Sensing:

Figure 2.32 summarizes the mechanism of self-assembly of M1-M3. From all the studies above it can be concluded that π-π stacking of the Fmoc moieties and the hydrophobic effect are the two most important forces driving the self-assembly of M1-M3. Hydrogen bonding seems trivial in this process. Involvement of the urea NH ($N\text{-}H_a$) in intra molecular hydrogen bond, forming the six membered ring is supported by the NMR experiments and DFT studies (Figure 2.13b and 2.25a). The amino acid Phg amide proton is non-hydrogen bonded (Figure 2.13b) and remains so in the hydrophobic pockets even at concentrations greater than MGC indicating that intermolecular hydrogen bonds are not the driving forces for the self-assembly process. In the self-assembled state, adjacent molecules come close and the Fmoc groups are stacked together at 180° to each other. This is supported by the PXRD data where the interplaner distance of about 4.07 ± 0.1 Å is obtained which is the ideal distance for aromatic stacking. However stacking of the Fmoc moieties most probably occurs by approach of adjacent molecules from opposite sides (Figure 2.27).This happens firstly as the C terminal

end of the amino acid residue contains DCU moieties which impart non-planarity to the molecules, preventing adjacent molecules to approach as close as 4Å from the same side. Secondly, side chains of Phe and Phg contain bulky phenyl groups, in a plane which is almost perpendicular to that of the Fmoc moieties. This might also prevent same side approach of molecules. In M3, amino acid Gaba does not contain any side chains, which leads to better stacking of the molecules than in M1 and M2. This is supported by the presence of excimer peaks only in the fluorescence spectra of M3.

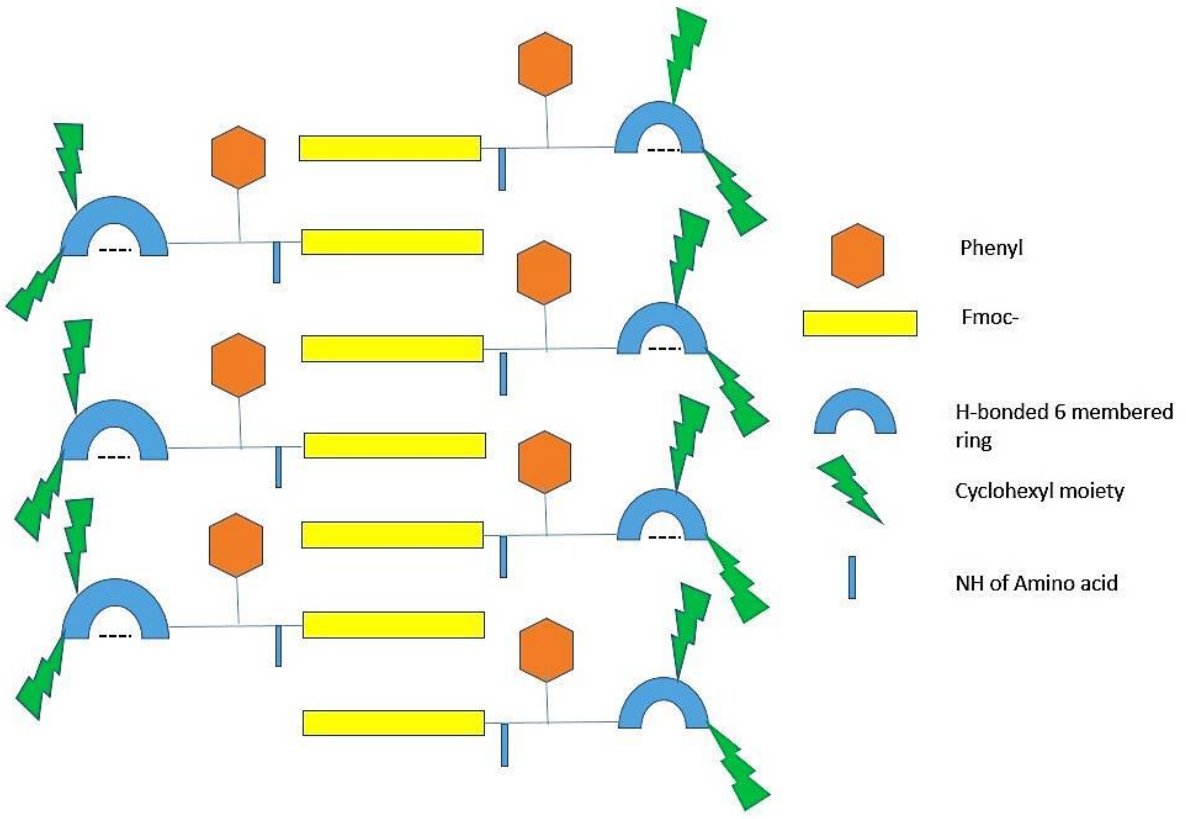

Figure 2.32: Schematic for self-assembly of the organogels from M1-M3.

As the NH of urea (N-H_a) is intramolecularly hydrogen bonded, the only NH available for the anion complexation is the N-H_b from the amino acid. Upon complexation with the anion, the backbone of the molecule gets distorted as seen from the DFT studies. This in turn prevents the approach of the molecules close enough to let π-π aromatic stacking possible and thus prevents gelation process. This explains the inability of M1-M3 to form gels in the presence

of anions. Once the gelation occurs, the non-hydrogen bonded N-H_b that complexes with the anions is housed deep in the hydrophobic pocket. This pocket is flanked by the Fmoc stacking on one side and the non-planer DCU moiety on the other. Moreover, fluoride and other anions being highly charged do not prefer to enter into the hydrophobic pocket to access the non- hydrogen bonded NH. This explains why the anions have no effect on the organogels.

2.7. Conclusion

In this study we have reported a new class of LMWG. Dicyclohexylurea derivatives of amino acids are extremely simple molecules that easily form organogels in a large range of organic solvents. The mechanism of gelation has been delineated and it has been proved that molecular self-assembly was driven by π-π interactions in between the Fmoc moieties and hydrophobic effect. The reported organogels are capable of absorbing different organic dyes highly efficiently and are recyclable in nature. M1-M3 can act as selective anion sensors for fluoride, hydroxide and acetate. The mechanism of fluoride sensing has been clearly understood and the mode of fluoride binding established both by experimental and computational methods. We may conclude by saying that this new class of amino acid derivatives of urea forms easily synthesizable and cost effective materials which can have multiple applications like water purification by removal of toxic dyes effectively and as anion sensors for selective anions like fluoride, acetate and hydroxide.

Chapter 3

Co-Assembly of Charged Complementary Peptides and Their Applications as Organic Dye / Heavy Metal Ion (Pb^{2+}, Hg^{2+}) Absorbents and Arsenic (III/V) Detectors

Chapter 3
Co-Assembly of Charged Complementary Peptides and Their Applications as Organic Dye / Heavy Metal Ion (Pb^{2+}, Hg^{2+}) Absorbents and Arsenic (III/V) Detectors

3.1. Peptide Hydrogels: Self-Assembly and Co-Assembly

Hydrogels are three dimensional polymeric networks capable of assimilating huge volumes of water. These are made of hydrophilic polymer chains that are chemically or physically interlinked.[516-518] Hydrogels constituted by chemical bonds and physical bonds are termed as chemical and physical gels respectively. The strength of the cross-linked system is dictated by the junctions which are tightly bound by strong forces like covalent, ionic bonds and/or weak forces such as hydrogen bonding, π-π stacking, hydrophobic interactions, hydrophilic interactions. [519-521] Molecular property of the hydrogelator is lost in the chemical gels while they remain intact in the physical gels. Many hydrogelating molecules are reported which can be assembled, under specific conditions, into gels through the self-assembly of small molecules. Owing to their large water content, hydrogels resemble biological tissues and can be put to various biomedical applications such as cell culture, [522, 523] tissue engineering, [524] drug delivery, [525,526] regenerative medicine.[527] Additionally hydrogels can also be used in environmental remediation and wastewater management. [528-530] Among various hydrogel building blocks, peptides are particularly attractive due to their facile synthesis, excellent gelation ability, good biocompatibility and bioactivity. [531] Being simple, robust and versatile biomaterials, peptide based hydrogels have gained significant attention in the recent years. [532] Peptide hydrogels have three dimensional fibrillar network structure[217] and are composed of α-helices, β-sheets or random coiled arrangements. [533-535] Peptide based hydrogels can be prepared in the presence of triggers like heating-cooling, sonication, adjustment of the pH of the solutions, addition of suitable salts or by performing enzymatic reactions on the gelator

precursors[536-538] Nature of amino acids in the peptide determines its hydrophobicity and hydrophilicity balance which is crucial for the gelation process.

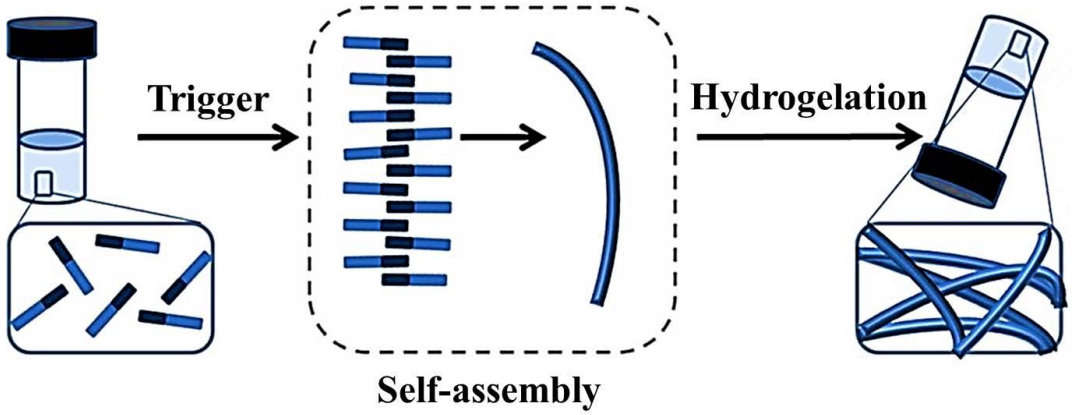

Figure 3.1: Schematic illustration of the hydrogelation process. The figure has been adapted with permission from reference 532. *Copyright 2013 Acta Materialia Inc. Published by Elsevier Ltd.*.

Supramolecular co-assembly of peptides involves the combination of two or more building blocks together to form an ordered organization. [539] Co-assembly results in multifunctionality or in generation of some special properties by the combination of the two partners which cannot be achieved by any one of them. In addition to co-assembly between molecules of same kind, for example peptide molecules, several different kinds of molecules like DNA, porphyrin rings, proteins etc. also have been shown to co-assemble with peptides[540-544] and give rise to materials with diverse applications. Supramolecular co-assembly between two or more distinct functional peptide building blocks results in structurally complex and diverse nanostructures. Co-assembly can take place in four possible ways, namely cooperative, orthogonal (self-sorting), random and destructive co-assembly (Figure 3.2).[545,546]

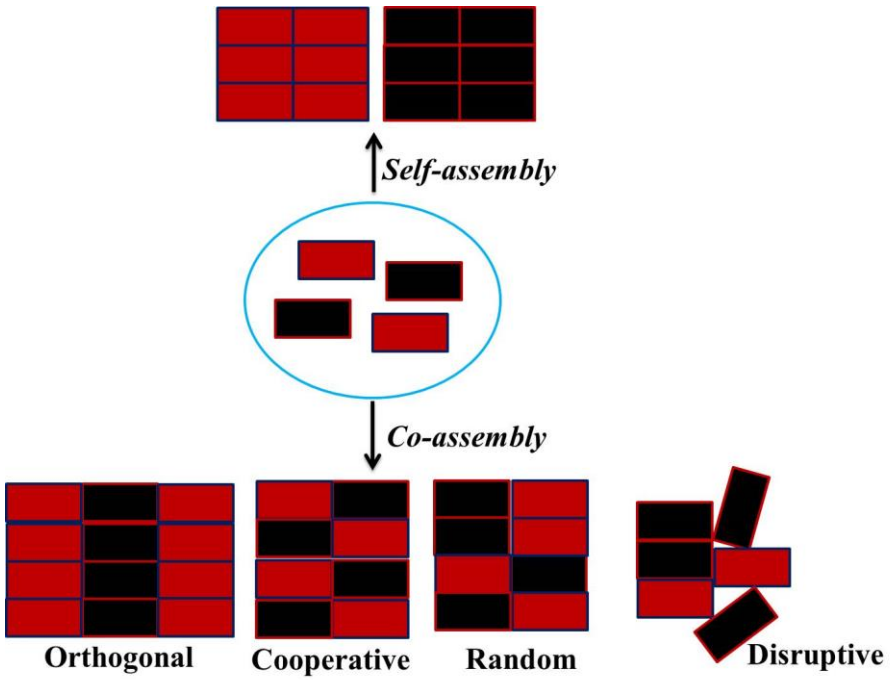

Figure 3.2: Peptide supramolecular co-assembly. Schematic illustration of how two peptide building blocks (black and red bricks) can self-assemble into an ordered architecture. Mixing them results in a complex co-assembled architecture (wall comprising of both black and red bricks) *via.* four possible supramolecular arrangements such as cooperative, orthogonal (or self-sorting), random and disruptive co-assembly.

In cooperative self-assembly, two peptide building blocks interact with each other to give rise to architectures in which both the components are arranged in alternate fashion. This kind of assembly usually occurs in cases where the individual components are very much similar to each other with minor differences. In contrast, orthogonal self-assembly or self-sorted co-assembly occurs when the constituent partners assemble independently on their own in the presence of the other. Such phase separated co-assembly is particularly necessary in fabricating p-n heterojunction photovoltaics. Designing of orthogonally co-assembled systems is quite challenging as the two components involves different kinds of non-covalent interactions. Co-assembly in between different components can also occur in between the two extremes which involve various degrees of mixing and self-sorting. In random self-assembly,

organization in between the partners does not occur in any precise manner while in destructive self-assembly, organization of one of the components is disrupted by the other. The interplay between the mixing ratios of the individual building blocks allows adaptable co-assembly mechanism to tune the morphology and the resulting physical, chemical and mechanical properties leading to relevant applications of these multifunctional supramolecular architectures. [327, 546] Different kinds of non-covalent forces, most importantly aromatic interactions[545, 547-549] and electrostatic interactions[227,550] have been used in the design of co-assembled systems. Enantiomeric peptides,[397,551] chemical[552] and electrochemical stimuli[553] and enzymatic reactions[554] have also been exploited in various studies to generate co-assembled systems. Co-assembled systems have been vastly employed in controlling physical dimensions of nanostructures,[555,556] generating non-canonical complex topologies, [557] light harvesting systems, [558] conducting architectures, [559] biocatalytic assemblies[560] and biomimetic scaffolds for tissue cultures.[334]

As discussed in the last chapters, water pollution is an eminent threat to the health of modern world and requires urgent action. Removal of toxic organic dyes and metal ions from water is an important application of hydrogels.[304, 305, 561] Peptide hydrogels are extremely efficient in removal of contaminants from water, since they are water permeable, possess a high surface area, are biodegradable and reusable.

3.2. Arsenic Detection

Arsenic poisoning of the underground water is a severe environmental problem worldwide. Millions of people in more than 70 countries are affected by arsenic poisoning of the drinking water. The exposure to Arsenic can have disastrous health consequences if not detected at correct time.[562] The most toxic forms are the oxo anions of Arsenic in its +III and +V oxidation states., namely arsenites (AsO_2^-) and arsenates (AsO_3^-).[563] This evokes an urgent need for highly selective and robust moieties for detecting arsenic. There are only very few

examples where peptides have been used for detection of arsenic. [443, 563, 564] A unique As(III)-binding peptide with a sequence of T-Q-S-Y-K-H-G was obtained through the repeated positive screening against As(III) with Limit of Detection (LOD) of 54 nM and negative screening against some representative foreign metals from a phage peptide library.[564]

3.3. Present Study

In this chapter, we have designed two charge complementary peptides A1 (WLVFFK) and A2 (WLVFFE) with an intention of studying the self-assembly of each of the peptides and their co-assembly. We rationally designed the peptides with features that would facilitate assembly. Both the peptides consisted of the LVFF moiety which is derived from the Alzheimer's amyloid β peptide sequence[565] and is known to form β-sheet conformation[566]. In order to make the peptides water soluble, we added basic Lys and acidic Glu in the sequence of A1 and A2 respectively. Electrostatic interaction in between the oppositely charged side chains at physiological pH would facilitate co-assembly of the two peptides. A Tryptophan (Trp) residue was added at the N-terminus of the peptides, to be able to use its intrinsic fluorescence properties in monitoring the self-assembly process. Also, the aromatic side chain of Trp might help in the stacking of the peptides to form self- assembled structures leading to gelation. We have thoroughly studied the mechanisms of self-and co-assembly in these systems. We have employed these hydrogels obtained in wastewater management. A1 hydrogel and the co-assembled gels of A1 and A2 were capable of absorbing cationic, anionic and neutral organic dyes individually and from a mixture in water with high efficiency (≥80% efficiency). The gels could be used recyclably for about three consecutive cycles. Both kinds of hydrogels were also capable of absorbing toxic heavy metal ions like Pb^{2+} and Hg^{2+} from water in addition to that of metal ions like Co^{2+} and Ni^{2+}. Peptides A1 and A2 could act as selective sensors for anions like AsO_2^- and AsO_3^- where arsenic is present in

its most toxic oxidation states like As (III) and As (V) respectively. Figure 3.3 gives an overview of the work done in the present Chapter.

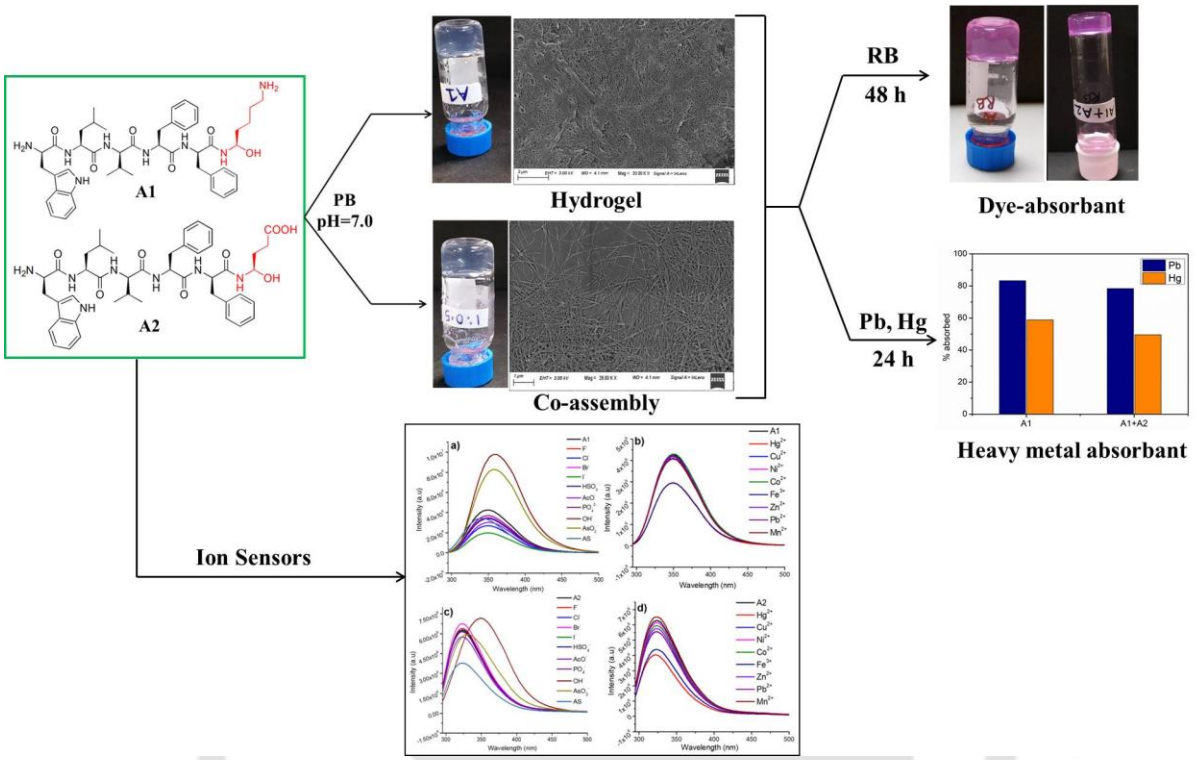

Figure 3.3: Schematic of the work done in the present chapter.

3.4. Experimental Details

3.4.1. Synthesis and Purification:

The two peptides A1 (H_2N-WLVFFK-COOH) and A2 (H_2N-WLVFFE-COOH) were synthesized by standard solid phase peptide synthesis (SPPS) using Fmoc Chemistry on Wang resin (0.1 mmol). Deprotection of the Fmoc group was achieved by 20 % piperidine in DMF. The amino acids were coupled using hydroxybenzotriazole (HOBt) and benzotriazole-1-yl-oxy-tris-pyrrolidino-phosphonium hexafluorophosphate (PyBOP) as coupling reagents in DMF. After attaching all the amino acids, the peptides were cleaved from the resin using 95% TFA and were precipitated in cold diethyl ether. The peptides were purified using reverse phase HPLC on a C18 column using acetonitrile/water gradient. After purification, the peptides were characterized using analytical HPLC on C18 column to check its purity

using acetonitrile/water as solvent system (Appendix A, Figure A5a, b, Page III). Further they were characterized by ESI-MS (Appendix A, Figure A6a, b, Page IV) and ^{1}H NMR spectroscopy (600 MHz) (Appendix A, Figure A7 and A8, Page IV, V).

ESI-MS of A1. Calculated mass= 838.4741 Da, Calculated $(M+H)^{+}$=839.4775 Da, Observed $(M+H)^{+}$= 839.4917 Da, Observed $(M+2H/2)^{+}$= 420.2499 Da

ESI-MS of A2. Calculated mass= 839.4218 Da, Calculated $(M+H)^{+}$=840.4251 Da, Observed $(M+H)^{+}$= 840.4435 Da, Observed $(M+2H/2)^{+}$= 420.2528 Da.

A1: ^{1}H NMR ((Appendix A, Figure A7) (600 MHz, DMSO-d_6) δ 10.98 (s, 1H, -COOH at the C-terminus), 8.63 (s, 1H, -NH of Trp indole ring), 8.15 (d, 1H, backbone NH), 8.00 (d,1H, backbone NH), 7.93 (d, 1H, backbone NH), 7.71 (d,1H, backbone NH), 7.36 (d,1H, backbone NH), 7.24 – 6.99 (m, 14 Hs, Phenyl rings of Phe and Trp), 4.57 – 4.48 (m, 3Hs, α H of Phe and Lys), 4.43 (d, 1H, α H of Trp), 4.21-4.09 (m, 3Hs, α Hs of Leu, Val and Lys; merged), 3.91 (s, 1H, -CH of indole ring) 3.05-3.00 (m, 2Hs, beta Hs of Trp), 2.98-2.88(3Hs, β Hs of Leu and Val) , 2.83-2.68 (m, 4H, β Hs of Phe), 2.29-2.24 (m, 2Hs, ε Hs of Lys), 1.92 – 1.78 (m, 4H, -NHs at the N-terminus), 1.62-1.53 (m, 2H, β Hs of Lys), 1.48 – 1.41 (m, 2H, δ Hs of Lys), 1.41 – 1.35 (m, 2H, γ Hs of Lys), 0.90 – 0.70 (m, 12H, methyl Hs of Leu and Val), (δ 2.50 for solvent residual peak, δ 3.33 for H_2O).

A2: ^{1}H NMR ((Appendix A, Figure A8) (600 MHz, DMSO-d_6) δ 10.99 (s, 2Hs, -COOH of Glu, -COOH at the C-terminus), 8.63 (s, 1H, -NH of Trp indole ring), 8.23 (s, 1H, backbone NH), 8.11 (s, 1H, backbone NH), 8.03 (d, 1H, backbone NH), 7.94 (d, 1H, backbone NH), 7.71 (d, 1H, backbone NH), 7.43 – 6.94 (m, 14Hs, Phenyl rings of Phe and Trp), 4.59 – 4.50 (m, 2Hs, α H of Phe), 4.43 (s, 1H, α H of Trp), 4.16-4.10 (m, 3Hs, α H of Glu, Val, Leu), 3.91 (s, 1H, -CH of indole ring), 3.03 (m, 1H, β H of Val), 2.94 (m, 2H, β Hs of Trp), 2.85 – 2.68 (m, 4H, β Hs of Phe), 1.89-1.69 (m, 2Hs, β Hs of Leu), 1.65 – 1.50 (m, 4H, β and γ Hs

of Glu), 1.45 (m, 1H, γ H of Leu), 1.35 (q, 2H, -NHs at the N-terminus), 0.94 – 0.65 (m, 12Hs, methyl Hs of Leu and Val), (δ 2.50 for solvent residual peak, δ 3.33 for H_2O).

3.4.2. Formation of Hydrogels:

1.0 mg of A1 peptide was taken in 500 µL of sodium phosphate buffer (0.2 % wt/v; 2.38 mM) (pH=7.0) and then heated on a hot plate till the peptide dissolved which was then kept undisturbed at room temperature. It resulted in the formation of hydrogel after 2-3 hs of standing which was stable to inversion of the glass vial. We tried for the hydrogelation of A2 under same conditions but it did not form any gel. A1 also formed gel in 20% EtOH/phosphate buffer mixture at 0.2 % wt/v. A1 and A2 when taken in the ratio of 1:0.5 and 1:1 (wt/wt) formed hydrogel in sodium phosphate buffer at pH=7.0 whereas 1:2 and 1:3 resulted in the formation of viscous solution.

3.4.3. Determination of the Gel to Sol Transition Temperature for the Hydrogels:

For the hydrogels, the T_{gel} was obtained by placing the gel containing vial in an oil bath and then slowly raising the temperature of the bath at the rate of 1ºC per minute. The temperature was monitored using a thermometer and was recorded accordingly.

3.4.4. FESEM:

For the morphology of the hydrogels, preheated samples were casted on the silicon wafer and allowed to dry under vacuum before imaging. Peptide hydrogel A1 was taken at its MGC in sodium phosphate buffer system and in sodium phosphate buffer/EtOH mixture. The viscous solution of A2 in sodium phosphate buffer at 5 mM concentration was used for imaging. The morphology of the co-assembled systems of A1 and A2 was taken in the ratio of 1:0.5, 1:1, 1:2 and 1:3 in phosphate buffer.

3.4.5. FETEM:

FETEM studies were performed by casting 3 μL of the co-assembled hydrogels at 1:0.5 and 1:1 ratios in sodium phosphate buffer on carbon-coated copper grids (300 mesh). The grid was allowed to dry under vacuum at room temperature before imaging.

3.4.6. FT-IR Spectroscopy:

IR spectra of the samples were recorded using KBr pellet within the range of 1000-4000 cm^{-1}. FTIR of peptides A1, A2 and xerogels obtained from freeze drying the hydrogels of A1, A1+A2 (1:0.5 and 1:1) were recorded.

3.4.7. Rheology:

The viscoelastic properties of hydrogels A1, A1+A2 (1:0.5) and A1+A2 (1:1) were determined by rheological studies at 25 ºC. For measuring rheology, A1 hydrogel was prepared at 4.5 mg/mL (0.45 % wt/v) in phosphate buffer (pH=7.0) and in a mixture of EtOH/buffer system. The co-assembled hydrogels were prepared at 2:1 (wt/wt) and 2:2 (wt/wt) in 1 mL of phosphate buffer (pH=7.0). A strain sweep test was performed over a range from 0.1-100% strain at a fixed oscillatory frequency of 1 $rads^{-1}$. Furthermore, the mechanical strength of hydrogels was determined from the oscillatory test, i.e. frequency sweep, which was carried out under an appropriate strain 0.1% with the frequency ranging from 1-100 $rads^{-1}$.

3.4.8. Fluorescence Spectroscopy:

To look into the self-assembly pattern of the peptide A1 and A2, fluorescence experiment was performed by monitoring the fluorescence emission of the Trp moiety. A concentration dependent fluorescence was performed for A1 in 20% EtOH/ phosphate buffer and A2 in 40% EtOH/phosphate buffer system (0.00487-5 mM) keeping excitation wavelength at 280 nm.

3.4.9. PXRD:

Wide angle X-ray diffraction analysis was done (Cu-Kα radiation, λ = 1.5406 Å) for both the powdered samples of A1, A2 and the xerogels obtained from lyophilising the hydrogels of A1 and the co-assembled hydrogels.

3.4.10. Dye Absorption Studies:

At first the hydrogel was prepared as mentioned in the gelation experiment (1 mg in 500 µL of phosphate buffer, pH =7.0). Then, aqueous solutions of RB (20 µM), CV (40 µM), NR (110 µM) and Methyl Orange (MO) (70 µM) were added into the preformed gel and allowed to absorb. Also, aqueous solutions of two metal ions, Ni^{2+} (100 mM) and Co^{2+} (100 mM) were added to absorb. The dye/metal ion absorption was measured using UV-Vis spectroscopy from time to time to know the trend in absorption by the hydrogel. Further, the amount of dye unabsorbed in the supernatant was checked by monitoring the UV of the supernatant aqueous solution after 48 h and calculating the concentration from a standard calibration curve of the dye/metal ion (Appendix A, Figure A10a-d, A11a, b, Page VI). The dye absorption by the co-assembled hydrogel A1+A2 (1:1) was done in the similar fashion as described with two dyes RB and MO. The amount of dye/metal ion loaded in the hydrogel and the dye/metal ion loading efficiency were then calculated as follows:

Dye/Metal ion absorbed =Initial dye/metal ion- Unabsorbed dye/metal ion

% absorbed= Dye/metal ion absorbed/Initial dye/metal ion X 100

The dye and metal ion absorption from an all component mixture by the hydrogels was also checked using UV-Vis spectroscopy in which the aqueous solution of dyes (RB, MO, NR and CV) and the metal ion (Co^{2+} and Ni^{2+}) was mixed together and was added to the preformed hydrogel to absorb.

3.4.11. Reusability of the Hydrogel A1:

The hydrogel from A1 was prepared as discussed earlier at its MGC in phosphate buffer. Then 500 µL of 20 µM aqueous solution of RB was added into it and the dye was allowed to be absorbed for 24 h. After 24 h, the supernatant solution at the top was taken and its absorbance was measured from which the % of dye absorbed was calculated. Then to the dye absorbed gel ether was added as the release medium and it was kept undisturbed for 2 days after which the gel became clear. On the clear, dye free hydrogel, fresh solution of 20 µM RB was added again and left to be absorbed for 24 h. This cycle continued for 2 times after which the hydrogel was no longer be used further for dye absorption.

3.4.12. Anion Sensing:

A stock solution of 1 mM of the peptide A1 and A2 in 20 % and 40 % respectively in EtOH/water system was prepared. Stock solutions of 10 mM tetrabutylammonium salts of F^-, Cl^-, Br^-, I^-, $H_2PO_4^-$, OH^-, AcO^- and HSO_4^-; sodium salt of arsenite (AsO_2^-) and arsenic acid were prepared in water. Then a solution of 0.2 mM of the A1 and A2 were prepared from the stock solution. Also, 0.2 mM of all the anion solutions was prepared from the 10 mM stock solution. For monitoring UV and fluorescence spectra 500 µL of 0.2 mM of the peptide solution was taken and into it 500 µL of 0.2 mM anion solution was added so that the final concentration of the both the solutions become 0.1 mM. The fluorescence was monitored for all the anions with the peptide molecules at 280 nm.

3.4.13. Metal Ion Sensing:

A stock solution of 1 mM of A1 and A2 in EtOH/water system was prepared was prepared. Stock solutions of 10 mM of metal ion salts ($CoCl_2$, $PbCl_2$, $NiCl_2$, $CuCl_2$ $MnCl_2$, $Zn(NO_3)_2$, $Hg(OAc)_2$, $FeCl_3^+$) were prepared in water. Then a solution of 0.2 mM of A1 and A2 were prepared from the stock solution. Also, 0.2 mM of all the metal ion solutions were prepared

from the 10 mM stock solution. For monitoring fluorescence spectra 500 µL of 0.2 mM of the peptide solution was taken and into it 500 µL of 0.2 mM metal ion solution was added so that the final concentration of the peptide and the metal ion solution became 0.1 mM. The fluorescence was then monitored at 280 nm.

3.4.14. Titration of the Gelator Molecules with Specific Anions and Metal Ions:

500 µL of 0.2 mM of peptide solution in 20 % and 40 % respectively in EtOH/water system was taken in different 1 mL volumetric flasks and into it 500 µL of different concentration of the anion and metal ion solution were added so that the final concentration of the peptide solution becomes 0.1 mM. The Trp fluorescence these solutions was then monitored for the solutions at 280 nm.

3.4.15. Detection Limit:

For detection limit calculation, fluorescence of 0.01 mM solution of A1 and A2 in EtOH/water solvent system was measured at 280 nm for ten times. Then standard deviation (σ) of the intensity at the emission wavelength was calculated. Then titration of A1 and A2 with the anions and metal ions at very low concentrations were monitored (0.002-0.025 mM) and a linear plot of concentration versus intensity was obtained. From the linear plot, the slope (k) was calculated and was put into the equation below:

$$DL=3\ \sigma/k\ ;\ n=10$$

3.4.16. Pb^{2+} and Hg^{2+} Removal by Hydrogels A1 and A1+A2:

Hydrogel A1 and the co-assembled hydrogel A1+A2 were prepared at 2 mg and 2:2 (wt/wt) in 2 mL respectively in phosphate buffer system. Into it 2 mL of 20 mg/L aqueous solution of Pb^{2+} and 2 mL of 100 mg/L Hg^{2+} solution was added and left to be absorbed for 24 h. After that, the supernatant solution was analysed using atomic absorption spectroscopy. The

experiment was done in duplicate and the values obtained were average of two readings. The % absorbed was then calculated using the following equation,

Concentration of metal ion absorbed =Initial metal ion- Unabsorbed metal ion

% absorbed= Metal ion absorbed/Initial metal ion X 100

For Pb^{2+}, 217 nm was used as the wavelength for analysis, with 1 nm slit width for an optimum working range of 0.1-30 µg/mL and for Hg^{2+}, wavelength of 253 nm was used for analysis with 0.5 nm slit width with optimum working range of 2-400 µg/mL.

3.5. Results and Discussions

3.5.1. Gelation Study:

The chemical structures of the two peptides A1 and A1 are shown in Figure 3.4a, b highlighting the different structural components of the peptides. When subjected to gelation, it was found that A1 formed hydrogel in sodium phosphate buffer and also in 20% EtOH/sodium phosphate buffer upon heating and subsequent cooling (Figure 3.4c), whereas A2 under similar conditions failed to form gel. Also, when A1 and A2 were taken together in 1:1 and 1:0.5 ratios and subjected to similar treatment as that of A1, co-assembled hydrogel was formed (Figure 3.4d). It should be noted that the other ratios of A1 and A2, like 1:2 and 1:3 failed to form hydrogel under similar conditions. Thus it was obvious that either stoichiometric ratio or an excess of A1 favoured gelation. A mixture with excess of A2 failed to do so. Table 3.1 gives the characteristic features of the gels formed from A1 and A2.

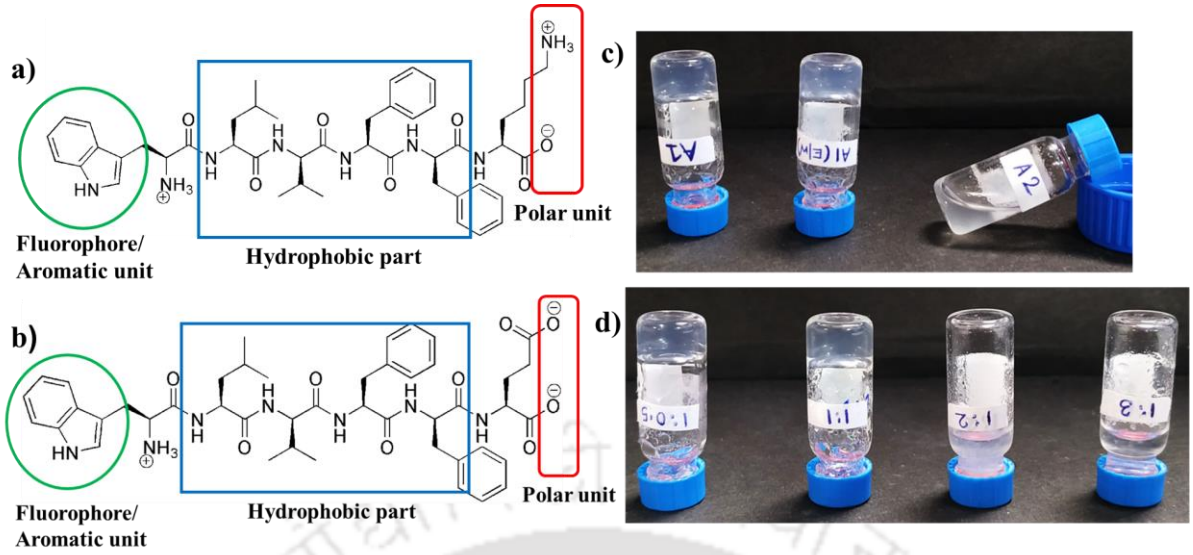

Figure 3.4: Chemical structures of a) A1, b) A2, c) Gel formation by A1 in sodium phosphate buffer (pH-7.0), EtOH/sodium buffer system and viscous solution of A2 in sodium phosphate buffer (pH-7.0) and d) Gelation by different ratios of A1 and A2. A1, A2 mixtures of 1:1 and 1:0.5 ratios produced gels while those of 1:2 and 1:3 ratios did not.

Table 3.1: Table summarizing gelation properties, physical state, Minimum Gelation Concentration (MGC) and sol-gel conversion temperature (T_{gel}) of A1, A2 and various ratios of A1+A2 mixtures

Peptides	Solvent system	MGC	T_{gel} (°C)	State
A1	PB (pH=7.0)	0.20 %w/v	60	Transparent
A1	PB (pH=7.0)+ EtOH	0.20 %w/v	54	Translucent
A2	PB (pH=7.0)	-	-	Viscous solution
A1+A2	PB (pH=7.0)	1 mg each in 0.5 mL (0.40%w/v)	56	Translucent
A1+A2	PB (pH=7.0)	1+ 0.5 mg in 0.5 mL (0.30%w/v)	52	Translucent
A1+A2	PB (pH=7.0)	1+ 2 mg in 0.5 mL (0.60%w/v)	-	Viscous solution
A1+A2	PB (pH=7.0)	1+ 3 mg in 0.5 mL (0.80%w/v)	-	Solution

Since A1 and A2 contained charged amino acid residues in them and had unprotected termini, therefore, their overall charge was pH dependent. The pKa of the α-carboxyl group and the amino groups are about 3 and 8 respectively, while the pKa of the side chain in Glu and Lys are about 4 and 11 respectively. Thus at acidic pH(<3), A1 had +2 charge, at neutral pH(~ 7.0), it had +1 charge while at the basic pH(>11), it had -1 charge. A2 on the other hand had +1 charge at acidic pH (<3), -1 charge at neutral pH and a -2 charge at basic pH(>11). As self-assembly of the peptides requires close approach of the molecules, it would be difficult for A1 to assemble in acidic pH, and A2 in basic pH due to the electrostatic repulsion in between them, owing to in the double positive and negative charges respectively. A1 neither formed gel nor any well characterized morphology in water at neutral (pH=7.0) or alkaline pH (pH=10), wherein it carried either a single positive or negative charge. A1 formed hydrogel in sodium phosphate buffer at pH 7.0 and in a mixture of 20% EtOH/ sodium phosphate buffer pH 7.0 upon heating and subsequent cooling (Figure 3.4c). Phosphate ions present in the buffer might play a crucial role in neutralizing the electrostatic repulsive forces amongst the A1 molecules, leading to their close approach and formation of the hydrogel. This might explain the inability of A1 to form gel in water alone. A2 on the other hand, did not form gel under any experimental conditions that were tried by changing the solvent, pH, salt concentration and gelation stimulants (sonication, vortexing, heating etc.). In order to investigate if the position of the charged residue in the primary sequence of A2 had any influence on its gelation capability, peptide A3 (Figure 3.5) was designed in which the Glu residue was positioned at the N terminus. However just like A2, A3 did not form gel under any of the experimental conditions that were tried. This proved that the position of the amino acid residue did not have any effect on its gelation ability of the negatively charged peptide.

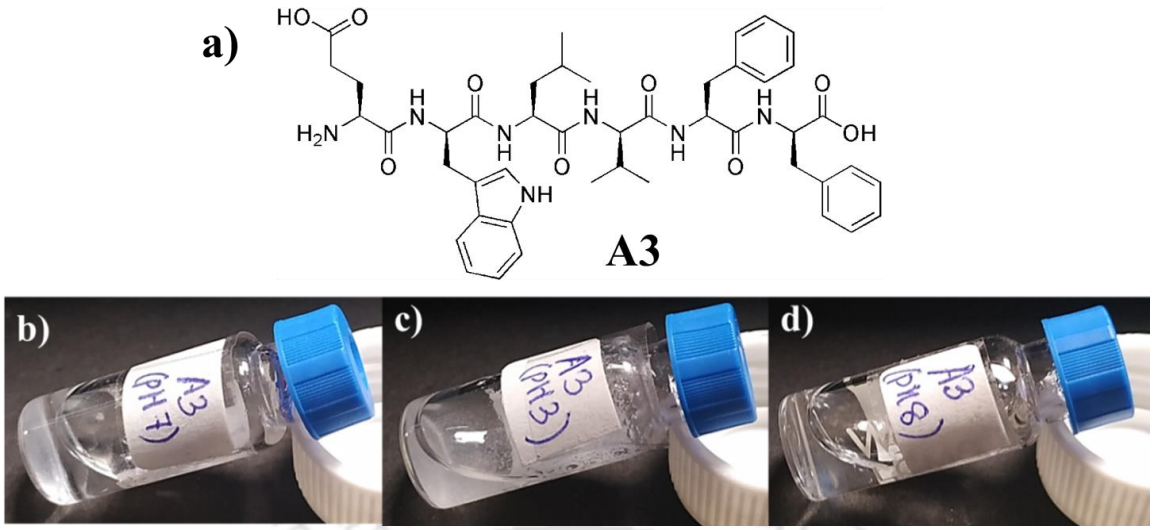

Figure 3.5: a) Chemical structures of A3 (EWLVFF). Photographs of A3 in different pH systems b) sodium phosphate buffer pH=7, c) citrate buffer pH 3.0 and d) sodium phosphate buffer pH=8 at 2mg / 0.5 mL concentration. All the systems (b-d) were first heated and the cooled to check the gelation ability.

The very small positive ion Na^+, present in the buffer, was most probably unable to diffuse the negative charge on A2 at neutral pH and induce assembly in them. The slight difference in the length of the hydrophobic side chain of the Lys and Glu residues might be responsible for such a difference in the gelation behaviour of A1 and A2. Additionally the point charge in the side chain of Lys compared to the delocalized charge on the carboxylate group of Glu residue might also contribute to this difference. In the co-assembled systems, mixtures that contained higher proportions of A2, resulting in an overall negative charge at the neutral pH, failed to form hydrogels proving the point further. This further proved that electrostatic interactions mediated *via.* counter ions from the buffer was the most important factor propelling assembly on these systems.

3.5.2. Morphological Studies:

Morphological features of the gel formed by A1, A2 and (A1+A2) have been studied by FESEM and FETEM. In Figure 3.6a-c, it was found that, A1 formed a dense mesh like

morphology in sodium phosphate buffer, pH 7.0 (Figure 3.6a), while it formed well entangled fibrous network like morphology in EtOH/ sodium phosphate buffer mixture (Figure 3.6b). A2 formed irregular aggregate-like morphology in sodium phosphate buffer (pH=7.0) (Figure 3.6c).

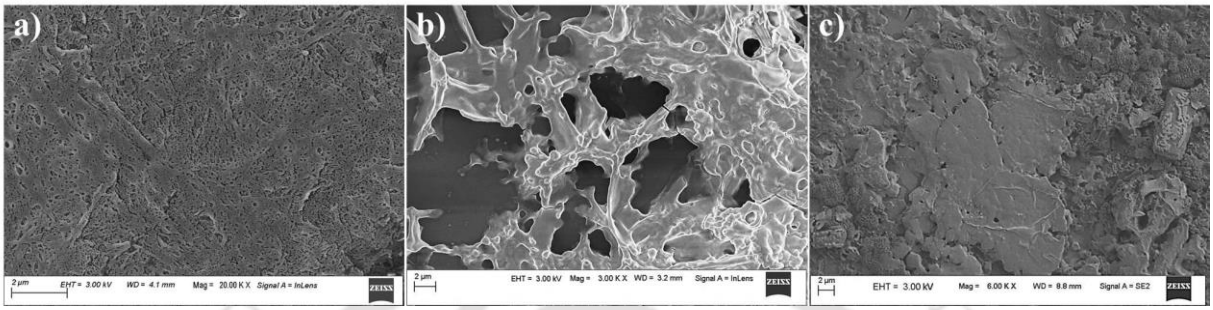

Figure 3.6: FESEM images of a) A1 hydrogel in sodium phosphate buffer (pH=7.0), b) A1 hydrogel in EtOH/sodium phosphate buffer system at CGC and c) viscous solution of A2 at 5 mM in sodium phosphate buffer (pH=7.0).

Figure 3.7a-d shows the morphology of the co-assembled systems formed from A1 and A2 taken in various ratios. It is found that, a well entangled fibrous network was observed in case of the co-assembled hydrogel formed by taking A1 and A2 in the ratio of 1:0.5 and 1:1. The viscous solutions obtained by other ratios gave an aggregate kind of morphology when visualised in FESEM.

To have a closer look at the morphology of the co-assembled hydrogels, FETEM was performed on the two co-assembled hydrogels. Both the 1:1 and 1:0.5 hydrogels contained fiber like morphology. The hierarchical self-assembly is clearly observable in the images where finer fibers are seen to form flatter fiber-bundles. (Figure 3.8a-b). Formation of uniform fibre like morphology in both the co-assembled gels is a clear indication of cooperative self-assembly in the system.

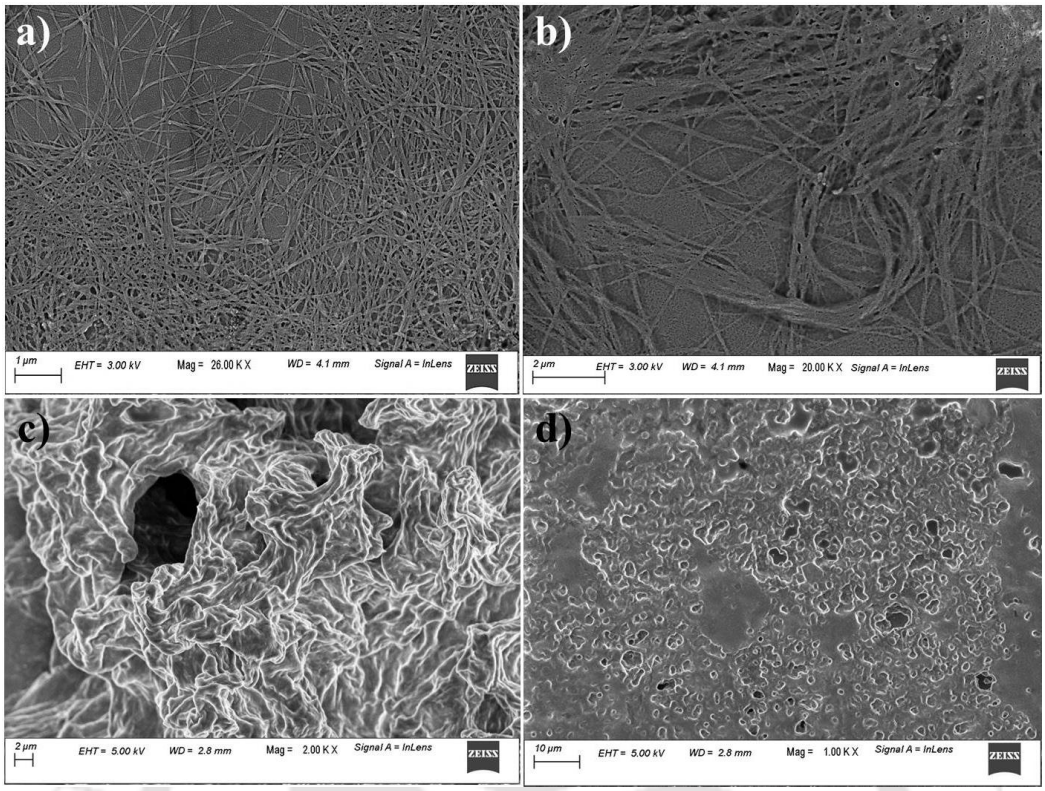

Figure 3.7: FESEM images of hydrogel of A1+A2 in the ratio of a) 1:0.5 wt/wt, b) 1:1 wt/wt, c) 1:2 wt/wt and d) 1:3 wt /wt ratio in sodium phosphate buffer at pH=7.0.

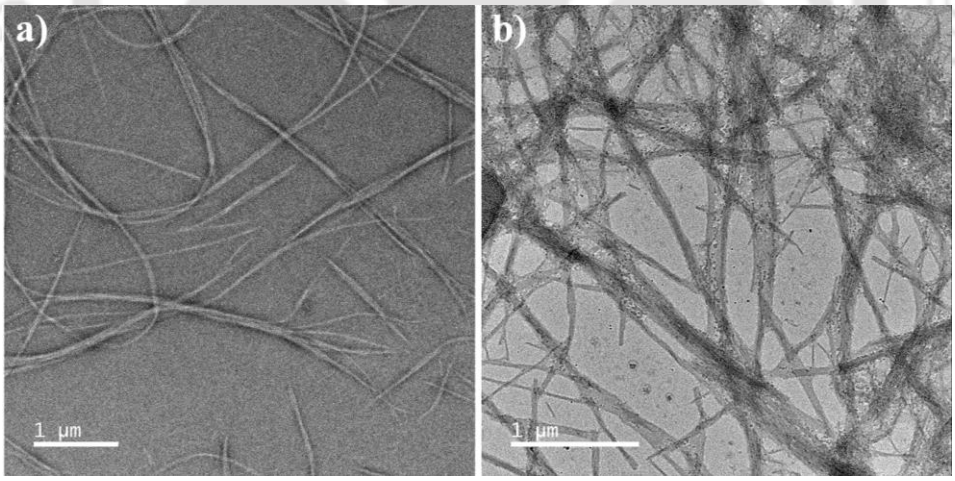

Figure 3.8: FETEM of A1+A2 hydrogel in sodium phosphate buffer, pH=7.0, a) 1:0.5 and b) 1:1 (wt/wt).

3.5.3. Viscoelastic Properties of the Hydrogels:

Viscoelastic property of the hydrogel was studied by rheology using 0.45 w/v % A1 hydrogel in a) phosphate buffer at pH 7.0 (Figure 3.9a, b) and b) 20% EtOH/phosphate buffer (Figure 3.9c, d). In the angular frequency sweep experiment performed at a constant strain of 0.1% at 25°C, for both the hydrogels, G′ was found to be dominating over G″ till about 100 rad/s (Figure 3.9a, c). Also, G′ and G″ were found to be independent of angular frequency, in the region of 1-100 rad/s which indicated the formation of stable hydrogels. The value of storage moduli G´ was of the order of 10^2-10^3 Pa for A1 hydrogel in sodium phosphate buffer and in the EtOH/ sodium phosphate buffer suggesting that the hydrogels formed in both the systems were mechanically robust. In strain sweep experiment, G′ was found to be higher than G″ till a particular strain (Figure 3.9b, d), beyond which the two crossed each other, indicating loss of gel nature for both the systems.

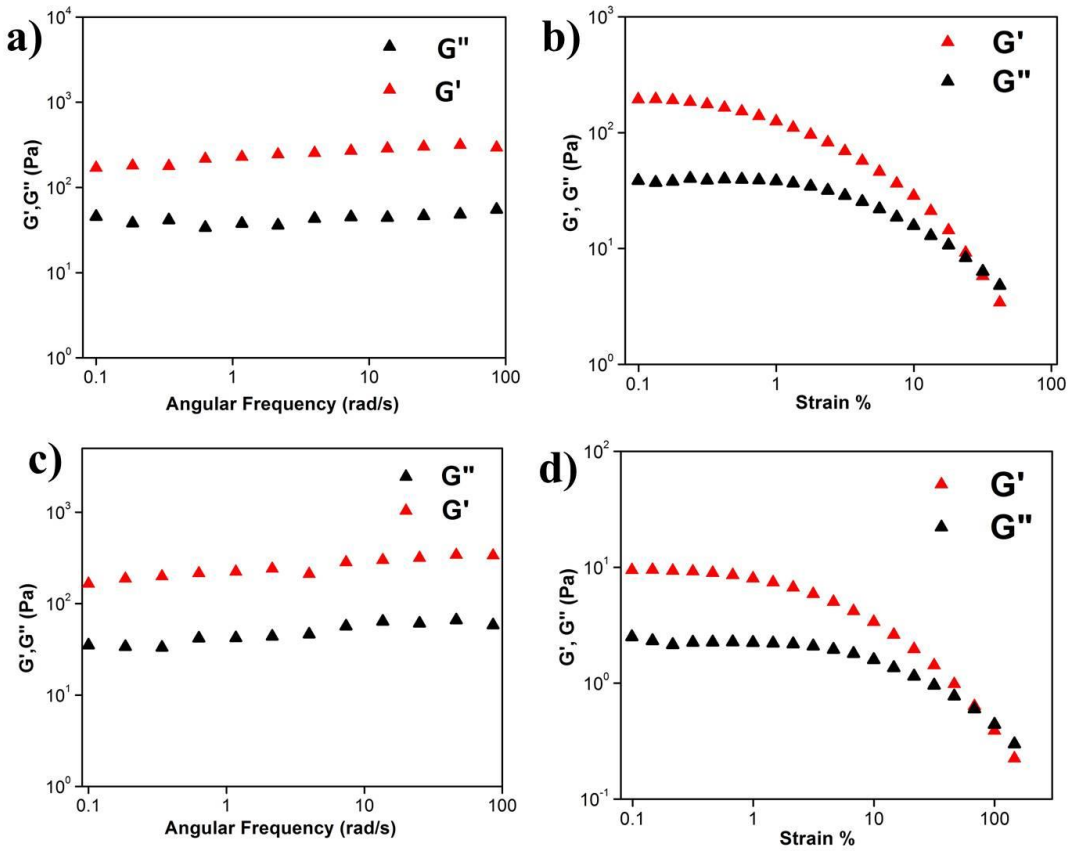

Figure 3.9: Angular frequency and strain dependence of the dynamic storage moduli (G′) and the loss moduli (G″) of hydrogel A1 at 0.45 % wt/v in a, b) sodium phosphate buffer; c, d) 20% EtOH/sodium phosphate system respectively.

We have then checked the mechanical strength of the co-assembled hydrogels formed from A1 and A2 taken in ratios 1:0.5 (2 mg and 1 mg respectively for A1 and A2) and 1:1 (2 mg and 2 mg respectively for A1 and A2) in 1 mL of the solvent. We observed that in the frequency sweep experiment (Figure 3.10a,c), the G′ values for the co-assembled hydrogels 1:0.5 and 1:1 were between 10^0-10^1 and 10^2-10^3, which were lower and higher than the A1 hydrogel respectively, suggesting that the 1:0.5 and 1:1 co-assembled hydrogels were weaker and stronger than A1 respectively.

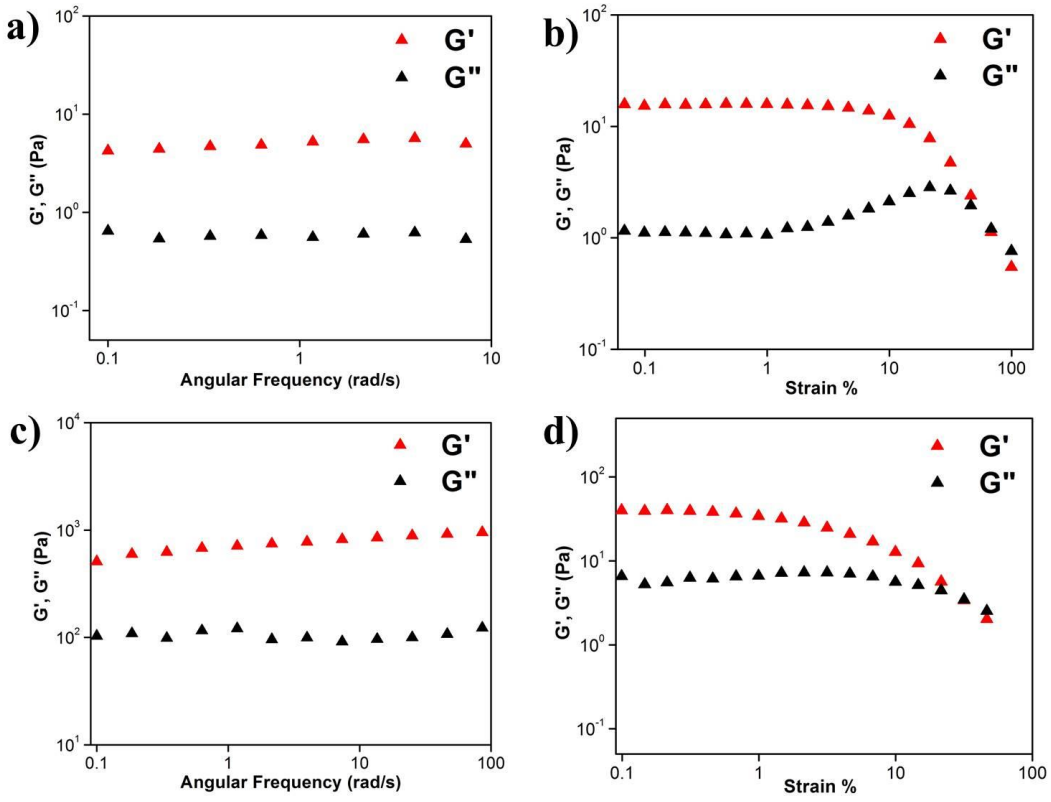

Figure 3.10: Angular frequency and strain dependence of the dynamic storage moduli (G′) and the loss moduli (G″) of co-assembled hydrogels formed from a, b) A1+A2=1:0.5 and c, d) A1+A2=1:1 in sodium phosphate buffer (pH=7.0).

The increased robustness of the 1:1 co-assembled hydrogel with respect to the A1 self-assembled hydrogel might be attributed to the additional electrostatic interactions in between the differently charged peptides in the co-assembled system. In the A1 hydrogel, assembly was mediated through the phosphate ions while in the co-assembled hydrogel, this was not necessary. Complementary charges on A1 and A2 led to favourable interactions in the 1:1 co-assembled hydrogel. However, in the 1:0.5 co-assembled gel, there was an excess of positive charges and hence the assembly had to be mediated through the phosphate ions. Thus the 1:0.5 hydrogel was weaker than the 1:1 hydrogel. In strain sweep experiment, G′ was found to be higher than G″ till a particular strain (Figure 3.10b, d) for both the co-assembled gels, beyond which the two crossed each other, indicating loss of gel nature for both the systems.

3.5.4. Factors Driving Self-Assembly:

3.5.4.1. Fluorescence Study: Both the designed peptides A1 and A2 had a Trp residue each in them. We used the intrinsic fluorescence of the Trp residue to study the assembly processes in the peptides A1 and A2. The fluorescence emission maxima of Trp was monitored as a function of peptide concentration (Figure3.11 a-b). The fluorescence emission intensity (λ_{max} = 353 nm) increased proportionately with the increase in the concentration of both the peptides till 0.625 mM (Figure 3.11a) and 1.25 mM (Figure 3.11b) for A1 and A2 respectively, beyond which it quenched with further increase in the concentration. In A1, the quenching in the fluorescence emission maxima was accompanied by a blue shift ($\Delta\lambda$ = 10 nm) which is indicative of increase in the hydrophobicity, while in A2, no shift in peak position was observed. Quenching of the fluorescence intensities of the peptides with increasing concentration indicates π-π stacking of the aromatic indole rings. This establishes that the aromatic stacking is one of the covalent interactions that drive molecular assembly. Quenching of the fluorescent emission intensity at a lower concentration for A1 compared to that of A2 indicates the better assembling nature of A1 compared to A2. Secondly, the

hypsochromic shift observed in A1, indicating increase in the hydrophobicity in the system with increased concentration, is an indicator of the better assembling ability of A1 in comparison to A2, where no shift was observed in the emission maxima. From the above experiments, we clearly understand that A1 has considerably greater assembling nature in comparison to A2 which probably leads to gelation in the former.

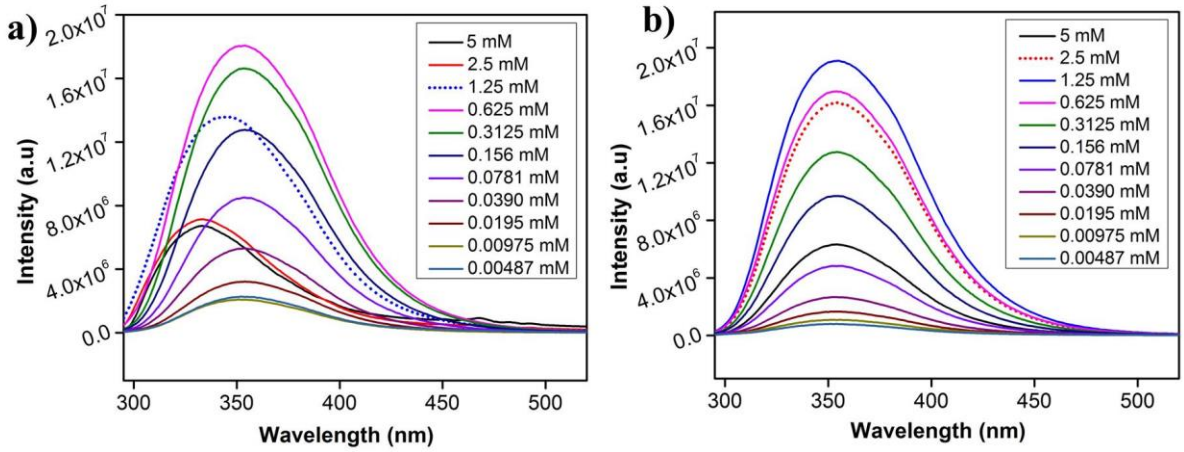

Figure 3.11: Concentration dependent fluorescence of a) A1 in 20% EtOH/sodium phosphate buffer, b) A2 in 40% EtOH/sodium phosphate buffer.

3.5.4.2. Backbone Conformation and Role of Hydrogen Bonding: In order to understand the backbone conformation of A1 and A2 and the role of hydrogen bonding in the self-assembly and co-assembly processes, solid state FTIR spectroscopy was performed on powdered samples of A1 and A2 and xerogels of A1 and A1+ A2 hydrogels (1:1 and 1:0.5 ratios) (Figure 3.12). Presence of peaks at around 1631 and 1682 cm^{-1} in all the systems, clearly indicated antiparallel β-sheet conformation for the peptides in individual powdered form or in hydrogel state. This is quite expected from the presence of the LVFF backbone moiety present in the peptides. Even in both the co-assembled systems (1:1 and 1:0.5), peptides A1 and A2 adopted an antiparallel β-sheet conformation. Presence of NH stretching peak at 3279 cm^{-1} in the FTIR spectrum of both powdered and xerogels indicated presence of extensive hydrogen bonding in the system.

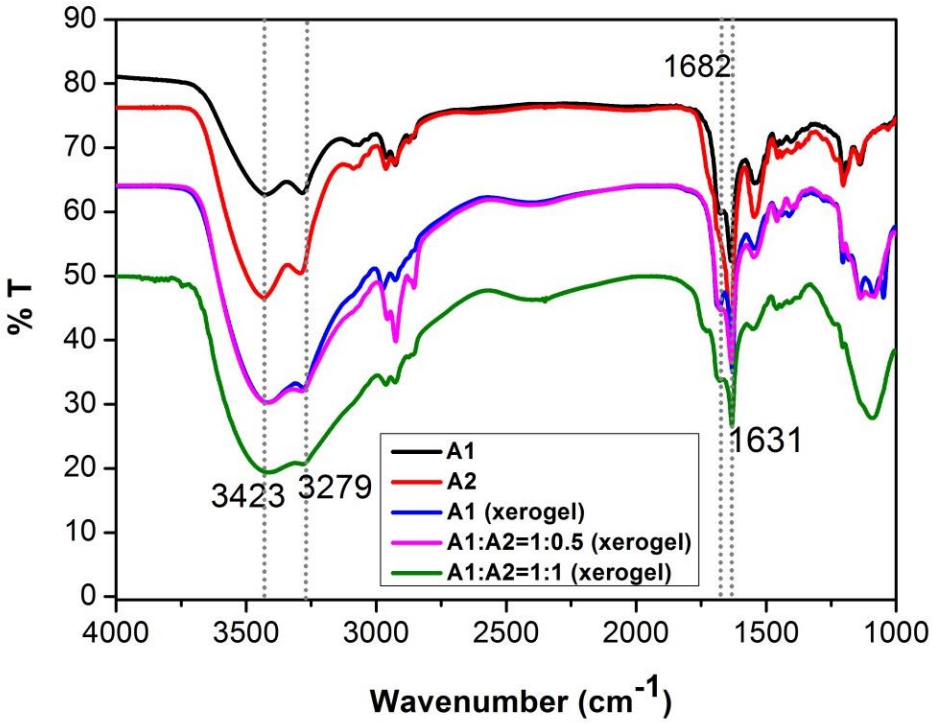

Figure 3.12: FTIR spectra of A1, A2, A1 xerogel, 1:0.5 and 1:1 ratio of the xerogels of A1+A2.

3.5.4.3. Molecular Packing: To understand the ordered arrangement of the peptides A1, A2 and the self and co-assembled systems, PXRD was performed (Figure 3.13, Table 3.2). In all the systems studied, a promiment peak at around 23° was obtained that corresponded to an interplaner distance of ~3.8Å. The typical centroid to centroid distance upon face to face interaction of two benzyl rings is about 3.8Å, indicating that very strong aromatic π-π interaction was present in all the systems. Additionally, in A1 and A2 another prominent interplaner distance of ~11.5Å was observed. This could be attributed to the distance in between the subsequent β-sheets. In all the xerogels studied, an interplaner distance of ~12.4Å was observed. This spacing was attributed to the distance in between the subsequent β-sheets in the xerogel structures.

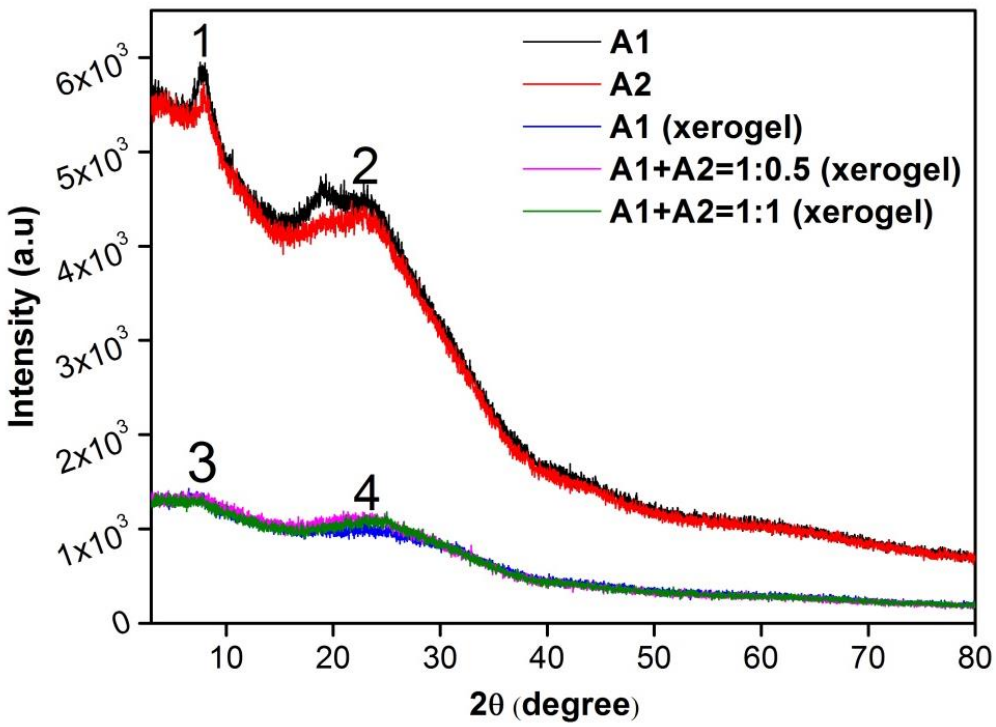

Figure 3.13: PXRD of A1, A2, A1 xerogel, 1:0.5 and 1:1 co-assembled xerogels of A1+A2.

It must be remembered that the xerogels were derived from the hydrogels that were formed in sodium phosphate buffer. Presence of water, ions in between the subsequent β-sheet layers might be responsible for increasing inter-sheet spacings observed in the xerogels. Thus, in summary, A1 and A2 consistently form β-sheet conformation in powdered state and in self-assembled or co-assembled xerogel state. As A1 and A2 have similar motifs in them (LVFF), their co-assembly occured in a facile manner without perturbing the backbone conformation of the peptides. The co-assembly between A1 and A2 was cooperative in nature. Presence of uniform fibers as seen from FETEM corroborates the fact. Secondly, strong aromatic π-π stacking interactions exist in all the systems and is another important interaction driving self-assembly.

Table 3.2: Interplanar distances observed from the PXRD in A1, A2, A1 xerogel, 1:0.5 and 1:1 co-assembled xerogels of A1+A2.

	Peak 1	**Peak 2**	**Peak 3**	**Peak 4**
A1	2θ=7.64°, d=11.56 Å	2θ=23.16°, d=3.84 Å	-	-
A2	2θ=7.82°, d=11.29 Å	2θ=22.86°, d=3.88 Å	-	-
A1 (xerogel)	-	-	2θ=7.20°, d=12.27 Å	2θ=23.12°, d=3.84 Å
A1+A2 (1:0.5) (xerogel)	-	-	2θ=7.02°, d=12.58Å	2θ=22.92°, d=3.87 Å
A1+A2 (1:1) (xerogel)	-	-	2θ=7.12°, d=12.40 Å	2θ=25.02°, d=3.55 Å

3.5.5. Mechanism of Self-Assembly:

As seen from the various experiments, electrostatic interaction, aromatic π-π stacking interaction and hydrogen bonding played important roles in the self-assembly and the co-assembly processes being studied here. At neutral pH, formation of hydrogel in the presence of phosphate buffer, suggested that the phosphate ions played a crucial role in diffusing the positive charge on the A1 peptides, bringing them close together to form the hydrogel. In the case of A2, the positive counter ions of phosphate buffer, being extremely small, might not have been able to diffuse the negative charge on A2 and bring about gelation. Hence electrostatic interactions played a very important role in these assembly processes. Difference in the nature of the charged groups and the slight difference in the hydrophobicity of the side chains of the charged amino acid residues might also have contributed to the difference in the gelation behaviour of the otherwise identical peptides A1 and A2. Figure 3.14 depicts the molecular arrangement involved in the self-assembly of A1.

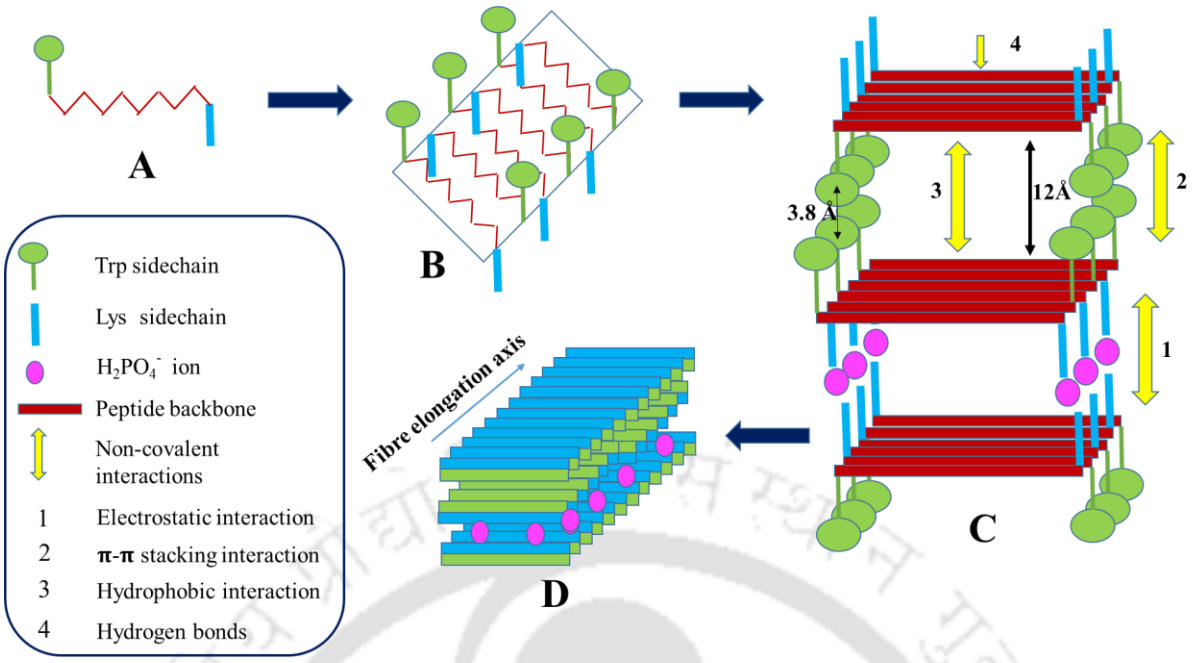

Figure 3.14: Schematic representation of the molecular arrangement involved in the self-assembly of A1.

A1 monomers formed antiparallel β-sheets as evidenced from the IR spectroscopy. The sheets were amphipathic in nature, having two distinct faces. One of the faces was hydrophobic in nature which contained the Trp side chain while the other face contained the charged Lys side chains. The side chains of the intervening LVFF moiety alternately faced opposite directions and pointed both towards the hydrophobic and charged faces of the β-sheets. Due to the formation of the antiparallel β-sheets, the positively charged amino terminus of one monomeric unit faced the negatively charged carboxylate end of the adjacent monomeric unit. This compensated the charge on the edges of the sheets. Next, the sheets stacked on each other in such a way that the hydrophobic face of one sheet confronted the hydrophobic face of the other. This stacking was favoured by the hydrophobic interaction in between them. Additionally, the Trp rings from one sheet formed π-π stacking with that from the other sheet. The stacking of the β-sheets was also favoured by the hydrophobic interactions in between the side chains of the LVFF moiety. The charged faces of the adjacent

β-sheets faced each other. The phosphate ions stacked in between such positively charged faces and neutralized the repulsion, thus bringing stability to the system. As this charge stabilization was absent in water, hydrogelation of A1 did not occur there. The stacking of the sheets led to formation of fibres. Such fibres came close together along the edges of the sheets. This was favoured by the electrostatic interactions in between the terminal charges, giving rise to thicker fibre bundles. The thick bundles entangled with each other and eventually gave rise to the mesh like morphology that was observed by FESEM.

Figure 3.15 summarized the mechanism of co-assembly of A1 and A2 in 1:1 ratio. Presence of an uniform fibre like morphology as seen from microscopic techniques like FESEM and FETEM, accompanied by the evidences that the backbone conformation of A1, A2 in the co-assembled gel was the same as in the self-assembled gel and interplaner spacings in the co- and self-assembled gels were identical, suggested that A1 and A2 underwent cooperative co-assembly. This was expected as peptides A1 and A2 were similar in their structure. As shown in the figure 3.15, A1 and A2 alternated to form β-sheets in which one face of the sheet was hydrophobic and contained the Trp side chain. The other surface of the sheet contained both the positive and the negative side chains of Lys and Glu residues from A1 and A2 respectively. Stacking of the β-sheets involved hydrophobic interactions and aromatic π-π stacking interactions in between the indole rings of the Trp chains in the hydrophobic faces. The charged face of the β-sheet contained positive and negative charges along the two edges. While stacking of the charged faces, the sheets approached an alternate fashion so that the oppositely charged edges faced each other giving rise to favourable electrostatic interactions. It was due to this interaction that the 1:1 co-assembled gel was stronger than the A1 hydrogel as observed from rheology. While in the later, the phosphate ions mediated the interaction in between the positive faces of the β-sheets, in the former co-assembled system, complementary charges on the constituent peptides gave rise to the favourable electrostatic

interactions that stabilized the system. The 1:0.5 hydrogel system underwent self-assembly pretty much the same way as the 1:1 system, with some minor differences. In the 1:0.5 co-assembled hydrogel, the peptides might have repeated as A1:A2:A1 units. This would give rise to β-sheets with edges containing mixed charges and the charged face containing overall positive charge. In this case phosphate ions from the phosphate buffer would help neutralizing the repulsive forces and bringing about stacking of the β-sheets as in the case of A1 hydrogel. Thus the 1:0.5 co-assembled gel was weaker than the 1:1 co-assembled gel. In the mixture ratios of A1 and A2, with higher amounts of A2, the system acquired excess negative charge which could not be stabilized by the small positively charged ions of the phosphate buffer and hence, there was no resultant hydrogelation just like A2.

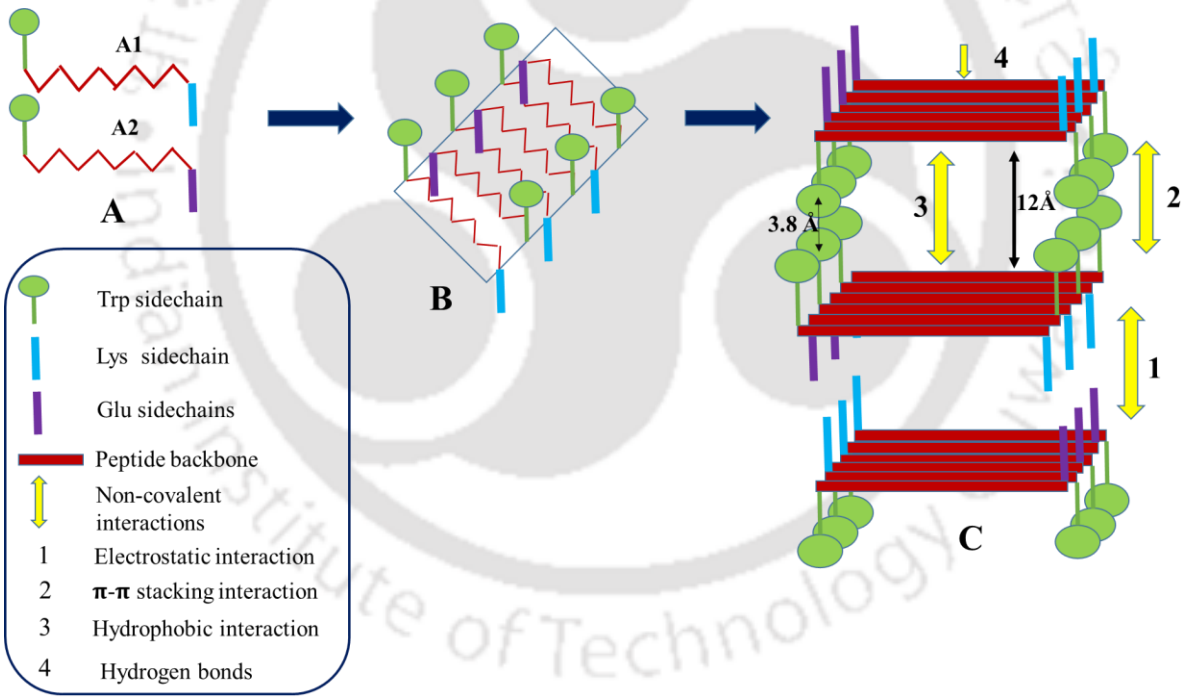

Figure 3.15: Schematic representation depicting the mechanism of co-assembly of A1 and A2 in 1:1 ratio.

3.5.6. Application of the Hydrogels in Dye and Metal Ion Absorption:

We have used the A1 hydrogel and the co-assembled gels of A1 and A2 for dye and metal ion absorption studies. The aqueous solution of the dyes or the metal ions was allowed to stand with the gel for 48 h. The UV absorbance of the solution was monitored over the time to obtain the amount of unabsorbed dye (Figure 3.16a-f). Amount of dye absorbed was back calculated from the initial concentration of the solution as discussed in the experimental section. All our hydrogels (self and co-assembled) acted as very efficient absorbents for the organic dyes like RB, CV, NR, MO and divalent metal ions Ni^{2+} and Co^{2+} (Figure 3.17, 3.18). It is mention worthy that the gels could absorb cationic, anionic and neutral organic dyes. The detailed quantification of the absorption efficiency of the hydrogels for the different hydrogels is tabulated in Table 3.3.

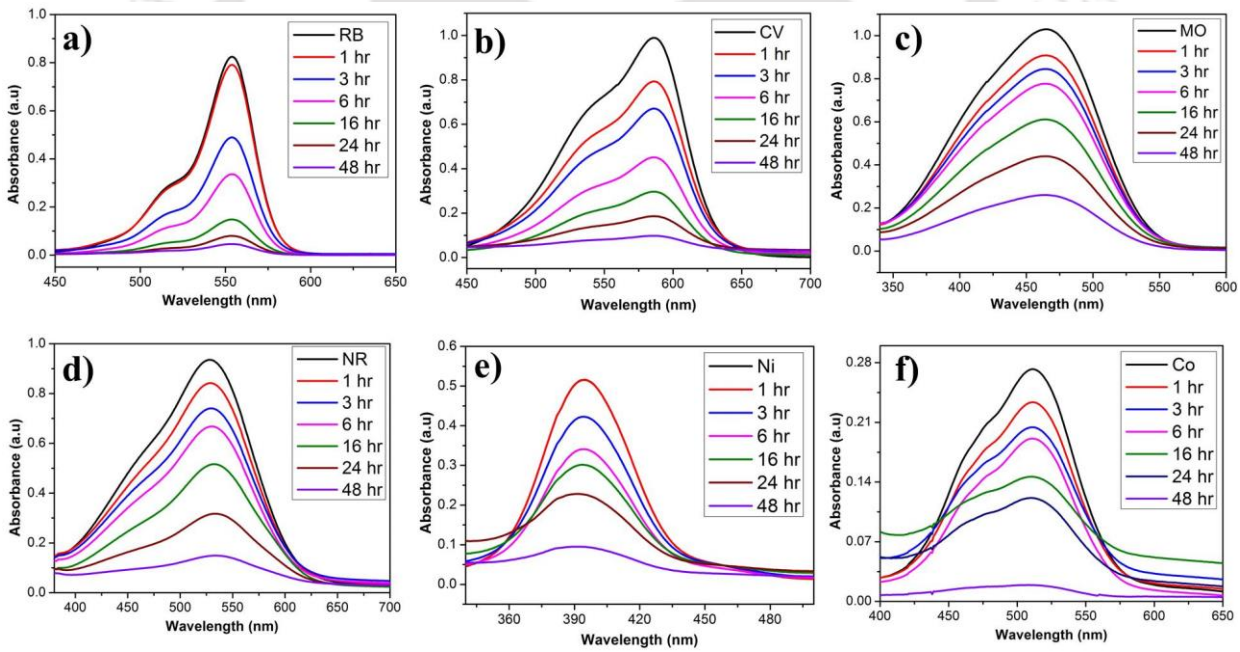

Figure 3.16: Dye/Metal ion absorption by A1 hydrogel a) RB b) CV c) MO d) NR e) Nickel Chloride and f) Cobalt Chloride by UV-Vis spectroscopy.

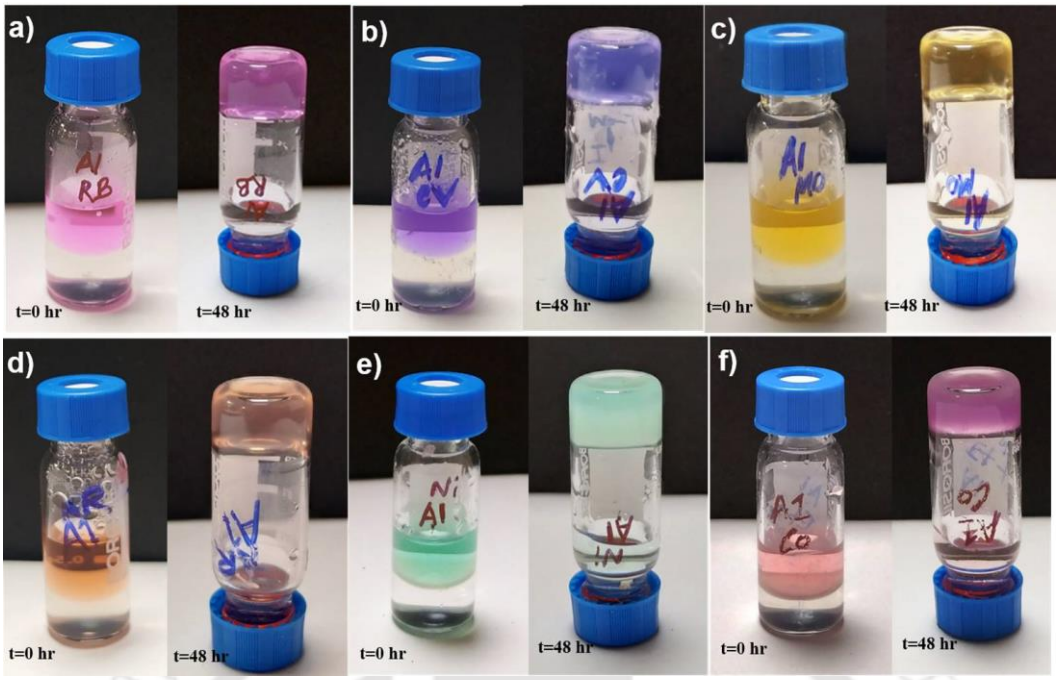

Figure 3.17: Gel pictures of dye/metal ion absorption by A1 hydrogel. a) RB, b) CV, c) MO, d) NR, e) Nickel Chloride (Ni^{2+}) and f) Cobalt Chloride (Co^{2+})

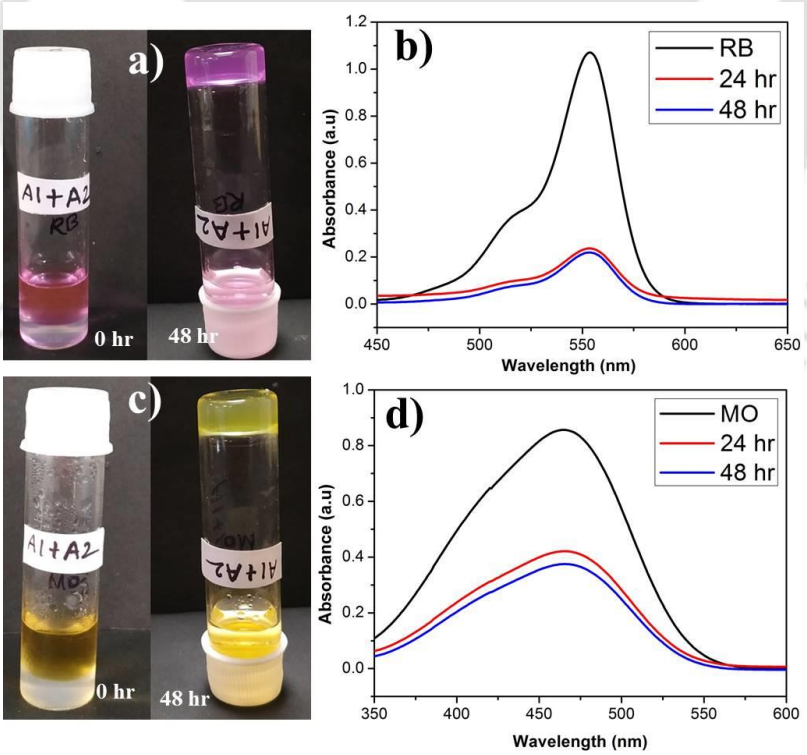

Figure 3.18: Dye absorption by hydrogel A1+A2=1:1. Photograph of dye absorbed hydrogel a) RB, c) MO; UV-Vis studies for dye absorption by the co-assembled hydrogel for b) RB, d) MO.

Table 3.3: Dye and metal ion absorption by the studied hydrogel systems

Dye/Metal salt	Nature	Loaded	% absorbed	Hydrogel system
RB	Cationic	20 µM	96.92	A1
CV	Cationic	40 µM	79.93	
MO	Anionic	70 µM	88.92	
NR	Neutral	110 µM	81.52	
Nickel Chloride (Ni^{2+})	Metal ion	100 mM	83.32	
Cobalt Chloride (Co^{2+})	Metal ion	100 mM	93.65	
RB	Cationic	20 µM	84.28	A1+A2
MO	Anionic	70 µM	83.47	

After looking at the efficiency of the hydrogels for absorption of individual dyes, we wanted to look at the efficiency of the hydrogels for the absorption of mixtures of dyes. As seen from the figure 3.19, both the self-assembled and the co-assembled hydrogels were capable of absorbing dyes (CV, NR, MO and RB) and metal ions (Co^{2+} and Ni^{2+}) from a mixture. Thus such hydrogels can be used in the real life applications, where the water is contaminated by several contaminants.

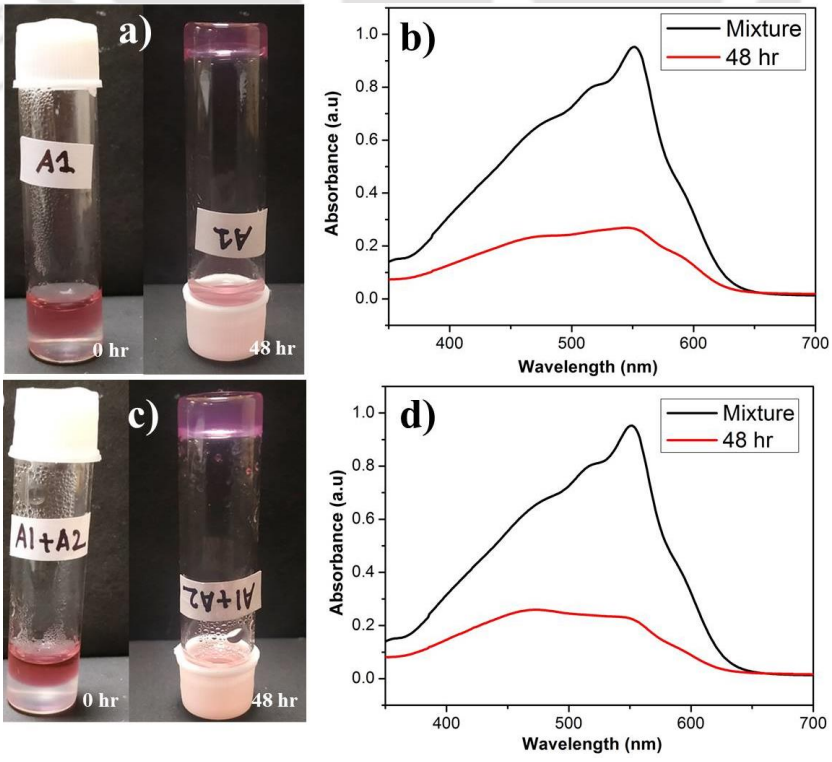

Figure 3.19: Photograph of mixture of dye/metal ion absorbed by hydrogel formed from a) A1, c) A1+A2; UV-Vis studies to show an all component mixture absorption by hydrogel b) A1, d) A1+A2.

3.5.7. Reusability of the Hydrogel A1:

In order to be efficiently used as a material for water purification, the material should be economic and hence, reusable. A1 hydrogel could be reused over three cycles for subsequent loading and release of the dye, after which the quality of the hydrogel degraded. Figure 3.20a is the pictorial representation of the hydrogel loaded with dye RB, its subsequent release in ether and reloading of the dye for the next cycle. Figure 3.20b shows the UV-Vis studies performed to quantify the amount of dye that could be loaded to the hydrogel in each cycle.

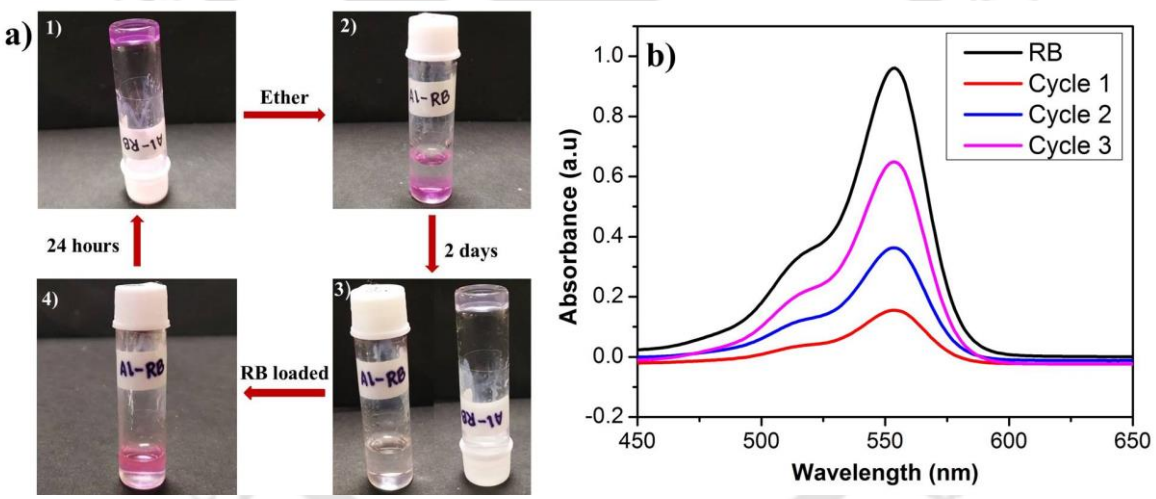

Figure 3.20: Reusability of hydrogel A1: a) Reusing hydrogel A1 for dye absorption, b) UV-Vis studies for quantifying the amount dye RB which could be loaded onto the hydrogel A1 after each cycle after a time period of 24 h.

It was observed that in the first cycle, the hydrogel A1 was capable of absorbing about 89% of RB. Upon addition of ether, the release medium to the dye loaded gel, and leaving it for 48 hs, the loaded dye was released. This was visibly evident from hydrogel becoming colourless and the ether layer turning pink. The integrity of the gel was intact as can be proved by the

vial inversion test. In the second and third cycles about 74% and 53% of dye was loaded onto the gel (Table 3. 4). After the third cycle, the gel degraded and could not be used further.

Table 3.4: Percentage of RB absorbed by hydrogel A1 in three cycles

No. of Cycles	RB absorbed (%)
Cycle 1	88.95
Cycle 2	73.80
Cycle 3	52.90

3.5.8. Removal of Toxic Metal Ions: Absorption of Pb^{2+} and Hg^{2+}:

A1 hydrogel and A1+A2 co-assembled hydrogels were utilized for the absorption of toxic heavy metal ions Pb^{2+} and Hg^{2+} from the aqueous solutions. After addition of the metal solutions on the hydrogels, and letting them stand for 24 h, the supernatant was analysed using AAS. The amount of unabsorbed ions in the supernatant was used to back calculate the amount of ions that was absorbed by the hydrogels. For both the self-assembled and the co-assembled hydrogels, Pb^{2+} ions was absorbed better (~80%) than the Hg^{2+} ions (~55%). Both the metal ions were dipositively charged, and Hg^{2+} was smaller in size than Pb^{2+} (Table 3.5). Thus the better absorption efficiency for Pb^{2+} was attributed to the smaller size of the counter ion (Cl^-) in comparison to that of $Hg^{2+}(OAc^-)_2$. Ni^{2+} and Co^{2+} which were also absorbed very efficiently (~ 80%) by the hydrogel systems were small in size accompanied by small counterions (Cl^-). Thus the metal ion absorption efficiency of the hydrogels may be dependent on the size of their counter ions.

Table 3.5: Pb^{2+} and Hg^{2+} absorption by the self- and co-assembled hydrogels:

Hydrogels	Metal ion	Conc. loaded (mg/L)	Conc. in the supernatant (mg/L)	Conc. absorbed (mg/L)	% absorbed
A1	Pb	20	3.34	16.66	83.30
	Hg	100	41.20	58.80	58.80
A1+A2 (1:1)	Pb	20	4.31	15.69	78.45
	Hg	100	50.45	49.55	49.55

In summary, we have been able to prove that our self and co-assembled hydrogels are highly efficient in absorbing different organic dyes and metal ions from water individually or from a mixture. It is mention worthy that these hydrogels can also absorb toxic metal ions like Pb^{2+} and Hg^{2+} from water efficiently. Thus, these cheap and robust materials are extremely prospective for future use in water remediation.

3.5.9. Ion Sensing Studies by Peptides A1 and A2:

We have employed our peptides A1 and A2 in sensing different kinds of ions. We have monitored the fluorescence of A1 and A2 in the absence and the presence of various anions like F^-, Cl^-, Br^-, I^-, HSO_4^-, $H_2PO_4^-$, CH_3COO^-, OH^- (as their Bu_4N^+ salts), AsO_2^- and AsO_3^- (Figure 3.21a, b) and also various metal ions like Hg^{2+}, Co^{2+}, Pb^{2+}, Ni^{2+}, Cu^{2+}, Mn^{2+}, Zn^{2+} and Fe^{3+} (Figure 3.24a,b). The spectroscopic studies were performed in water/EtOH as the peptides are not completely soluble in water. The anion and the metal salts were dissolved in water.

3.5.9.1. Response Towards Anions: Peptides A1 and A2 responded for arsenite (AsO_2^-), arsenate (AsO_3^-) and hydroxide (OH^-) anions. In the presence of other anions (F^-, Cl^-, Br^-, I^-, HSO_4^-, $H_2PO_4^-$, AcO^-), there was no change in the λ_{max} of the fluorescence emission and minor changes in peak intensities (Figure 3.21a, b). In the absence of anions, upon being excited at 280 nm, the fluorescence emission maxima for A1 and A2 were at 349 nm and 323 nm respectively. For, A1, upon addition of 0.1 mM AsO_2^- and OH^- the peak at 349 nm red

shifted to 357 nm and 358 nm respectively with an enhancement in fluorescence signal intensity (about 2 folds). In case of addition of 0.1 mM of AsO_3^- solution to A1, there was a blue shift to 341 nm, although the fluorescence intensity was not changed remarkably (Figure 3.21a). There was negligible effect on the fluorescence spectra of A1 in the presence of other ions. For A2, upon addition of 0.1 mM AsO_2^- and OH^-, the peak at 323 nm was red shifted to 330 nm and 349 nm respectively. In case of addition of 0.1 mM of AsO_3^- solution to A2, there was a decrease in the fluorescent intensity without any change in the peak position (Figure 3.21b). There was negligible effect on the fluorescence spectra of A2 in the presence of other ions. Thus it can be concluded that molecules A1 and A2 selectively sensed AsO_2^-, AsO_3^- and OH^- in solution.

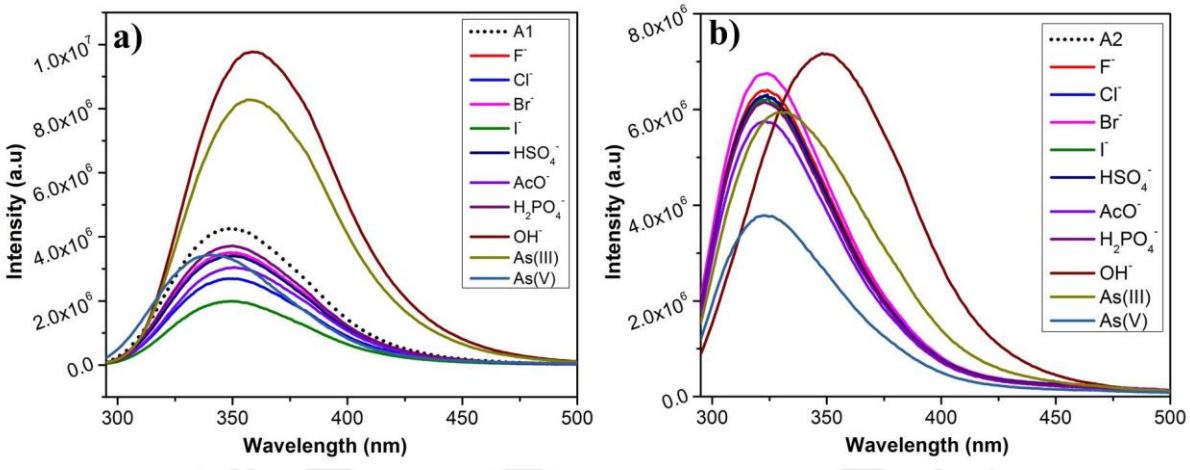

Figure 3.21: Sensing of Anions by a) A1 and b) A2 (Anions=0.1 mM, A1=0.1 mM and A2=0.1 mM).

To determine the sensitivity of the peptides towards the sensed anions, the fluorescence response of A1 and A2 was monitored as a function of anion concentration (Figure 3.22a-c, 3.23a-c). The concentration of the anions was varied from 0.02 mM to 2 mM. In case of A1, it was observed that for AsO_2^- and OH^-, upon increasing the concentration of the anions, there was a steady enhancement in the intensity of fluorescence signal upto 0.07 mM, after which the signal abruptly intensified accompanied by a red shift (Figure 3.22a, b). In case AsO_3^-

solution, there was an irregular shuffle in fluorescent intensity although, it eventually decreased upon increasing the concentration of AsO_3^- solution without any shift in the peak position. (Figure 3.22c).

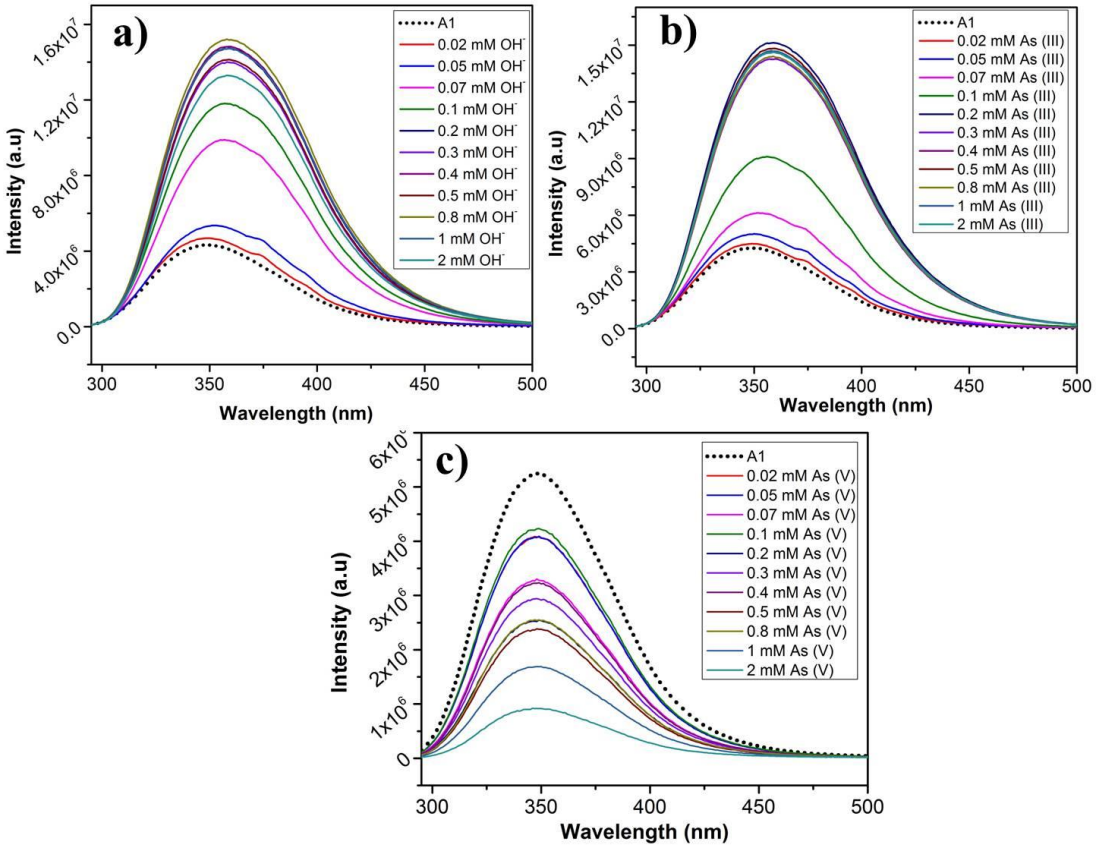

Figure 3.22: Anion sensing by A1: Titration of A1 with a) OH^- , b) As (III), and c) As (V).

In case of A2, similar trend in fluorescence signal was observed for AsO_2^- and OH^- ions as observed for A1. When the concentration of AsO_2^- and OH^- was increased from 0.02 mM, the fluorescence signal did not changed much except a red shift to 330 nm till 0.1 mM, after which there was a sudden increase in the signal along with a major red shift to 356 nm beyond which the fluorescence signal got saturated till 2 mM (Figure 3.23 a, b). In case of increasing concentration of AsO_3^-, at first the fluorescence intensity slightly increased, after which there was an irregular intensity shift of the signal followed by an eventual decrease in the signal intensity (at ~0.4mM) accompanied by a red shift to 347 nm (Figure 3.23c). The

mode of interaction of the anions OH- and AsO_2^- seem to be similar from their fluorescence response. This might be due to the similarity in the size of these two anions in comparison to AsO_2^- .

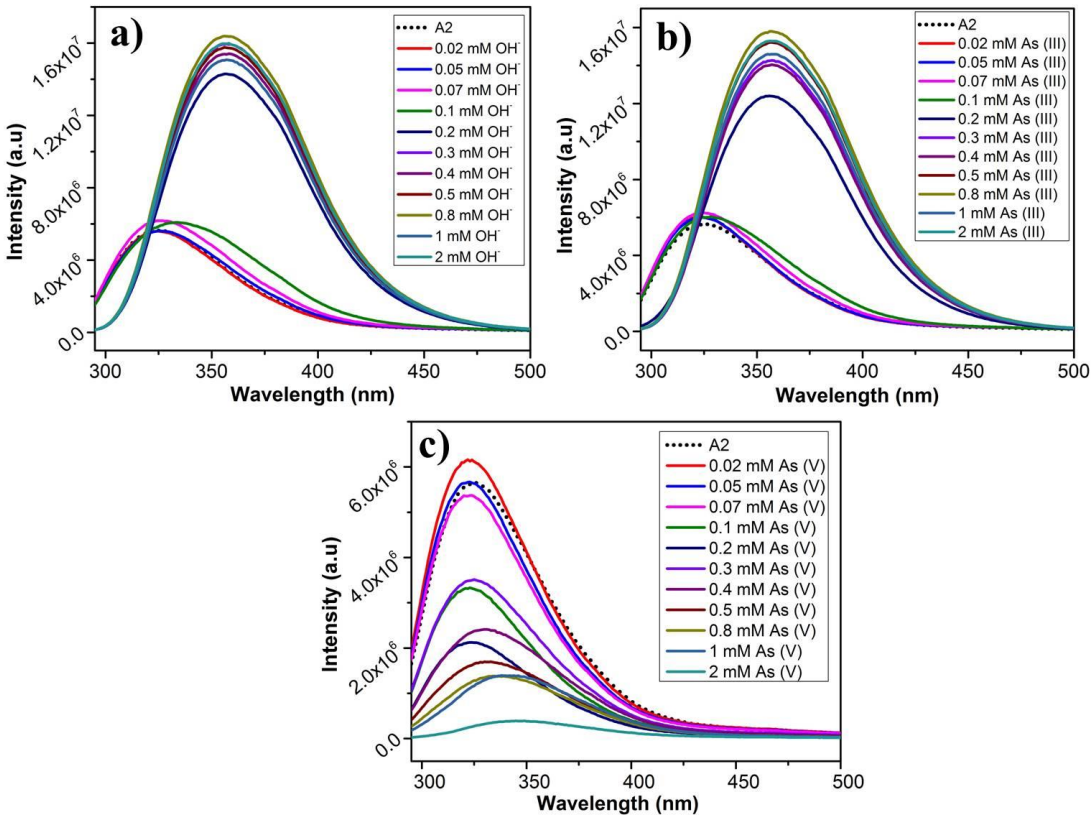

Figure.3.23: Anion sensing by A2: Titration of A2 with a) OH^- , b) As (III), and c) As (V).

The detection limit of A1 and A2 for the anions is tabulated in Table 3.6. A1 had a lower LOD for all the anions in comparison to A2. This most probably was owing to the negative charge on the anions electrostatically favouring the positively charged A1 molecule over the negatively charged A2 molecule. LODs for the detection of AsO_2^- and AsO_3^- by A1 are 2.57 µM and 7.06 µM and by A2 are 33.08 µM and 10.96 µM respectively. AsO_2^- and AsO_3^- contain Arsenic in the most toxic oxidation states which have very grave health implications causing serious diseases and death. In several parts of the world, contamination of the underground drinking water with arsenic causes severe problems. Though the limits of

detection of the molecules A1 and A2 is above the recommended safety levels of Arsenic in drinking water (10 µg/L, 0.13µM), it is still highly relevant. There are very few examples of peptide based arsenic detectors which make these sensors even more prospective candidates for selective Arsenic detection.

3.5.9.2. Response Towards Metal Ions: We have studied the response of our peptides A1 and A2 towards different metal ions (Cu^{2+}, Hg^{2+}, Fe^{3+}, Pb^{2+}, Zn^{2+}, Ni^{2+}, Co^{2+} and Mn^{2}). A decrease in fluorescence intensity for A1 and A2 was observed upon addition of 0.1 mM of Hg^{2+} and Fe^{3+} without any change in the peak position (λ_{em} = 349 nm and 323 nm for A1 and A2). In the presence of other metal ions Co^{2+}, Pb^{2+}, Ni^{2+}, Cu^{2+}, Mn^{2+}, Zn^{2+} there was no change in peak positions or intensity of the signal (Figure 3.24a,b).

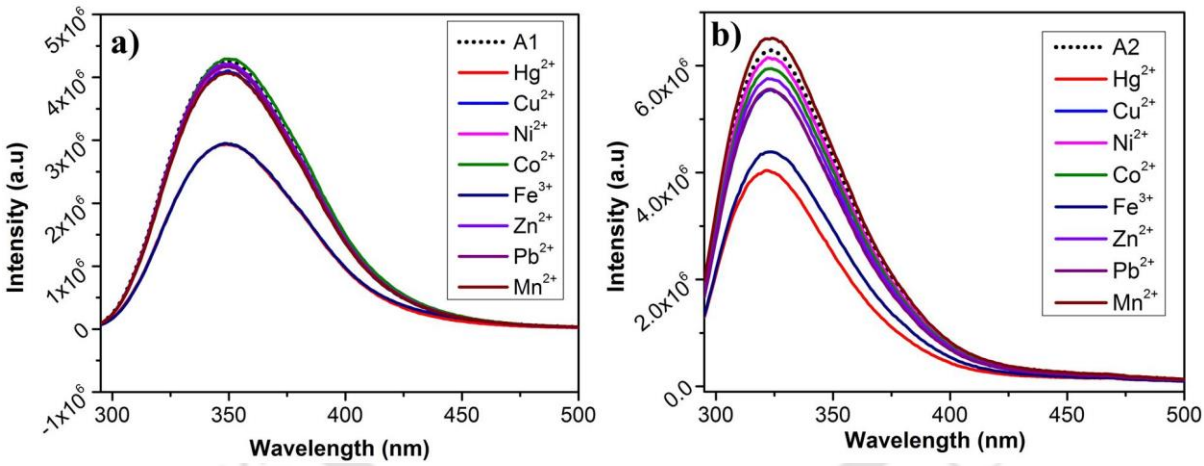

Figure 3.24: Sensing of metal ions by a) A1 and b) A2 (Metal ions=0.1mM, A1=0.1 mM and A2=0.1 mM).

To find out the sensitivity of Fe^{3+} ion detection, the fluorescence response of A1 and A2 was monitored as a function of metal ion concentration (Figure 3.25a, b). The concentration of the Fe^{3+} was varied from 0.02 mM to 2 mM. It was observed that for both A1 and A2, there was a quenching in fluorescence signal upon increasing the concentration of Fe^{3+} without any

change in the peak position. A1 and A2 had a detection limit of 2.19 µM and 18.82 µM respectively towards Fe^{3+} (Table 3.6).

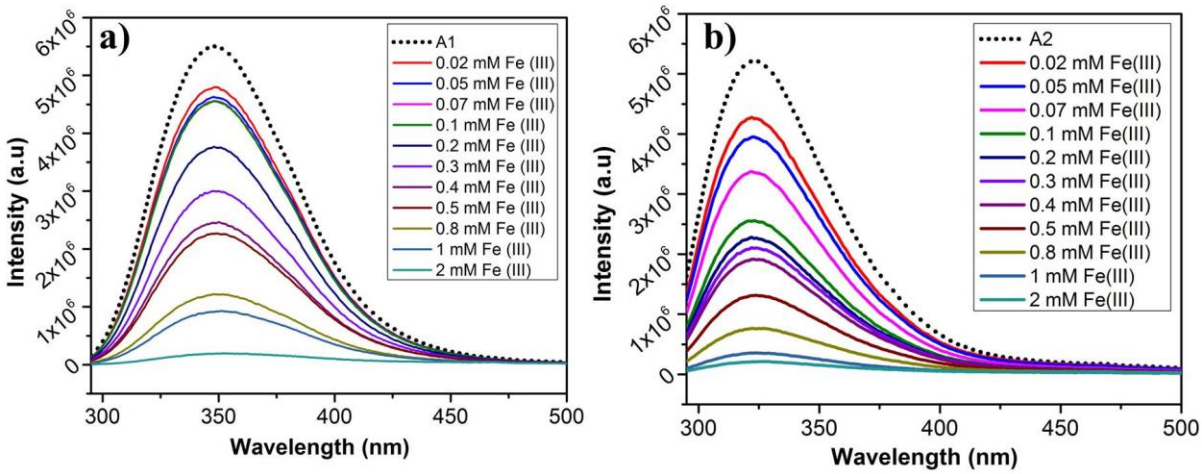

Figure 3.25: Fe^{3+} sensing by A1 and A2: Titration of a) A1 and b) A2 with different concentrations of Fe^{3+}.

Table 3.6: Detection limit of the different ions by A1 and A2.

Ions	A1	A2
As(III)	2.57 µM	33.08 µM
OH^-	2.86 µM	39.68 µM
As(V)	7.06 µM	10.96 µM
Fe^{3+}	2.19 µM	18.82 µM

3.6. Conclusion

In this study, we have reported two charge complementary peptides, A1 and A2, containing Lys and Glu and studied their self-assembly and co-assembly in molecular details. A1 formed hydrogel in phosphate buffer pH 7.0 while A2 did not. Co-assembled gels were formed only with equal or greater amounts of A1 in the mixture. Electrostatic interaction was the most important driver though hydrogen bonding, π-π stacking interactions and hydrophobic

interactions were also instrumental in the assembly process. Peptides adopted β-sheet conformation and the stacking of the sheets gave rise to the formation of the fibre-like structure. Electrostatic interaction played a pivotal role in the stacking of the β-sheets that led to the formation of fibers. The thinner fibers assembled together laterally giving rise to the thicker ones, which entangled to form the mesh like architecture that eventually constituted the hydrogel. Similarity in the structure of the constituent peptides led to cooperative co-assembly in the system, wherein electrostatic interactions between the charge complementary peptides gave rise to the tougher co-assembled gels. Applications of the self- and co-assembled hydrogels in wastewater remediation were probed. All the reported hydrogels were efficient absorbants of different types of organic dyes (Rhodamine B, Crystal Violet, Neutral Red, Methyl Orange), small divalent metal ions (Ni^{2+}, Co^{2+}) as well as heavy toxic metal ions like Pb^{2+} and Hg^{2+}. These materials could be recyclably deployed making their use economically viable. Ability to remove contaminants individually and from a mixture of several components makes these hydrogels highly prospective for practical uses of water remediation. Peptides A1 and A2 can selectively detect arsenite and arsenate ions, the most toxic forms of arsenic responsible for contamination of drinking water, in addition to detection of OH^- and Fe^{3+}. The materials developed in the present study can thus be employed for several applications. Understanding of the molecular details of the assembly processes would empower scientists to develop such simple materials with versatile applications through rational design in the future.

Chapter 4

Peptide Hydrogels as Platforms for Sustained Release of Antimicrobial and Antitumor Drugs and Proteins

Chapter 4

Peptide Hydrogels as Platforms for Sustained Release of Antimicrobial and Antitumor Drugs and Proteins

4.1. Peptide Hydrogels in Biomedical Applications

The versatility, diversity, biocompatibility, stimuli-responsiveness, low immunogenicity and biodegradability of the peptide hydrogels have extended their applications to several biomedical fields like delivery platform[567-569,577], 3D cell culture,[572] anti-bacterial agents,[570,573,574] wound dressings,[569,575] and tissue engineering/regeneration[571,576] to name but a few (Figure 4.1). Of the various applications mentioned, peptide based hydrogels have evoked extreme importance as delivery platforms. Possession of features such as biocompatibility and non-cytotoxicity, the hydrogel network has become an obvious choice for usage as a delivery vehicle for drug/gene or other therapeutic molecules such as proteins.

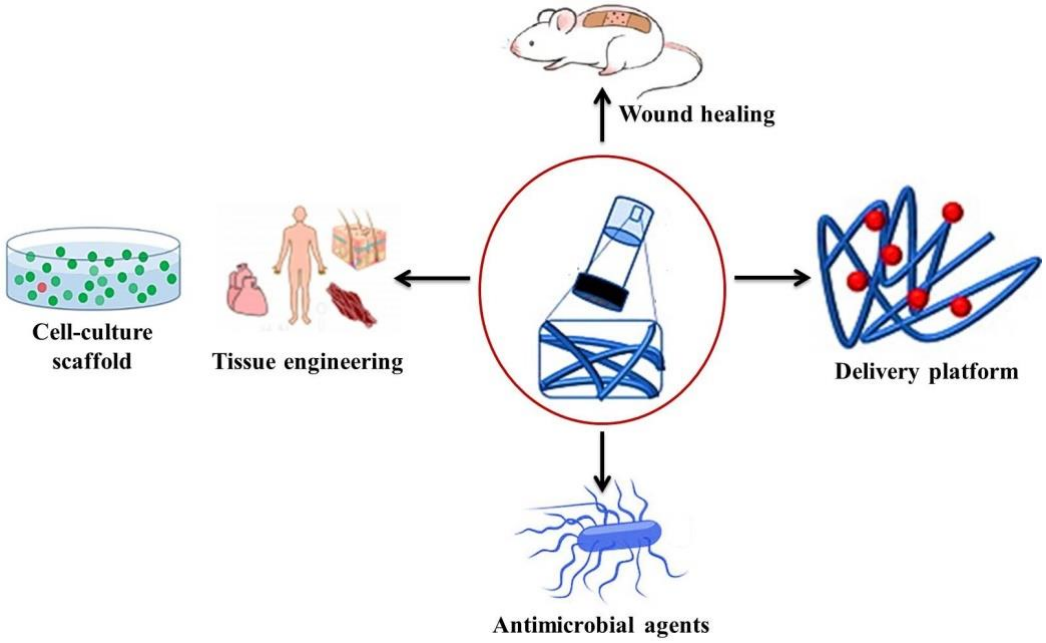

Figure 4.1: Peptide hydrogels in biomedical applications.

4.1.1. Peptide Hydrogels in Drug Delivery: With the advancement in the field of therapeutic research, there has been an increased need for the development of suitable drug delivery systems or platforms.[578] It has been established that efficacy of the drug depends on its mode of administration. Issues like solubility, systemic stability, target specific delivery etc. makes drug delivery a complicated problem. Different modes of drug delivery (Figure 4.2) have been studied which includes liposomes, hydrogels, DNA aptamers,[579, 580] oligonucleotides,[581] biodegradable polymers, nanoparticles and peptide based drug delivery vehicles [521, 567, 582] like peptide hydrogels[521, 567, 583, 584] and cell penetrating peptides[585] These approaches involve either (a) formation of a prodrug involving covalent attachment of the therapeutic molecules to the drug delivery vehicles like peptides, polymers, dendrimers and nanoparticles [586-590] or (b) an entrapment of the drug followed by release.[591, 592] For instance, Lin and co-workers studied doxorubicin incorporated RGD-conjugated polypeptide vesicles with high drug loading content (45%) and loading efficiency (95%) which showed excellent stability, accelerated intracellular drug release (pH and enzyme-responsive), higher tumor accumulation, and lower systemic toxicity.[591]

Several difficulties like systemic toxicity of the drug delivery platforms and stimuli dependent release of the drugs make drug delivery a challenging issue inspite of various techniques that are available. Additionally, for maintaining proper dosage of the drugs, controlled and sustainable release of drug over long periods of time is one of the primary requirements for a drug delivery platform.[567] Most of the strategies mentioned above involve burst release of drugs which transiently increase the local concentration of the drug and require multiple and frequent administration.[517, 567]

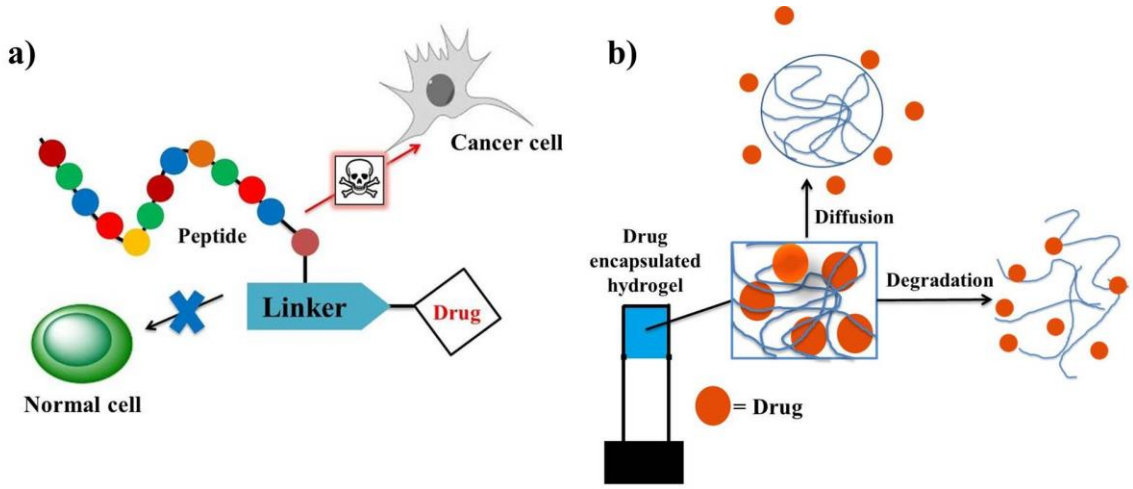

Figure 4.2: Different modes of drug delivery: a) formation of a prodrug involving covalent attachment of drug molecules, b) entrapment of the drug followed by release *via.* diffusion or degradation pathways.

4.1.2. Peptide Hydrogels in Protein Delivery: Therapeutic proteins are an important class of molecules that are becoming increasingly relevant for the biopharmaceutical industry.[593, 594] Challenges in the delivery of therapeutic proteins includes their large size and complicated structures which lead to limited solubility, stability, denaturation, enzymatic degradation and membrane permeability[593, 595]. Therefore, the ideal protein delivery vehicles must have desirable properties which include high protein loading and biocompatibility; the ability to shield the proteins from enzymatic degradation and rapid clearance; the function to provide sustained release in a desired and therapeutically effective way. Peptide hydrogels are also promising candidates for protein delivery applications.[271, 567, 596-601] The high water content in peptide-based supramolecular hydrogels provides the favourable space to store the proteins. Either hydrophilic or hydrophobic molecules could be entrapped in the inter- or intra-fiber areas, greatly increasing the solubility of biologics to be delivered. The interior of the supramolecular hydrogels mimics the extra cellular milieu and helps in protection and stabilization of the proteins to help retain their activity before they reach the desired location.[567] Zhang and his group studied the sustained release of a variety of proteins,

including lysozyme, trypsin inhibitor, BSA, and human IgG using a peptide hydrogel formed from Ac-$(RADA)_4$-$CONH_2$ peptide[271]. In a subsequent study, his group studied the sustained release of IgG over 3 months through the permeable structure of nanofiber scaffold hydrogels formed from the self-assembling peptides Ac-$(RADA)_4$-$CONH_2$ and Ac-$(KLDL)_3$-$CONH_2$.[596] In addition to therapeutic proteins, other biomolecules such Vitamins can also be delivered using peptide hydrogels. For example, Banerjee and his group reported entrapment and slowl release of vitamin B_{12} at a low pH (~2.0) from a metallohydrogel formed from a bolaamphiphilic peptide.[305]

4.2. Present Study

Hydrogel formed by positively charged peptide A1 (H_2N-WLVFFK-COOH) from Chapter 3 was exploited to act as a universal drug and protein delivery platform. Antibiotic drug ciprofloxacin (CP), anticancer drug 5 fluorouracil (5-FU) and proteins like BSA and lysozyme were co-assembled/loaded into the hydrogel and released sustainably with the retention of activity in the case of the drugs and the retention of secondary structure in the case of the proteins respectively. We have investigated the co-assembly of the peptide with the drug molecules using various experimental details. We have demonstrated a sustainable release of anticancer drug 5-FU and antibiotic CP from the co-assembled hydrogel over a span of 3 days. Representative proteins like BSA and lysozyme were loaded on the peptide hydrogel and their release was monitored. In all the cases, released drugs retained their activity while the released proteins retained their native secondary structure. The novelty of the work lies in the fact that these simple biocompatible materials could be used as delivery platform for cargoes of different sizes, charges and chemistries and were capable of addressing important issues in drug delivery like sustained and tissue specific release. The overview of the work done in the present chapter is summarized in the Figure 4.3.

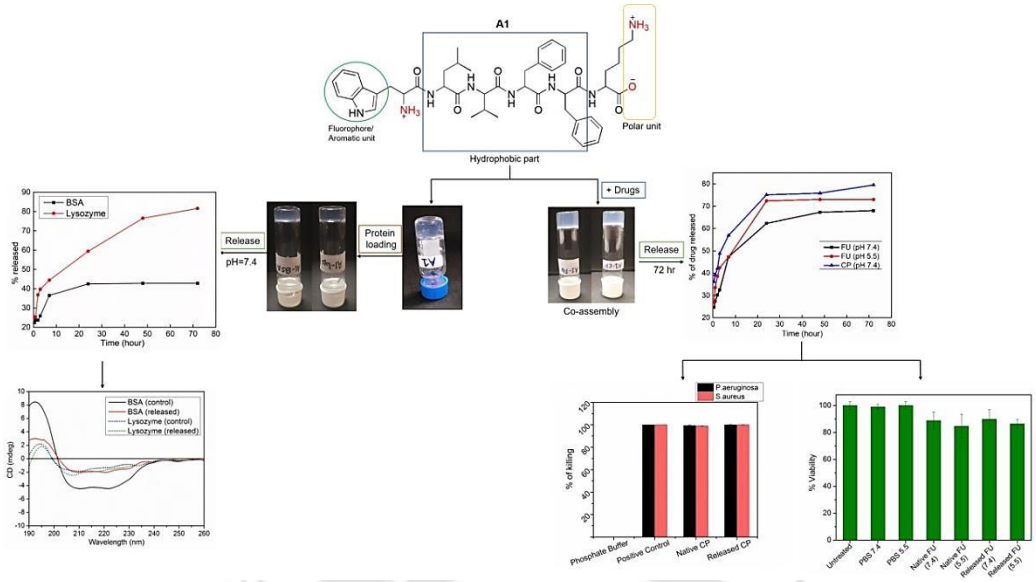

Figure 4.3: Schematic illustration of the work of this Chapter.

4.3. Experimental Details

4.3.1. Synthesis and Purification:

A1 (**H_2N-WLVFFK-COOH**) was synthesised and purified as described in Chapter 3. (3.4.1). Characterisation of the peptide is available in Appendix A (Figure A5a, A6a and A7; Page III and IV).

4.3.2. Formation of Hydrogel:

The hydrogel from A1 was prepared as mentioned in Chapter 3 (3.4.2).

4.3.3. Co-Assembly of Drugs CP and 5-FU with A1 to Form Hydrogels:

2 mg of peptide A1 was taken in 350 µL of 10 mM sodium phosphate buffer (pH=7.0) and into it 75 µL of 1 mM 5-FU solution in water was added to attain a final concentration of 150 µM for the drug. The solution was then heated till the peptide dissolved and was left for cooling at RT to form the 5-FU incorporated hydrogel.

For loading CP, 2 mg of the peptide A1 was taken in 400 µL of 10 mM phosphate buffer (pH=7.0). Into it, 50 µL of 1 mM CP solution in water was added so that the concentration of

the drug becomes 100 µM. The solution was then heated till the peptide dissolved and was left for cooling at RT to form the CP loaded hydrogel.

4.3.4. Loading of BSA and Lysozyme to Hydrogel A1:

Hydrogel A1 was prepared as mentioned in chapter 3 at its MGC. 1 mL of each of aqueous solutions of 1.5 mg/mL BSA and 0.7 mg/mL lysozyme were added into the preformed gel and was allowed to stand. The protein/enzyme loading was measured using UV-Vis spectroscopy. Unabsorbed biomolecules in the supernatant was estimated by monitoring the UV of the supernatant aqueous solution and calculating the concentration from a standard calibration curve (Appendix A, Figure A13a, b, Page VII). The amount of biomolecules loaded in the hydrogel and loading efficiency were then calculated as follows:

Biomolecules Loaded = Initial concentration of the biomolecules - Unabsorbed concentration of the biomolecules

Loading efficiency= Loaded concentration/Initial concentration X 100

4.3.5. FESEM:

For the morphology of the co-assembled gels, preheated samples were casted on the silicon wafer, cooled and the gels that formed were allowed to dry at RT before imaging. Co-assembled gels were formed from a mixture of peptide at its CGC, i.e. 2.38 mM and the drugs CP and 5-FU at a final concentration of was 150 µM and 100 µM respectively. The heated mixtures were casted on silicon wafer, cooled and dried before imaging.

4.3.6. Rheology:

The viscoelastic properties of hydrogels A1-CP and A1-5-FU were determined by rheological studies at 25 ºC. For measuring rheology of A1-CP and A1-5-FU, the hydrogels were prepared in 10 mM sodium phosphate buffer (pH=7) at 2 mg/mL concentration. A strain sweep test was performed over a range from 0.1-100% strain at a fixed oscillatory frequency of 1 rad s^{-1}. Furthermore, the mechanical strength of hydrogels was determined from the

oscillatory test, i.e. frequency sweep, which was carried out under an appropriate strain 0.1% with the frequency ranging from 1-100 rad/s.

4.3.7. Fluorescence Spectroscopy:

To check the interaction of drugs CP and 5-FU with A1 in the co-assembled hydrogel, fluorescence emission of the Trp of the peptide A1 was monitored in the presence of different concentrations of CP and 5-FU added to A1, at an excitation wavelength of 280 nm in 20% EtOH/ phosphate buffer.

4.3.8. FT-IR Spectroscopy:

FT-IR spectra was recorded within the range of 1000-4000 cm^{-1} for A1-CP and A1-5-FU xerogels and compared with that of A1 xerogel.

4.3.9. PXRD:

Wide angle X-ray diffraction analysis was done (Cu-Kα radiation, χ = 1.5406 Å) for the xerogels obtained from the lyophilisation of A1-CP and A1-5-FU hydrogels, for understanding their molecular packing in the co-assembled xerogel state. The results were compared with the self-assembled A1 xerogel.

4.3.10. Circular Dichroism:

CD spectra of the native and released BSA and lysozyme at 0.3304 mg/mL and 0.3742 mg/mL in PBS 7.4 respectively were recorded using a 200 µL quartz cuvette of 1 mm path length at room temperature. Spectra were collected at a scan rate of 200 nm·min−1 and 2 nm bandwidth from 190 to 260 nm with three scans for averaging. Before running the sample, respective solvent system were run to correct the baseline.

4.3.11. Release of Drug/Biomolecules:

1 mL of PBS, used as release medium, was placed on the drug-peptide co-assembled hydrogel. 500 µL of the release medium was taken out at different time intervals to measure

the UV absorbance. Release studies were monitored for 72 h. For CP, release studies were done in PBS pH 7.4, to mimic physiological milieu while release of 5-FU was studied both at PBS pH 7.4 and 5.5, to mimic healthy and cancerous tissue environments. From the standard curves of the drug molecules obtained from UV spectroscopy (Appendix A, Figure A13 c,d, Page VII) the amount of drug released was calculated.

For release of proteins, PBS buffer of pH 7.4 was added to the BSA and lysozyme loaded hydrogels. 500 µL of the release medium was taken out at different time intervals and its UV absorbance was measured. Release studies have been monitored for 72 h.

The release efficiency was then calculated as:

Release % = Released concentration/Loaded concentration X 100

4.3.12. Potency of the Drug Released:

CP: To compare the activity of the released CP from the hydrogel with the native drug, antimicrobial assays were performed.

a) Micro-Broth Dilution Assay: Overnight grown cultures of the pathogens were used to obtain mild log phase cultures of *Staphylococcus aureus* MTCC 96 (g+) and *Pseudomonas aeruginosa* MTCC 2488 (g-). The cell suspensions were centrifuged at 6000 rpm for 5 min, cell pellets were washed thrhice with 10 mM PBS of pH 7.4 and resuspended in the same buffer to obtain the cell suspension containing 5×10^5 CFU/mL. The reaction was set in a 96 well plate. 50 µl of the cell suspension was incubated with 50µL (79 µM) CP (native and released from hydrogel in PBS 7.4) and incubated at 310 K for 4 h. A negative control containing only cell suspension and a positive control containing 10 µM polymyxin B with cell suspension were maintained. Next, 150 µL of suitable media was added to reaction well and incubated overnight with shaking at 310 K temperature. The peptide concentration at which 90% growth inhibition was observed served as its MIC90%. Absorbance was

monitored at 630 nm. Polymyxin B was used to normalize the data. All experiments were performed in triplicates.

b) Disc Diffusion Assay: It was done to find out the antibacterial activity of released CP from the peptide hydrogel. *Staphylococcus aureus* MTCC 96 (g+) and *Pseudomonas aeruginosa* MTCC 2488 (g-) were utilized for antimicrobial test. Typically, 100 µL of bacterial suspension (10^8 CFU/mL) was spread by sterile L spreader over the solidified nutrient agar plate and dried for 15 minutes under laminar flow. Then sterile paper discs (6 mm) were dipped into the respective dose solution and placed on the bacterial lawn. Thereafter plates are sealed with parafilm and incubated at 310K for 18 h. The antibacterial activity for CP before and after release from the hydrogel was measured as "zone of inhibition" where released buffer was used as a control. All experiments were performed in triplicates to find out standard deviation along with one control plate without any treatment.

5-FU*:* To compare the activity of the released 5-FU from the hydrogel with the native drug, MTT assay was done on cancerous cell line MCF-7 (human breast cancer cells). Cells were seeded in 96 well plate at the density of 6000 cells/well. Then, native 5-FU and that released in PBS at pH 7.4 and 5.5, were added on cells at 10 µM concentration and incubated for 24 h. After completion of the treatment, 3-(4,5-dimethylthiazol-2-yl)-2,5-diphenyl tetrazolium bromide (MTT) reagent mixed with Dulbecco's Modified Eagle Medium (DMEM) medium was added onto the cells and the plates were incubated in CO_2 incubator for 2 h. In the next step, MTT containing medium was removed and 150 µl DMSO was added into each well. The absorbance of the dissolved formazan product was measured at 570 nm, while reference was taken at 650 nm.

4.3.13. Cytotoxicity of Peptide A1:

The effects of the peptide A1 on the cell viability was studied by MTT assay on healthy human embryonic cell line HEK and cancerous cell line MCF7. HEK and MCF cells were

seeded into 96 well plate at the density of 10^4 cells/well. After overnight incubation, cells were treated with different concentrations (0 µM to 100 µM) of the A1 for 24 h. Subsequently, MTT (0.3 mg/mL) reagent in DMEM was incubated with the cells for another 3 h and the formed formazan crystals were solubilized by adding 200 µl of DMSO. Cell viability was calculated by measuring absorbance at 570 nm by using a Tecan plate reader

4.4. Results and Discussions

4.4.1. Hydrogelation of A1:

As mentioned in the last chapter (Chapter 3), A1 formed hydrogel in phosphate buffer at pH 7.0 and organogel in 20% EtOH/phosphate buffer upon being heated and subsequently cooled (Figure 3.4c, Chapter 3). A1 hydrogel had a dense continuous matrix like morphology in sodium phosphate buffer at pH 7.0 (Figure 3.6a, Chapter 3) while A1 organogel formed entangled fibrous network in EtOH/ sodium phosphate buffer mixture (Figure 3.6b, Chapter 3).

4.4.2. Factors Driving Self-Assembly:

Detailed investigation on the forces driving self-assembly were performed as entailed in Chapter 3 using various experiment techniques like fluoresence spectroscopy, PXRD, FTIR, etc. Though aromatic π-π interactions, hydrogen bonding and hydrophobic interactions were found to be the important factors in driving hydrogelation of A1, the process was overall governed by electrostatic interactions.

4.4.3. Delivery of Drug Molecules from Hydrogel A1:

In this chapter, we have tested the capability of A1 to form co-assembled hydrogels with two drugs: a) anticancer drug, 5-FU and b) antibiotic, CP. We have also studied the subsequent release of these drugs from these co-assembled hydrogels. 5-FU is a known chemotherapeutic anticancer drug that is used to treat stomach, pancreatic, breast, cervical, respiratory, head,

breast and neck cancer.[602] Several drug delivery systems like nanoparticles, liposomes, niosomes, beads, lipoproteins and hydrogels have been used for the delivery of 5-FU.[603] However, its clinical application is limited due to a number of reasons such as low bioavailability and side effects generated by nonspecific absorption.[604] CP on the other hand is a broad spectrum antibiotic effective against both gram positive and gram negative bacteria that is administered to tackle bacterial infections and is a gold standard for topical applications. Limited solubility in water and low bioavailability are the reasons for limited applications of this drug.[605]

4.4.3.1. Co-Assembly of Drugs and the Peptide: Gelation and Morphology of the Drug Incorporated Hydrogels:

A1 formed co-assembled hydrogel with both CP and 5-FU. The co-assembly occurred upon heating and subsequent cooling of the mixtures of A1 with the drugs in sodium phosphate buffer, pH 7.0 (Figure 4.4 a, d). The morphology of the gels was studied using FESEM. Interestingly in the A1-5-FU hydrogel (Figure 4.4b), two discrete types of morphologies were evident. Banana plantation type of morphology was present along with the mesh-like morphology that was seen for the pristine peptide A1 hydrogel. The banana plantation like morphology was probably formed by the drug molecule 5-FU. This suggested that incorporation of 5-FU in the A1-5-FU hydrogel did not disturb the self-assembly of the peptide rather, both the components showed self-sorted self-assembly.

Figure 4.4e shows the morphology of the co-assembled A1-CP hydrogel. In this case, a network of nanotube like structures, most probably formed by the CP was found along with a continuous mesh-like morphology in the background, formed by the peptides. Coexistence of both the two distinct morphologies proved that even for A1-CP co-assembled gel, the co-assembly occurred *via* self-sorting. These are beautiful examples of orthogonal self-assembly. There are a few examples in the literature of such kind of self-assembly.[606] Webber and co-

workers reported electrostatic-driven self-sorting of two peptides DWDW and KWKW upon co-assembly.[606]

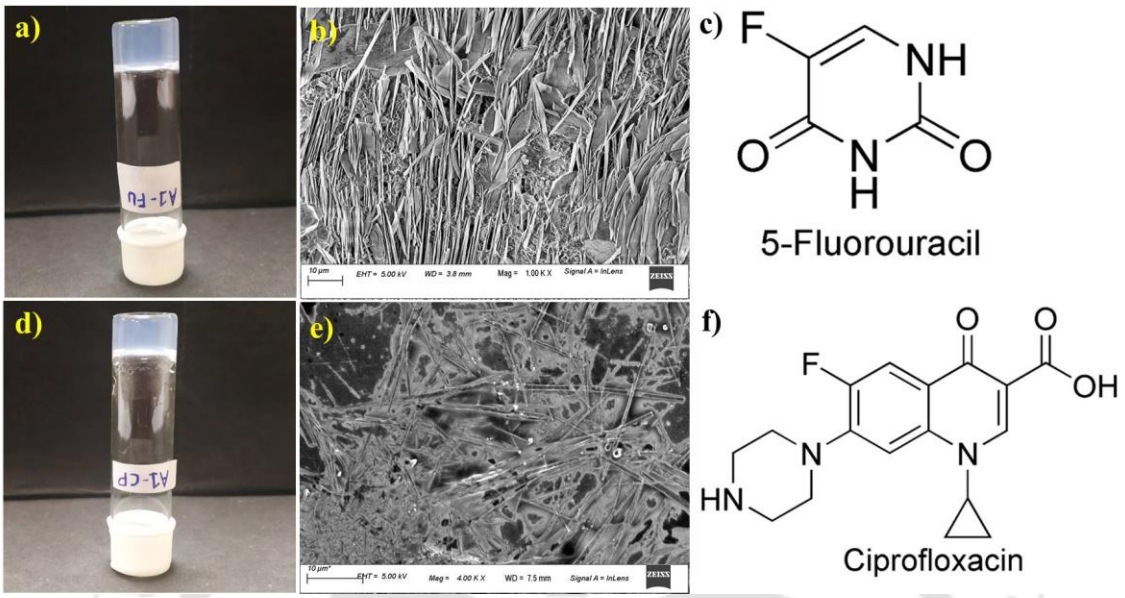

Figure 4.4: Co-assembled gels A1-5FU and A1-CP. Photographs of co-assembled hydrogels (a) A1-5-FU and (d) A1-CP respectively. FESEM images of co-assembled hydrogels (b) A1-5-FU and (e) A1-CP. Chemical structures of the drug molecules (c) 5-FU and (d) CP respectively.

4.4.3.2. Viscoelastic Properties:

Both A1-5-FU and A1-CP were found to be mechanically robust as seen from the rheology studies (Figure 4.5b, c and 4.5e, f). In the angular frequency sweep experiment, G′ was found to be greater than the G′′ till a frequency of 100 rad/sec. The value of G′ was of the order of $10\text{-}10^2$ for both the A1-CP and A1-5-FU co-assembled gels, which was a little lower than that observed for the pristine hydrogel (Figure 4.5a), indicating that the co-assembly reduced the robustness of the A1-CP and A1-5-FU gels. Figure 4.5e, f revealed that in the strain sweep experiment for both the co-assembled hydrogels, the storage modulus was higher than the loss modulus till a particular strain (~50%) beyond which the two crossed each other, indicating loss of gel nature. Co-assembly of the drugs with A1 led to formation

of softer and more malleable hydrogels which might be of advantage for the release of the drugs. The self-sorting and orthogonal assembly of the individual components might be the reason for the formation of the softer gels.

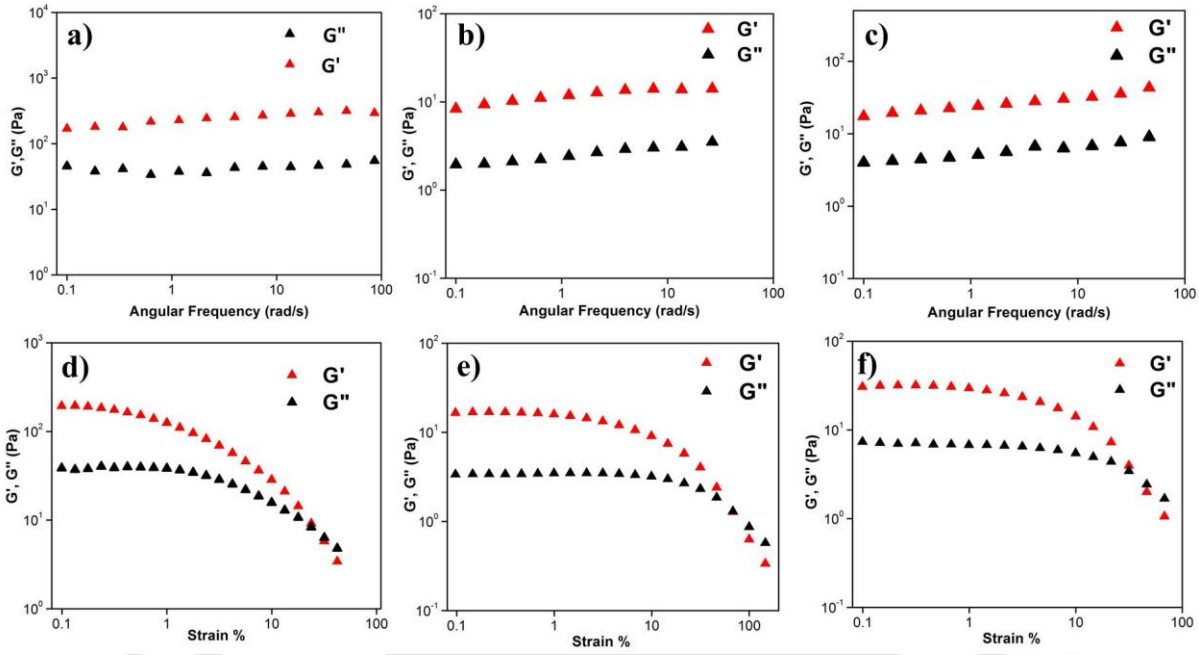

Figure 4.5: Frequency dependence of the dynamic storage moduli (G′) and the loss moduli (G″) of hydrogels a) A1, b) A1-5-FU, c) A1-CP and strain dependence of the dynamic storage moduli (G′) and the loss moduli (G″) hydrogels, d) A1, e) A1-5-FU and f) A1-CP at 0.20 % wt/v in phosphate buffer.

4.4.3.3. Interaction Between the Drug Molecules and A1 in the Co-Assembled Gels:

In order to understand the nature of interaction in between the drug molecules and A1 in the co-assembled gels, we monitored the intrinsic Trp fluorescence emission of A1 as a function of the varying concentrations of the drugs (Figure 4.6a, b). In the case of both 5-FU and CP, the fluorescence emission intensity of Trp quenched upon addition of increasing concentration of the drugs. This indicated an increased π-π stacking in between the Trp indole rings and the aromatic moieties present in the drugs (Figure 4.4c, f). In the case of CP co-assembled hydrogel, a prominent band appeared at a λ_{max} = 401 nm which might be attributed

to excimer/exciplex formation due to increased aromatic π-π stacking upon enhanced assembly. The intensity of this band diminished with the increase in the concentration of CP suggesting the formation of exciplex.[607] Upon addition of the drug, aromatic π-π stacking occured in between Trp of A1 and the aromatic moiety of CP leading to the formation of exciplex. Increase in the concentration of the exciplex, upon addition of increased amounts of drug, led to quenching in the intensity of the band. Thus, it is clear that aromatic π-π stacking played an important role in the co-assembly process of A1 with the drugs.

FTIR were studied to look at the backbone conformation of A1 in the drug incorporated hydrogels (Figure 4.6c). Characteristic peaks at around 1630 and 1683 cm^{-1} for A1-5-FU and A1-CP xerogel indicated that A1 adopted β-sheet conformation in both the cases, similar to the pristine A1 xerogel. NH stretching peaks at around 3276 cm^{-1} indicated presence of hydrogen bonding in the co-assembled xerogels. Similarity in the backbone conformation of A1 in the self-assembled and the co-assembled gels supported the formation of orthogonal co-assembly as seen from the FESEM experiments earlier.

To understand the arrangement of the molecules in the co-assembled gels in the solid state, PXRD was performed on the co-assembled xerogels A1-CP and A1-5-FU (Figure 4.6d). Upon comparison of the spectra obtained from both A1-5FU, A1-CP with the pristine A1 xerogels, it was clear that all of them had similar interplaner distances suggesting that the arrangements of the molecules remained the same in all the three cases. It was interesting to note the presence of interplaner distance of around 3.8Å in both the co-assembled xerogels, which corresponded to the centroid to centroid distance for the face –to –face stacking of aromatic rings. This observation once again supported the presence of orthogonal co-assembly over that of cooperative co-assembly as observed from the FESEM experiments.

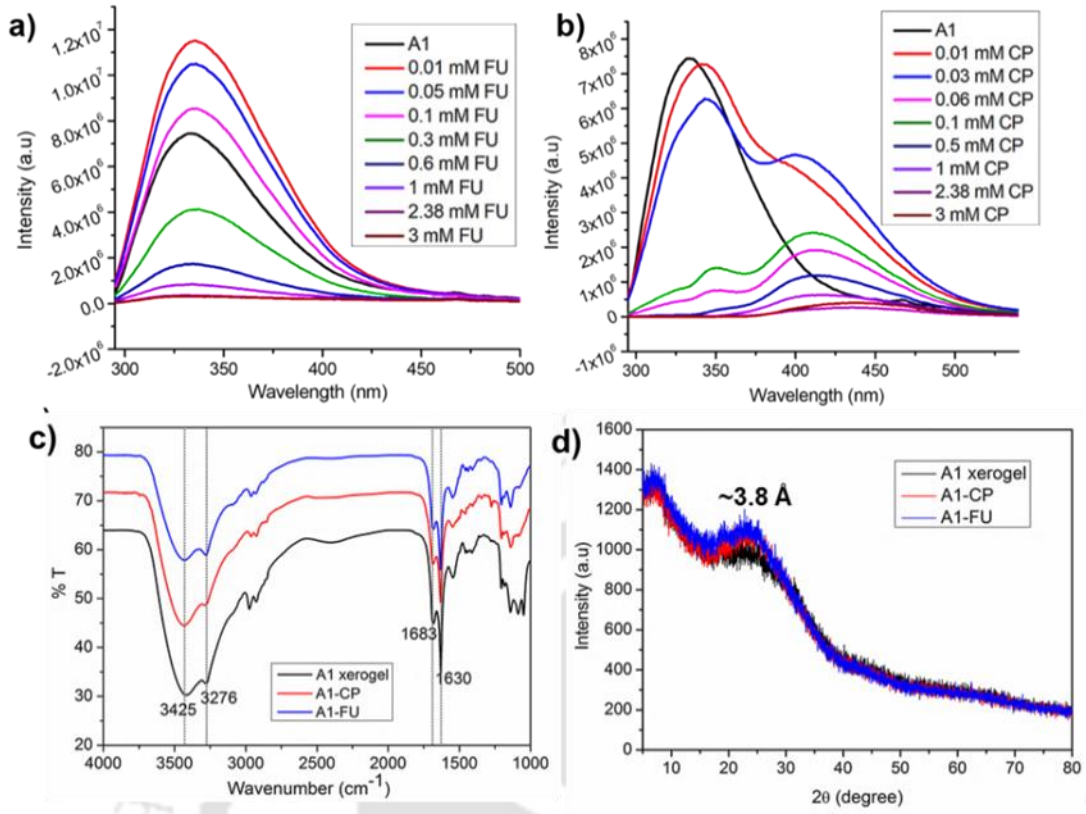

Figure 4.6: Interaction between the drug molecules and A1 in the co-assembled gels. Fluorescence of A1 in presence varying concentrations (0.01-3 mM) of a) 5-FU and b) CP. Comparison between the c) FTIR of xerogels A1, A1-CP and A1-5-FU and d) PXRD of xerogels A1, A1-CP and A1-5-FU.

In summary, co-assembly of A1 with the drugs led to softer hydrogels formed from orthogonal self-sorting of the two. Non-covalent forces like aromatic π-π stacking and hydrogen bonding interactions in between A1 and the drug molecules and in between each class of molecules, played crucial roles in the co-assembly process.

The decrease in the mechanical strength of the self-assembled gel upon co-assembly with the drugs could be attributed to the disruption of continuous self-assembled structure and non-covalent interactions in A1 for the insertion of the self-assembled patches of the drug in the co-assembled gel. Though favourable aromatic interactions and hydrogen bonded interactions might be present among A1 and the drug moieties (as seen from fluorescence studies), it must

be energetically less favourable in comparison to interactions among molecules of each class, leading to the decrease in the mechanical strength of the co-assembled gels. This was also indicated in the formation of orthogonal co-assembly instead of cooperative co-assembly, where both the components interact one on one at the molecular level to produce a totally new kind of self-assembled pattern. In the present case of orthogonal co-assembly, interaction in between the A1 and the drug molecules occur only at the surfaces where the two self-assembled patches come in contact with each other.

4.4.3.4. Release of 5-FU and CP:

One of the major disadvantage of the earlier studies on delivery of 5-FU involved unspecific release of the drugs, causing harm to the healthy cell lines. We studied the release of 5-FU in release media of two different pH's: a) pH 5.5, to mimic the acidic cancerous tissues and b) pH 7.4, to mimic the healthy tissues (Figure 4.7a, b). The time dependent release of the drug was followed by monitoring the UV absorption of the release media (Figure 4.7a, b). It was observed that about 73% and 68% of 5-FU was released over a span of 72 h in the acidic pH of 5.5 and neutral pH of 7.4 respectively (Figure 4.7d) (Table 4.1). As the cancer tissues tend to be acidic in nature, facilitated release of 5-FU in the acidic medium would diminish unspecific release of the drug making this material a potential drug release platform for anticancer drugs. Release of antibiotic CP was studied at a pH of 7.4 (Figure 4.7c) for a span of 72 h. About 80% of the drug was released in 72 h (Figure 4.7d) (Table 4.1) beyond which the release plateaued out. Thus the co-assembled gels were good platforms for sustained release of different kinds of drug molecules.

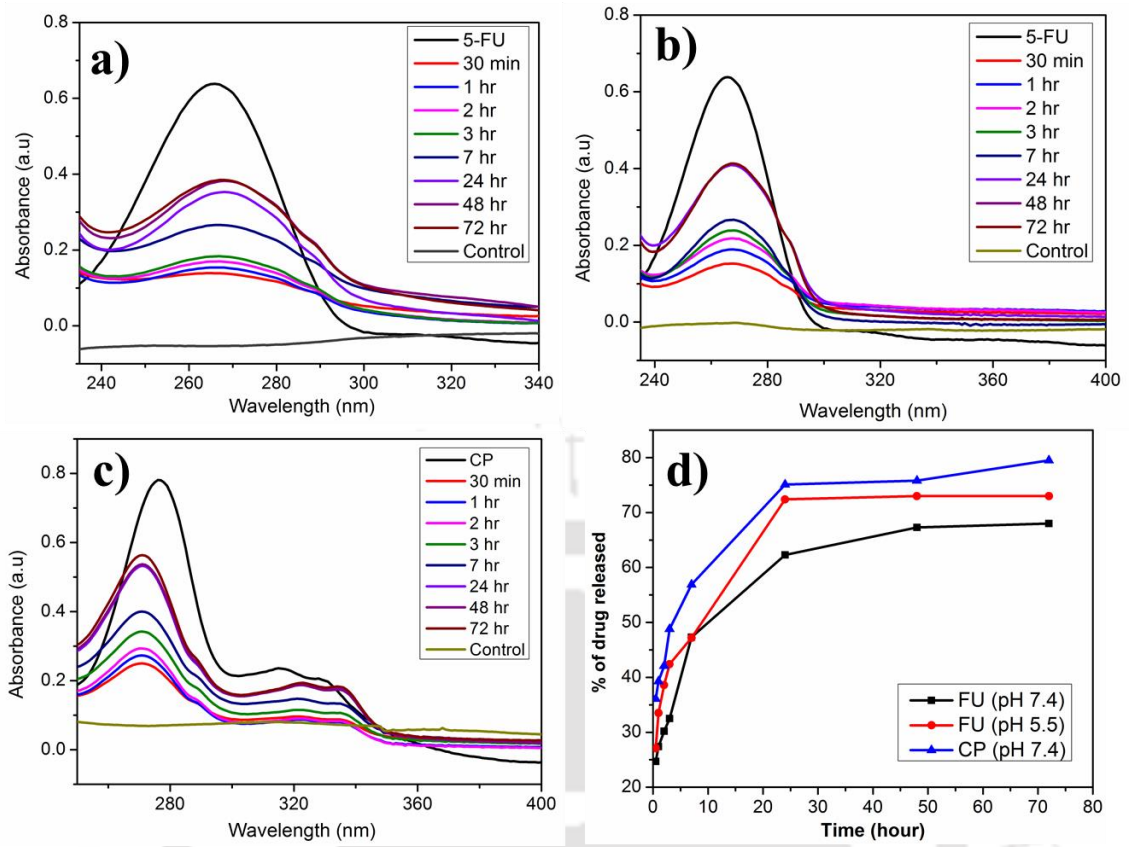

Figure 4.7: UV-Visible study to monitor the release of a) 5-FU in PBS 7.4, b) 5-FU in PBS 5.5, c) CP in PBS 7.4 and d) Release kinetics of drugs from A1 hydrogel over a span of 72 h.

Table 4.1: Release studies of drug molecules loaded onto and released from A1 hydrogel.

Drug loaded hydrogels	Release medium	Drug loaded	Concentration of the released material after 72 h	% released
A1-CP	PBS 7.4	100 µM	79.00 µM	79.00
A1-5-FU	PBS 7.4	150 µM	102.14 µM	68.09
A1-5-FU	PBS 5.5	150 µM	109.57 µM	73.04

4.4.3.5. Activity of the Released Drugs:

To access if the drugs retained their activity post storage and release from the hydrogel, we performed their respective activity assays. MIC of the released antibiotic CP was evaluated against gram negative bacteria *P. aeruginosa* and a gram positive bacteria *S. Aureus*. Figure 4.8a shows the effect of released CP on the microbes in comparison to the neat antibiotic, taken as positive control. It was found that the released drug was as efficient as the neat antibiotic. Additionally, standard plate growth inhibition assay was employed for relative qualitative estimation of the antimicrobial activity of the released antibiotic on *P. aeruginosa* and *S. Aureus* (Figure 4.8b). The diameter of the growth inhibition zone was measured after 24 h of incubation at 37°C and compared with the positive control, which was the neat drug. The diameter of the growth inhibition zone of the released CP was about 69% and 81% of that of the neat control antibiotic for *P. aeruginosa* and *S. Aureus* respectively (Table 4.2). In summary, the antibiotic retained its activity considerably upon being loaded and released from the hydrogel material.

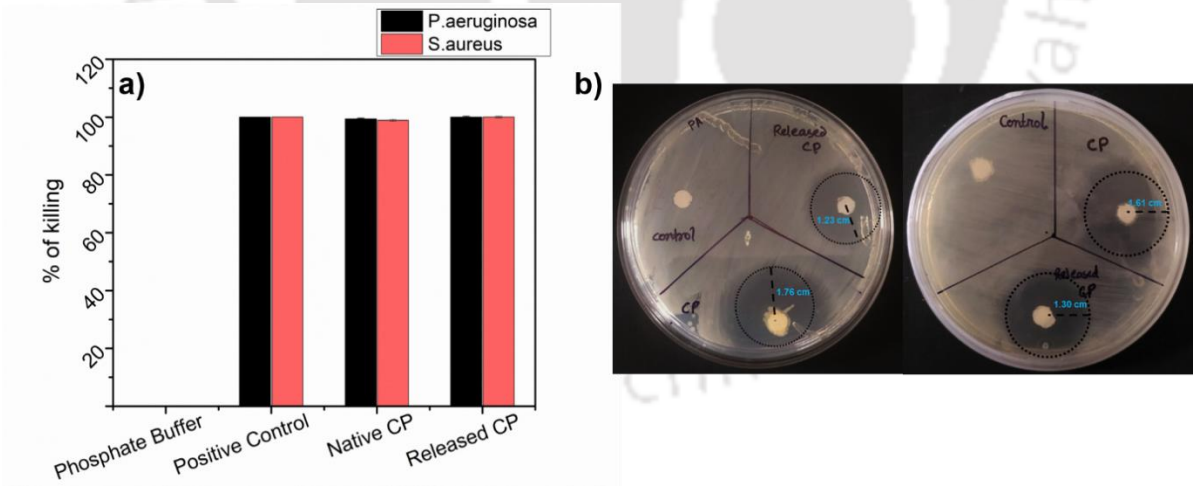

Figure 4.8: Antimicrobial activity of the CP released from co-assembled gel A1-CP in *P.aeruginosa* and *S.aureus.* a) MIC90% as obtained from the micro-broth dilution assay. Each experiment was done in triplicate. b) Representative patterns of zone inhibition experiment.

Table 4.2: Diameter of zone inhibition of bacterial growth obtained from disc diffusion assay

Bacteria	Fresh CP	CP post release	-ve control
Pseudomonas aeruginosa	3.5±0.32 cm.	2.63±0.13 cm.	N.D
Staphylococcus aureus	3.23±0.25 cm.	2.6±0.16 cm.	N.D

−ve control = Sterile PBS (pH 7.4) and N.D. = not detected

In order to access the anticancer activity of the released 5-FU, viability of MCF 7 cells upon incubation with the released drug was studied. As the release of the drug was studied at two different pHs, so was the anticancer activity (Figure 4.9).

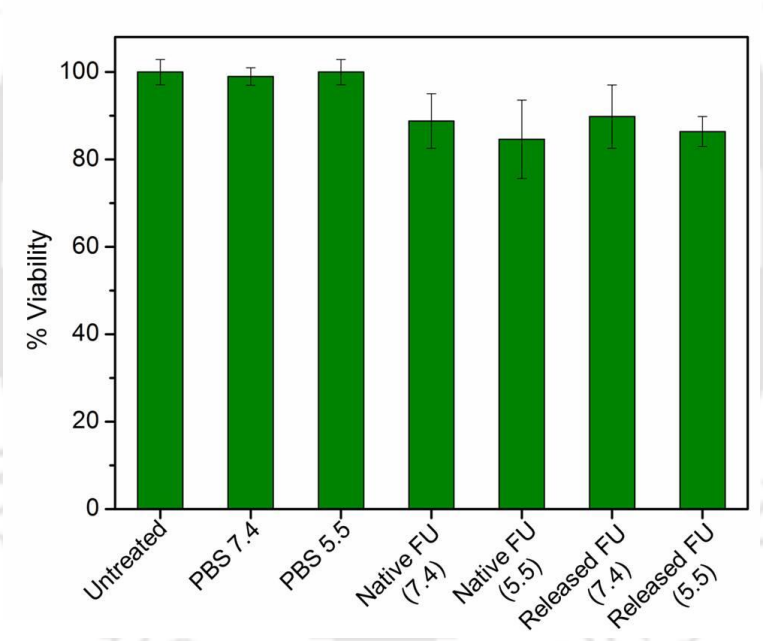

Figure 4.9: Anticancer activity of 5-FU released from co-assembled gel A1-5-FU on human breast cancer MCF7 cell lines. The assay has been performed after about 10X dilution of the released drug. Cell Viability was quantified by measuring the absorption at 570 nm. All experiments were performed in triplicates.

The concentration of the released drug was very high, and thus it was diluted about 10 times before checking the cell viability of the cancerous MCF7 cells. The cell viability of the

released drug was comparable to that of the neat drug indicating that the released 5-FU retained its activity completely upon storage and release from the hydrogel.

4.4.4. Loading and Sustained Release of Proteins BSA and Lysozyme from the Hydrogelator A1:

For studying whether A1 hydrogel was capable of storage and release of proteins, two representative proteins, BSA and lysozyme were loaded (Figure 4.10a, b) into A1 hydrogel and their release was monitored subsequently for over a period of 3 days (Figure 4.10c, d). The model proteins were chosen such that they were very diverse in their size and pI values. While the BSA was a large protein containing 583 amino acid residues and hydrodynamic radius of 3.8-4.3 nm, lysozyme was a much smaller protein containing only 129 amino acid residues and a hydrodynamic radius of 2 nm. pI BSA and lysozyme were 4.7 and 11.1 in water. Thus in PBS pH 7.4, BSA would be negatively charged while lysozyme would be positively charged. Amount of protein loaded into or released from the hydrogel was quantitated by monitoring the UV absorbance of the supernatant. About 51.39% and 65.50% of BSA and lysozyme were loaded into the hydrogel respectively. BSA was clearly loaded to a much lesser extent than lysozyme and this may be attributed to the larger size of the former compared to that of the later.

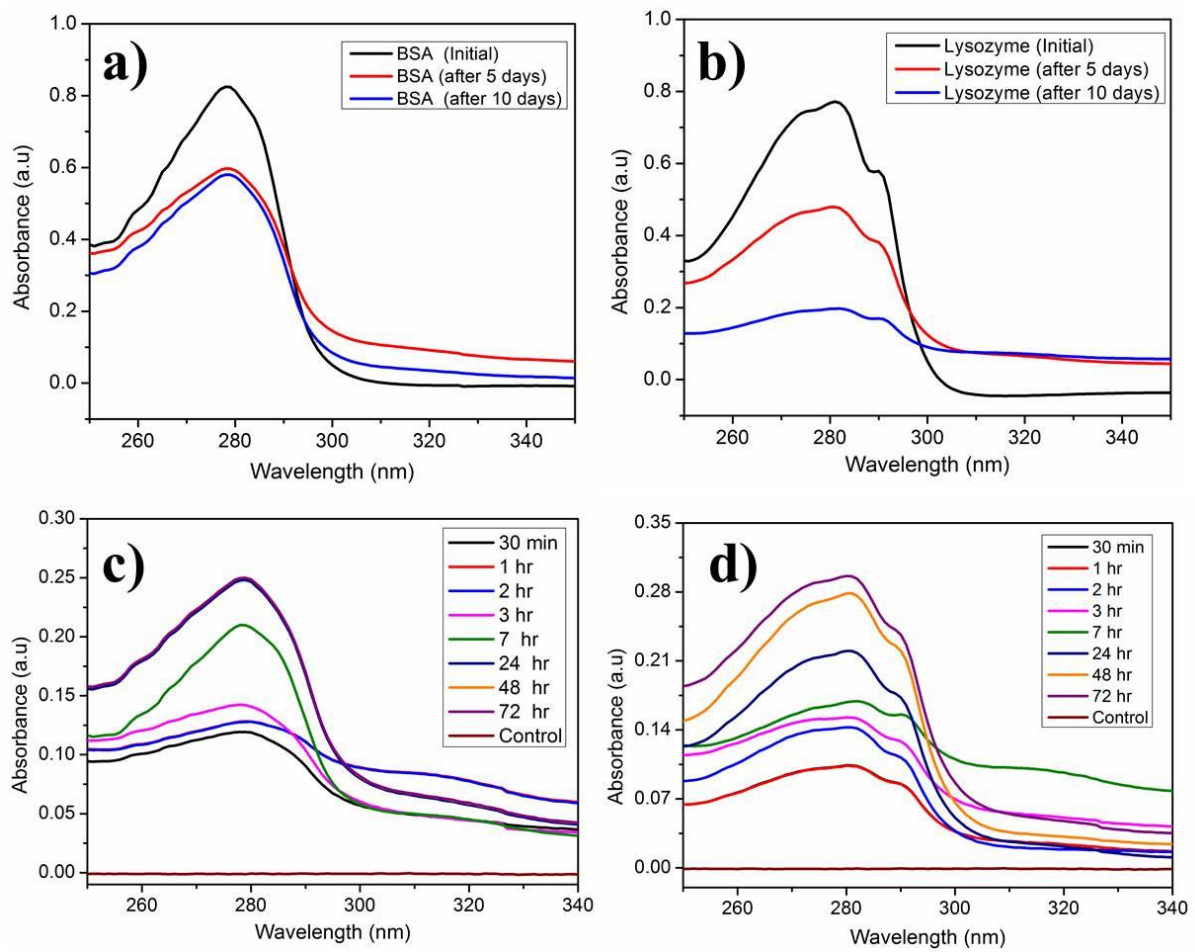

Figure 4.10: UV-Visible study monitoring the loading of a) BSA, b) lysozyme into A1 hydrogel and release of c) BSA, d) lysozyme from A1 hydrogel in PBS, pH = 7.4.

Upon following the release kinetics of the proteins, it was noted that there was an initial burst phase with rapid release of proteins from the hydrogel which subsequently slowed down and finally plateaued out (Figure 4.11). The initial burst might have been caused by the release of the proteins present at or near the surface of the hydrogel-solvent interface. The subsequent slowing down of the release was due to the protein molecules embedded deep within the hydrogel that had to diffuse to the surface through the fibrillar mesh of the hydrogel for being released. About 82% and 43% of lysozyme and BSA were released from the hydrogel over a period of three days (Table 4.3).

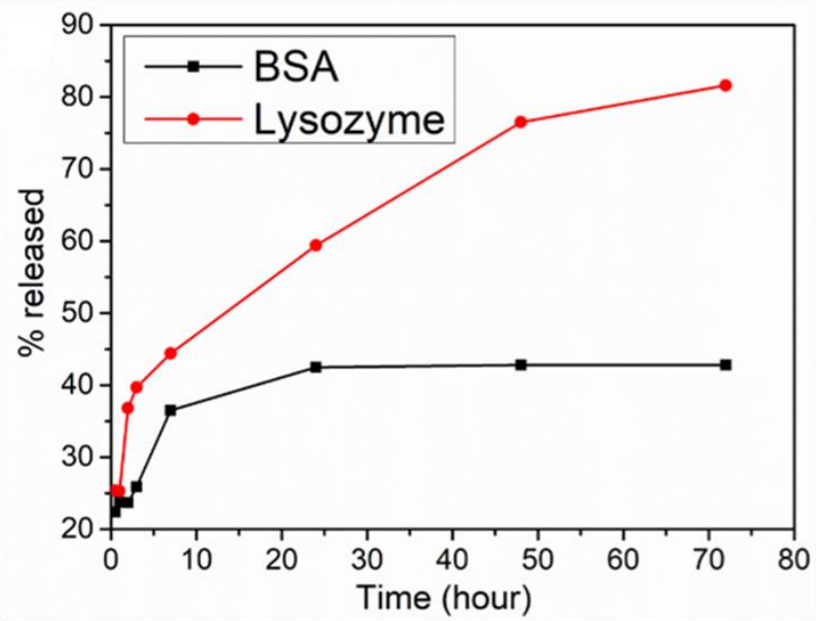

Figure 4.11: Release kinetics of proteins like BSA and lysozyme from A1 hydrogel over a span of 72 h

Table 4.3: Release studies of proteins loaded onto and released from A1 hydrogel

Protein loaded hydrogels	Release medium	Protein loaded	Concentration of the released protein after 72 h	% released
A1-BSA	PBS 7.4	0.7709 mg/mL	0.3304 mg/mL	42.85
A1-Lysozyme	PBS 7.4	0.4585 mg/mL	0.3742 mg/mL	81.61

The rate of release of lysozyme was significantly higher than that of BSA. This might be due to the considerably larger size of BSA (583 amino acids) compared to that of lysozyme (129 amino acids). Larger size of BSA might lead to slower movement of the protein through the fibrillary network of the hydrogel in comparison to that of lysozyme. Additionally, BSA with pI of 4.7 was negatively charged in PB (pH 7.4) in comparison to lysozyme, which was positively charged (pI being 11.1) at that condition. A1 being positively charged would have a favourable electrostatic interaction with the negatively charged BSA, leading to its slower release. Lysozyme, on the other hand, being positively charged did not have any favourable

electrostatic interaction with the hydrogel and was released quickly. However, in this context it must be remembered that inspite of having a favourable electrostatic interaction with the hydrogel, the loading of BSA was lesser than lysozyme. It was the smaller size and thus better diffusivity of the lysozyme through the hydrogel network that led to its better uptake. Thus, the size of the protein seems to have the determining role in the loading and release of proteins in this case.

4.4.5. Secondary Structure and Chemical integrity of Released Proteins:

We wanted to investigate if the encapsulation and the storage of the proteins had any effect on their stability and secondary structure. MALDI-MS performed on the release media showed presence of intact proteins in them indicating that loading and storage of the proteins inside the hydrogel prevented any chemical denaturation of the proteins (Figure 4.12). The released proteins retained their secondary structures as seen from the CD spectroscopy (Figure 4.13). As in the case of structured proteins, the structure and the function are closely related to each other, it may be concluded that the released proteins also retained their activity.

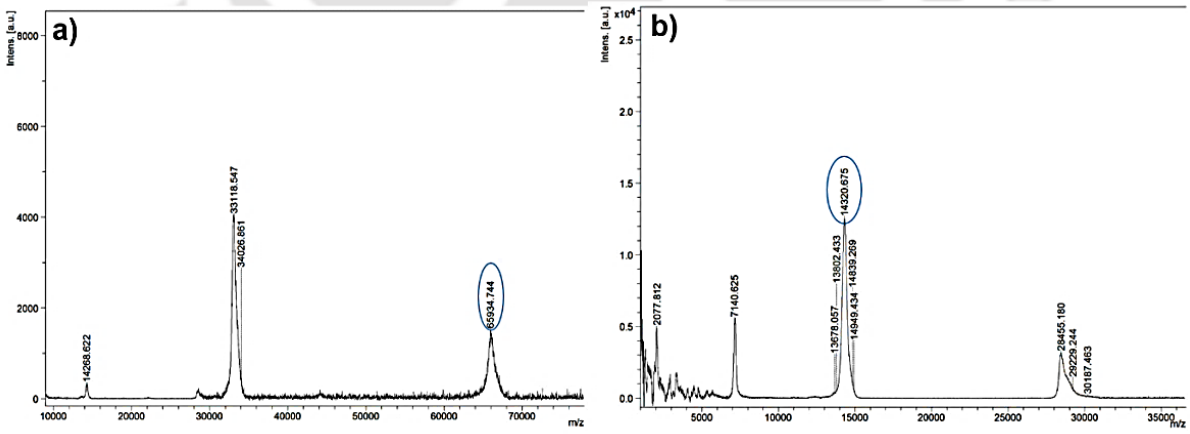

Figure 4.12: MALDI spectrum of the release medium (PBS, pH 7.4) showing presence of intact proteins a) BSA and b) lysozyme.

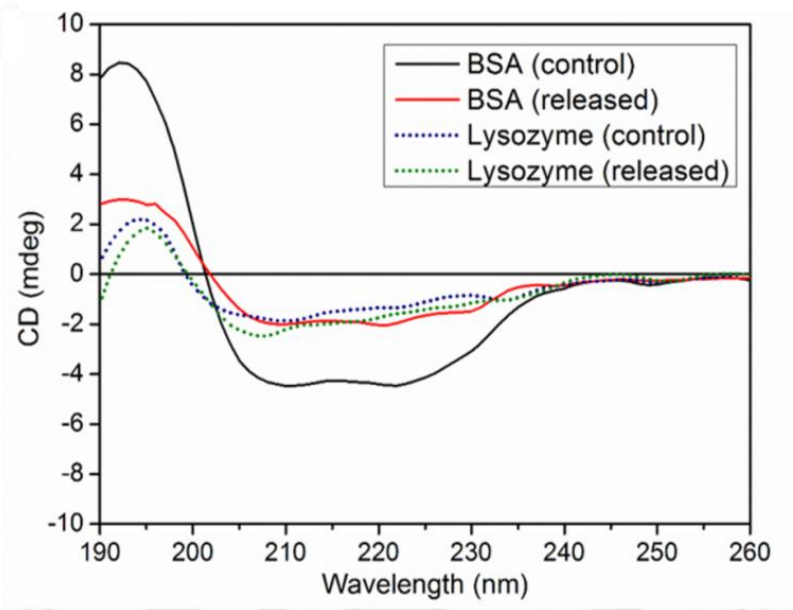

Figure 4.13: CD spectra of the native and released proteins BSA and lysozyme in PBS 7.4.

4.4.6. Cytotoxicity of A1:

In order to be used as a drug delivery platform, the hydrogel should be non-cytotoxic to the systemic tissues. One of the bottle necks in being able to use polymeric materials as drug delivery platforms stems from the systemic toxicity generated by them. Cytotoxicity of A1 was assessed using the MTT cell viability assay. Figure 4.14 shows the effect of A1 on the cell viability of MCF7 and HEK cell lines. A1 was found to be non-cytotoxic for 24 h over the entire concentration range (0-100 µM) for which the experiment was conducted. This concentration was very high compared to that which might result from the dissolution of molecules from the surface of the hydrogel. Thus for practical purposes, peptide A1 was non-cytotoxic and ideal to be used as a drug delivery platform.

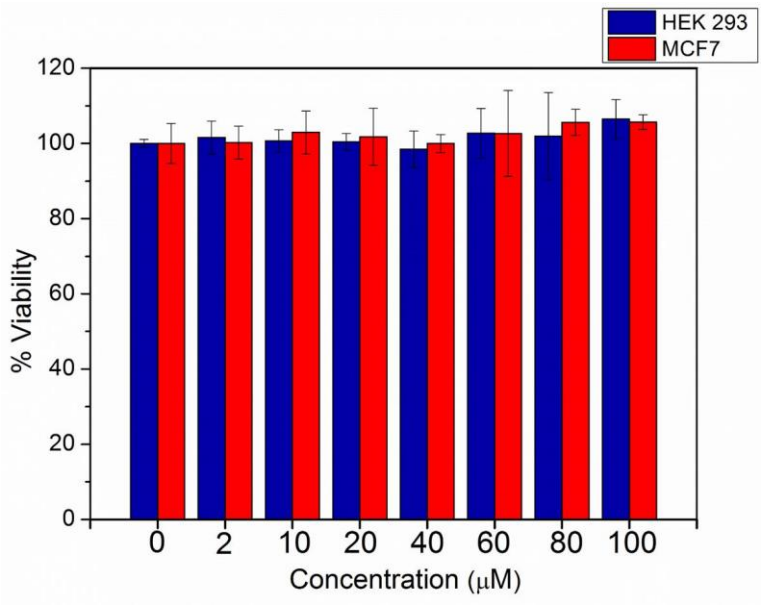

Figure 4.14: MTT assay of A1 on HEK 293 and MCF7 cell lines. Cell Viability was quantified by measuring the absorption at 570 nm. All experiments were performed in triplicate.

4.5. Conclusion

We have designed a drug delivery platform from a charged peptide based hydrogel, which can be used for sustained release of various kinds of drugs and proteins. We have investigated the co-assembly of the peptide with the drug molecules in details. Co-assembly of the peptide with the drugs was of orthogonal nature wherein the peptide and the drugs self-sorted and co-assembled individually. This led to the formation of softer co-assembled gels. Aromatic π-π stacking, hydrogen bonding and the electrostatic interactions were the key players facilitating hydrogelation and co-assembly processes. Anticancer drug 5-FU was shown to be released better in acidic pH compared to normal physiological pH, which might diminish the problem of unspecific release of the drug. All the cargoes were released sustainably from the hydrogels and retained their biological activity and secondary structure post-release. Such "all in one" kind of non-cytotoxic delivery platform might be of great importance in biomedical applications the future.

Chapter 5

Investigation of the Self-Assembly Mechanism of a Tryptophan Containing Tetrapeptide

Chapter 5
Investigation of the Self-Assembly Mechanism of a Tryptophan Containing Tetrapeptide

5.1. Peptide Self-Assembly

As discussed in the earlier chapters, self-assembly of molecules is an unique way of fabrication of materials with complex architectures that can be employed in various applications. Choice of the molecular building blocks and their judicious design helps in directing the assembly process Self-assembly can be further tuned by manipulating the various factors/ stimuli that drive the process. Diphenylalanine (FF) moiety was the first peptide system that showed exceptional self-assembling ability and have been extensively used in various studies. The self-assembling property of this dipeptide unit occurred due strong aromatic π-π stacking interactions of its side chains. However, the two other aromatic amino acids Trp and Tyr, have only been used to a limited extent. Di-Trp peptide (WW) does not show similar aggregation properties as the FF peptide, in spite of having an aromatic side chain that could have aromatic interaction.[150] S. Verma and co-workers demonstrated that a tetrapeptide containing diTrp moiety self-assembled to form nano-vesicles.[608] They also demonstrated that di-Trp moiety when attached to a tridentate ligand also gave rise to spherical vesicular structures.[609]

5.2. Present Study

In this study we have designed a simple tetrapeptide Boc-Trp-Leu-Trp-Leu-OMe (P), containing two Trps, that are interspersed by a Leu residue, and studied its self-assembly mechanism. The peptide shows a concentration dependent morphological transition from unilayered discrete nanospheres to clustered microspheres (Figure 5.1). Intrinsic Trp fluorescence was used as a reporter entity that helped in studying the mechanism of self-assembly of the peptide. Dye/drug binding studies were employed to understand the details of

the self-assembled morphology (Figure 5.1). We demonstrated that the peptide microspheres could interact, intercalate and restrain the hydrophobic dye carboxyfluorescein (CF) and drug molecule Curcumin on its surface, in addition to encapsulating them. The dye and the drug molecules could be released in the presence of physiologically relevant cations and acidic pH. This dual-mode drug binding helped us to gain thorough understanding of the mechanism of self-assembly of our designed peptide. Additionally, since the drug release could be stimulated by lowering the pH, and the cancer tissues are acidic in nature, this model might find potential applications in cancer drug delivery in future.

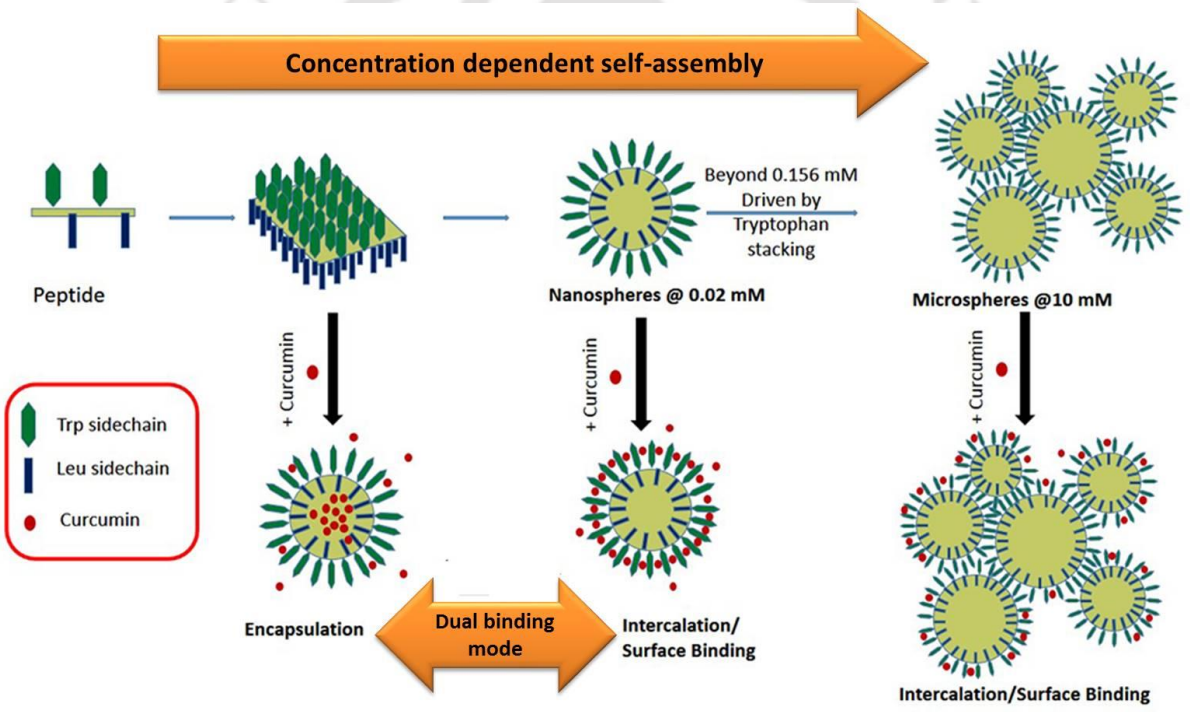

Figure 5.1: Schematic illustration of the work of this Chapter

5.3. Experimental Details

5.3.1. Synthesis of the Peptide:

5.3.1.1. General Procedure:

Racemization free, fragment condensation technique based solution phase method was employed for the synthesis of the tetrapeptide (Boc-Trp-Leu-Trp-Leu-OMe) (P). Tertiary butyloxycarbonyl (Boc) and methyl ester group were used for the protection of amino and

carboxyl groups. The Boc group and the ester group were deprotected using formic acid and saponification reactions respectively. Coupling was mediated *via.* N-(3-dimethylaminopropyl)-N′-ethylcarbodiimide hydrochloride EDC.HCl and HOBt. The progress of the reaction was monitored using thin layer chromatography (TLC). The final peptide was obtained with high purity by column chromatography using silica gel (100-200) mesh as the stationary phase and mixture of ethyl acetate and hexane in the ratio of 3:2 as the mobile phase. The peptide was further purified using HPLC for further removal of any impurities. The synthesized peptide was fully characterized by ^{1}H NMR study, ESI-MS and FT-IR Spectroscopy.

5.3.1.2. Synthesis of Boc Protected L-Trp (Boc-W-OH):

L-Trp (20 mmol, 1 equiv.) was dissolved in 5N NaOH, stirred and cooled to 0 ℃. To the stirring solution, Boc anhydride (24 mmol, 1.2 equiv.) dissolved in 1, 4-dioxane was added. The pH of the reaction was maintained at >12. The reaction mixture was allowed to stir overnight. Dioxane was evaporated completely over rota vapour. Water was added to the reaction mixture, washed with ethyl acetate (3 x 30 mL) and acidified with 6N HCl (pH = 2). The aqueous layer was extracted with ethyl acetate (3 x 30 mL), the organic layers pooled and washed with 25% brine solution. The organic layer was dried over Na_2SO_4 and evaporated to get the Boc protected L-Trp. (Boc-W-OH).

Yield of the reaction was 5.89 g (19.4 mmol, 97%).

HRMS (ESI-MS): m/z $(M+H)^+$ calculated for $C_{16}H_{20}N_2O_4$ = 305.1496 Da, Obs $(M+H)^+$ = 305.1451 Da (Appendix A, Figure A14, Page VIII).

^{1}H NMR (DMSO-d_6 , 600 MHz, δ ppm) (Appendix A, Figure A15, Page VIII): 1.33 (s, 9H, BOC-H); 2.96-3.02 (m,1H, Cβ H); 3.12-3.17 (m,1H, Cβ H); 4.12 - 4.19 (m, 1H, Cα H); 6.94-6.97 (d,1H, *J* = 12 Hz, C_7H w.r.t indole ring); 6.98-7.02 (t, 1H, *J* = 9 Hz, C_5H w.r.t indole ring); 7.05-7.10 (t, 1H, *J* = 6Hz, C_6H w.r.t indole ring); 7.14-7.20 (broad singlet, 1H, C_2H

w.r.t indole ring); 7.33-7.37 (d, 1H, J= 12Hz, C_4H w.r.t indole ring); 7.52-7.55 (d, 1H, *J* = 6 Hz, amide NH); 10.83 (s, 1H, NH indole) .

5.3.1.3. Synthesis of Methyl Ester of L-Leu (L-OMe. HCl):

L-Leu (50 mmol, 1 eq.) and dry methanol (50 mL) were taken in a round bottom flask, covered with a calcium chloride guard tube and cooled in an ice bath. Into the stirring reaction mixture, $SOCl_2$ (75 mmol, 1.5 equivalent) was drop-wise added. The reaction mixture was stirred for another 30 minutes under ice cooled condition. After 30 minutes the reaction mixture was refluxed for 4 h. After four h the reaction mixture was cooled down and then evaporated to get the methyl ester of L-Leu.

Yield of the reaction was7.67g (42.5 mmol, 85%).

5.3.1.4. Synthesis of Dipeptide Boc-Trp-Leu–OMe:

L-OMe. HCl (15 mmol) was dissolved in minimum amount of dry DCM (30 mL) to which 5.9 mL (2.8 equiv.) of triethyl amine was added at 0 ℃ and stirred for 15 minutes. This was added to a precooled solution of Boc-protected Trp Boc-W-OH (15mmol) in dry DCM (30 mL), preactivated with EDC.HCl (1.2 equiv.) and HOBt (1.2 equiv.). After 12 h, the reaction mixture was washed with distilled water and brine for three times. The organic layer was dried over anhydrous sodium sulphate, filtered and was evaporated in vacuum to yield an off-white solid. The dipeptide was purified with column chromatography using silica gel as stationary phase and mixture of ethyl acetate and hexane in the ratio of 3:2 as eluent.

Yield of the reaction was5.4 g (12.5 mmol, 83.2 %).

HRMS (ESI-TOF): $m/z(m+H)^+$ calc. for $C_{23}H_{33}N_3O_5$ 432.2493 Da, found 432.2490 Da (Appendix A, Figure A16, Page IX).

^1H NMR (DMSO-d_6, 600 MHz, δ ppm) (Appendix A, Figure A17, Page IX) : 0.84, 0.9 (d, 3H, *J* = 6 Hz, Leu δ H); 1.3 (s, 9H, BOC-H); 1.46-1.56 (m, 1H, Leu γ H); 1.56-1.7 (m, 2H,

Leu β H); 2.86-2.92, 3.04-3.08 (m, 2H, Trp βH); 3.06 (s, 3H, methyl group); 4.24 (m, 1H Leu αH); 4.35 (m, 1H, Trp αH); 6.73-6.77 (d, 1H, *J* = 6Hz, C_7H w.r.t. indole ring); 6.97-6.99 (t,1H, *J* = 6, C_5H w.r.t indole ring); 7.05-7.08 (t, 1H, *J* = 6, C_6Hw.r.t indole ring); 7.13 (broad singlet, 1H, C_2H w.r.t indole ring);7.33 (d, 1H, J = 6 Hz, amide NH); 7.61(d, 1H, *J* = 6 Hz, C_4H w.r.t indole ring); 8.25 (d, 1H, *J* = 6 Hz, amide NH), 10.80 (1H, NH, indole ring).

5.3.1.5. Synthesis of Boc-Trp-Leu-OH:

The synthesized dipeptide Boc-WL-OMe (6.2 mmol, 2.672 g) was dissolved in methanol (MeOH) followed by the drop wise addition of 10 N NaOH till pH of the reaction was> 12 (mixture turned turbid). The reaction was allowed to stir for 36 h and progress of the reaction was monitored by TLC. After 36 h, the reaction mixture was evaporated. Water was added to the residue and extracted with ethyl acetate (3 x 30 mL). The aqueous layer was cooled and acidified with 6 N HCl (pH =2) and then extracted with ethyl acetate (3x 30 mL). The organic layers were pooled, washed with brine solution, dried over Na_2SO_4andevaporated to obtain the product Boc-WL-OH.

The yield of the reaction: 1.9 g, (4.8 mmols, 77.41 %).

5.3.1.6. Synthesis of Peptide Boc-Trp-Leu-Trp-Leu-OMe:

10 mL formic acid was added to the di-peptide Boc-Trp-Leu-OMe (4.8 mmol) and kept for 3 h. Thereafter, formic acid was completely removed under pressure. The residue so obtained was taken in water and the pH of the solution was adjusted to 11 using sodium bicarbonate and then extracted with ethyl acetate (3x 30 mL). Organic layers were pooled, washed with brine, dried over sodium sulphate and concentrated to a viscous liquid which responds to ninhydrine test. The Boc deprotected dipeptide (NH_2-Trp-Leu-OMe) was dissolved in DCM and triethyl amine was added to it at 0℃ and the reaction mixture was stirred for 15 minutes. This was added to the precooled Boc-Trp-Leu-OH in dry DCM, preactivated with EDC.HCl and HOBt. After 72 h the reaction was washed with distilled water and brine (3x 30 mL).

The organic layer was dried over anhydrous sodium sulphate, filtered and was evaporated in vacuum to yield an off white solid. The tetra peptide was purified using silica gel as stationary phase and mixture of ethyl acetate and hexane in the ratio of 3:2 as eluent. Final purification was done by reverse phase HPLC using acetonitrile/H_2O solvent mixtures. Tetrapeptide was obtained as a white powder.

Yield of the reaction was 2.0 g (2.8 mmols, 58.10 %).

Melting point: 154°C.

The peptide purity was confirmed by analytical HPLC trace (Appendix A, Figure A18, Page X) and characterised by ESI-MS (Appendix A, Figure A19, Page X) and ^{1}H NMR spectra (Appendix A, Figure A20, Page XI).

^{1}H NMR (DMSO-d_6, 600 MHz, δ ppm): 0.78-0.83 (m, 12 H, Leu *δ*-H); 1.07-1.09 (t, 2 H, Leu γ-H); 1.26 (s, 9 H, Boc-H merged with Leu β-H); 1.3-1.5 (m, 4 H, Leu β-H merged with Boc-H); 2.8-3.14 (m, 4H, Trp β-H); 3.6 (s, 3H, OMe); 4.1-4.6 (s, 4H, chiral); 6.81,7.88,8.07, 8.26 (d, 4H, *J* = 6 Hz, amide N-H); 6.91-6.97 (t, 2H, *J* = 12 Hz, C_6Hw.r.t. indole ring); 7.02-7.05 (t, 2H, *J* = 6Hz, C_5H w.r.t. indole ring); 7.08-7.11 (d, 2H, *J* = 6 Hz, C_4Hw.r.t. to indole ring); 7.28-7.30 (d, 2H, *J* = 12 Hz, C_7Hw.r.t. indole ring); 7.52-7.58 (d, 2H, *J* = 6 Hz, C_2H w.r.t. indole ring); 10.79-10.80 (s, 2H, indole ring N-H).

HRMS (ESI-TOF): m/z$(m+H)^+$ calc. for $C_{40}H_{54}N_6O_7$731.4127 Da, found 731.4187 Da (Appendix A, Figure A19, Page X)

5.3.2. FT-IR Spectroscopy: IR spectra was recorded in KBr pellet in the region of 1000-4000 cm^{-1}.

5.3.3. FESEM: The morphologies of the reported materials were studied by FESEM.

a) For the FESEM study in different solvents, lyophilized peptide was incubated for 5 minutes in different solvents (DMSO, toluene, MeOH and EtOH) at peptide concentration of

10 mM. The peptide solutions were drop casted on a silicon wafer and dried under vacuum at room temperature overnight (7 days for DMSO solution).

b) For the morphology study at lower concentration, 0.02 mM ethanolic peptide solution was prepared and after 2 minutes 5µL of this solution was taken out and drop casted on a wafer. Another part of the solution was allowed to age for 10 days and 5 µL of the same was drop casted on a wafer thereafter. 20 µL of 0.01 mM of KCl and 50 µL of HCOOH were added to two batches of 10 days- aged peptide solution (5 mL each), incubated for 48 h respectively and drop casted on a silicon wafer.

c) 1.46 mg of lyophilized peptide was added to 100 mL of 2.5 µM Curcumin solution to a final peptide concentration of 0.02 mM and incubated for 2 days. 5 µL of this solution was drop casted on a silicon wafer. Water was added to the peptide solution and it was freeze dried in two batches in which 5 µL of 0.01 mM of KCl and 50 µL of HCOOH were added, incubated for 48 h and 5 µL of each batch were casted on wafer and dried before imaging.

5.3.4. FETEM: FETEM studies were performed by casting 3 µL of 0.02 mM ethanolic solution of peptide on carbon - coated copper grids (300 mesh). EtOH was removed by slow evaporation and the grid was allowed to dry under vacuum at room temperature for 3 days. 3 µL of uranyl acetate solution was added to the grid and dried under vacuum overnight. Images were taken in both the transmission mode and diffraction mode.

5.3.5. AFM: For AFM study, 5 µL ethanolic solution of the peptide (10 mM and 0.02 mM) were placed on microscope glass coverslip and dried by slow evaporation under vacuum for 3 days.

5.3.6. DLS: Particle size of the peptide spheres was determined by DLS with different concentrations (0.01, 0.02, 0.03, 0.04 mM) of ethanolic peptide solutions.

5.3.7. CD Spectroscopy: The CD spectra of all the samples were recorded by using a 200 µL quartz cuvette of 1 mm path length at RT. Spectra were collected at a scan rate 100 $nm.min^{-1}$ and 2 nm bandwidth from 195 to 260 nm with 5 scans for averaging. Before running the sample, ethanol was run to correct the baseline.

5.3.8. Fluorescence Spectroscopy: Intrinsic Trp fluorescence of peptide was monitored to study the peptide self-assembly process. Emission spectra were recorded for peptide solutions at different concentrations in between 10 mM- 0.04 mM at excitation wavelength of 280 nm and a slit width of 3.

5.3.9. Fluorescence Microscopy: Ethanolic solution of peptide (0.02 mM) was incubated with 50 µM of CF for 24 h. Then one drop (10 µL) of this solution was drop casted on a cover slide and dried at room temperature under vacuum. Fluorescence microscopic image was then taken.. For salt triggered disruption studies with the spheres, KCl solution (1 mM 5 µL) was added to the dye solution of peptide, incubated for 12 h and image taken subsequently.

5.3.10. Peptide Microsphere- Dye/Drug Interaction: This was studied by monitoring fluorescence emission of dye CF and drug Curcumin using fluorescence spectroscopy.

a. <u>Peptide-CF Interaction:</u> 5 mL of peptide solution was mixed with 5 mL of ethanolic CF solution to attain final peptide and CF concentrations of 0.02 mM and 90 µM respectively. Emission spectra of CF were recorded at different time intervals with excitation wavelength at 493 nm and bandwidth 5 nm. Finally after 24 h, 5 µL of 0.01 mM KCl was added to 5 mL of the above solution, incubated for 24 h and florescence was measured. To the other 5 mL of the above solution, 50 µL of HCOOH was added, incubated for 24 h and fluorescence measured.

b. <u>Curcumin Peptide Interaction:</u> Experiment was done in two different ways.

1. To ethanolic peptide solution, Curcumin solution was added to make final peptide concentration of 0.02 and 10 mM and final Curcumin concentration of 20 μM respectively. Florescence emission was monitored at different time intervals. After 36 h, KCl and HCOOH were added to different portions of the above solution as described previously and florescence was recorded.

2. 1.46 mg of lyophilized peptide was added to 100 mL of 20 μM ethanolic solution of Curcumin to make a final peptide concentration of 0.02 mM. Emission spectra with excitation maxima at 430 nm and bandwidth of 5 was recorded at different time intervals upto 36 h. KCl and HCOOH were added to different portions of the above solution as described previously and florescence was recorded.

5.3.11. Proof of Curcumin Encapsulation:

Peptide (1.5 mg) of peptide was added to 20 μM Curcumin solution. The microspheres containing Curcumin were coagulated using water and centrifuged down. The supernatant's mass was checked. After several cycles of washing followed by centrifugation, the precipitate was resuspended in ethanol and water and lyophilized. Lyophilized microspheres loaded with Curcumin were again resuspended in EtOH and its mass checked. Finally KCl was added to rupture the microspheres to release Curcumin and mass was checked.

5.4. Results and Discussions

5.4.1. Self-Assembly of P in Different Solvent Systems:

Figure 5.2 gives the chemical structure and the gas phase optimized geometry of the synthesised peptide P. We wanted to study the self-assembly behaviour P in different solvents and conditions. To gain insight into the type of morphology formed by the peptide P in different solvents upon self-assembly, we performed various kinds of electron microscopic studies like FESEM, TEM and AFM.

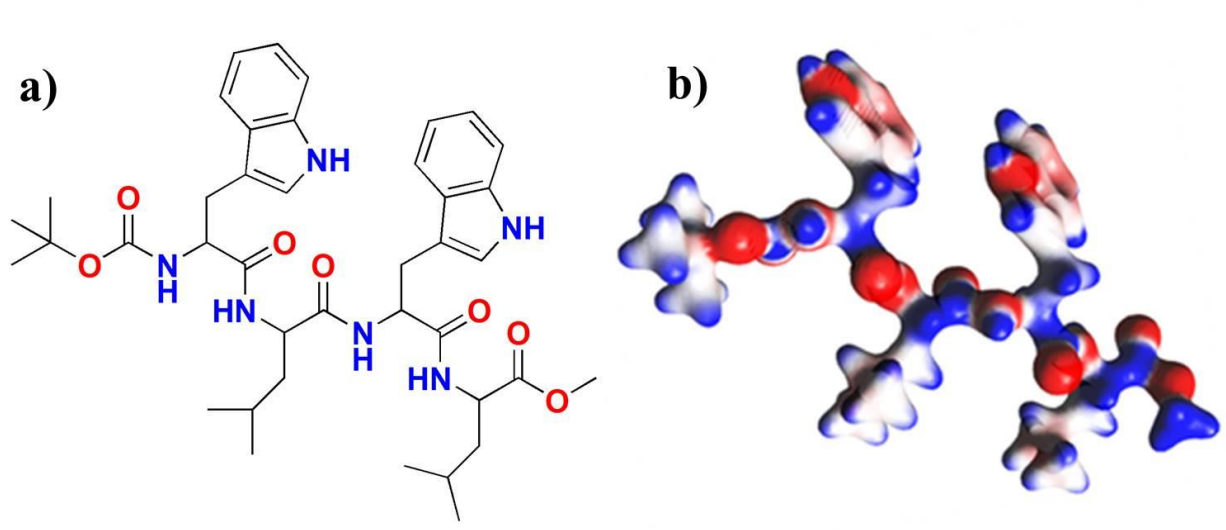

Figure 5.2: a) Chemical structure of Peptide Boc-Trp-Leu-Trp-Leu-OMe (P). b) Electrostatic potential map of Gas phase optimized geometry (Method: Hartree–Fock (HF) Basis set: 6-31+g*) of P. Blue and red indicate positive and negative charge respectively.

The morphology of the peptide P at 10 mM concentration in various solvents like DMSO, toluene, MeOH and EtOH observed by FESEM is shown in Figure 5.3a-d. It is clearly evident from the images that P adopts different morphologies in various solvents. Thus the solute-solvent interaction has a predominant role on modifying the solute-solute interactions that bring about self-assembly. In our study, we focused on the spherical morphology which was obtained in two solvents namely EtOH and MeOH. As MeOH is carcinogenic and in the practical scenario may not be suitable for applications, we decided to continue our studies further with EtOH. The particle size distribution of the microspheres at 10 mM MeOH and EtOH is shown in Figure 5.4a, b respectively where we have observed that at 10 mM concentration of P, microspheres with diameters ranging from 2-3 μm were formed predominantly in EtOH. To probe the effect of concentration on the self-assembly of P, FESEM was done at different concentrations. P self-assembled into nanospheres of 200-300

nm diameters at as low a concentration as 0.02 mM (Figure 5.5a). Thus the size of the microspheres was proportional to the concentration of the peptide solution.

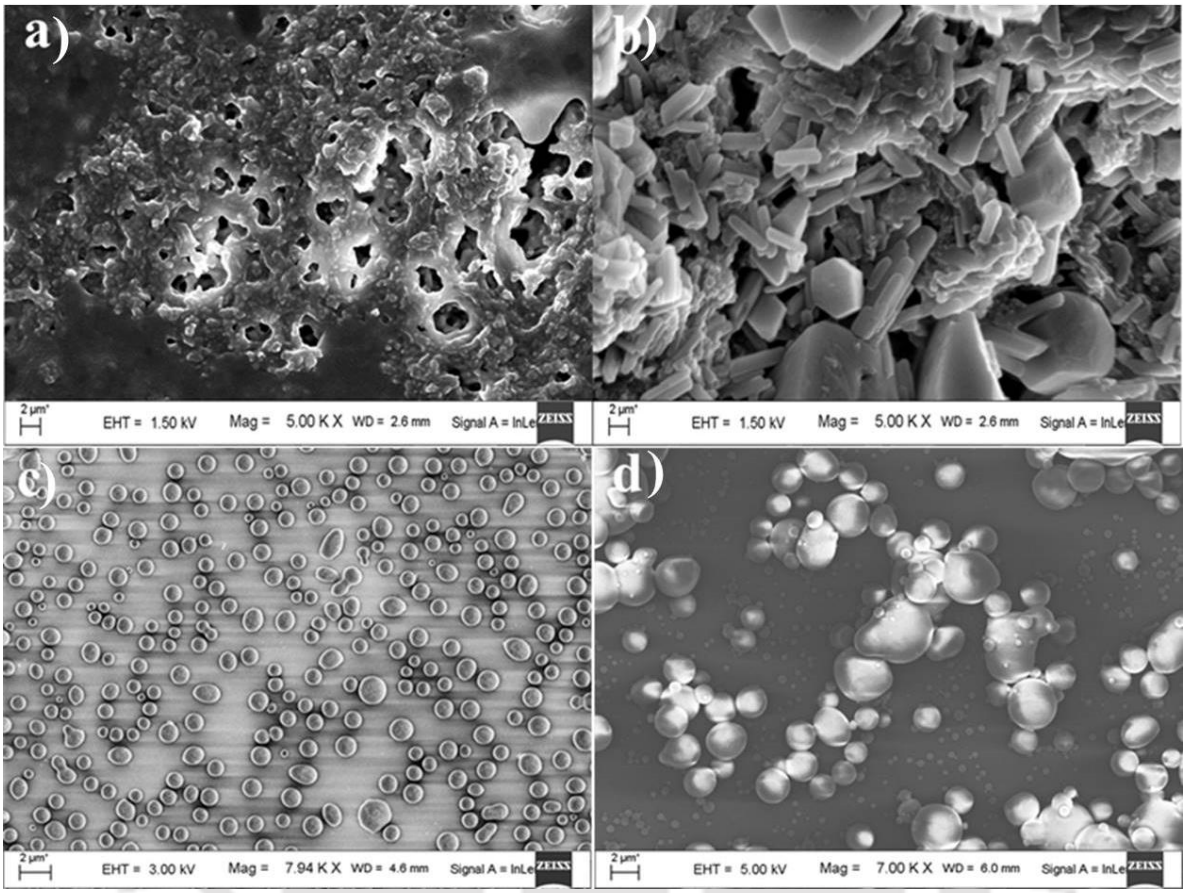

Figure 5.3: FESEM image of P in a) DMSO b) toluene c) MeOH and d) ETOH at 10 mM peptide concentration. P adopts different morphologies in various solvents.

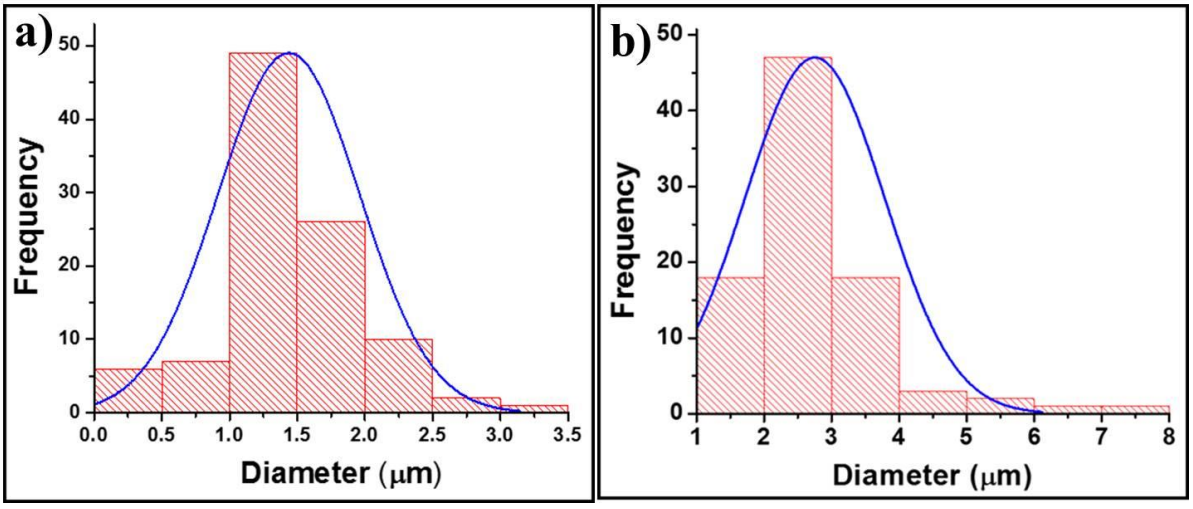

Figure 5.4: Particle size distribution of P microspheres in a) MeOH and b) EtOH at 10 mM peptide concentration. This has been obtained from the analysis of Figure 5.3c, d.

We wanted to find out whether this self-assembly process was kinetically or thermodynamically governed. Figures 5.5a and 5.5b show the morphologies of P at 0.02 mM, after incubation for 2 minutes and 10 days. There was no visible difference in the morphology indicating that the self-assembled morphology of the reported peptide may be a thermodynamically controlled product. The self-assembled microspheres disrupted upon addition of KCl and formic acid as is clear from FESEM images (Figure 5.5c-d).

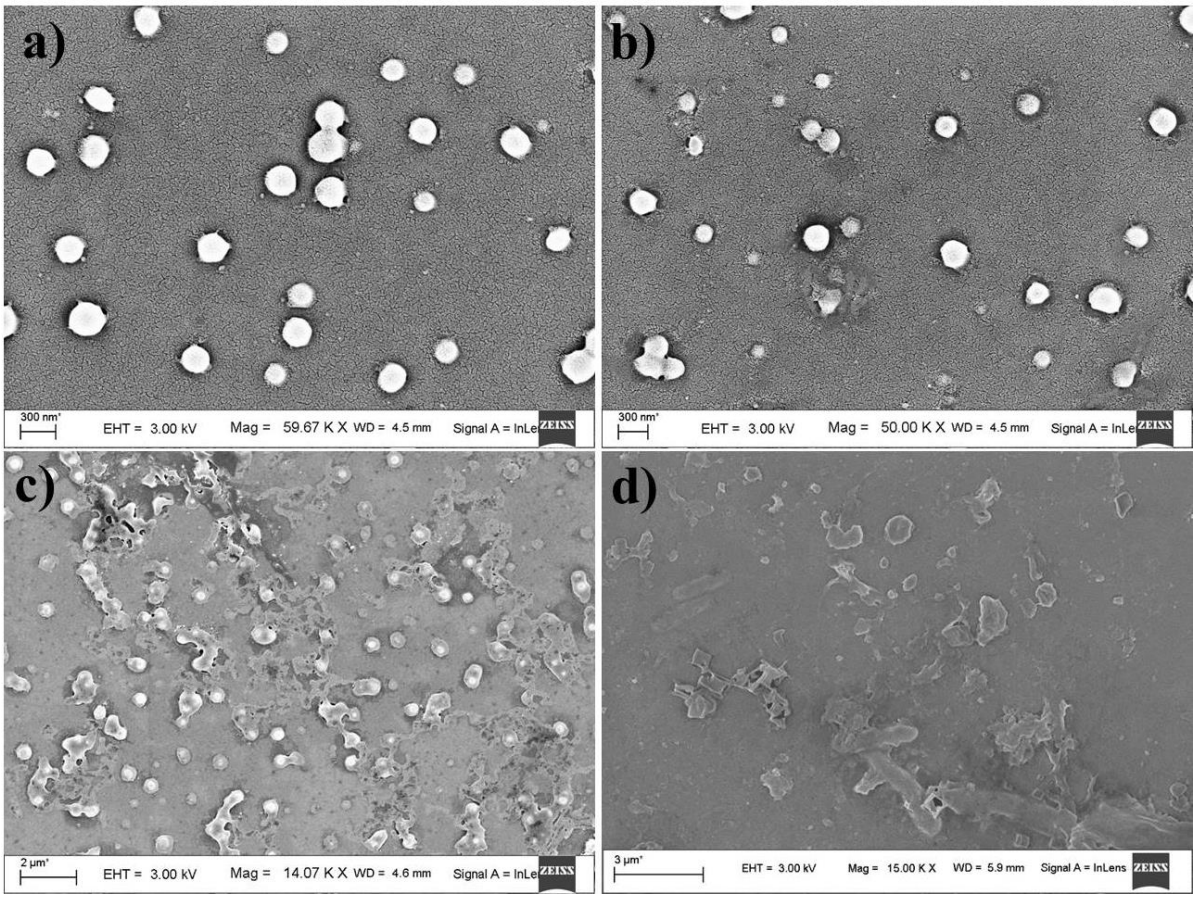

Figure 5.5: FESEM image of P in EtOH at 0.02 mM after incubation for a) 2 min and b) 10 days and after addition of c) of 0.1 mM KCl and d) 5µl HCOOH to a.

For further insight into the self-assembled morphology, FETEM studies were performed. It was observed that P formed nanospheres of the diameter of about 200-400 nm at a

concentration of 0.02 mM and microspheres of diameter of about 1-1.1 µm at a concentration of 10 mM which is in corroboration with the FESEM data (Figure 5.6a, b). The electron diffraction pattern in Figure 5.6c shows that the microspheres are partly crystalline. However, attempts of growing single crystals of P have been unsuccessful so far. The particle size distribution of the microspheres as seen by FETEM at 10 mM is shown in Figure 5.6d. The average particle size was found to be 1 µm.

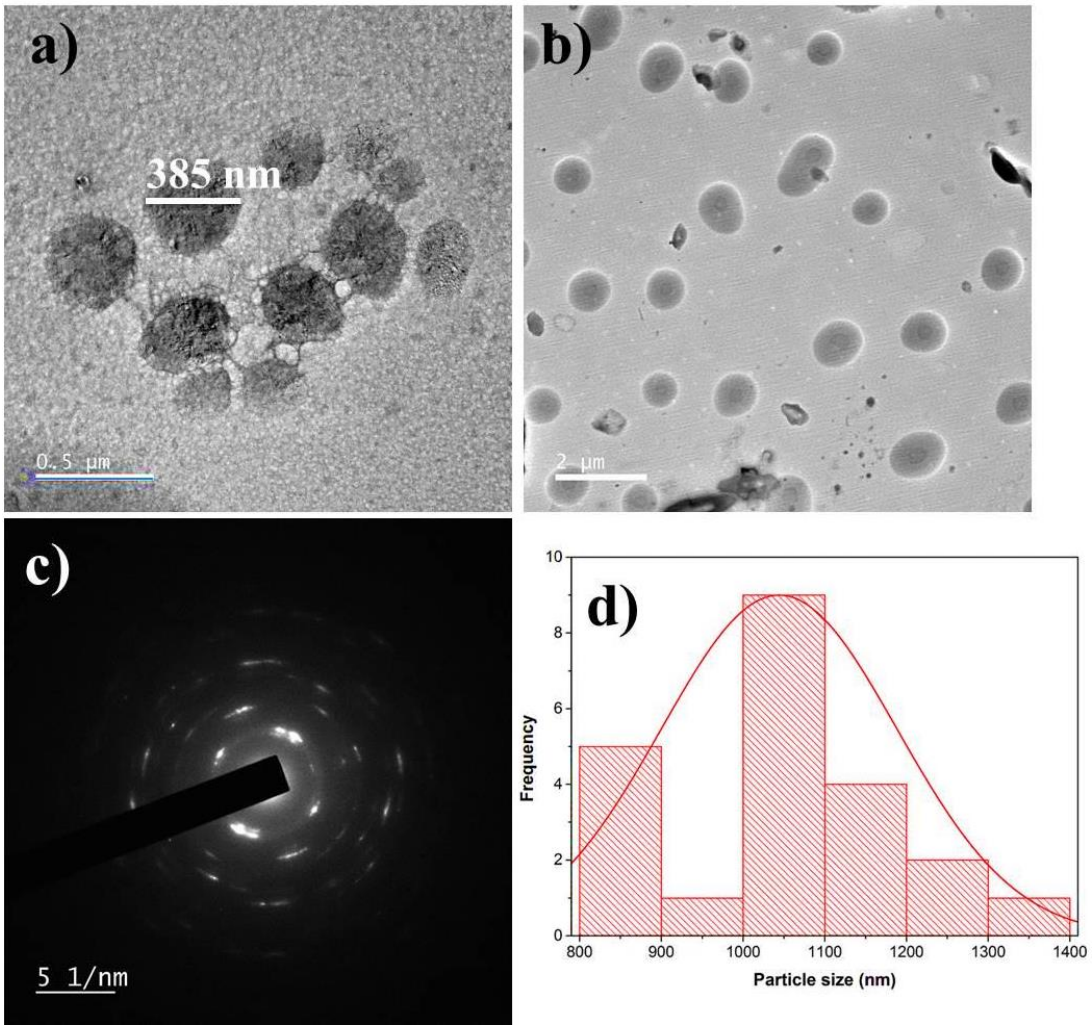

Figure 5.6: FETEM image of P at a) 0.02 mM and b) 10 mM respectively, c) Electron micrograph image of P at 0.02 mM and d) Particle size distribution of microspheres at 10 mM concentration of P as analysed from b.

Further, the topology of the self-assembled structures was studied using AFM (Figure 5.7a-c) at 0.02 mM peptide concentration. Nanospheres of 400 nm diameter were seen which also supported FESEM and FETEM data. Figure 5.7b and 5.7c shows the 3D plot and the surface profile analysis of the particles to see the width and flatness of the particles at that concentration.

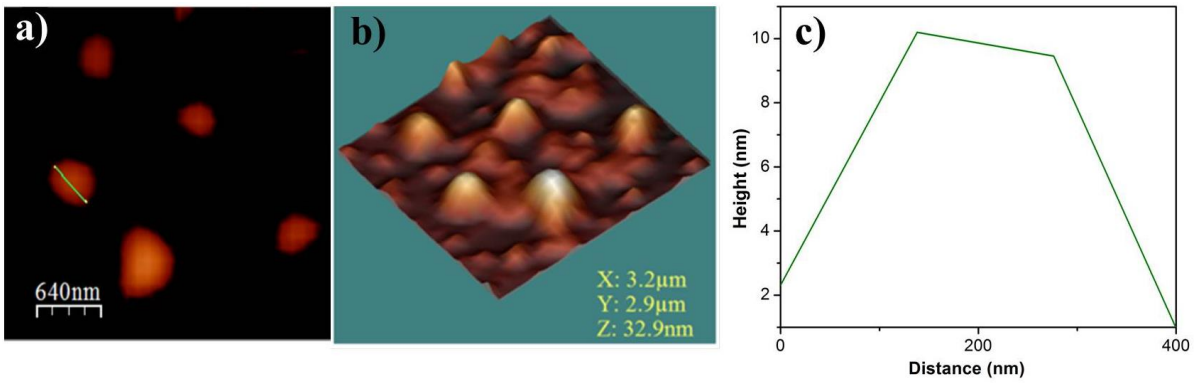

Figure 5.7: a) 2D AFM image of P at 0.02 mM concentration, b) 3D AFM image and c) height profile plot for the peptide nanospheres formed by P at 0.02 mM concentration.

5.4.2. Size Distribution of the Nanospheres: In order to study the dependence of the size of the self-assembled nanospheres on the concentration of the peptide solution, DLS experiments were performed. At peptide concentrations of 0.01, 0.02, 0.03 and 0.04 mM, the diameter of the nanospheres varied from 248 nm, 638 nm, 971 nm and 1410 nm (Figure 5.8a-d). Thus it was clearly seen that with the increase in concentration, the size of the microsphere increased as was previously seen in the FESEM studies. The peptide formed smaller nanospheres at lower concentration which started fusing with each other to form larger microspheres at higher concentration.

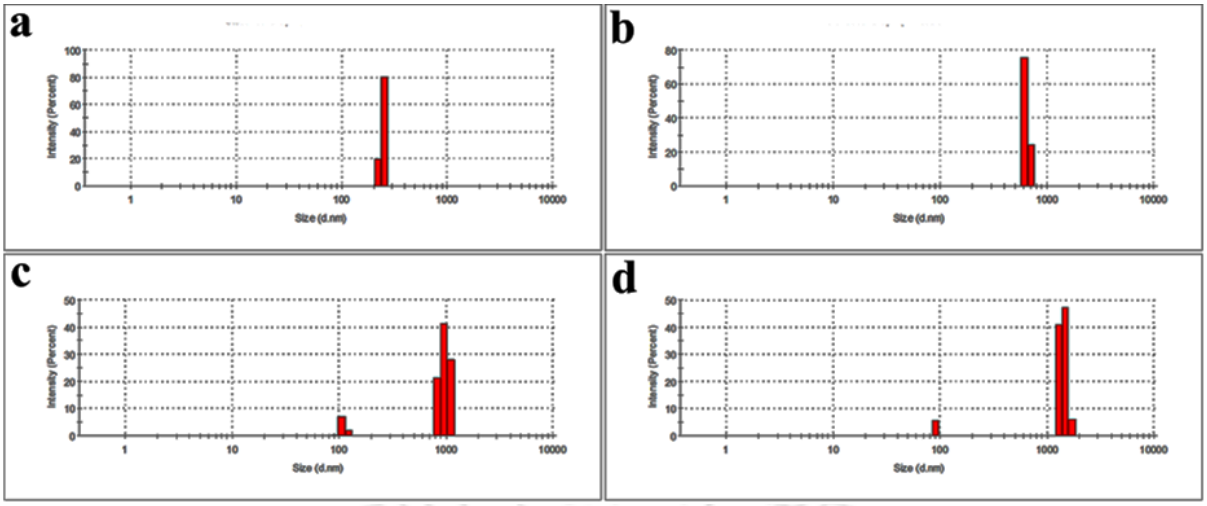

Figure 5.8: DLS study of P at a) 0.01 mM, b) 0.02 mM c) 0.03 mM and d) 0.04 mM peptide concentrations showing increasing diameters of 248 nm, 638 nm, 971 nm and 1410 nm respectively.

5.4.3. Backbone Conformation and Hydrogen Bonding in P: FTIR experiment was performed to look into the backbone conformation of tetrapeptide P (Figure 5.9) and the extent of hydrogen bonding of the peptides in the solid state. The most informative frequency ranges for peptides are (a) 3500-3200 cm^{-1}, corresponding to the N-H stretching vibrations of the peptide and (b) 1800-1600 cm^{-1}, corresponding to the stretching vibrations of the peptide urethane, and ester groups.[610-613] Two intense bands were obtained at 3416 cm^{-1} and 3312 cm^{-1} indicating non-hydrogen bonded and intermolecularly hydrogen-bonded NHs respectively.[611, 613] The intensity of the NH band at 3312 cm^{-1} is more than that at 3416 cm^{-1} indicating hydrogen bonded structures for the peptide in solid state. The characteristic IR absorption bands at about 1641 cm^{-1} (amide I) and 1531 cm^{-1} (amide II) of the tetrapeptide are typical of β-sheet[610-612] conformations. Moreover, existence of band at 1689 cm^{-1} gave a hint of the presence of antiparallel *β*-sheet structures.[611]

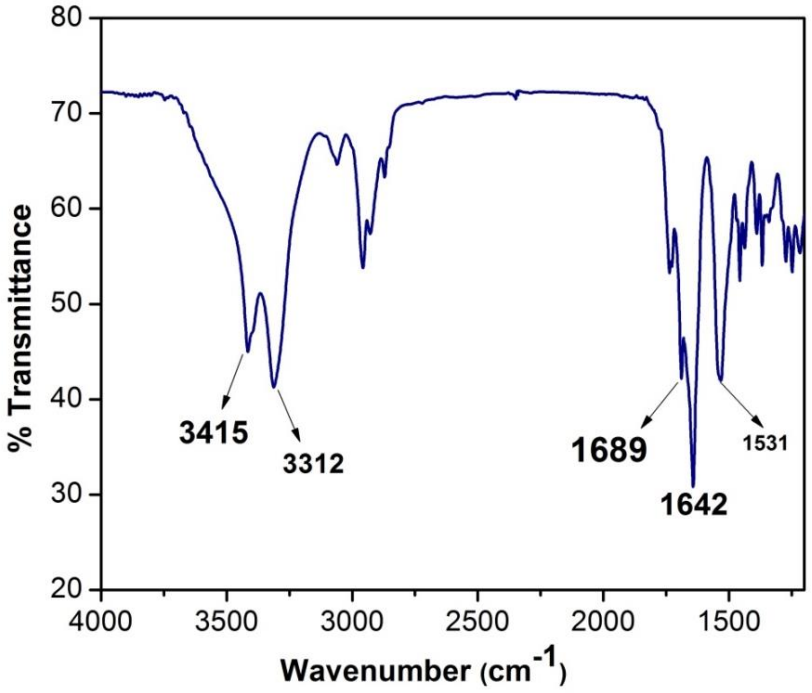

Figure 5.9: FTIR spectrum of P indicating β-sheet like solid state conformation.

5.4.4. Secondary Structure of P: Circular dichroism was performed at different concentrations of the peptide (Figure 5.10). Though CD is a sensitive technique for the prediction of secondary structure of polypeptides,[614] the limitations on the use of CD for conformational analysis of small linear peptides with aromatic residues have been reported.[615, 616] Moreover, secondary structure formation has been shown to be dependent on the length of the polymers. As P is very small, presence of random coil like CD peaks was not surprising.[617] Upon increasing the concentration of P beyond 0.15 mM, a noteworthy exiton-coupled band appeared at 215 nm (negative) and 229 nm (positive), which indicated interaction between aromatic chromophores of Trp[618] (Figure 5.10). These bands were not seen at lower concentrations which suggested that the self-assembly which was obtained at a lower concentration of 0.02 mM did not involve stacking of the indole rings of Trp. Observation of exciton coupled band at high concentration of peptide suggested that some change in self-assembly occurred at high peptide concentration that involved aromatic stacking of Trp side chains.

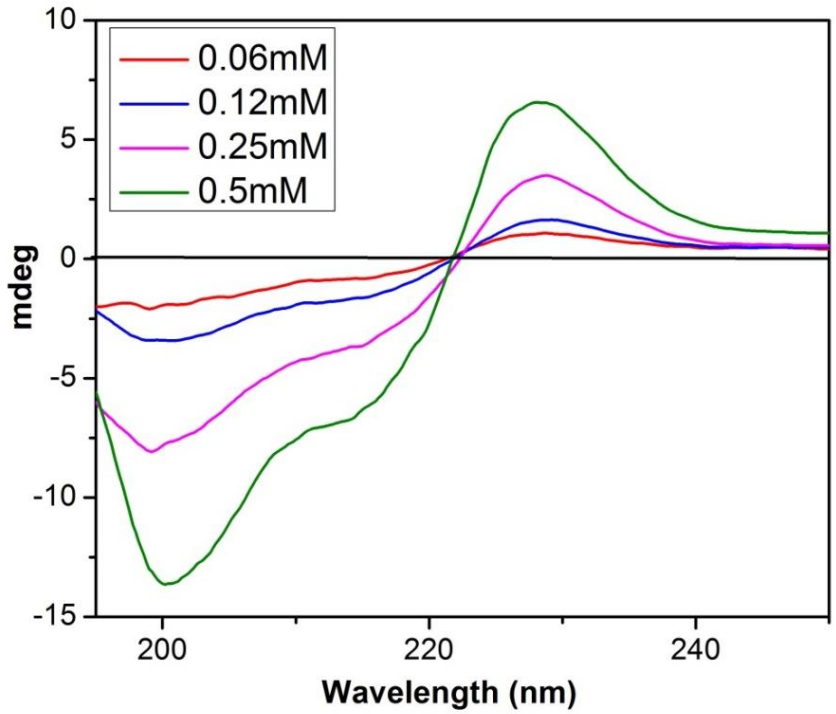

Figure 5.10: CD spectrum of P showing exciton coupled bands at 215 nm (negative) and 229 nm (positive) at higher P concentration.

5.4.5. Self-Assembly of P:

5.4.5.1. Role of π-π Stacking: To probe the self-assembly of the peptide further, we decided to monitor the intrinsic fluorescence of Trp residues present in the peptide. As the intrinsic fluorescence of Trp gets quenched upon aromatic stacking interactions of the indole rings during self-assembly, this study is immensely important in monitoring the self-assembly driven by aromatic stacking of Trp. Upon increasing the concentration of the peptide, the fluorescence intensity at 345 nm steadily increased till 0.156 mM, beyond which the fluorescence intensity got quenched upon increasing the concentration (Figure 5.11). This suggested that aromatic stacking of indole rings occurred beyond 0.156 mM and was absent at lower concentrations. This data corroborated the CD data and suggested that the self-assembly into nanospheres at a low concentration of 0.02 mM was not assisted by Trp stacking. With increase in the concentration of the peptide, not only did the size of the

peptide nanospheres increase as seen by DLS, but a significant change in the self-assembly pattern also occurred, which involved aromatic stacking of Trp.

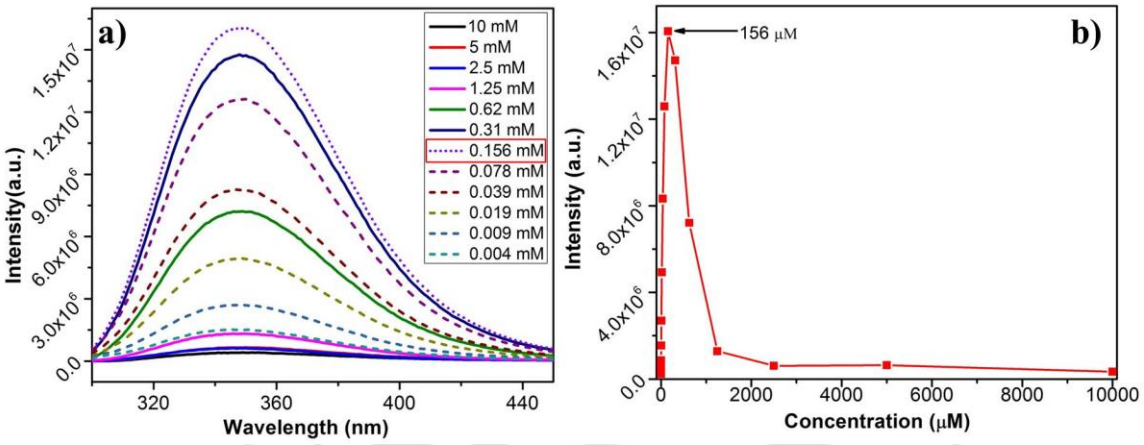

Figure 5.11: a) Concentration dependent fluorescence spectra of P b) Plot of fluorescence emission intensity vs. concentration of P.

Thus, from the FESEM, IR, CD and fluorescence data we can suggest that the self-assembly process of P was guided not only by aromatic stacking of the Trp moieties but also other non-covalent forces like hydrogen bonding. Although we have seen from fluorescence data that beyond 156 μM concentration of P the stacking of Trp moieties drives the self-assembly of P, but from FESEM data we have observed that even at lower concentration of 0.02 mM peptide nanospheres were formed. This suggested that self-assembly at lower concentration was not guided by aromatic stacking but by other interactive forces like hydrogen bonding. This brings us to a conclusive idea about the interplay of more than one non-covalent force in the self –assembly of peptide P. For gaining deeper insight into the molecular arrangement in the assembly process, we have done extensive fluorescence experiments of the peptide with curcumin and CF, a fluorescent drug and dye respectively.

5.4.5.2. Studies on Binding/Encapsulation of Dye CF and Hydrophobic Drug Curcumin to the Peptide Microspheres:

At first, we have chosen the fluorescent dye CF to study the peptide-CF interaction using fluorescence microscopy. Figure 5.12a shows the brightfield image of the peptide nanospheres at 0.02 mM peptide concentration. Figure 5.12b is the fluorescence image of the dye, showing its localization at certain zones. Figure 5.12c is the superimposition of the two earlier images which demonstrates the co-localization of dye CF and the peptide nanospheres. However, this picture does not explain whether the peptide is surface bound or entrapped within the nanospheres. Figure 5.12d shows the loss of localization/scattering of CF upon addition of KCl which is an effect of the disruption of the vesicles upon addition of KCl, as already seen from FESEM earlier (Figure 5.5c). This disruption of peptide self-assembly leads to the loss of interaction in between the peptide and CF.

We have then used fluorescence spectroscopy to understand the interaction of the dye with the peptide P by using the intrinsic fluorescence emission of the dye. Figure 5.13a shows the time dependent fluorescence emission spectrum of CF upon being incubated with peptide solution (0.02 mM). Initially, after addition of the dye to the peptide solution, the fluorescence emission intensity of the dye got quenched which indicated the interaction of the dye with the peptide. The fluorescence emission intensity of the dye kept steadily decreasing over the time till about 10 h. Upon addition of KCl, the fluorescence emission of the CF increased again. This might be a consequence of release of the dye molecules due to disruption of peptide nanospheres upon addition of KCl. Disruption of nanospheres in presence of KCl has already been demonstrated earlier with FESEM (Figure 5.5c).The regain of fluorescence in the case of CF was almost 100% as KCl seemed to have very little effect on it (Figure 5.13b).

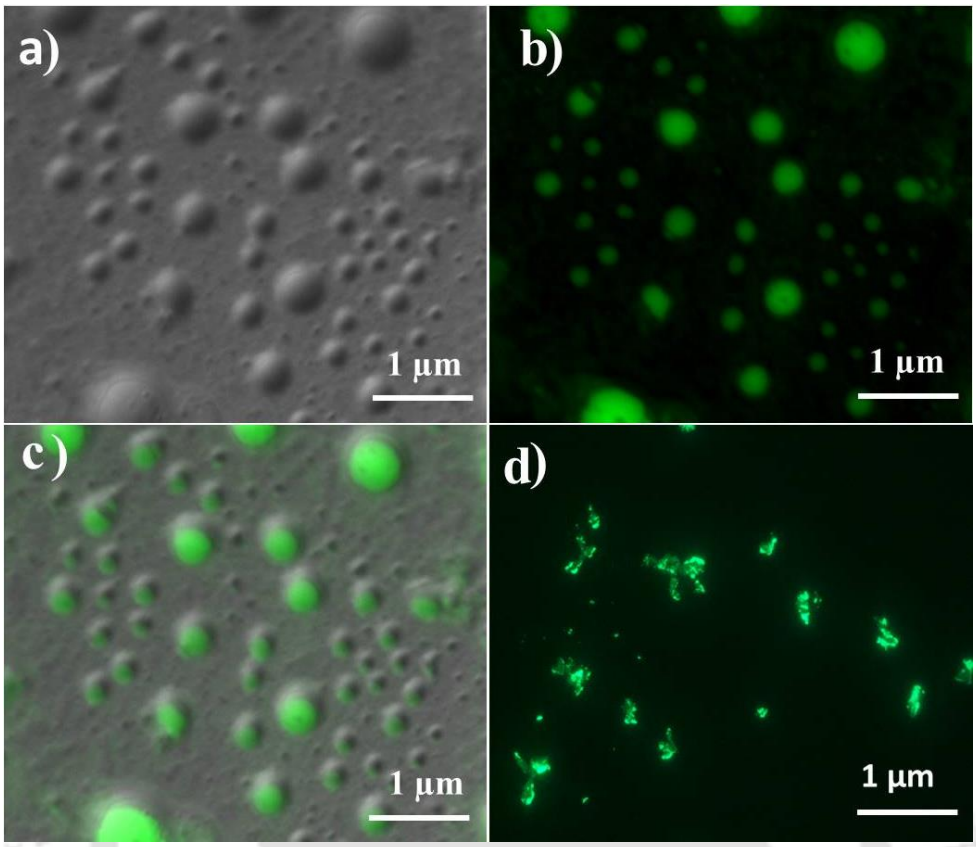

Figure 5.12: Fluorescence microscopic image of P at 0.02 mM upon addition of CF. a) Bright field image, b) Fluorescence image, c) Superposition of a and b and d) Fluoresence image upon addition of KCl.

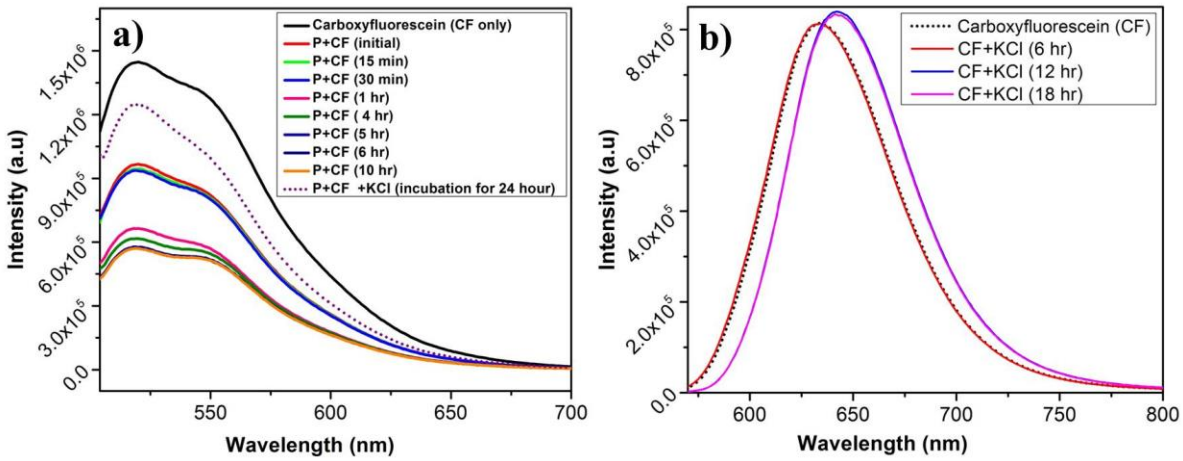

Figure 5.13: a) Time dependent fluoresence spectra of CF upon being added to 0.02 mM solution of P and b) Effect of KCl on the fluorescence emission of a) CF. The fluorescence emission maxima of CF is slightly red shifted while intensity remains unchanged in the presence of KCl.

To have a much better understanding of the peptide self-assembly process, we have studied the interaction of the peptide with another aromatic moiety, an anticancer drug Curcumin. This time we have studied the interaction between them in two different ways: One was similar to that we have been done in case of CF, i.e. we have added the ethanolic solution of drug into the peptide solution in ethanol assuming that the peptide nanospheres were already formed and secondly, we have allowed the formation of nanospheres in the ethanolic solution of Curcumin, i.e. added solid peptide to it. We have monitored the change in fluorescence emission of the Curcumin moiety in either cases.

In the first case, when Curcumin was incubated with peptide solution (0.02 mM), we observed similar kind of result as was obtained in case of CF, i.e. after addition of the drug to the peptide solution, the fluorescence emission of Curcumin got quenched which was indicative of the interaction of the drug with the peptide (Figure 5.14a). The fluorescence kept steadily decreasing over the time till about 36 h for Curcumin and stayed stable till 48 h (not shown in figure). Upon addition of KCl or HCOOH, the fluorescence emission of the Curcumin increased again as a result of the disruption of the nanospheres; however the regain of fluorescence intensity of curcumin was not 100% as in the presence of KCl, the fluorescence of Curcumin was modified as shown in Figure 5.14b.

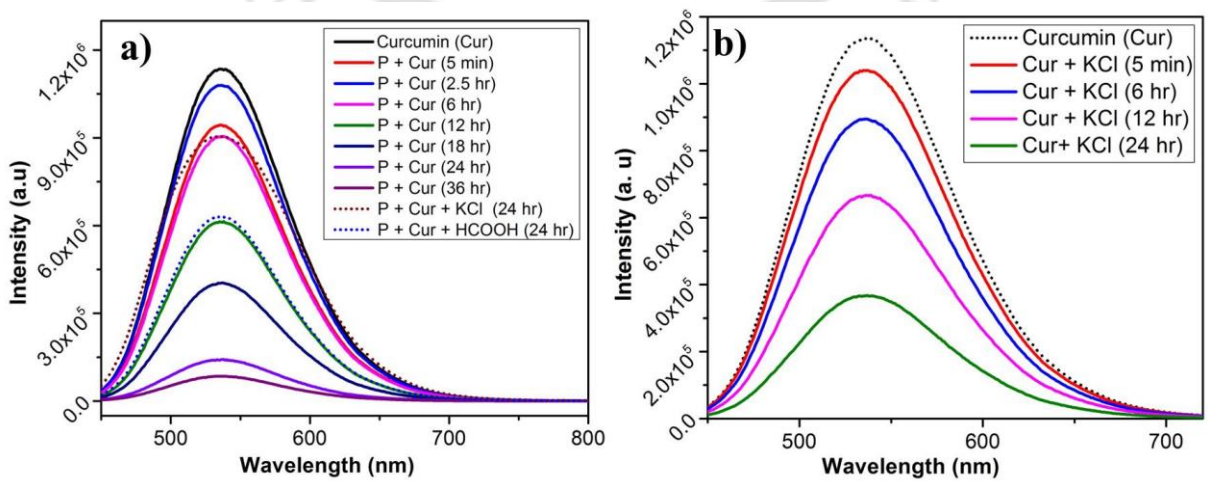

Figure 5.14: a) Time dependent fluorescence spectra of Curcumin upon being added to 0.02 mM solution of P and b) Effect of KCl on the fluorescence emission of Curcumin. Fluorescence emission of Curcumin was severely quenched in the presence of KCl.

In the second way, time dependent fluorescence emission of Curcumin was monitored (Figure 5.15a) upon addition of solid peptide to curcumin solution. Nanospheres formed in the presence of Curcumin were visualised upon performing FESEM (Figure 5.15b). In this scenario, a lot of dye was encapsulated inside the nanospheres. Interestingly, this time the fluorescence intensity of Curcumin did not diminish appreciably, unlike the earlier case where Curcumin solution was added to the peptide solution, i.e. to already formed nanospheres (Figure 5.14a). This result suggested that Curcumin was not entrapped within the nanospheres, rather surface bound in the earlier case. As interaction of Curcumin with the surface of the nanospheres led to appreciable quenching of fluorescence, it may be argued that the surface of the nanospheres contained some aromatic groups that interacted with aromatic moieties of Curcumin. This suggested that Trp side chains stick out on the outer surface of the nanospheres formed at 0.02 mM peptide concentration. When Curcumin was entrapped inside the nanospheres, there was a slight fluorescence quenching indicating that the inside of the nanospheres did not have aromatic groups to interact with the Curcumin. The slight decrease in fluorescence intensity may have occurred due to the untrapped Curcumin molecules in solution that interacted with the Trp residues on the surface. This is a clear hint that the interior of nanospheres did not contain any indole moieties of Trp but contained Leu side chains instead.

Thus these drug encapsulation studies proved a good way to indirectly understand the self-assembled morphology of P. Upon addition of KCl and formic acid to the Curcumin entrapped nanospheres, the fluorescence emission of Curcumin changed significantly. This was due to the rupture of the microspheres releasing the encapsulated and bound Curcumin.

This changed fluorescence of Curcumin was similar to that observed earlier upon release of surface bound Curcumin. Figure 5.15c and d shows the FESEM image of rupture of the Curcumin loaded nanospheres in the presence of KCl and HCOOH that validates the change in fluorescence emission of Curcumin as seen in Figure 5.14a.

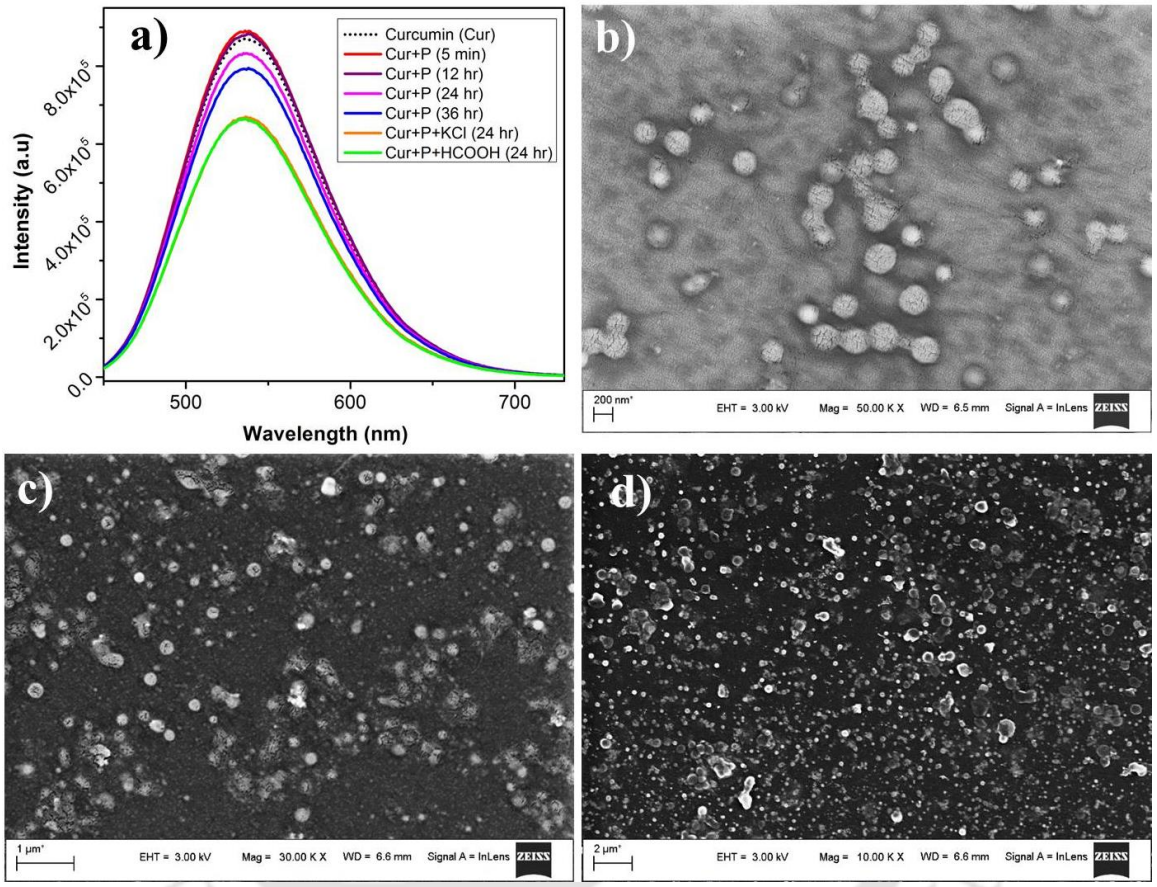

Figure 5.15: a) Time dependent fluoresence spectra of curcumin upon addition of freeze dried P (final conc. 0.02 mM) to curcumin solution. b) FESEM image of peptide nanospheres formed in the presence of curcumin. FESEM images of ruptured curcumin loaded P nanospheres upon addition of c) KCl and d) HCOOH.

Furthermore, in order to prove that Curcumin was indeed encapsulated in the microspheres, the Curcumin solution with solid peptide added to it was coagulated with the addition of water and centrifuged. The precipitate was washed several times with water to remove any unbound curcumin from the surface and subsequently resuspended in EtOH. Mass analysis

was performed on the EtOH before (control) and after addition of KCl to the solution. Presence of Curcumin mass in EtOH, after disruption of Curcumin loaded peptide microspheres with KCl, clearly proved that Curcumin was entrapped in the microspheres (Appendix A, Figure A21, Page XI).

Next, we thought of understanding the microsphere morphologies at 10 mM peptide concentration. For this, Curcumin was added to the peptide microspheres formed at 10 mM and its fluorescence emission was monitored (Figure 5.16b) and compared with the data obtained upon addition of Curcumin to peptide solution at 0.02 mM (Figure 5.16a). Trends in the fluorescence quenching of the Trp fluorescence with time for both 0.02 mM and 10mM peptide concentration were identical, indicating interaction of the peptide with dye. This proved that even at 10mM concentration of the peptide, the microspheres had Trp sticking out of the surface, just like the case of P nanospheres formed at 0.02mM. To ensure that the binding of Curcumin to the surface of nanospheres was indeed through aromatic interaction between the aromatic moiety of the drug and indole ring of Trp, fluorescence emission of Trp upon addition of Curcumin to preformed nano-assemblies at both 0.02mM (Figure 5.16c) and 10mM (Figure 5.16d) was monitored. In both the cases, quenching of Trp fluorescence was observed proving that Curcumin was indeed surface bound to the nano/microspheres by aromatic interaction between the Trp side chains and the aromatic moieties present in the drug.

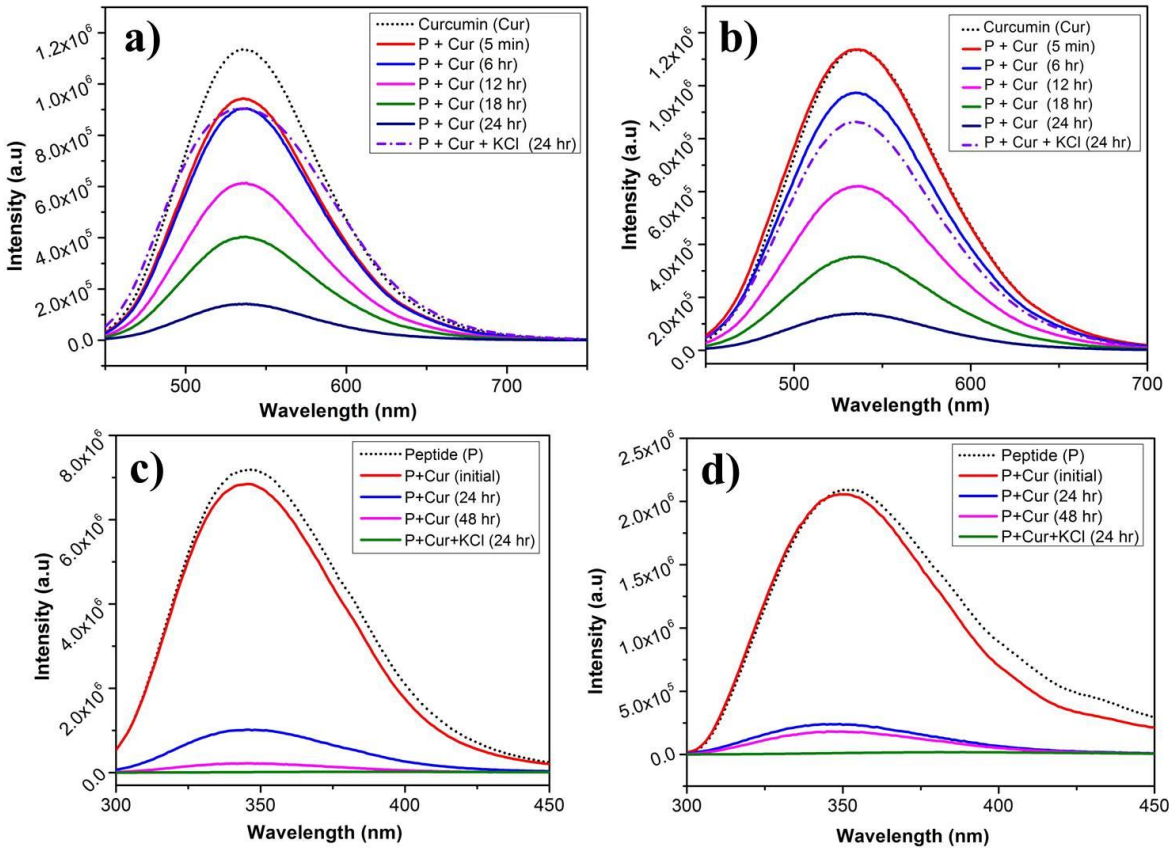

Figure 5.16: Time dependent Fluoresence spectra of Curcumin upon being added to a) 0.02 mM and b) 10 mM solution of P. Time dependent fluorescence spectra of P (Trp) upon addition of Curcumin to c) 0.02 mM and d) 10 mM solution of P.

5.4.6. Mechanism of Self-Assembly:

Tetrapeptide Boc-Trp-Leu-Trp-Leu-OMe spontaneously self-assembled into spherical nano-/microspheres upon dissolution in EtOH, as seen from FESEM. On the basis of the experiments described above and the energy-optimized structure of the peptide (Figure 5.2b), it was possible to understand the mechanism of self-assembly of the tetrapeptide. Figure 5.17 is a schematic which attempts to explain the mechanism of concentration-dependent self-assembly of the tetrapeptide. From the energy-minimized structure of the peptide, the orientation of the Trp ring was seen to be roughly about perpendicular to the plane containing the peptide bond. From FTIR, the peptide was found to adopt anti-parallel β-sheet conformation. When peptide strands hydrogen-bonded to form anti-parallel β-sheets, the Trp

residues pointed toward one side of the β sheet and the Leu side chains pointed toward the opposite side (Figure 5.17B). The Trp aromatic rings were poised in such a fashion that they did not stack with each other upon forming the anti-parallel β-sheet. Thus, even upon forming the anti-parallel β-sheet, the intrinsic fluorescence of Trp in the peptides increased proportionately with the concentration. This peptide sheet folded to form the nanospheres which were seen in FESEM at as low as 0.02 mM concentration (Figure 5.17C). These nanospheres were formed in such a way that the Trp side chains pointed outwards while the hydrophobic Leu side chains pointed inwards. The formation of nanospheres at the 0.02 mM concentration did not need the aromatic stacking of Trp and was driven by the hydrophobic effect. Because of the low concentration, the nanospheres remained discrete and did not cluster with each other (Figure 5.5a). Upon increasing the concentration of the peptide, self-assembly via the above mentioned mode continued and the size of the nanospheres increased by fusion of the smaller spheres forming larger spheres (microspheres), as seen by DLS studies (Figure 5.8). Beyond a certain concentration (0.156 mM), the microspheres came close together and formed clusters of microspheres (Figure 5.17D). This clustering was stabilized by aromatic interactions of Trp side chains pointing out of the microspheres. This led to quenching of Trp intrinsic fluorescence (Figure 5.11a) and appearance of exciton-coupled CD peaks (Figure 5.10) upon increasing the concentration of the peptide beyond 0.156 mM. The proximity of the microspheres at higher concentrations is seen in the FESEM images at 10 mM (Figure 5.3d). Figure 5.17E−G indicates surface binding and encapsulation of curcumin at different peptide concentrations and mode of addition. This provides additional information about the interaction between the aromatic groups of the drug with the trptophan sidechains present at the surface of the nanospheres/microspheres and leads to a conclusive idea about how the nanospheres are decorated with the sidechains of Trp residues of P.

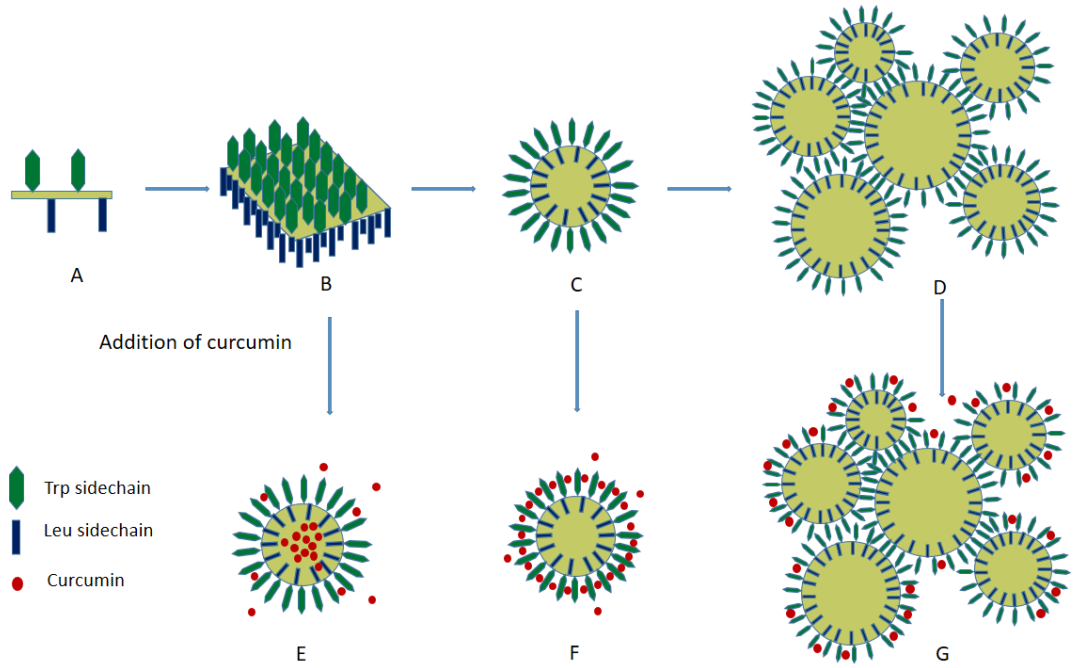

Figure 5.17: Schematic representation of concentration dependent self-assembly and drug binding pattern of P. A) P monomer, B) β-sheet like conformation of P, C) P nanospheres at 0.02 mM, D) Clustered P microspheres at 10mM, E) Entrapment of dye in nanospheres, F) Binding of Curcumin on at the surface of P nanospheres and G) Binding of Curcumin on at the surface of P microspheres at 10 mM.

5.5. Conclusion

In conclusion, we have been able to explain the mechanism of self-assembly of a tetrapeptide containing Trp. This is a befitting example showing how self-assembly is governed by an interplay of several forces. At the low concentration range, intra-strand hydrogen bonding leads to the formation of anti-parallel β-sheets that is driven to assemble into unilayered nanospheres by hydrophobic effect, with the Leu side chains pointed towards to core of the nanosphere and Trp side chains pointing outwards. Upon increasing the concentration of the peptide, the size of the peptide spheres increase which eventually form unilayered microspheres. Beyond a certain concentration, clustering of microspheres occur which is stabilized by aromatic stacking interactions between the Trp side chains sticking out of the

microspheres. We have also demonstrated the mechanism of self-assembly of the nanospheres using aromatic moieties such as Curcumin. We found that when Curcumin was added to P nanospheres, it was intercalated on the surface of the nanospheres instead of being encapsulated in the spheres. Curcumin interacted with the peptide nanospheres *via.* aromatic interactions between the indole ring of the Trp sticking out of the nanosphere surface and its aromatic moiety. On the other hand, upon forming the peptide nanospheres in the presence of Curcumin, encapsulation occured. In both cases, the drug was released in the presence of physiologically relevant ions like potassium and in acidic conditions, upon disruption of the peptide self-assembly. With dual drug encapsulation and intercalation capabilities, this prototype helps us in a better understanding of the self-assembly mechanism of the peptide P into nanospheres.

Chapter 6

Conclusions

Chapter 6

Conclusions

This thesis is about the exploration and understanding of self-assembly mechanism in small designed peptides and applying the peptide nanostructures in diverse applications. Peptides and amino acid derivatives have been synthesized using standard solution and solid phase peptide synthesis. Thereafter we have undertaken various studies and delineated the mechanism of self-assembly in molecular details, unravelling the supramolecular interactions that are involved in the process. Finally we have employed the self-assembled materials in wastewater treatment and drug delivery applications.

Chapter 1 introduces the process of self-assembly, the governing supramolecular interactions and external factors/stimuli that control self-assembly. We have summarized the advancements in the field of peptide self-assembly, the plethora of structures that are formed and the spectrum of applications they have been employed in. We have also discussed the various characterisation techniques which are required for proper study of the mechanistic details of the peptide nanostructures.

In the second chapter, we have shown dicyclohexyl urea derivatives of amino acids Fmoc-Phe-DCU (M1), Fmoc-Phg-DCU (M2) and Fmoc-Gaba-DCU (M3) to form phase selective, thermo-reversible and mechanically robust gels in a large range of organic solvents. We have proved that self-assembly leading to gelation in this system is mainly propelled by hydrophobicity and π-π stacking interactions in between Fmoc groups. Interestingly, the organogels were found to absorb several kinds of organic dyes namely, CV, RB and NR efficiently and could be reused for dye absorption for multiple cycles. Additionally, M1-M3 acted as sensors for anions like fluoride, acetate. NMR and DFT calculations suggested involvement of the amino acid NH in fluoride binding while urea NH was involved in a six

membered intramolecular hydrogen bond. Urea moiety was believed to have an indirect role in modulating the electronic levels of the sensors which led to interaction with the anions.

In the third chapter, we have designed and studied the self- and co-assembly of two charge complementary peptides A1 (WLVFFK) and A2 (WLVFFE) into hydrogels. Though, aromatic π-π interactions, hydrogen bonding and hydrophobic interactions were the most important drivers for hydrogelation, electrostatic interaction was the governing factor that led to self-assembly. Co-assembly of the two peptides was of cooperative nature and the stability of the coassembled gels varies on their composition. The self- and co-assembled gels were highly efficient in removal of organic dyes (acidic, basic and neutral) and toxic metal ions (Co^{2+}, Ni^{2+}, Pb^{2+}, Hg^{2+}) from wastewater recyclably. Both the peptides acted as selective sensors for anions like arsenite (AsO_2^-), arsenate (AsO_3^-) and hydroxide (OH^-) ions and cation Fe^{3+}.

In the fourth chapter, the non-cytotoxic A1 hydrogel have been used for the sustained release of different kinds (chemistries, sizes, charges and bioactivities) of drugs and protein molecules. All the cargoes retained their chemical identity, structure and bioactivity upon loading, storage and release from the hydrogel. Anticancer (5-FU) and antimicrobial (CP) drugs were co-assembled orthogonally with the peptide to form hydrogels, where each components self-sorted and assembled individually. π-π stacking interactions and H-bonding in between the components led to the co-assembly. 5-FU was more efficiently released in acidic pH compared to neutral pH, which might aid the tissue specific delivery of drugs.

In the fifth chapter, we studied the concentration dependent self-assembly of a tryptophan rich tetrapeptide. The peptide formed nanospheres at a lower concentration which was driven by hydrogen bonding and hydrophobic interactions. The surface of the nanospheres were decorated with the tryptophan side chains. At higher concentrations, peptides formed microspheres which adhered to each other via the intercalation of the tryptophan side chains

present on the surface. The nano/microspheres were capable of encapsulating as well as binding drug/dye molecules on the surface. Physiological salt concentrations and acids disrupted the assembly leading to release of the drug/dye molecules. This prototype might be a promising strategy to be adopted in drug delivery in the future.

Understanding the underlying molecular interactions of different assembled systems would help in the design of custom peptides with desired properties and tailor-made applications. Though, with the extensive studies in the field, and the present understanding, peptide self-assembly is no more a serendipitous phenomenon, the success to failure ratio of the rational design is also significant. The field remains at the frontiers of material research community owing to its ability to generate materials which are economically viable, simple and robust, with versatile applicability. We hope that the research entailed in this thesis has advanced the field in a significant way.

References

1. Whitesides, G.M.; Boncheva, M. Beyond molecules: Self-assembly of mesoscopic and macroscopic components. *PNAS* **2002**, *99*, 4769–4774.
2. Stupp, S.I.; Palmer, L.C. Supramolecular Chemistry and Self-Assembly in Organic Materials Design. *Chem. Mater.* **2014**, *26*, 507–518.
3. Ozin, G.A.; Hou, K.; Lotsch, B.V.; Cademartiri, L.; Puzzo, D. P.; Scotognella, F.; Ghadimi, A.; Thomson, J. Nanofabrication by self-assembly. *materials today* **2009**, *12*, 12-23.
4. Whitesides, G.M.; Grzybowski, B. Self-Assembly at All Scales. *Science* **2002**, *295*, 2418-2421.
5. Arigaa, K.; Nishikawaa, M.; Moria, T.; Takeya, J.; Shrestha, L. K.; Hill, J. P. Self-assembly as a key player for materials nanoarchitectonics. *Science and Technology of Advanced Materials* **2019**, *20*, 51–95.
6. Boles, M.A.; Engel, M.; Talapin, D. V. Self-Assembly of Colloidal Nanocrystals: From Intricate Structures to Functional Materials. *Chem. Rev.* **2016**, *116*, 11220−11289.
7. Whitesides, G. M.; Mathias, J. P.; Seto, C. T. Molecular Self-Assembly and Nanochemistry: A Chemical Strategy for the Synthesis of Nanostructures. Science **1991**, *254*, 1312-1319.
8. Gerbelli, B. B.; Vassiliades, S. V.; Rojas, J. E. U.; Pelin, J. N. B. D.; Mancini, R. S. N.; Pereira, W. S. G.; Aguilar, A. M.; Venanzi, M.; Cavalieri, F.; Giuntini, F.; Alves, W. A. Hierarchical Self-Assembly of Peptides and its Applications in Bionanotechnology. *Macromol. Chem. Phys*. **2019**, *220*, 1900085, 1-22.
9. Menger, F. M. Supramolecular chemistry and self-assembly. *PNAS* **2002**, *99*, 4818–4822.
10. Sakurai, M.; Shimojima, A.; Heishi, M.; Kuroda, K. Preparation of Mesostructured Siloxane-Organic Hybrid Films with Ordered Macropores by Templated Self-Assembly. *Langmuir* **2007,** *23*, 10788-10792.
11. Huesing, N.; Raab, C.; Torma, V.; Roig, A.; Peterlik, H. Periodically Mesostructured Silica Monoliths from Diol-Modified Silanes. *Chem. Mater.* **2003**, *15*, 2690-2692.
12. Wei, G.; Reichert, J.; Bossert, J.; Jandt, K. D. Novel Biopolymeric Template for the Nucleation and Growth of Hydroxyapatite Crystals Based on Self-Assembled Fibrinogen Fibrils. *Biomacromolecules* **2008**, *9*, 3258–3267.

13. Kim, W.; Thevenot, J.; Ibarboure, E.; Lecommandoux, S.; Chaikof, E. L. Self-Assembly of Thermally Responsive Amphiphilic Diblock Copolypeptides into Spherical Micellar Nanoparticles. *Angew. Chem. Int. Ed*. **2010**, *49*, 4257 –4260.
14. Li, J.; Xu, B. Enzyme-mediated self-assembly. *Self-assembling Biomaterials Molecular Design, Characterization and Application in Biology and Medicine* **2018**, 399-417.
15. Gao, T.; Wang, T.; Wu, W.; Liu, Y.; Huo, Q.; Qiao, Z.; Sheng Dai, S. Solvent-Induced Self-Assembly Strategy to Synthesize Well-Defined Hierarchically Porous Polymers. *Adv. Mater*. **2019**, *31*, 1806254, 1-7.
16. Liu, J.; Song, K.; Shin, Y.; Liu, X.; Chen, J.; Yao, K. X.; Pan, J.; Yang, C.; Yin, J.; Xu, L-J.; Yang, H.; El-Zohry, A.M.; Xin, B.; Mitra, S.; Hedhili, M. N.; Roqan, I. S.; Mohammed, O. F.; Han, Y.; Bakr, O. M. Light-Induced Self-Assembly of Cubic $CsPbBr_3$ Perovskite Nanocrystals into Nanowires. *Chem. Mater*. **2019**, *31*, 6642−6649.
17. Bhattacharyya, K.; Mukherjee. S. Fluorescent Metal Nano-Clusters as Next Generation Fluorescent Probes for Cell Imaging and Drug Delivery. *Bull. Chem. Soc. Jpn*. **2018**, *91*, 447–454.
18. Komiyama, M.; Mori, T.; Ariga, K. Molecular Imprinting: Materials Nanoarchitectonics with Molecular Information. *Bull. Chem. Soc. Jpn*. **2018**, *91*, 1075–1111.
19. Rogers, W. B.; Shih, W. M.; Manoharan, V. N. Using DNA to program the self-assembly of colloidal nanoparticles and microparticles. *Nat. Rev. Mater*. **2016**, *1*, 16008.
20. Bai, Y.; Luo, Q.; Liu, J. Protein self-assembly *via* supramolecular strategies. *Chem. Soc. Rev*. **2016**, *45*, 2756-2767.
21. Hu, X.; Liao, M.; Gong, H.; Zhang, L.; Cox, H.; Waigh, T. A.; Lu, J. R. Recent advances in short peptide self-assembly: from rational design to novel applications. *Current Opinion in Colloid & Interface Science* **2020**, *45*, 1–13.
22. Milles, S.; Jensen, M. R.; Communie, G.; Maurin, D.; Schoehn, G.; Ruigrok, R. W. H.; Martin Blackledge, M. Self-Assembly of Measles Virus Nucleocapsid-like Particles: Kinetics and RNA Sequence-Dependence. *Angew Chem Int Ed Engl*. **2016**, *55*, 9356-9360.
23. Feng Z.; Wang, H.; Chen, X.; Xu, B. Self-Assembling Ability Determines the Activity of Enzyme-Instructed Self-Assembly for Inhibiting Cancer Cells. *J. Am. Chem. Soc*. **2017**, *139*, 15377-15384.
24. Lin, Y.; Chapman, R.; Stevens, M. M. Integrative Self-Assembly of Graphene Quantum Dots and Biopolymers into a Versatile Biosensing Toolkit. *Adv. Funct. Mater*. **2015**, *25*, 3183-3192.

25. Wang, L.; Gong, C.; Yuan, X.; Wei, G. Controlling the Self-Assembly of Biomolecules into Functional Nanomaterials through Internal Interactions and External Stimulations: A Review. *Nanomaterials* **2019**, *9*, 285, 1-27.
26. Joshi, A.; Singh, N.; Verma, G. Preparation and applications of self-assembled natural and synthetic nanostructures. *Fabrication and Self-Assembly of Nanobiomaterials* **2016**, 29-55.
27. O'Mahony, C. T.; Farrell, R. A.; Goshal, T.; Holmes, J. D.; Morris, M. A. The Thermodynamics of Defect Formation in Self-Assembled Systems. *Thermodynamics - Systems in Equilibrium and Non-Equilibrium*, Dr. Juan Carlos Moreno PirajÃ¡n (October Ed.) **2011**, 279-306.
28. Wang, J.; Liu, K.; Xinga, R.; Yan, X. Peptide self-assembly: thermodynamics and kinetics. *Chem. Soc. Rev*. **2016**, *45*, 5589-5604.
29. Berg, J. M.; Tymoczko, J. L.; Stryer, L. Section 1.3. Chemical Bonds in Biochemistry. *Biochemistry. 5th edition. New York: W H Freeman* **2002**.
30. Das, A.; Ghosh, S. H-bonding directed programmed supramolecular assembly of naphthalene-diimide (NDI) derivatives. *Chem. Commun*. **2016**, *52*, 6860-6872.
31. Pantos¸ G. D.; Pengo, P.; Sanders, J. K. M. Hydrogen-Bonded Helical Organic Nanotubes. *Angew. Chem. Int. Ed***. 2007**, *46*, 194 –197.
32. Li, Q.; Jia, Y.; Dai, L. Yang, Y.; Li, J. Controlled Rod Nanostructured Assembly of Diphenylalanine and Their Optical Waveguide Properties. *ACS Nano* **2015**, *9*, 2689–2695.
33. Li, P.; Chen, X.; Yang, W. Graphene-Induced Self-Assembly of Peptides into Macroscopic-Scale Organized Nanowire Arrays for Electrochemical NADH Sensing. *Langmuir* **2013**, *29*, 8629–8635.
34. Cheng, C-C.; Wang, J-H.; Chuang, W-T.; Liao, Z-S.; Huang, J-J.; Huang, S-Y.; Fana, W-L.; Leed, D-J. Dynamic supramolecular self-assembly: hydrogen bonding-induced contraction and extension of functional polymers. *Polym. Chem*. **2017**, *8*, 3294-3299.
35. Gavel, P.; Dev, D.; Parmar, H. S.; Bhasin, S.; Das, A. K. Investigations of Peptide-Based Biocompatible Injectable Shape-Memory Hydrogels: Differential Biological Effects on Bacterial and Human Blood Cells. *ACS Appl. Mater. Interfaces.* **2018**, *10*, 10729–10740.
36. Wang, J.; Zhao, X.; Li, J.; Kuang, X.; Fan, Y.; Wei, G.; Su, Z. Electrostatic Assembly of Peptide Nanofiber−Biomimetic Silver Nanowires onto Graphene for Electrochemical Sensors. *ACS Macro Lett*. **2014**, *3*, 529–533.

37. Kuroiwa, K.; Masaki, Y.; Koga, Y.; Deming, T. J. Self-Assembly of Discrete Metal Complexes in Aqueous Solution via Block Copolypeptide Amphiphiles. *Int. J. Mol. Sci.* **2013**, *14*, 2022-2035.
38. Sun, H.; Zhang, X.; Miao, L.; Zhao, L.; Luo, Q.; Xu, J.; Liu, J. Micelle-Induced Self-Assembling Protein Nanowires: Versatile Supramolecular Scaffolds for Designing the Light-Harvesting System. *ACS Nano* **2016**, *10*, 421–428.
39. Liu, L-H.; Li, Z-Y.; Rong, L.; Qin, S-Y.; Lei, Q.; Cheng, H.; Zhou, X.; Zhuo, R-X.; Zhang, X-Z. Self-Assembly of Hybridized Peptide Nucleic Acid Amphiphiles. *ACS Macro Lett*. **2014**, *3*, 467−471.
40. McGuinness, K.; Nanda, V. Collagen mimetic peptide discs promote assembly of a broad range of natural protein fibers through hydrophobic interactions. *Org. Biomol. Chem*. **2017**, *15*, 5893–5898.
41. Liao, H-S.; Lin, J.; Liu, Y.; Huang, P.; Jin, A.; Chen, X. Self-Assembly Mechanisms of Nanofibers from Peptide Amphiphiles in Solution and on Substrate Surfaces. *Nanoscale* **2016**, *8*, 14814-14820.
42. Yang, H.; Fung, S-Y.; Pritzker, M.; Chen, P. Modification of Hydrophilic and Hydrophobic Surfaces Using an Ionic-Complementary Peptide. *PLoS One* **2007**, *2*, e1325.
43. Anand, B. G.; Dubey, K.; Shekhawat, D. S.; Prajapati, K. P.; Kar, K. Strategically Designed Antifibrotic Gold Nanoparticles to Prevent Collagen Fibril Formation. *Langmuir* **2017**, *33*, 13252–13261.
44. Wang, E.; Desai, M. S.; Lee, S-W.; Light-Controlled Graphene-Elastin Composite Hydrogel Actuators. *Nano Lett.* **2013**, *13*, 2826–2830.
45. Gazit. E. A possible role for -stacking in the self-assembly of amyloid fibrils. *FASEB J.* **2002**, *16*, 77-83.
46. Gillard, R. E.; Raymo, F. M.; Stoddart, J. F. Controlling Self-Assembly. *Chem. Eur. J.* **1997**, *3*, 1933-1940.
47. Claessens, C. G.; Stoddart, J. F. π-π Interactions In Self-Assembly. *Journal of Physical Organic Chemistry*, **1997**, *10*, 254–272.
48. Shetty, A. S.; Zhang, J.; Moore, J. S. Aromatic π-Stacking in Solution as Revealed through the Aggregation of Phenylacetylene Macrocycles. *J. Am. Chem. Soc*. **1996**, *118*, 1019-1027.

49. Bujosa, S.; Castellanos, E.; Frontera, A.; Rotger, C.; Costa, A.; Soberats, B. Self-assembly in water of amphiphilic aryl-squaramides driven by dipolar π-π interactions. *Org. Biomol. Chem*. **2020**, *18*, 888-894.
50. McGaughey, G. B.; Gagne´§, M.; Rappe, A. K. π-Stacking Interactions Alive and Well In Proteins. *J. Biol. Chem*. **1998**, *273*, 15458-15463.
51. Hunter, C. A. Arene- Arene Interactions: Electrostatic or Charge Transfer? *Angew. Chem. Int. Ed. Engl.* **1993**, *32*, 1584-1586.
52. Su, Z.; Shen, H.; Wang, H.; Wang, J.; Li, J.; Nienhaus, G. U.; Li L.; Wei, G. Motif-Designed Peptide Nanofi bers Decorated with Graphene Quantum Dots for Simultaneous Targeting and Imaging of Tumor Cells. *Adv. Funct. Mater*. **2015**, *25*, 5472–5478.
53. Li, D.; Zhang, W.; Yu, X.; Wang, Z.; Su, Z.; Wei, G. When biomolecules meet graphene: from molecule-level interactions to material design and applications. *Nanoscale* **2016**, *8*, 19491-19509.
54. Yun, W.; Xiong, W.; Wu, H.; Fu, M.; Huang, Y.; Liu, X.; Yang, L. Graphene oxide-based fluorescent "turn-on" strategy for Hg^{2+} detection by using catalytic hairpin assembly for amplification. *Sensors and Actuators B* **2017**, *249*, 493–498.
55. Huang, J-Y.; Zhao, L.; Lei, W.; Wen, W.; Wang, Y-J. Bao, T.; Xiong, H-Y.; Zhang, X-H.; Wang, S-F. A high-sensitivity electrochemical aptasensor of carcinoembryonic antigen based on graphene quantum dots-ionic liquid-nafion nanomatrix and DNAzyme-assisted signal amplification strategy. *Biosensors and Bioelectronics* **2018**, *99*, 28–33.
56. Faul, F.J.; Antonietti, M. Ionic Self-Assembly: Facile Synthesis of Supramolecular Materials. *Adv. Mater*. **2003**, *15*, 673-683.
57. Caplan, M. R.; Moore, P. N.; Zhang, S.; Kamm, R. D.; Lauffenburger, D. A. Self-Assembly of a β-Sheet Protein Governed by Relief of Electrostatic Repulsion Relative to van der Waals Attraction. *Biomacromolecules* **2000**, *1*, 627-631.
58. Tahara, K.; Lei, S.; Adisoejoso, J.; Feyter, S. D.; Tobe, Y. Supramolecular surface-confined architectures created by self-assembly of triangular phenylene–ethynylene macrocycles *via* van der Waals interaction. *Chem. Commun*. **2010**, *46*, 8507–8525.
59. Dougherty, D. A. Cation-π Interactions in Chemistry and Biology: A New View of Benzene, Phe, Tyr, and Trp. *Science* **1996**, *271*, 163-168.
60. Chen, C-C.; Hsu, W.; Kao, T-C.; Horng, J-C. Self-Assembly of Short Collagen-Related Peptides into Fibrils *via* Cation-π Interactions. *Biochemistry* **2011**, *50*, 2381–2383.

61. Luo, J.; Chen, K.; Yin, P.; Li, T.; Wan, G.; Zhang, J.; Ye, S.; Bi, X.; Pang, Y.; Wei, Y.; Liu, T. Effect of Cation-π Interaction on the Macroionic Self-Assembly. *Angew. Chem. Int. Ed*. **2018**, *57*, 4067-4072.
62. Seonki Hong, S.; Wang, Y.; Park, S. Y.; Lee, H. Progressive fuzzy cation-π assembly of biological catecholamines. *Sci. Adv*. **2018**; *4*, eaat7457.
63. Gebbie, M.; Wei, W.; Schrader, A. *et.al*. Tuning underwater adhesion with cation–π interactions. *Nature Chemistry*, **2017**, *9*, 473–479.
64. Ma, J. C.; Dennis A. Dougherty, D. A. The Cation-π Interaction. *Chem. Rev*. **1997**, *97*, 1303-1324.
65. Slutsky, M. M.; Marsh, E. N. G. Cation–π interactions studied in a model coiled-coil peptide. *Protein Science* **2004**, *13*, 2244–2251.
66. Hsieh, M-C.; Liang, C.; Mehta, A. K.; Lynn, D. G.; Grover, M. A. Multi-step Conformation Selection in Amyloid Assembly. *J. Am. Chem. Soc*. **2017**, *139*, 17007–17010.
67. Ghosh, A.; Haverick, M.; Stump, K.; Yang, X.; Tweedle, M. F.; Goldberger, J. E. Fine-Tuning the pH Trigger of Self-Assembly. *J. Am. Chem. Soc*. **2012**, *134*, 3647−3650.
68. Lu, C-H.; Cecconello, A.; Elbaz, J.; Credi, A.; Willner, I. A Three-Station DNA Catenane Rotary Motor with Controlled Directionality. *Nano Lett*. **2013**, *13*, 2303−2308.
69. Wu, N.; Willner, I. pH-Stimulated Reconfiguration and Structural Isomerization of Origami Dimer and Trimer Systems. *Nano Lett*. **2016**, *16*, 6650−6655.
70. Elbaz, J.; Wang, Z-G.; Orbach, R.; Willner, I. pH-Stimulated Concurrent Mechanical Activation of Two DNA "Tweezers". A "SET-RESET" Logic Gate System. *Nano Lett.* **2009**, *9*, 4510-4514.
71. Hamley, I. W.; Dehsorkhi, A.; Castelletto, V.; Furzeland, S.; Atkins, D.; Seitsonen, J.; Ruokolainen, J. Reversible helical unwinding transition of a self-assembling peptide amphiphile. *Soft Matter* **2013**, *9*, 9290-9293.
72. Huang, Y.; Mai, Y.; Yang, X.; Beser, U.; Liu, J.; Zhang, F.; Yan, D.; Müllen, K.; Feng, X. Temperature-Dependent Multidimensional Self-Assembly of Polyphenylene-Based "Rod−Coil" Graft Polymers. *J. Am. Chem. Soc*. **2015**, *137*, 11602–11605.
73. Naota, T.; Koori, H. Molecules That Assemble by Sound: An Application to the Instant Gelation of Stable Organic Fluids. *J. Am. Chem. Soc*. **2005**, *127*, 9324-9325.
74. Isozaki, K.; Takaya, H.; Naota, T. Ultrasound-Induced Gelation of Organic Fluids with Metalated Peptides. *Angew. Chem. Int. Ed*. **2007**, *46*, 2855 –2857.

75. Bardelang, D.; Camerel, F.; Margeson, J. C.; Leek, D. M.; Schmutz, M.; Zaman, B.; Yu, K.; Soldatov, D. V.; Ziessel, R.; Ratcliffe, C. I.;. Ripmeester, J. A. Unusual Sculpting of Dipeptide Particles by Ultrasound Induces Gelation. *J. Am. Chem. Soc*. **2008**, *130*, 3313-3315.
76. Pan, S.; Luo, S.; Li, S.; Lai, Y.; Geng, Y.; He, B.; Gu, Z. Ultrasound accelerated gelation of novel L-lysine based hydrogelators. *Chem. Commun.* **2013**, *49*, 8045-8047.
77. Berthon, G. Stability Constants of Metal Complexes of Amino Acids? With Polar Side Chains (Technical Report*). Pure and Applied Chemistry* **1995**, *67*, 1117-1240.
78. Lenz, G. R.; Martell, A. E. Metal Chelates of Some Sulfur-containing Amino Acids. *Biochemistry*, **1964**, *33*, 745-750.
79. Dong, J.; Canfield, J. M.; Mehta, A. K.; Shokes, J. E.; Tian, B.; Childers, W. S.; Simmons, J. A.; Mao, Z.; Scott, R. A.; Warncke, K.; Lynn, D. G. Engineering metal ion coordination to regulate amyloid fibril assembly and toxicity. *PNAS* **2007**, *104*, 13313–13318.
80. Micklitsch, C. M.; Knerr, P. J.; Branco, M. C.; Nagarkar, R.; Pochan, D. J.; Schneider, J. P. Zinc-Triggered Hydrogelation of a Self-Assembling b-Hairpin Peptide. *Angew. Chem. Int. Ed*. **2011**, *50*, 1577 –1579.
81. Knerr, P. J.; Branco, M. C.; Nagarkar, R.; Pochan, D. J.; Schneider, J. P. Heavy metal ion hydrogelation of a self-assembling peptide via cysteinyl chelation. *J. Mater. Chem.* **2012**, *22*, 1352-1357.
82. Collier, J. H.; Hu, B-H.; Ruberti, J. W.; Zhang, J.; Shum, P.; Thompson, D. H.; Messersmith, P. B. Thermally and Photochemically Triggered Self-Assembly of Peptide Hydrogels. *J. Am. Chem. Soc.* **2001**, *123*, 9463-9464.
83. Ye, Q.; Huo, M.; Zeng, M.; Liu, L.; Peng, L.; Wang, X.; Yuan, J. Photoinduced Reversible Worm-to-Vesicle Transformation of Azo- Containing Block Copolymer Assemblies Prepared by Polymerization-Induced Self-Assembly. *Macromolecules* **2018**, *51*, 3308−3314.
84. Muraoka, T.; Cui, H.; Stupp, S. I. Quadruple Helix Formation of a Photoresponsive Peptide Amphiphile and Its Light-Triggered Dissociation into Single Fibers. *J. Am. Chem. Soc*. **2008**, *130*, 2946-2947.
85. Ma, H.; Fei, J.; Li, Q.; Li, J. Photo-induced Reversible Structural Transition of Cationic Diphenylalanine Peptide Self-Assembly. *Small* **2015**, *11*, 1787-1791.

86. Tanaka, F.; Mochizuki, T.; Liang, X.; Asanuma, H.; Tanaka, S.; Suzuki, K.; Kitamura, S.; Nishikawa, A.; Tei, K.; Hagiya, M. Robust and Photocontrollable DNA Capsules Using Azobenzenes. *Nano Lett*. **2010**, *10*, 3560–3565.
87. Huebner, D.; Rossner, C.; Vana, P. Light-induced self-assembly of gold nanoparticles with a photoresponsive polymer shell. *Polymer* **2016**, *107*, 503-508.
88. Yang, Y.; Endo, M.; Hidaka, K.; Sugiyama, H. Photo-Controllable DNA Origami Nanostructures Assembling into Predesigned Multiorientational Patterns. *J. Am. Chem. Soc*. **2012**, *134*, 20645–20653.
89. Haines, L. A.; Rajagopal, K.; Ozbas, B.; Salick, D. A.; Pochan, D. J.; Schneider, J. P. Light-Activated Hydrogel Formation via the Triggered Folding and Self-Assembly of a Designed Peptide. *J. Am. Chem. Soc*. **2005**, *127*, 17025-17029.
90. Irie, M. Diarylethenes for Memories and Switches. *Chem. Rev*. **2000**, *100*, 1685-1716.
91. Yamauchi, K.; Takashima, Y.; Hashidzume, A.; Yamaguchi, H.; Harada, A. Switching between Supramolecular Dimer and Nonthreaded Supramolecular Self-Assembly of Stilbene Amide-r-Cyclodextrin by Photoirradiation. *J. Am. Chem. Soc*. **2008**, *130*, 5024–5025.
92. Qiu, Z.; Yu, H.; Li, J.; Wang, Y.; Zhang, Y. Spiropyran-linked dipeptide forms supramolecular hydrogel with dual responses to light and to ligand–receptor interaction. *Chem. Commun*. **2009**, 3342-3344.
93. Huang, Y.; Qiu, Z.; Xu, Y.; Shi, J.; Lina, H.; Zhang, Y. Supramolecular hydrogels based on short peptides linked with conformational switch. *Org. Biomol. Chem*. **2011**, *9*, 2149–2155.
94. He, H.; Xu, B. Instructed-Assembly (iA): A Molecular Process for Controlling Cell Fate. *Bull Chem Soc Jpn*. **2018**, *91*, 900–906.
95. Wang, Q.; Yang, Z.; Gao, Y.; Ge, W.; Wanga, L.; Bing Xu, B.; Enzymatic hydrogelation to immobilize an enzyme for high activity and stability. *Soft Matter* **2008**, *4*, 550–553.
96. Gao, Y.; Kuang, Y.; Guo, Z-F.; Guo, Z.; Krauss, I. J.; Xu, B. Enzyme-Instructed Molecular Self-assembly Confers Nanofibers and a Supramolecular Hydrogel of Taxol Derivative. *J. Am. Chem. Soc*. **2009**, *131*, 13576–13577.
97. Gao, Y.; Shi, J.; Yuan, D.; Xu, B. Imaging enzyme-triggered self-assembly of small molecules inside live cells. *Nat. Commun*. **2012**, *3:1033*, 1-8.
98. Gao, J.; Wang, H.; Wang, L.; Wang, J.; Kong, D.; Yang, Z. Enzyme Promotes the Hydrogelation from a Hydrophobic Small Molecule. *J. Am. Chem. Soc.* **2009**, *131*, 11286–11287.

99. Yang, Z.; Ho, P-L.; Liang, G.; Chow, K. H..; Wang, Q.; Cao, Y.; Guo, Z.; Xu, B. Using β-Lactamase to Trigger Supramolecular Hydrogelation. *J. Am. Chem. Soc*. **2007**, *129*, 266-267.

100. Yang, Z.; Xu, K.; Guo, Z.; Guo, Z.; Bing Xu, B. Intracellular Enzymatic Formation of Nanofibers Results in Hydrogelation and Regulated Cell Death. *Adv. Mater*. **2007**, *19*, 3152–3156.

101. Yang, Z.; Maa, M.; Xu, B. Using matrix metalloprotease-9 (MMP-9) to trigger supramolecular hydrogelation. *Soft Matter* **2009**, *5*, 2546–2548.

102. Bremmer, S. C.; Anne J. McNeil, A.J.; Soellner, M. B. Enzyme-triggered gelation: targeting proteases with internal cleavage sites. *Chem. Commun*. **2014**, *50*, 1691—1693.

103. Qin, X.; Xie ,Q. X.; W.; Tian, S.; Cai, J.; Yuan, H.; Yu, Z.; Butterfoss, G. L.; Khuonga, A. C.; Gross, R. A. Enzyme-triggered hydrogelation via self-assembly of alternating peptides. *Chem. Commun*. **2013**, *49*, 4839-4841.

104. Bremmer, S.C.; Chen, J.; McNeil, A. J.; Soellner, M. B. A general method for detecting protease activity *via* gelation and its application to artificial clotting. *Chem. Commun*. **2012**, *48*, 5482–5484.

105. Zhao, F.; Weitzel, C. S.; Gao, Y.; Browdy, H. M.; Shi, J.; Lin, H-C.; Susan T. Lovett, S. T.; Bing Xu, B. β-Galactosidase-instructed formation of molecular nanofibers and a hydrogel. *Nanoscale* **2011**, *3*, 2859–2861.

106. Chronopoulou, L.; Lorenzoni, S. *et.al.* Lipase-supported synthesis of peptidic hydrogels. *Soft Matter* **2010**, *6*, 2525–2532.

107. Song, F.; Zhang, L-M. Enzyme-Catalyzed Formation and Structure Characteristics of A Protein-Based Hydrogel. *J. Phys. Chem. B.* **2008**, *112*, 13749–13755.

108. Toledano, S.; Williams, R. J.; Jayawarna, V.; Ulijn, R. V. Enzyme-Triggered Self-Assembly of Peptide Hydrogels via Reversed Hydrolysis. *J. Am. Chem. Soc*. **2006**, *128*, 1070-1071.

109. Liu, Y.; Javvaji, V.; Raghavan, S. R.; Bentley, W. E. Payne, G. F. Glucose Oxidase-Mediated Gelation: A Simple Test To Detect Glucose in Food Products. *J. Agric. Food Chem.* **2012**, *60*, 8963−8967.

110. Sakai, S.; Komatani, K.; Taya, M. Glucose-triggered co-enzymatic hydrogelation of aqueous polymer solutions. *RSC Advances* **2012,** *2*, 1502–1507.

111. Choi, Y. C.; Choi, J. S.; Junga, Y. J.; Cho, Y. W. Human gelatin tissue-adhesive hydrogels prepared by enzyme-mediated biosynthesis of DOPA and Fe^{3+} ion crosslinking. *J. Mater. Chem. B.* **2014**, *2*, 201–209.

112. Yang, Z.; Gu, H.; Fu, D.; Gao, P.; Lam, J. K.; Xu, B. Enzymatic Formation of Supramolecular Hydrogels. *Adv. Mater*. **2004**, *16*, 1440-1444.

113. Amir, R.J.; Zhong, S.; Pochan, D. J.; Hawker, C. J. Enzymatically Triggered Self-Assembly of Block Copolymers. *J. Am. Chem. Soc*. **2009**, *131*, 13949–13951.

114. Yuan, D.; Shi, J.; Du, X.; Huang, Y.; Gao, Y.; Baoum, A. A.; Xu, B. The enzyme-instructed assembly of the core of yeast prion Sup35 to form supramolecular hydrogels. *J. Mater. Chem. B*. **2016**, *4*, 1318-1323.

115. Qi, J.; Yan, Y.; Cheng, B.; Deng, L.; Shao, Z.; Sun, Z.; Li, X. Enzymatic Formation of an Injectable Hydrogel from a Glycopeptide as a Biomimetic Scaffold for Vascularization. *ACS Appl. Mater. Interfaces.* **2018**, *10*, 6180−6189.

116. Bowerman, C. J.; Nilsson, B. L. A Reductive Trigger for Peptide Self-Assembly and Hydrogelation *J. Am. Chem. Soc.* **2010**, *132*, 9526–9527.

117. Ren, C.; Song, Z.; Zheng, W.; Chen, X.; Wang, L.; Kong D.; Yang, Z. Disulfide bond as a cleavable linker for molecular self-assembly and hydrogelation. *Chem. Commun*. **2011**, *47*, 1619–1621.

118. Rasale, D. B.; Maity, I.; Konda, M.; Das, A. K. Peptide self-assembly driven by oxo-ester mediated native chemical ligation. *Chem. Commun*. **2013**, *49*, 4815-4817.

119. Zhao, F.; Gao, Y.; Shi, J.; Browdy, H. M.; Xu, B. Novel Anisotropic Supramolecular Hydrogel with High Stability over a Wide pH Range. *Langmuir* **2011**, *27*, 1510–1512.

120. Sun, Y.; Zhang, Y.; Tian, L.; Zhao, Y.; Wu, D.; Xue, W.; Ramakrishna, S.; Wu, W.; He, L. Self-assembly behaviors of molecular designer functional RADA16-I peptides: influence of motifs, pH, and assembly time. *Biomed. Mater.* **2017**, *12*, 1-11.

121. Shao, Y.; Jia, H.; Cao, T.; Liu, D. Supramolecular Hydrogels Based on DNA Self-Assembly. *Acc. Chem. Res*. **2017**, *50*, 659−668.

122. Wei, G.; Su, Z.; Reynolds, N. P.; Arosio, P.; Hamley, I. W.; Gazit, E.; Mezzenga, R. Self-assembling peptide and protein amyloids: from structure to tailored function in nanotechnology. *Chem. Soc. Rev*. **2017**, *46*, 4661—4708.

123. Dai, B.; Li, D.; Xi, W.; Luo, F.; Zhang, X.; Zou, M.; Cao, M.; Hu, J.; Wang, W.; Wei, G.; Zhang, Y.; Liu, C. Tunable assembly of amyloid-forming peptides into nanosheets as a retrovirus carrier. *PNAS* **2015,** *112*, 2996-3001.

124. Abraham, S. N.; Beachey, E. H. Assembly of a Chemically Synthesized Peptide of Escherichia coli Type 1 Fimbriae into Fimbria-Like Antigenic Structures. *Journal of Bacteriology* **1987**, 2460-2465.

125. Imanishi, Y.; Kimura, S. Peptide Self-Assembly in Phospholipid Bilayer Membrane *Proc. Japan Acad*. **1992**, *68*, 121-126.

126. Ghadiri, M.; Granja, J.; Milligan, R. *et.al.* Self-assembling organic nanotubes based on a cyclic peptide architecture. *Nature* **1993,** *366*, 324–327.

127. Gortner, R. A.; Hoffman, W. F. An Interesting Colloid Gel. Paper No. 263. *Journal Series, Minnesota Agricultural Experiment Station* **1921**, 2199-2202.

128. Menger, F. M.; Yamasaki, Y.; Catlin, K. K.; Nishimi, T. X-Ray Structure of a Self-Assembled Gelating Fiber. *Angew. Chem. Int. Ed. Engl*. **1995**, *34*, 585-586.

129. Menger, F. M.; Caran, L. K. Anatomy of a Gel. Amino Acid Derivatives That Rigidify Water at Submillimolar Concentrations *J. Am. Chem. Soc*. **200**0, *122*, 11679-11691.

130. Zelzer, M.; Ulijn, R. V. Next-generation peptide nanomaterials: molecular networks, interfaces and supramolecular functionality. *Chem. Soc. Rev*. **2010**, *39*, 3351–3357.

131. Guan, J.; Jiang, Z.; Wang, M.; Liu, Y.; Liu, J.; Yang, Y.; Ding, T.; Lu, W.; Gao, C.; Qian, J.; Zhan, C. Short Peptide-Mediated Brain-Targeted Drug Delivery with Enhanced Immunocompatibility. *Mol. Pharmaceutics.* **2019**, *16*, 907–913.

132. Bumbaca, B.; Li, Z.; Shah, K. D.; Pharmacokinetics of Protein and Peptide Conjugates. *Drug Metab Pharmacokinet*. **2019**, *34*, 42–54.

133. Dehsorkhi, A.; Castelletto, V.; Hamley, I. W. Self-assembling amphiphilic peptides. *J. Pept. Sci*. **2014**, *20*, 453–467.

134. Hutchinson, J. A.; Burholt, S.; Hamley, I. W. Peptide hormones and lipopeptides: from self-assembly to therapeutic applications. *J. Pept. Sci*. **2017,** *23*, 82– 94.

135. Ulijn, R. V.; Smith, A. M. Designing peptide based nanomaterials. *Chem. Soc. Rev*. **2008**, *37*, 664–675.

136. Leite, D. M.; Barbu, E.; Pilkington, G. J.; Lalatsa, A. Peptide Self-Assemblies for Drug Delivery. *Current Topics in Medicinal Chemistry* **2015**, *15*, 2277-2289.

137. Berndt, P.; Fields, B. G.; Tirrell, M. Synthetic Lipidation of Peptides and Amino Acids: Monolayer Structure and Properties. *J. Am. Chem. Soc*. **1995**,*117*, 9515-9522.

138. Bhattacharya, S.; Ghosh, K. Y. First report of phase selective gelation of oil from oil/water mixtures. Possible implications toward containing oil spills. *Chem. Commun*. **2001**, 185–186.

139. Pal, A.; Dey, J. Water-Induced Physical Gelation of Organic Solvents by N-(n-Alkylcarbamoyl)-L-alanine Amphiphiles. *Langmuir* **2011**, *27*, 3401–3408.

140. Chu, X.; Xing, P.; Li, S.; Ma, M.; Hao, J.; Hao, A. Dual-tuning multidimensional superstructures based on a T-shaped molecule: vesicle, helix, membrane and nanofiber-constructed gel. *RSC Adv*. **2015**, *5*, 1969–1978.

141. Huang, Z.; Luo, Q. *et.al*. Redox control of GPx catalytic activity through mediating self-assembly of Fmoc-phenylalanine selenide into switchable supramolecular architectures. *Soft Matter* **2014**, *10*, 9695–9701.

142. Reddy, A.; Srivastava, A. Mechano-responsive gelation of water by a short alanine-derivative. *Soft Matter* **2014**, *10*, 4863–4868.

143. Yang, Z.; Wang, L.; Wang, J.; Gao, P.; Xu, B. Phenyl groups in supramolecular nanofibers confer hydrogels with high elasticity and rapid recovery. *J. Mater. Chem.* **2010**, *20*, 2128–2132.

144. Wang, Q.; Yang, Z.; Ma, M.; Chang, K.; Xu, B. High Catalytic Activities of Artificial Peroxidases Based on Supramolecular Hydrogels That Contain Heme Models. *Chem. Eur. J*. **2008**, *14*, 5073 – 5078.

145. Suzuki, M.; Yumoto, M.; Kimura, M.; Shirai, H.; Hanabusa, K. New Low-Molecular-Mass Gelators Based on L-Lysine: Amphiphilic Gelators and Water-Soluble Organogelators. *HCA* **2004**, *87*, 1-10.

146. Suzuki, M.; Yumoto, M.; Kimura, M.; Shirai, H.; Hanabusa, K. Supramolecular hydrogels containing inorganic salts and acids. *Tetrahedron Letters* **2004**, *45*, 2947–2950.

147. Fu, X.; Wang, N.; Zhang, S.; Wang, H.; Yang, Y. Formation mechanism of supramolecular hydrogels in the presence of L-phenylalanine derivative as a hydrogelator. *Journal of Colloid and Interface Science* **2007**, *315*, 376–381.

148. Cao, S.; Fu, X.; Wang, N.; Wang, H.; Yang, Y. Release behavior of salicylic acid in supramolecular hydrogels formed by L-phenylalanine derivatives as hydrogelator. *International Journal of Pharmaceutics* **2008,** *357*, 95–99.

149. Fu, X. J.; Cao, S. Q.; Wang, N. X.; Zhang, S. Z.; Wang, H.; Yang, Y. J. Effect of hydrogen bonding and hydrophobic interaction on the formation of supramolecular hydrogels formed by L-phenylalanine derivative hydrogelator. *Chinese Chemical Letters* **2007**, *18*, 1001–1004.

150. Reches, M.; Gazit, E. Casting Metal Nanowires Within Discrete Self-Assembled Peptide Nanotubes. *Science* **2003,** *300*, 625-627.

151. Reches, M.; Gazit, E. Formation of Closed-Cage Nanostructures by Self-Assembly of Aromatic Dipeptides. *Nano Lett*. **2004,** *4*, 581-585.

152. Jayawarna1, V.; Smith, A.; Gough, J. E.; Ulijn, V. R. Three-dimensional cell culture of chondrocytes on modified di-phenylalanine scaffolds. *Biochemical Society Transactions* **2007**, *35*, 535-537.

153. Han, T. H.; Kim, J.; Park, J. S.; Park, C. B.; Ihee, H.; Kim, S. O. Liquid Crystalline Peptide Nanowires. *Adv. Mater*. **2007**, *19*, 3924–3927.

154. Wang, Y.; Lingenfelder, M.; Classen, T.; Costantin, G.; Kern, K. Ordering of Dipeptide Chains on Cu Surfaces through 2D Cocrystallization. *J. Am. Chem. Soc*. **2007**, *129*, 15742-15743.

155. Go¨rbitz, H. C. Nanotubes from hydrophobic dipeptides: pore size regulation through side chain substitution. *New J. Chem*. **2003**, *27*, 1789–1793.

156. Gˆrbitz, H. C. Nanotube Formation by Hydrophobic Dipeptides. *Chem. Eur. J.* **2001**, *7*, 5153-5159.

157. Fan, Z.; Sun, L.; Huang, Y.; Wang, Y.; Zhang, M. Bioinspired fluorescent dipeptide nanoparticles for targeted cancer cell imaging and real-time monitoring of drug release. *Nature Nanotechnology* **2016**, *11*, 388-394.

158. Reches, M.; Gazit E. Self-Assembly of Peptide Nanotubes and Amyloid-like Structures by Charged-Termini-Capped Diphenylalanine Peptide Analogues. *Israel Journal of Chemistry* **2005,** *45*, 363–371.

159. Ni, M.; Zhuo, S. Applications of self-assembling ultrashort peptides in bionanotechnology. *RSC Adv*. **2019**, *9*, 844–852.

160. Cui, H.; Webber, M. J; Stupp, S. I. Invited Review Self-Assembly of Peptide Amphiphiles: From Molecules to Nanostructures to Biomaterials. *Biopolymers* **2010**, *94*, 1-18.

161. Löwik, D.; van Hest, J. C. M. Peptide based amphiphiles. *Chem. Soc. Rev.* **2004**, *33*, 234-245.

162. Hartgerink, D. J.; Beniash, E.; Stupp, I. S. Self-Assembly and Mineralization of Peptide-Amphiphile Nanofibers. Science **2001**, *294*, 1684-1688.

163. Zhang, S.; Greenfield, M. A.; Mata, A.; Palmer, L. C.; Bitton, R.; Mantei, J. R.; Aparicio, C.; Olvera de la Cruz, M.; Stupp, S. I. A self-assembly pathway to aligned monodomain gels. *Nature materials* **2010**, 594-601.

164. L´opez-P´erez, E. D.; L´opez, R. G.; Hamley, I. W.; Alem´an, C. Molecular insights into aggregates made of amphiphilic Fmoc-tetrapeptides. *Soft Matter* **2013**, *9*, 11021–11032.

165. Ou, C.; Zhang, J.; Zhang, X.; Yang, Z.; Chen, M. Phenothiazine as an aromatic capping group to construct a short peptide-based 'super gelator. *Chem. Commun*. **2013**, *49*, 1853-1855.

166. Rodriguez, L. A.; Parish, L. C.; Nisbeta, R. D.; Williams, J. R. Tuning the amino acid sequence of minimalist peptides to present biological signals via charge neutralised self-assembly. *Soft Matter* **2013**, *9*, 3915–3919.

167. Kuang, Y.; Gao, Y.; Shi, J.; Lin, H-C.; Xu, B. Supramolecular hydrogels based on the epitope of potassium ion channels. *Chem. Commun*. **2011**, *47*, 8772–8774.

168. Debnath, S.; Roy, S.; Ulijn, V. R.; Peptide Nanofibers with Dynamic Instability through Nonequilibrium Biocatalytic Assembly. *J. Am. Chem. Soc*. **2013**, *135*, 16789−16792.

169. Qin, S-Y.; Pei, Y.; Liu, X-J.; Zhuo, R-X.; Zhang, X-Z. Hierarchical self-assembly of a β-amyloid peptide derivative. *J. Mater. Chem. B.* **2013**, *1*, 668–675.

170. Li, Y.; Ding, Y.; Qin, M.; Caoc, Y.; Wang, W. An enzyme-assisted nanoparticle crosslinking approach to enhance the mechanical strength of peptide-based supramolecular hydrogels. *Chem. Commun*. **2013**, *49*, 8653—8655.

171. Bhattacharjee, S.; Bhattacharya, S. Phthalate mediated hydrogelation of a pyrene based system: a novel scaffold for shape-persistent, self-healing luminescent soft material. *J. Mater. Chem. A*, **2014**, *2*, 17889–17898.

172. Jones, S.; Wong, K. H.; Thordarson, P.; Ladouceu, F. Electroactive self-assembling hydrogels for flexible display technology. *J. Phys.: Condens. Matter* **2010**, *22*, 494105, 1-7.

173. Vauthey, S.; Santoso, S.; Gong, H.; Watson, N.; Zhang, S. Molecular self-assembly of surfactant-like peptides to form nanotubes and nanovesicles. *PNAS* **2002**, *99*, 5355–5360.

174. Zhao, X. Design of self-assembling surfactant-like peptides and their applications. *Current Opinion in Colloid & Interface Science* **2009**, *14*, 340–348.

175. Castelletto, V.; Barnes, R. H.; Karatzas, K-A.; Edwards-Gayle, C. J. C.; Greco, F.; Hamley, I. W.; Rambo, R.; Seitsonen, J.; Ruokolainen, J. Arginine-Containing Surfactant-Like Peptides: Interaction with Lipid Membranes and Antimicrobial Activity. *Biomacromolecules* **2018**, *19*, 2782–2794.

176. Wang, J.; Han, S.; Meng, G.; Xu, H.; Xia, D.; Zhao, X.; Schweins, R.; Lu, J. R. Dynamic self-assembly of surfactant-like peptides A_6K and A_9K. *Soft Matter* **2009**, *5*, 3870–3878.

177. Chen, P. Self-assembly of ionic-complementary peptides: a physicochemical viewpoint. *Colloids and Surfaces A: Physicochem. Eng. Aspects* **2005**, *261*, 3–24.

178. Zhang, S.; Altman, M. Peptide self-assembly in functional polymer science and engineering. *Reactive & Functional Polymers* **1999**, *41*, 91–102.

179. Hong, Y.; Legge, R. L.; Zhang, S.; Chen, P. Effect of Amino Acid Sequence and pH on Nanofiber Formation of Self-Assembling Peptides EAK16-II and EAK16-IV. *Biomacromolecules* **2003**, *4*, 1433-1442.

180. Zhang, S.; Holmest, T.; Lockshin, C.; Rich, A. Spontaneous assembly of a self-complementary oligopeptide to form a stable macroscopic membrane. *Proc. Natl. Acad. Sci. USA* **1993**, *90*, 3334-3338.

181. Zhang, S.; Lockshin, C.; Cook, R.; Rich, A. Unusually Stable β-Sheet Formation in an Ionic Self-Complementary Oligopeptide. *Biopolymers* **1994**, *34*, 663-672.

182. Joo, S. H. Cyclic Peptides as Therapeutic Agents and Biochemical Tools. *Biomol. Ther*.**2012**, *20*, 9-26.

183. Fernandez-Lopez, S. Kim, H-S.; Choi, E. C.; Delgado, M.; Granja, J. R.; Khasanov, A.; Kraehenbuehl, K.; Long, G.; Weinberger, D. A.; Wilcoxen, K. M.; Ghadiri, M. R. Antibacterial agents based on the cyclic D, L-α-peptide architecture. *Nature* **2001**, *412*, 452-455.

184. Chapman, R.; Danial, M.; Koh, M. L.; Jolliffe, K. A.; Perrier, S. Design and properties of functional nanotubes from the self-assembly of cyclic peptide templates. *Chem. Soc. Rev*. **2012**, *41*, 6023–6041.

185. Ishihara, Y.; Kimura, S. Nanofiber formation of amphiphilic cyclic tri-β-peptide. *J. Pept. Sci.* **2010**, *16*, 110–114.

186. Scanlon, S.; Aggeli, A. Self-assembling peptide nanotubes. *nanotoday* **2008**, *3*, 22-30.

187. Claussen, R. C.; Rabatic, B. M.; Stupp, S. I. Aqueous Self-Assembly of Unsymmetric Peptide Bolaamphiphiles into Nanofibers with Hydrophilic Cores and Surfaces *J. Am. Chem. Soc***. 2003**, *125*, 12680-12681.

188. da Silva, E. R.; Alves, W. A.; Castelletto, V.; Reza, M.; Ruokolainen, J.; Hussain, R.; Hamley, I. W. Self-Assembly Pathway of Peptide Nanotubes Formed by a Glutamatic Acid-Based Bolaamphiphile. *Chem. Commun*. **2015**, *51*, 11634-11637.

189. Bai, S.; Debnath,S.; Javid, N.; Frederix, P. W. J. M.; Fleming, S.; Pappas, C.; Ulijn, R. V. Differential Self-Assembly and Tunable Emission of Aromatic Peptide *Bola*-Amphiphiles Containing Perylene Bisimide in Polar Solvents Including Water. *Langmuir* **2014**, *30*, 7576−7584.

190. Maity, I.; Rasale, D. B.; Das, A. K. Exploiting a self-assembly driven dynamic nanostructured library. *RSC Adv*. **2013**, *3*, 6395–6400.

191. Deechongkit, S.; Powers, E. T.; You, S-L.; Kelly, J. W. Controlling the Morphology of Cross β-Sheet Assemblies by Rational Design *J. Am. Chem. Soc.* **2005**, *127*, 8562-8570.

192. Sanders, A. M.; Dawidczyk, T. J.; Katz, H. E.; Tovar, J. D. Peptide-Based Supramolecular Semiconductor Nanomaterials via Pd-Catalyzed Solid-Phase "Dimerizations". *ACS Macro Lett*. **2012**, *1*, 1326−1329.

193. Wall, B. D.; Diegelmann, S. R.; Zhang, S.; Dawidczyk, T. J.; Wilson, W. L.; Katz, H. E.; Mao, H-Q.; Tovar, J. D. Aligned Macroscopic Domains of Optoelectronic Nanostructures Prepared via Shear-Flow Assembly of Peptide Hydrogels. *Adv. Mater*. **2011**, *23*, 5009–5014.

194. Ryadnov, M. G.; Woolfson, D. N. MaP Peptides: Programming the Self-Assembly of Peptide-Based Mesoscopic Matrices. *J. Am. Chem. Soc*. **2005**, *127*, 12407-12415.

195. Duan, P.; Qin, L.; Zhu, X.; Liu, M. Hierarchical Self-Assembly of Amphiphilic Peptide Dendrons: Evolution of Diverse Chiral Nanostructures through Hydrogel Formation over a Wide pH Range. *Chem. Eur. J*. **2011**, *17*, 6389 – 6395.

196. Li, W.; Li, J.; Lee, M. Fabrication of Artifical Toroid Nanostructures by Modified β-sheet Peptide. *Chem. Commun*. **2013**, *49*, 8238-8240.

197. Doran, T. M.; Ryan, D. M.; Nilsson, B. L. Reversible photocontrol of self-assembled peptide hydrogel viscoelasticity. *Polym. Chem*. **2014**, *5*, 241-248.

198. Seliktar, D. Designing Cell-Compatible Hydrogels for Biomedical Applications. *Science* **2012**, *336*, 1124-1128.

199. Lee, S.; Oh, S. *et.al*. Stimulus-Responsive Azobenzene Supramolecules: Fibers, Gels, and Hollow Spheres. *Langmuir* **2013**, *29*, 5869–5877.

200. Lin, Y.; Qiao, Y.; Tang, P.; Li, Z.; Huang, J. Controllable self-assembled laminated nanoribbons from dipeptide-amphiphile bearing azobenzene moiety. *Soft Matter* **2011**, *7*, 2762–2769.

201. Beck, K.; Brodsky, B. Supercoiled Protein Motifs: The Collagen Triple-Helix and the α-Helical Coiled Coil. *Journal of Structural Biology* **1998**, *122*, 17–29.

202. Potekhin, S. A.; Melnik, T. N.; Popov, V.; Lanina, N. F.; Vazina, A. A.; Rigler, P.; Verdini, A. S.; Corradin, G.; Kajava, A. V. De novo design of fibrils made of short α-helical coiled coil peptides. *Chemistry & Biology* **2001**, *8*, 1025-1032.

203. Wagner, D. E.; Phillips, C. L.; Ali, W. M.; Nybakken, G. E.; Crawford, E. D.; Schwab, A. D.; Smith, W. F.; Fairman, R. Toward the development of peptide nanofilaments and nanoropes as smart materials. *PNAS* **2005**, *102*, 12656–12661.

204. Moutevelis, E.; Woolfson, D. N. A Periodic Table of Coiled-Coil Protein Structures. *J. Mol. Biol.* **2009**, *385*, 726–732.

205. Gribbon, C.; Channon, K. J.; Zhang, W.; Banwell, E. F.; Bromley, E. H. C.; Chaudhuri, J. B.; Oreffo, R. O. C.; Woolfson, D. N. MagicWand: A Single, Designed Peptide That Assembles to Stable, Ordered α-Helical Fibers. *Biochemistry* **2008**, *47*, 10365–10371.

206. Xu, C.; Breedveld, V.; Kopecˇek, J. Reversible Hydrogels from Self-Assembling Genetically Engineered Protein Block Copolymers. *Biomacromolecules* **2005**, *6*, 1739-1749.

207. Smith, A. M.; Banwell, E. F.; Edwards, W. R.; Pandya, M. J.; Woolfson, D. N. Engineering Increased Stability into Self-Assembled Protein Fibers. *Adv. Funct. Mater.* **2006**, *16*, 1022–1030.

208. Fishwick, C. W. G.; Beevers, A. J.; Carrick, L. M.; Whitehouse, C. D.; Aggeli, A.; Boden, N. Structures of Helical β-Tapes and Twisted Ribbons: The Role of Side-Chain Interactions on Twist and Bend Behavior. *Nano Letters* **2003**, *3*, 1475-1479.

209. Kun Lu, K.; Jacob, J.; Thiyagarajan, P. Conticello, V. P.; Lynn, D. G. Exploiting Amyloid Fibril Lamination for Nanotube Self-Assembly. *J. Am. Chem. Soc*. **2003**, *125*, 6391-6393.

210. Xu, G.; Wang, W.; Groves, J. T.; Hecht, M. H. Self-assembled monolayers from a designed combinatorial library of de novo β-sheet proteins. *PNAS* **2001**, *98*, 3652–3657.

211. Aggeli, A.; Bell, M.; Carrick, L. M.; Fishwick, C. W. G.; Harding, R.; Mawer, P. J.; Radford, S. E.; Strong, A. E.; Boden, N. pH as a Trigger of Peptide β-Sheet Self-Assembly and Reversible Switching between Nematic and Isotropic Phases. *J. Am. Chem. Soc*. **2003**, *125*, 9619-9628.

212. Powers, E. T.; Yang, S. I.; Lieber, C. M.; Kelly, J. W. Ordered Langmuir-Blodgett Films of Amphiphilic β-Hairpin Peptides Imaged by Atomic Force Microscopy. *Angew. Chem. Int. Ed.* **2002**, *41*, 127-130.

213. Schneider, J. P.; Pochan, D. J.; Ozbas, B.; Rajagopal, K.; Pakstis, L.; Kretsinger, J. Responsive Hydrogels from the Intramolecular Folding and Self-Assembly of a Designed Peptide. *J. Am. Chem. Soc.* **2002**, *124*, 15030-15037.

214. King, P. J. S.; Lizio, M. G.; Booth, A.; Collins, R. F.; Gough, J. E.; Aline F. Miller, A. F.; Webb, S. J. A modular self-assembly approach to functionalised β-sheet peptide hydrogel biomaterials. *Soft Matter* **2016**, *12*, 1915-1923.

215. Yuan, C.; Li, S.; Zou, Q.; Ren, Y.; Yan, X. Multiscale simulations for understanding the evolution and mechanism of hierarchical peptide self-assembly. *Phys. Chem. Chem. Phys*. **2017**, *19*, 23614-23631.

216. Sun, H.; Luo, Q.; Hou, C.; Liu, J. Nanostructures based on protein self-assembly: From hierarchical construction to bioinspired materials. *Nano Today* **2017**, *14*, 16–41.

217. Dasgupta, A.; Mondal, J. H.; Das, D. Peptide hydrogels. *RSC Adv*. **2013**, *3*, 9117–9149.

218. Martin, C. R.; Kohli, P. The Emerging Field Of Nanotube Biotechnology. *Nat Rev Drug Discov*. **2003**, *2*, 29–37.

219. Yan, X.; He, Q.; Wang, K.; Duan, L.; Cui, Y.; Li, J. Transition of Cationic Dipeptide Nanotubes into Vesicles and Oligonucleotide Delivery. *Angew. Chem. Int. Ed*. **2007**, *46*, 2431 –2434.

220. Gupta, M.; Bagaria, A.; Mishra, A.; Mathur, P.; Basu, A.; Ramakumar, S.; Chauhan, V. S. Self-Assembly of a Dipeptide-Containing Conformationally Restricted Dehydrophenylalanine Residue to Form Ordered Nanotubes. *Adv. Mater*. **2007**, *19*, 858–861.

221. Guha, S.; Banerjee, A. Self-Assembled Robust Dipeptide Nanotubes and Fabrication of Dipeptide-Capped Gold Nanoparticles on the Surface of these Nanotubes. *Adv. Funct. Mater*. **2009**, *19*, 1949–1961.

222. Bonetti, A. *et.al*. Dipeptide Nanotubes Containing Unnatural Fluorine-Substituted $\beta^{2,3}$-Diarylamino Acid and L-Alanine as Candidates for Biomedical Applications. *Org. Lett*. **2015**, *17*, 4468–4471.

223. Vale´ry, C.; Paternostre, M.; Robert, B.; Gulik-Krzywicki, T.; Narayanan, T.; Dedieu, J-C.; Keller, G.; Torres, M-L.; Cherif-Cheikh, R.; Calvo, P.; Artzner, F. Biomimetic organization: Octapeptide self-assembly into nanotubes of viral capsid-like dimension. *PNAS* **2003**, *100*, 10258–10262.

224. Rosenthal-Aizman, K.; Svensson, G.; Unde´n, A. Self-Assembling Peptide Nanotubes from Enantiomeric Pairs of Cyclic Peptides with Alternating D and L Amino Acid Residues. *J. Am. Chem. Soc*. **2004**, *126*, 3372-3373.

225. Santoso, S.; Hwang, W.; Hartman, H.; Zhang, S. Self-assembly of Surfactant-like Peptides with Variable Glycine Tails to Form Nanotubes and Nanovesicles. *Nano Letters* **2002**, *2*, 687-691.

226. Bucak, S.; Cenker, C.; Nasir, I.; Olsson, U.; Zackrisson, M. Peptide Nanotube Nematic Phase. *Langmuir* **2009**, *25*, 4262–4265.

227. Behanna, H. A.; Donners, J. J. J. M.; Gordon, A. C.; Stupp, S. I. Coassembly of Amphiphiles with Opposite Peptide Polarities into Nanofibers. *J. Am. Chem. Soc.* **2005**, *127*, 1193-1200.

228. Silva, G. A.; Czeisler, C.; Niece, K. L.; Beniash, E.; Harrington, D. A.; Kessler, J. A.; Stupp, S. I. Selective Differentiation of Neural Progenitor Cells by High–Epitope Density Nanofibers. *Science* **2004**, *303*, 1352-1355.

229. Marini, D. M.; Hwang, W.; Lauffenburger, D. A.; Zhang, S.; Kamm, R. D. Left-Handed Helical Ribbon Intermediates in the Self-Assembly of a β-Sheet Peptide. *Nano Letters* **2002**, *2*, 295-299.

230. van Hell, A. J.; Costa, C. I. C. A.; Flesch, F. M.; Sutter, M.; Jiskoot, W.; Crommelin, D. J. A.; Hennink, W. E.; Mastrobattista, E. Self-Assembly of Recombinant Amphiphilic Oligopeptides into Vesicles. *Biomacromolecules* **2007**, *8*, 2753-2761.

231. Bellomo, E. G.; Wyrsta, M. D.; Pakstis, L.; Pochan, D. J.; Deming, T. J. Stimuli-responsive polypeptide vesicles by conformation-specific assembly. *nature materials* **2004**, *3*, 244-248.

232. Holowka, E. P.; Pochan, D. J.; Deming, T. J. Charged Polypeptide Vesicles with Controllable Diameter. *J. Am. Chem. Soc.* **2005**, *127*, 12423-12428.

233. Rodriguez-Herna´ndez, J.; Lecommandoux, S. Reversible Inside-Out Micellization of pH-responsive and Water-Soluble Vesicles Based on Polypeptide Diblock Copolymers. *J. Am. Chem. Soc.* **2005**, *127*, 2026-2027.

234. Dreher, M. R.; Simnick, A. J.; Fischer, K.; Smith, R. J.; Patel, A.; Schmidt, M.; Chilkoti, A. Temperature Triggered Self-Assembly of Polypeptides into Multivalent Spherical Micelles. *J. Am. Chem. Soc*. **2008**, *130*, 687-694.

235. Yoon, Y-R.; Lim, Y-b.; Lee, E.; Lee, M. Self-assembly of a peptide rod–coil: a polyproline rod and a cell-penetrating peptide Tat coil. *Chem. Commun*. **2008**, 1892–1894.

236. Lim, Y-b.; Lee, E.; Lee, M. Controlled Bioactive Nanostructures from Self-Assembly of Peptide Building Blocks. *Angew. Chem. Int. Ed*. **2007**, *46*, 9011 –9014.

237. Mandal, D.; Tiwari, R. K.; Shirazi, A. M.; Oh, D.; Ye, G.; Banerjee, A.; yadav, A.; Parang, K. Self-Assembled Surfactant Cyclic Peptide Nanostructures as Stabilizing Agents. *Soft Matter* **2013**, *9*, 9465-9475.

238. Cherny, I.; Gazit, E. Amyloids: Not Only Pathological Agents but Also Ordered Nanomaterials. *Angew. Chem. Int. Ed***. 2008**, *47*, 4062 – 4069.

239. Reches, M.; Porat, Y.; Gazit, E. Amyloid Fibril Formation by Pentapeptide and Tetrapeptide Fragments of Human Calcitonin. *The Journal of Biological Chemistry* **2002**, *277*, 35475–35480.

240. Tenidis, K.; Waldner, M.; Bernhagen, J.; Fischele, W.; Bergmann, M.; Weber. M.; Merkle, M-L.; Voelter, W.; Brunner, H.; Kapurniotu, A. Identification of a Penta- and Hexapeptide of Islet Amyloid Polypeptide (IAPP) with Amyloidogenic and Cytotoxic Properties. *J. Mol. Biol*. **2000** *295*, 1055-1071.

241. Lomander, A.; Hwang, W.; Zhang, S. Hierarchical Self-Assembly of a Coiled-Coil Peptide into Fractal Structure. *Nano Letters* **2005**, *5*, 1255-1260.

242. Ryadnov, M. G. A Self-Assembling Peptide Polynanoreactor. *Angew. Chem. Int. Ed.* **2007**, *46*, 969 –972.

243. Orbach, R.; Adler-Abramovich, L.; Zigerson, S.; Mironi-Harpaz, I.; Dror Seliktar, D.; Gazit, E. Self-Assembled Fmoc-Peptides as a Platform for the Formation of Nanostructures and Hydrogels. *Biomacromolecules* **2009**, *10*, 2646–2651.

244. Ligorio, C.; Zhou, M.; Wychowaniec, J. K.; Zhu, X.; Bartlam, C.; Miller, A. F.; Vijayaraghavan, A.; Hoyland, J .A.; Saiani, A. Graphene oxide containing self-assembling peptide hybrid hydrogels as a potential 3D injectable cell delivery platform for intervertebral disc repair applications. *Acta Biomaterialia* **2019**, *92*, 92–103.

245. Hiew, S. H.; Mohanram, H.; Ning, L.; Guo, J.; Sánchez-Ferrer, A.; Shi, X.; Pervushin, K.; Mu, Y.; Mezzenga, R.; Miserez, A. A Short Peptide Hydrogel with High Stiffness Induced by 3_{10}-Helices to β-Sheet Transition in Water. *Adv. Sci*. **2019**, *6*, 1901173, 1-11.

246. Zhang, Y.; Gu, H.; Yang, Z.; Xu, B. Supramolecular Hydrogels Respond to Ligand-Receptor Interaction. *J. Am. Chem. Soc*. **2003**, *125*, 13680-13681.

247. Thota, C. K.; Yadav, N.; Chauhan, V. S. "A novel highly stable and injectable hydrogel based on a conformationally restricted ultrashort peptide". *Sci. Rep*. **2016,** *6*, 31167, 1-12.

248. Podder, D.; Chowdhury, S. R.; Nandia, S. K.; Haldar, D. Tripeptide based super-organogelators: structure and function. *New J. Chem*. **2019**, *43*, 3743-3749.

249. Chetia, M.; Debnath, S.; Chowdhuri, S.; Chatterjee, S. Self-assembly and multifunctionality of peptide organogels: oil spill recovery, dye absorption and synthesis of conducting biomaterials. *RSC Adv*. **2020**, *10*, 5220–5233.

250. Das, A. K.; Bose, P. P.; Drew, M. G. B.; Banerjee, A. The role of protecting groups in the formation of organogels through a nano-fibrillar network formed by self-assembling terminally protected tripeptides. *Tetrahedron* **2007**, *63*, 7432–7442.

251. Adhikari, B.; Nanda, J.; Banerjee, A. Pyrene-Containing Peptide-Based Fluorescent Organogels: Inclusion of Graphene into the Organogel. *Chem. Eur. J.* **2011**, *17*, 11488 – 11496.

252. Langer, R. Drug delivery and targeting. *Nature* **1998**, *392*, 5-10.

253. Su, C-W.; Chiang, C-S.; Li, W-M.; Hu, S-H.; Chen, S-Y. Multifunctional nanocarriers for simultaneous encapsulation of hydrophobic and hydrophilic drugs in cancer treatment. *Nanomedicine* **2014**, *9*, 1499–1515.

254. Ro¨sler, A.; Vandermeulen, G. W. M.; Klok, H-A. Advanced drug delivery devices via self-assembly of amphiphilic block copolymers. *Advanced Drug Delivery Reviews* **2001**, *53*, 95–108.

255. Webber, M. J.; Matson, J. B.; Tamboli, V. K.; Stupp, S. I. Controlled release of dexamethasone from peptide nanofiber gels to modulate inflammatory response. *Biomaterials* **2012**, *33*, 6823-6832.

256. Zhang, P.; Cheetham, A.G.; Lin, Y-A.; Cui, H. Self-Assembled Tat Nanofibers as Effective Drug Carrier and Transporter. *ACS Nano* **2013**, *7*, 5965–5977.

257. Yishay-Safranchik, E.; Golana, M.; David, A. Controlled release of doxorubicin and Smac-derived pro-apoptotic peptide from self-assembled KLD-based peptide hydrogels. *Polym. Adv. Technol*. **2014**, *25*, 539–544.

258. Silva, R. F.; Araújo, D. R.; Silva, E. R.; Ando, R.A.; Alves, W. A. L-Diphenylalanine Microtubes as a Potential Drug-Delivery System: Characterization, Release Kinetics, and Cytotoxicity. *Langmuir* **2013**, *29*, 10205−10212.

259. Lu, S.; Wang, H.; Sheng, Y.; Liu, M.; Chen, P. Molecular binding of self-assembling peptide EAK16-II with anticancer agent EPT and its implication in cancer cell inhibition. *Journal of Controlled Release* **2012**, *160*, 33–40.

260. Li, N.; Li, N.; Yi, Q.; Luo, K.; Guo, C.; Pan, D.; Gu, Z. Amphiphilic peptide dendritic copolymer-doxorubicin nanoscale conjugate self-assembled to enzyme-responsive anti-cancer agent. *Biomaterials* **2014**, *35*, 9529-9545.

261. von Maltzahn, G.; Vauthey, S.; Santoso, S.; Zhang, S. Positively Charged Surfactant-like Peptides Self-assemble into Nanostructures. *Langmuir* **2003**, *19*, 4332-4337.

262. Jabbari, E.; Yang, X.; Moeinzadeh, S.; He, X. Drug release kinetics, cell uptake, and tumor toxicity of hybrid VVVVVVKK peptide-assembled polylactide nanoparticles. *European Journal of Pharmaceutics and Biopharmaceutics* **2013**, *84*, 49–62.

263. Sadatmousavi, P.; Soltani, M.; Nazarian, R.; Jafari, M.; Chen, P. Self-Assembling Peptides: Potential Role in Tumor Targeting. *Current Pharmaceutical Biotechnology* **2011**, *12*, 1089-1100.

264. Zhao, F.; Ma, M. L.; Xu, B. Molecular hydrogels of therapeutic agents. *Chem. Soc. Rev.* **2009**, *38*, 883–891.

265. Murphy, E. A.; Majeti, B. K.; Barnes, L. A.; Makale, M.; Weis,S. M.; Lutu-Fuga, K.; Wrasidlo, W.; Cheresh, D. A. Nanoparticle-mediated drug delivery to tumor vasculature suppresses metastasis. *PNAS* **2008**, *105*, 9343–9348.

266. Luo, G.; Yu, X.; Jin, C.; Yang, F.; Fu, D.; Long, J.; Xu, J.; Zhan, C.; Lu, W. LyP-1-conjugated nanoparticles for targeting drug delivery to lymphatic metastatic tumors. *International Journal of Pharmaceutics* **2010**, *385*, 150–156.

267. Jiang, T.; Zhang, Z.; Zhang, Y.; Lv, H.; Zhou, J.; Li, C.; Hou, L.; Zhang, Q. Dual-functional liposomes based on pH-responsive cell-penetrating peptide and hyaluronic acid for tumor-targeted anticancer drug delivery. *Biomaterials* **2012**, *33*, 9246-9258.

268. Shah, A.; Malik, M. S.; Khan, G. S.; Nosheen, E.; Iftikhar, F. J.; Khan, F. A.; Shukla, S. S.; Akhter, M. S.; Kraatz, H-B.; Aminabhavi, T. M. Stimuli-responsive peptide-based biomaterials as drug delivery systems, *Chemical Engineering Journal* **2018**, *353*, 559-583.

269. Yang, C.; Wang, Z.; Ou, C.; Chen, M.; Wang, L.; Yang, Z. A supramolecular hydrogelator of curcumin. *Chem. Commun*. **2014**, *50*, 9413-9415.

270. Gong, C.; Shan, M.; Li, B.; Wu, G. A pH and redox dual stimuli-responsive poly(amino acid) derivative for controlled drug release. *Colloids and Surfaces B: Biointerfaces* **2016**, *146*, 396–405.

271. Koutsopoulosa, S.; Unsworth, L. D.; Nagai, Y.; Zhang, S. Controlled release of functional proteins through designer self-assembling peptide nanofiber hydrogel scaffold. *PNAS* **2009**, *106*, 4623–4628.

272. Rea, J. C.; Gibly, R. F.; Barron, A. E.; Shea, L. D. Self-assembling peptide–lipoplexes for substrate-mediated gene delivery. *Acta Biomaterialia* **2009**, *5*, 903–912.

273. Chen, J-X.; Xu, X-D.; Yang, S.; Yang, J.; Zhuo, R-X.; Zhang, X-Z. Self-Assembled BolA-like Amphiphilic Peptides as Viral-Mimetic Gene Vectors for Cancer Cell Targeted Gene Delivery. *Macromol. Biosci*. **2013**, *13*, 84–92.

274. Genta, I.; Chiesa, E.; Colzani, B.; Modena, T.; Conti, B.; Dorati, R. GE11 Peptide as an Active Targeting Agent in Antitumor Therapy: A Minireview. *Pharmaceutics* **2018**, *10*, 2, 1-14.

275. Lin, W. J.; Chien, W. H. Peptide-conjugated micelles as a targeting nanocarrier for gene delivery. *J. Nanopart. Res*. **2015**, *17*, 349, 1-14.

276. Holmes, T. C.; de Lacalle, S.; Su, X.; Liu, G.; Rich, A.; Zhang, S. Extensive neurite outgrowth and active synapse formation on self-assembling peptide scaffolds. *PNAS* **2000**, *97*, 6728–6733.

277. Gelain, F.; Bottai, D.; Vescovi, A.; Zhang, S. Designer Self-Assembling Peptide Nanofiber Scaffolds for Adult Mouse Neural Stem Cell 3-Dimensional Cultures. *PLoS ONE* **2006,** e119, 1-11.

278. Cunha, C.; Panseri, S.; Villa, O.; Silva, D.; Gelain, F. 3D culture of adult mouse neural stem cells within functionalized self-assembling peptide scaffolds. *International Journal of Nanomedicine* **2011**, *6*, 943–955.

279. Nune, M.; Kumaraswamy, P.; Krishnan, U. M.; Sethuraman, S. Self-Assembling Peptide Nanofibrous Scaffolds for Tissue Engineering: Novel Approaches and Strategies for Effective Functional Regeneration. *Current Protein and Peptide Science* **2013**, *14*, 70-84.

280. Wan, A. C. A.; Ying, J. Y. Nanomaterials for in situ cell delivery and tissue regeneration. *Advanced Drug Delivery Reviews* **2010**, *62*, 731–740.

281. Kisiday, J.; Jin, M.; Kurz, B.; Hung, H.; Semino, C.; Zhang, S.; Grodzinsky, A. J. Self-assembling peptide hydrogel fosters chondrocyte extracellular matrix production and cell division: Implications for cartilage tissue repair. *PNAS* **2002**, *99*, 9996–10001.

282. Hutmacher, D. W.; Loessner, D.; Rizzi, S.; Kaplan, D. L.; David J. Mooney, D. J.; Clements, J. A. Can tissue engineering concepts advance tumor biology research? *Trends in Biotechnology* **2010**, *28*, 125-133.

283. Jayawarna, V.; Ali, M.; Jowitt, T. A.; Miller, A. F.; Saiani, A.; Gough, J. E.; Ulijn, R. V. Nanostructured Hydrogels for Three-Dimensional Cell Culture Through Self-Assembly of Fluorenylmethoxycarbonyl–Dipeptides. *Adv. Mater*. **2006**, *18*, 611–614.

284. Mahler, A.; Reches, M.; Rechter, M.; Cohen, S.; Gazit, E. Rigid, Self-Assembled Hydrogel Composed of a Modified Aromatic Dipeptide. *Adv. Mater*. **2006**, *18*, 1365–1370.

285. Zhang, S.; Gelain, F.; Zhao, X. Designer self-assembling peptide nanofiber scaffolds for 3D tissue cell cultures. *Seminars in Cancer Biology* **2005**, *15*, 413–420.

286. Zhang, F.; Shi, G-S.; Ren, L-F.; Hu, F-Q.; Li, S-L.; Xie, Z-J. Designer self-assembling peptide scaffold stimulates pre-osteoblast attachment, spreading and proliferation. *J Mater Sci: Mater Med.* **2009**, *20*, 1475–1481.

287. Jung, J. P.; Nagaraj, A. K.; Fox, E. K.; Rudra, J. S.; Devgun, J. M.; Collier, J. H. Co-assembling peptides as defined matrices for endothelial cells. *Biomaterials* **2009**, *30*, 2400–2410.

288. Giancotti, F. G.; Ruoslahti, E. Integrin Signaling. *Science* **1999**, *285*, 1028-1033.

289. Zaidel-Bar, R.; Cohen, M.; Addadi, L.; Geiger, B. Hierarchical assembly of cell–matrix adhesion complexes. *Biochemical Society Transactions* **2004**, *32*, 416-420.

290. Pierschbacher, D. M.; Ruoslahti, E. Cell attachment activity of fibronectin can be duplicated by small synthetic fragments of the molecule. *Nature* **1984**, *309*, 30–33.

291. Pierschbacher, M. D.; Ruoslahti, E. Variants of the cell recognition site of fibronectin that retain attachment-promoting activity. *Proc. Natl. Acad. Sci. USA* **1984**, *81*, 5985-5988.

292. Storrie, H.; Guler, M. O.; Abu-Amara, S. N.; Volberg, T.; Rao, M.; Geiger, B.; Stupp, S. I. Supramolecular crafting of cell adhesion. *Biomaterials* **2007**, *28*, 4608–4618.

293. Chen, C.; Hu, J.; Zhang, S.; Zhou, P.; Zhao, X.; Xu, H.; Zhao, X.; Yaseen, M.; Lu, J. R. Molecular mechanisms of antibacterial and antitumor actions of designed surfactant-like peptides. *Biomaterials* **2012**, *33*, 592-603.

294. Li, J.; Chen, Z.; Zhou, M.; Jing, J.; Li, W.; Wang, Y.; Wu, L.; Wang, L.; Wang, Y.; Lee, M. Polyoxometalate-Driven Self-Assembly of Short Peptides into Multivalent Nanofibers with Enhanced Antibacterial Activity. *Angew. Chem. Int. Ed*. **2016**, *55*, 2592-2595.

295. Schnaider, L.; Brahmachari, S.; Schmidt, N.W.; Mensa, B.; Shaham-Niv, S.; Bychenko, D.; Adler-Abramovich, L.; Shimon, L. J. W.; Kolusheva, S.; DeGrado, W. F.; Gazit, E. Self-assembling dipeptide antibacterial nanostructures with membrane disrupting activity. *Nat. Commun*. **2017**, *8*:*1365*, 1-10.

296. Veiga, A. S; Sinthuvanich, C.; Gaspar, D.; Franquelim, H. G.; Castanho, M. A. R. B.; Schneider, J. P. Arginine-rich self-assembling peptides as potent antibacterial gels. *Biomaterials* **2012**, *33*, 8907-8916.

297. Chu-Kung, A. F.; Nguyen, R.; Bozzelli, K. N.; Tirrell, M. Chain length dependence of antimicrobial peptide–fatty acid conjugate activity. *Journal of Colloid and Interface Science* **2010**, *345*, 160–167.

298. Chu-Kung, A. F.; Bozzelli, K. N.; Lockwood, N. A.; Haseman , J. R.; Mayo, K. H.; Tirell, M. V. Promotion of Peptide Antimicrobial Activity by Fatty Acid Conjugation. *Bioconjugate Chem.* **2004**, *15*, 530-535.

299. Wang. X.; Wang, X. Aptamer-functionalized hydrogel diffraction gratings for the human thrombin detection. *Chem. Commun*. **2013**, *49*, 5957-5959.

300. Kim, J. H.; Lim, S. Y.; Nam, D. H.; Ryu, J.; Ku, S. H.; Park, C. B. Self-assembled, photoluminescent peptide hydrogel as a versatile platform for enzyme-based optical biosensors. *Biosensors and Bioelectronics* **2011**, *26*, 1860–1865.

301. Ren, C.; Wang, H.; Zhang, X.; Ding, D.; Wang, L.; Yang, Z. Interfacial self-assembly leads to formation of fluorescent nanoparticles for simultaneous bacterial detection and inhibition. *Chem. Commun*. **2014**, *50*, 3473-3475.

302. Ren, C.; Wang, H.; Mao, D.; Zhang, X.; Fengzhao, Q.; Shi, Y.; Ding, D.; Kong, D.; Wang, L.; Yang, Z. When Molecular Probes Meet Self-Assembly: An Enhanced Quenching Effect. *Angew. Chem. Int. Ed*. **2015**, *54*, 1-6.

303. de la Rica, R.; Pejoux, C.; Matsui, H.; Assemblies of Functional Peptides and Their Applications in Building Blocks for Biosensors. *Adv. Funct. Mater*. **2011**, *21*, 1018-1026.

304. Basak, S.; Nandi, N.; Paul, S.; Hamley, I. W.; Banerjee, A. A Tripeptide-based Self-Shrinking Hydrogel for Waste-Water Treatment: Removal of Toxic Organic Dyes and Lead (Pb^{2+}) Ions. *Chem. Commun*. **2017**, *53*, 5910-5913.

305. Ray, S.; Das, A. K.; Banerjee, A. pH-Responsive, Bolaamphiphile-Based Smart Metallo-Hydrogels as Potential Dye-Adsorbing Agents, Water Purifier, and Vitamin B_{12} Carrier. *Chem. Mater*. **2007**, *19*, 1633-1639.

306. Basu, K.; Nandi, N.; Mondal, B.; Dehsorkhi, A.; Hamley, I. W.; Banerjee, A. Peptide-based ambidextrous bifunctional gelator: applications in oil spill recovery and removal of toxic organic dyes for waste water management. *Interface Focus 7*, **2017**, *20160128*, 1-9.

307. Pramanik, B.; Ahmed, S.; Singha, N.; Das, D.; Self-Assembly Assisted Tandem Sensing of Pd^{2+} and CN^- by a Perylenediimide-Peptide Conjugate. *Chemistry Select* **2017**, *2*, 10061 –10066.

308. Zhang, C.; Wan L.Y.; Wu, S.; Wu, D.; Qin, X.; Ko, F. A reversible colorimetric chemosensor for naked-eye detection of copper ions using poly (aspartic acid) nanofibrous hydrogel. *Dyes and Pigments* **2015**, *123*, 380-385.

309. Acar, H.; Garifullin, R.; Guler, M. O. Self-Assembled Template-Directed Synthesis of One-Dimensional Silica and Titania Nanostructures. *Langmuir* **2011**, *27*, 1079–1084.

310. Tao, K.; Wang, J.; Li, Y.; Xia, D.; Shan, H.; Xu, H.; Lu, J. R. Short peptide-directed synthesis of one-dimensional platinum nanostructures with controllable morphologies. *Scientific Reports* **2013**, *3*:*2565*, 1-6.

311. Zhou, B.; Sun, Z.; Li, D.; Zhang, T.; Deng, L.; You-Nian Liu, Y-N. Platinum nanostructures via self-assembly of an amyloid-like peptide: a novel electrocatalyst for the oxygen reduction. *Nanoscale* **2013**, *5*, 2669-2673.

312. Williamson, M. P.; P. Waltho, J. P. Peptide Structure from NMR. *Chem. Soc. Rev*. **1992**, *21*, 227-236.

313. Singh, V.; Snigdha, K.; Singh, C.; Sinha, N.; Thakur, A. K. Understanding the self-assembly of Fmocphenylalanine to hydrogel formation. *Soft Matter* **2015**, *11*, 5353-5364.

314. Cohen, Y.; Avram, L.; Frish, L. Diffusion NMR Spectroscopy in Supramolecular and Combinatorial Chemistry: An Old Parameter-New Insights. *Angew. Chem. Int. Ed*. **2005**, *44*, 520-554.

315. Pappas, C. G.; Sasselli, I. R.; Ulijn. R. V. Biocatalytic Pathway Selection in Transient Tripeptide Nanostructures. *Angew. Chem. Int. Ed*. **2015**, *54*, 8119 –8123.

316. Jaroniec, C. P.; MacPhee, C. E.; Astrof, N. S.; Dobson, C. M.; Griffin, R. G. Molecular conformation of a peptide fragment of transthyretin in an amyloid fibril. *PNAS* **2002**, *99*, 16748–16753.

317. Nieuwland, M.; Ruizendaal, L.; Brinkmann, A.; Kroon-Batenburg, L.; van Hest, J. C. M.; L¨owik, D. W.P.M. A structural study of the self-assembly of a palmitoyl peptide amphiphile. *Faraday Discuss*. **2013**,*166*, 361-379.

318. Cormier, A. R.; Pang, X.; Zimmerman, M. I.; Zhou, H-X.; Paravastu, A. K. Molecular Structure of RADA16-I Designer Self-Assembling Peptide Nanofibers. *ACS Nano* **2013**, *7*, 7562–7572.

319. Wallace, M.; Iggo, J. A.; Adams, D. J. Probing the surface chemistry of self-assembled peptide hydrogels using solution-state NMR spectroscopy. *Soft Matter* **2017**, *13*, 1716-1727.

320. Leonard, S. R.; Cormier, A. R.; Pang, X.; Zimmerman, M. I.; Zhou, H-X.; Paravastu, A. K. Solid-State NMR Evidence for β-Hairpin Structure within MAX8 Designer Peptide Nanofibers. *Biophysical Journal* **2013**, *105*, 222–230.

321. Urry, D. W.; Mitchell, L. W.; Ohnishi, T. Solvent Dependence of Peptide Carbonyl Carbon Chemical Shifts And Polypeptide Secondary Structure: The Repeat Tetrapeptide of Elastin. *Biochemical and Biophysical Research Communications* **1974**, *59*, 62-69.

322. Whittemore, N. A.; Mishra, R.; Kheterpal, I.; Williams, A. D.; Wetzel, R.; Serpersu, E. H. Hydrogen-Deuterium (H/D) Exchange Mapping of Aβ1-40 Amyloid Fibril Secondary Structure Using Nuclear Magnetic Resonance Spectroscopy. *Biochemistry* **2005**, *44*, 4434-4441.

323. Rico, M.; Nieto, J. L.; Santoro, J.; Bermejo, F. J.; Herranz, J.; Gallego, E. Low-temperature ^{1}H-NMR evidence of the folding of isolated ribonuclease S-peptide. *FEBS Lett.* **1983**, *162*, 314-319.

324. Afonin, S.; Grage, S. L.; Ieronimo, M.; Wadhwani, P.; Ulrich, A. S. Temperature-Dependent Transmembrane Insertion of the Amphiphilic Peptide PGLa in Lipid Bilayers Observed by Solid State ^{19}F NMR Spectroscopy. *J. Am. Chem. Soc*. **2008**, *130*, 16512–16514.

325. Hamley, I. W.; Nutt, D. R.; Brown, G. D. Influence of the Solvent on the Self-Assembly of a Modified Amyloid Beta Peptide Fragment. II. NMR and Computer Simulation Investigation. *J. Phys. Chem. B.* **2010**, *114*, 940–951.

326. Truex, N. L.; Wang, Y.; Nowick, J. S. Assembly of Peptides Derived from β-Sheet Regions of β-Amyloid. *J. Am. Chem. Soc*. **2016**, *138*, 13882–13890.

327. Truex, N. L.; Nowick, J. S. Coassembly of Peptides Derived from β-Sheet Regions of β-Amyloid. *J. Am. Chem. Soc*. **2016**, *138*, 13891–13900.

328. Moore, W. H.; Krimm, S. Vibrational Analysis of Peptides, Polypeptides, and Proteins. II. β-Poly(L-alanine) and β-Poly(Lalanylglycine). *Biopolymers* **1976**, *15*, 2465-2483.

329. Fabian, H.; Schultz, C. P. Fourier Transform Infrared Spectroscopy in Peptide and Protein Analysis. In Encyclopedia of Analytical Chemistry (eds R.A. Meyers and C. Schöneich), **2006**, 1-23.

330. Kong, J.; Yu, S. Fourier Transform Infrared Spectroscopic Analysis of Protein Secondary Structures. *Acta Biochimica et Biophysica Sinica* **2007**, *39*, 549–559.

331. Wei, R.; Jin, C-C.; Quan, J.; Nie, H.; Zhu, L-M. A Novel Self-Assembling Peptide with UV-Responsive Properties. *Biopolymers* **2013**, *101*, 272-278.

332. Pappas, C. G.; Frederix, P. W. J. M.; Mutasa, T.; Fleming, S.; Abul-Haija, Y. M.; Kelly, S. M.; Gachagan, A.; Kalafatovic, D.; Trevino, J.; Ulijn, R.V.; Bai, S. Alignment of Nanostructured Tripeptide Gels by Directional Ultrasonication. *Chem. Commun*. **2015**, *51*, 8465-8468.

333. Pappas, C. G.; Mutasa, T.; Frederix, P. W. J. M.; Fleming, S.; Bai, S.; Debnath, S.; Kelly, S. M.; Gachagan, A.; Ulijn, R. V. Transient Supramolecular Reconfiguration of Peptide Nanostructures using Ultrasound. *Mater. Horiz*. **2015**, *2*, 198-202.

334. Zhou, M.; Self-assembled peptide-based hydrogels as scaffolds for anchorage dependent cells. *Biomaterials* **2009**, *30*, 2523–2530.

335. Amorin, M.; Perez, A.; Barbera, J.; Ozores, H. L.; Serrano, J. L.; Granja, J. R.; Sierra, T. Liquid crystal organization of self-assembling cyclic peptides. *Chem. Commun*. **2014**, *50*, 688-690.

336. Moretto, V.; Crisma, M.; Bonora, G. M.; Toniola, C.; Balaram, H.; Balaram, P. Comparison of the Effect of Five Guest Residues on the & Sheet Conformation of Host $(L\text{-Val})_n$ Oligopeptides. *Macromolecules* **1989**, *22*, 2939-2944.

337. Dado, G. P.; Gellman, S. H. Intramolecular Hydrogen Bonding in Derivatives of β Alanine and γ-Amino Butyric Acid: Model Studies for the Folding of Unnatural Polypeptide Backbones. *J. Am. Chem. Soc*. **1994**, *116*, 1054-1062.

338. Tuma, R. Raman spectroscopy of proteins: from peptides to large assemblies. *J. Raman Spectrosc*. **2005**, *36*, 307–319.

339. Ayas, S.; Cinar, G.; Ozkan, A. D.; Soran, Z.; Ekiz, O.; Kocaay, D.; Tomak, A.; Toren, P.; Kaya, Y.; Tunc, I.; Zareie, H.; Tekinay, T.; Tekinay, A. B.; Guler, M. O.; Dana, A. Label-Free Nanometer-Resolution Imaging of Biological Architectures through Surface Enhanced Raman Scattering. *Scientific Reports* **2013**, *3*:*2624*, 1-7.

340. Stewart, S.; Fredericks, P. M. Surface-enhanced Raman spectroscopy of peptides and proteins adsorbed on an electrochemically prepared silver surface. *Spectrochimica Acta Part A* **1999**, *55*, 1615–1640.

341. Bakshi, K.; Liyanage, M. R.; Volkin, D. B.; Middaugh, C. R. Circular Dichroism of Peptides. *Andrew E. Nixon (ed.), Therapeutic Peptides: Methods and Protocols*, *Methods in Molecular Biology* **2014**, *1088*, 247-253.

342. Singh, N.; Conte, M. P.; Ulijn, R. V.; Miraveta, J. F.; Escuder, B. Insight into the esterase like activity demonstrated by an imidazole appended self-assembling hydrogelator. *Chem. Commun*. **2015**, *51*, 13213-13216.

343. Tidhar, Y.; Weissman, H.; Wolf, S. G.; Gulino, A.; Rybtchinsky, B. Pathway-Dependent Self-Assembly of Perylene Diimide/Peptide Conjugates in Aqueous Medium. *Chem. Eur. J.* **2011**, *17*, 6068 – 6075.

344. Liebes-Peer, Y.; Rapaport, H.; Ashkenasy, N. Amplification of Single Molecule Translocation Signal Using β-Strand Peptide Functionalized Nanopores. *ACS Nano* **2014**, *8*, 6822–6832.

345. Punzi. P.; Giordano, C.; Marino, F.; Morosetti, S.; De Santis, P.; Scipioni, A. Metal chelates anchored to poly-l-peptides and linear D,L-α-peptides with promising nanotechnological applications. *Nanotechnology* **2012**, *23*, 395703, 1-10.

346. Pashuck, E. T.; Cui, H.; Stupp, S. I. Tuning Supramolecular Rigidity of Peptide Fibers through Molecular Structure. *J. Am. Chem. Soc*. **2010**, *132*, 6041–6046.

347. Hu, Y.; Lin, R.; Zhang, P.; Fern, J.; Cheetham, A. G.; Patel, K.; Schulman, R.; Kan, C.; Cui, H. Electrostatic-Driven Lamination and Untwisting of β-Sheet Assemblies. *ACS Nano* **2016**, *10*, 880–888.

348. Bowerman, C. J.; Liyanage, W.; Federation, A. J.; Nilsson, B. L. Tuning β-Sheet Peptide Self-Assembly and Hydrogelation Behavior by Modification of Sequence Hydrophobicity and Aromaticity. *Biomacromolecules* **2011**, *12*, 2735–2745.

349. Murphy, R. M. Static and dynamic light scattering of biological macromolecules: what can we learn? *Current Opinion in Biotechnology* **1997**, *8*, 25-30.

350. Kaszuba, M.; McKnight, D.; Connah, M. T.; McNeil-Watson, F. K.; Nobbmann, U. Measuring sub nanometre sizes using dynamic light scattering. *J. Nanopart. Res.* **2008**, *10*, 823–829.

351. Luo, T.; Kiick, K. L. Noncovalent Modulation of the Inverse Temperature Transition and Self-Assembly of Elastin-b-Collagen-like Peptide Bioconjugates. *J. Am. Chem. Soc*. **2015**, *137*, 15362–15365.

352. Zhang, Q.; Li, M.; Zhu, C.; Nurumbetov, G.; Li, Z.; Wilson, P.; Kempe, K.; Haddleton, D. M. Well-Defined Protein/Peptide−Polymer Conjugates by Aqueous Cu-LRP: Synthesis and Controlled Self-Assembly. *J. Am. Chem. Soc*. **2015**, *137*, 9344–9353.

353. Xiang, X.; Ding, X.; Moser, T.; Gao, Q.; Shokuhfar, T.; Heiden, P. A. Peptide-Directed Self-Assembly of Functionalized Polymeric Nanoparticles. Part II: Effects of Nanoparticle Composition on Assembly Behavior and Multiple Drug Loading Ability[a]. *Macromol Biosci*. **2015**, *15*, 568-582.

354. Choi, I.; Park, I-S.; Ryu, J-H.; Lee, M. Control of peptide assembly through directional interactions. *Chem. Commun*. **2012**, *48*, 8481–8483.

355. Berdugo, C.; Nalluri, S. K. M. Javid, N.; Escuder, B.; Miravet, J. F.; Ulijn, R. V. Dynamic Peptide Library for the Discovery of Charge Transfer Hydrogels. *ACS Appl. Mater. Interfaces* **2015**, *7*, 25946–25954.

356. Han, T. H.; Ok, T.; Kim, J.; Shin, D. O.; Ihee, H.; Lee, H-S.; Kim, S. O. Bionanosphere Lithography via Hierarchical Peptide Self-Assembly of Aromatic Triphenylalanine. *small* **2010**, *6*, 945–951.

357. Sadownik, J. W.; Leckie, J.; Ulijn, R. V. Micelle to fibre biocatalytic supramolecular transformation of an aromatic peptide amphiphile. *Chem. Commun*. **2011**, *47*, 728–730.

358. Ivnitski, D.; Amit, M.; Rubinov, B.; Cohen-Luria, R.; Ashkenasy, N.; Ashkenasy, G. Introducing charge transfer functionality into prebiotically relevant β-sheet peptide fibrils. *Chem. Commun*. **2014**, *50*, 6733—6736.

359. Hu, K.; Xiong, W.; Sun, C.; Wang, C.; Li, J.; Yin, F.; Jiang, Y.; Zhang, M-R.; Li, Z.; Wang, X.; Li, Z. Self-Assembly of Constrained Cyclic Peptides Controlled by Ring Size. *CCS Chem*. **2020**, *2*, 42–51.

360. Guo, Z.; Wang, Y.; Zhang, X.; Gong, R.; Mu, Y.; Wan, X. Solvent-Induced Supramolecular Assembly of a Peptide-Tetrathiophene-Peptide Conjugate. *Front. Chem*. **2019**, *7*:*467*, 1-8.

361. Hu, K.; Jiang, Y.; Xiong, W.; Li, H.; Zhang, P-Y.; Yin, F.; Zhang, Q.; Geng, H.; Jiang, F.; Li, Z.; Wang, X.; Li, Z. Tuning peptide self-assembly by an in-tether chiral center. *Sci. Adv.* **2018**, *4:eaar5907*, 1-8.

362. Mumcuoglu, D.; Sardan, M.; Tekinay, T.; Guler, M. O.; Tekinay, A. B. Oligonucleotide Delivery with Cell Surface Binding and Cell Penetrating Peptide Amphiphile Nanospheres. *Mol. Pharmaceutics* **2015**, *12*, 1584−1591.

363. Mammadov, R.; Cinar, G.; Gunduz, N.; Goktas, M.; Kayhan, H.; Tohumeken, s.; Topal, A. E.; Orujalipoor, I.; Delibasi, T.; Dana, A.; Ide, S.; Tekinay, A. B.; Guler, M. O. Virus-like nanostructures for tuning immune response. *Sci Rep*. **2015**, *5*:*16728*, 1-15.

364. Thomas, F.; Burgess, N. C.; Thomson, A. R.; Woolfson, D. N. Controlling the Assembly of Coiled–Coil Peptide Nanotubes. *Angew. Chem. Int. Ed*. **2016**, *55*, 987 –991.

365. Wang, Y.; Qi, W.; Huang, R.; Yang, X.; Wang, M.; Su, R.; He, Z. Rational Design of Chiral Nanostructures from Self-Assembly of a Ferrocene-Modified Dipeptide. *J. Am. Chem. Soc.* **2015**, *137*, 7869−7880.

366. Cao, M.; Shen, Y.; Wang, Y.; Wang, X.; Li, D. Self-Assembly of Short Elastin-like Amphiphilic Peptides: Effects of Temperature, Molecular Hydrophobicity and Charge Distribution. *Molecules* **2019**, *24*, 1-11.

367. Zhu, H.; Wang, H.; Shi, B.; Shangguan, L.; Tong, W.; Yu, G.; Mao, Z.; Huang, F. Supramolecular peptide constructed by molecular Lego allowing programmable self-assembly for photodynamic therapy. *Nature Communications* **2019**, *10*:*2412*, 1-10.

368. Rissanou, A. N.; Georgilis, E.; Kasotakis, E.; Mitraki, A.; Harmandaris, V. Effect of Solvent on the Self-Assembly of Dialanine and Diphenylalanine Peptides. *J. Phys. Chem. B* **2013**, *117*, 3962−3975.

369. Lakshmanan, A.; Cheong, D. W.; Accardo, A.; Fabrizio, E. D.; Riekel, C.; Hausera, C. A. E. Aliphatic peptides show similar self-assembly to amyloid core sequences, challenging the importance of aromatic interactions in amyloidosis. *PNAS* **2013**, *110*, 519–524.

370. Fan, Z.; Chang, Y.; Cui, C.; Sun, L.; Wang, D. H.; Pan, Z.; Zhang, M. Near infrared fluorescent peptide nanoparticles for enhancing esophageal cancer therapeutic efficacy. *Nature Communications* **2018**, *9*:*2605*, 1-11.

371. Hong, H.; Akbari, A.; Wu, J. Small amphipathic peptides are responsible for the assembly of cruciferin nanoparticles. *Scientific Reports* **2017**, *7:7819*, 1-13.

372. Babar, D. G.; Sarkar, S. Self-assembled nanotubes from single fluorescent amino acid. *Appl. Nanosci.* **2017**, *7*, 101–107.

373. Datta, D.; Tiwari, O.; Ganesh, K. N. New archetypes in self-assembled Phe-Phe motif induced nanostructures from nucleoside conjugated-diphenylalanines. *Nanoscale* **2018**, *10*, 3212–3224.

374. Goldsbury, C.; Kistler, J.; Aebi, U.; Arvinte, T.; Cooper, G. J. S. Watching Amyloid Fibrils Grow by Time-lapse Atomic Force Microscopy. *J. Mol. Biol.* **1999**, *285*, 33-39.

375. Lara, C.; Reynolds, N. P.; Berryman, J. T.; Xu, A.; Zhang, A.; Mezzenga, R. ILQINS Hexapeptide, Identified in Lysozyme Left-Handed Helical Ribbons and Nanotubes, Forms Right-Handed Helical Ribbons and Crystals. *J. Am. Chem. Soc*. **2014**, *136*, 4732−4739.

376. Bao, Y-X.; Yuan, M.; Du, Q.; Li, Y-B.; Gao, J-Y.; Khan, A. J.; Zhang, F. In situ AFM investigation of dual-mode self-assembling peptide. *Nucl. Sci. Tech.* **2019**, *30:117*, 1-11.

377. Pinotsi, D.; Buell, A. K.; Galvagnion, C.; Dobson, C. M.; Schierle, G. S. K.; Kaminski, C. F. Direct Observation of Heterogeneous Amyloid Fibril Growth Kinetics via Two-Color Super-Resolution Microscopy. *Nano Lett***. 2014**, *14*, 339−345.

378. del Mercato, L. L.; Pompa, P. P.; Maruccio, G.; Torre, A. D.; Sabella, S.; Tamburro, A. M.; Cingolani, R.; Rinaldi, R. Charge transport and intrinsic fluorescence in amyloid-like fibrils. *PNAS* **2007**, *104*, 18019–18024.

379. Pinotsi, D. A Label-Free, Quantitative Assay of Amyloid Fibril Growth Based on Intrinsic Fluorescence. *ChemBioChem* **2013**, *14*, 846-850.

380. Nelson, R.; Eisenberg, D. Recent atomic models of amyloid fibril structure. *Current Opinion in Structural Biology* **2006**, *16*, 260–265.

381. Nelson, R.; Eisenberg, D. Structural Models of Amyloid-Like Fibril. *Advances In Protein Chemistry* **2006**, *73*, 235-282.

382. Nelson, R.; Sawaya, M. R.; Balbirnie, M.; Madsen, A.; Riekel, C.; Grothe, R.; Eisenberg, D. Structure of the cross-β spine of amyloid-like fibrils. *Nature* **2005**, *435*, 7773–7778.

383. Hamley, I. W.; Castelletto, V.; Moulton, C. M.; Rodrı´guez-Pe´rez, J.; Squires, A. M.; Eralp, T.; Held, G.; Hicks, M. R.; Rodger, A. Alignment of a Model Amyloid Peptide Fragment in Bulk and at a Solid Surface. *J. Phys. Chem. B* **2010**, *114*, 8244-8254.

384. Balbach, J. J; Ishii, Y.; Antzutkin, O. N.; Leapman, R. D.; Rizzo, N. W.; Dyda, F.; Reed, J.; Tycko, R. Amyloid Fibril Formation by $A\beta_{16-22}$, a Seven-Residue Fragment of the Alzheimer's β-Amyloid Peptide, and Structural Characterization by Solid State NMR. *Biochemistry* **2000**, *39*, 13748-13759.

385. Naskar, J.; Palui, G.; Banerjee, A. Tetrapeptide-Based Hydrogels: for Encapsulation and Slow Release of an Anticancer Drug at Physiological pH. *J. Phys. Chem. B* **2009**, *113*, 11787–11792.

386. George, S. J.; Ajayaghosh, A. Self-Assembled Nanotapes of Oligo(p-phenylene vinylene)s: Sol–Gel- Controlled Optical Properties in Fluorescent π-Electronic Gels. *Chem. Eur. J.* **2005**, *11*, 3217-3227.

387. Bernado. P.; Mylonas, E.; Petoukhov, M. V.; Blackledge, M.; Svergun, D. I. Structural Characterization of Flexible Proteins Using Small-Angle X-ray Scattering. *J. Am. Chem. Soc.* **2007**, *129*, 5656-5664.

388. Guilbaud, J-B.; Saiani, A. Using small angle scattering (SAS) to structurally characterise peptide and protein self-assembled materials. *Chem. Soc. Rev.* **2011**, *40*, 1200–1210.

389. Veerman, C.; Rajagopal, K.; Palla, C. S.; Pochan, D. J.; Schneider, J. P.; Furst, E. M. Gelation Kinetics of â-Hairpin Peptide Hydrogel Networks *Macromolecules* **2006**, *39*, 6608-6614.

390. Orbach, R.; Mironi-Harpaz, I.; Adler-Abramovich, L.; Mossou, E.; Mitchell, E. P.; Forsyth, V. T.; Gazit, E.; Seliktar, D. The Rheological and Structural Properties of Fmoc-Peptide-Based Hydrogels: The Effect of Aromatic Molecular Architecture on Self-Assembly and Physical Characteristics. *Langmuir* **2012**, *28*, 2015-2022.

391. Jones, B. H.; Martinez, A. M.; Wheeler, J. S.; Spoerke, E. D. Surfactant-induced assembly of enzymatically stable peptide hydrogels. *Soft Matter* **2015**, *11*, 3572-3580.

392. Owczarz, M.; Bolisetty, S.; Mezzenga, R.; Arosio, P. Sol–gel transition of charged fibrils composed of a model amphiphilic peptide. *Journal of Colloid and Interface Science* **2015**, *437*, 244–251.

393. Sathaye, S.; Mbi, A.; Sonmez, C.; Chen, Y.; Blair, D. L.; Schneider, J. P.; Pochan, D. J. Rheology of peptide- and protein-based physical hydrogels: Are everyday measurements just scratching the surface? *Wiley Interdiscip. Rev. Nanomed. Nanobiotechnol*. **2015**, *7*, 34-68.

394. Kabiri, M.; Unsworth, L. D. Application of Isothermal Titration Calorimetry for Characterizing Thermodynamic Parameters of Biomolecular Interactions: Peptide Self-Assembly and Protein Adsorption Case Studies. *Biomacromolecules* **2014**, *15*, 3463-3473.

395. Lakshminarayanan, R. *et.al.* Structure, Self-Assembly, and Dual Role of β-Defensin-like Peptide from the Chinese Soft-Shelled Turtle Eggshell Matrix. *J. Am. Chem. Soc*. **2008**, *130*, 4660-4668.

396. Willerich, I.; Grohn, F. Molecular Structure Encodes Nanoscale Assemblies: Understanding Driving Forces in Electrostatic Self-Assembly. *J. Am. Chem. Soc*. **2011**, *133*, 20341–20356.

397. Swanekamp, R. J.; DiMaio, J. T. M. Bowerman, C. J. and Bradley L. Nilsson, B. L. Coassembly of Enantiomeric Amphipathic Peptides into Amyloid-Inspired Rippled β-Sheet Fibrils. *J. Am. Chem. Soc*. **2012**, *134*, 5556-5559.

398. Biswas, M. E.; Chatzis, I.; Ioannidis, M. A.; Chen, P. Modeling of adsorption dynamics at air–liquid interfaces using statistical rate theory (SRT). *Journal of Colloid and Interface Science* **2005**, *286*, 14–27.

399. Fung, S. Y.; Yang, H.; Chen, P. Sequence Effect of Self-Assembling Peptides on the Complexation and In Vitro Delivery of the Hydrophobic Anticancer Drug Ellipticine. *PLoS ONE* **2008**, *3*, e1956.

400. Hong, Y.; Lau, L. S.; Legge, R. L.; Chen, P. Critical Self-Assembly Concentration of an Ionic-Complementary Peptide EAK16-I. *The Journal of Adhesion* **2004**, *80*, 913-931,

401. Prodi, L. Luminescent chemosensors: from molecules to nanoparticles. *New. J. Chem*. **2005**, *29*, 20-31.

402. Hulanicki, A.; Glab, S.; Ingman, F. Chemical Sensors Definitions and Classification. *Pure and Appl. Chem*. **1991**, *63*, 1247-1250.

403. National Research Council **1995**. Expanding the Vision of Sensor Materials. Washington, DC: The National Academies.

404. Tchounwou, P. B.; Ayensu, W. K.; Ninashvili, N.; Sutton, D. Environmental Exposure to Mercury and Its Toxicopathologic Implications for Public Health. *Environ Toxicol*. **2003**, *18*, 149-175.

405. Wani, A. L.; Ara, A.; Usmani, J. A. Lead toxicity: a review. *Interdiscip Toxicol*. **2015**, *8*, 55–64.

406. Kobayashi, M.; Shimizu, S. Cobalt proteins. *Eur. J. Biochem*. **1999**, *261*, 1-9.

407. Okamoto, S.; Eltis, L. D. The biological occurrence and trafficking of cobalt. *Metallomics* **2011**, *3*, 963-970.

408. Berg, J. M.; Shi, Y. The Galvanization of Biology: A Growing Appreciation for the Roles of Zinc. *Science* **1996**, *271*, 1081-1085.

409. Ohyama, T. New Aspects of Magnesium Function: A Key Regulator in Nucleosome Self-Assembly, Chromatin Folding and Phase Separation. *Int. J. Mol. Sci.* **2019**, *20*, 1-15.

410. Egirani, D. E.; Latif, M. T.; Poyi, N. R.; Wessey, N.; Acharjee, S. Genesis, Uses and Environment Implications of Iron Oxides and Ores, Iron Ores and Iron Oxide Materials, Volodymyr Shatokha, IntechOpen **2018**, 23-38.

411. Abbate, V.; Hider, R. Iron in biology. *Metallomics* **2017**, *9*, 1467-1469.

412. Wang, X.; Mandal, A. K.; Saito, H.; Pulliam, J. F.; Lee, E. Y.; Ke, Z-J.; Lu, J.; Ding, S.; Li, L.; Shelton, B. J.; Tucker, T.; Evers, B. M.; Zhang, Z.; Shi, X. Arsenic and chromium in drinking water promote tumorigenesis in a mouse colitis-associated colorectal cancer model and the potential mechanism is ROS-mediated Wnt/β-catenin signaling pathway. *Toxicology and Applied Pharmacology* **2012**, *262*, 11–21.

413. Yoshida. T.; Yamauchi, H.; Sun, G. F. Chronic health effects in people exposed to arsenic via the drinking water: dose–response relationships in review. *Toxicology and Applied Pharmacology* **2004**, *198*, 243– 252.

414. Shahab, S.; Mustafa, G.; Khan, I.; Zahid, M.; Yasinzai, M.; Ameer, N.; Asghar, N.; Ullah, I.; Nadhman, A.; Ahmed, A.; Munir, I.; Mujahid, A.; Hussain, T.; Ahmad, M. N.; Ahmad, S. S. Effects of Fluoride Ion Toxicity on Animals, Plants, and Soil Health: A Review. *Research review Fluoride* **2017**, *50*, 393–408.

415. Trnkova, L.; Adam, V.; Hubalek, J.; Babula, P.; Kizek, R. Amperometric Sensor for Detection of Chloride Ions. *Sensors* **2008**, *8*, 5619-5636.

416. Graham, J.; Traylor, J. Cyanide Toxicity. In: StatPearls. Treasure Island (FL): StatPearls Publishing; **2020**.

417. Kanduti, D.; Sterbenk, P.; Artnik, B. Fluoride: A Review of Use And Effects On Health. *Mater Sociomed*. **2016,** 28, 133-137.

418. Konieczka, P. Validation and Regulatory Issues for Sample Preparation. *Comprehensive Sampling and Sample Preparation* **2012**, *2*, 699-711.

419. Cho, E. J.; Ryu, B. J.; Lee, Y. J.; Nam, K. C. Visible Colorimetric Fluoride Ion Sensors. *Org. Lett.* **2005**, 7, 2607-2609.

420. Sokkalingam, P.; Lee, C-H. Highly Sensitive Fluorescence "Turn-On" Indicator for Fluoride Anion with Remarkable Selectivity in Organic and Aqueous Media. *J. Org. Chem*. **2011**, *76*, 3820–3828.

421. Bozdemir, O. A.; Sozmen, F.; Buyukcakir, O.; Guliyev, R.; Cakmak, Y.; Akkaya, E. U. Reaction-Based Sensing of Fluoride Ions Using Built-In Triggers for Intramolecular Charge Transfer and Photoinduced Electron Transfer. *Org. Lett*. **2010**, *12*, 1400-1403.

422. Assadollahnejad, N.; Kargar, M.; Darabi H. R.; Abouali, N.; Jamshidi, S.; sharifi, A.; Aghapoor, K.; Sayahi, H. A new ratiometric, colorimetric and ''turn-on'' fluorescent chemosensor for detection of cyanide ion based on phenol–bisthiazolopyridine hybrid. *New J. Chem*. **2019**, *43*, 13001-13009.

423. Cheng, X.; Zhou, Y.; Qin, J.; Li, Z. Reaction-Based Colorimetric Cyanide Chemosensors: Rapid Naked-Eye Detection and High Selectivity. *ACS Appl. Mater. Interfaces* **2012**, *4*, 2133−2138.

424. Jiang, Y.; Sun, L-L.; Ren, G-Z.; Niu, X.; Hu, Z-Q. A novel colorimetric and fluorescent iminocoumarin-based chemosensor for acetate ion and its application to living cell imaging. *Talanta* **2016**, *146*, 732-736.

425. Gimeno, N.; Li, X.; Durrant, J. R.; Vilar, R. Cyanide Sensing with Organic Dyes: Studies in Solution and on Nanostructured Al_2O_3 Surfaces. *Chem. Eur. J*. **2008**, *14*, 3006-3012.

426. Guha, S.; Saha, S. Fluoride Ion Sensing by an Anion-π Interaction. *J. Am. Chem. Soc*. **2010**, *132*, 17674–17677.

427. Padghan, S. D.; Puyad, A. L.; Bhosale, R. S.; Bhosale, S. V.; Bhosale, S. V. Pyrene based fluorescent turn-on chemosensor: aggregation induced emission enhancement and

application towards Fe^{3+} and Fe^{2+} recognition. *Photochem. Photobiol. Sci*. **2017**, *16*, 1591-1595.

428. Shi, B.; Su, Y.; Zhang, L-L.; Huang, M.; Liu, R.; Zhao, S. Nitrogen and Phosphorus Co-doped Carbon Nanodots as a Novel Fluorescent Probe for Highly Sensitive Detection of Fe^{3+} in Human Serum and Living Cells. *ACS Appl. Mater. Interfaces* **2016**, *8*, 10717-10725.

429. Kumar, P.; Kumar, V.; Gupta, R. Arene-based fluorescent probes for the selective detection of iron. *RSC Adv*. **2015**, *5*, 97874-97882.

430. Maji, A.; Lohar, S.; Pal, S.; Chattopadhyay, P. A new rhodamine based 'turn-on' Cu^{2+} ion selective chemosensor in aqueous system applicable in bioimaging. *J. Chem. Sci.* **2017**, *129*, 1423-1430.

431. Cheng, D.; Liu, X.; Xie, Y.; Lv, H.; Wang, Z.; Yang, H.; Han, A.; Yang, X.; Zang, L. A Ratiometric Fluorescent Sensor for Cd^{2+} Based on Internal Charge Transfer. *Sensors* **2017**, *17*, 1-10.

432. Yang, X-B.; Yang, B-X.; Ge, J-F.; Xu, Y-J.; Xu, Q-F.; Liang, J.; Lu, J-M. Benzo[a]phenoxazinium-Based Red-Emitting Chemosensor for Zinc Ions in Biological Media. *Org. Lett.* **2011**, *13*, 2710–2713.

433. Zhou, Y.; Zhu, C-Y.; Gao, X-S.; You, X-Y.; Yao, C. Hg^{2+} -Selective Ratiometric and "Off-On" Chemosensor Based on the Azadiene-Pyrene Derivative. *Org. Lett.* **2010**, *12*, 2566-2569.

434. Huang, J.; Xu, Y.; Qian, X. A Rhodamine-Based Hg^{2+} Sensor with High Selectivity and Sensitivity in Aqueous Solution: A NS_2-Containing Receptor. *J. Org. Chem*. **2009**, *74*, 2167–2170.

435. Harford, C.; Sarkar, B. Amino Terminal Cu(II)- and Ni(II)-Binding (ATCUN) Motif of Proteins and Peptides: Metal Binding, DNA Cleavage, and Other Properties. *Acc. Chem. Res*. **1997**, *30*, 123-130.

436. Wang, P.; Wu, J.; Zhou, P.; Liu, W.; Tang, Y. A novel peptide-based fluorescent chemosensor for measuring zinc ions using different excitation wavelengths and application in live cell imaging. *J. Mater. Chem. B* **2015**, *3*, 3617-3624.

437. Xu, J.; Liu, N.; Hao, C.; Han, Q.; Duan, Y.; Wu, J. A novel fluorescence "on-off-on" peptide-based chemosensor for simultaneous detection of Cu^{2+}, Ag^{+} and S^{2-}. *Sensors & Actuators: B. Chemical* **2019**, *280*, 129-137.

438. Wang, P.; Wu, J.; Su, P.; Xu, C.; Ge, Y.; Liu, D.; Liu, W.; Tang, Y. Fluorescence "on-off-on" peptide-based chemosensor for selective detection of Cu^{2+} and S^{2-} and its application in living cells bioimaging. *Dalton Trans*. **2016**, *45*, 16246-16254.

439. Pang, X.; Wang, L.; Gao, L.; Feng, H.; Kong, J.; Li, L. Multifunctional peptide-based fluorescent chemosensor for detection of Hg^{2+} , Cu^{2+} and S^{2-} ions. *Luminescence*. **2019**, 1–10.

440. Wang, P.; An, Y.; Liao, Y. A novel peptide-based fluorescent chemosensor for Cd(II) ions and its applications in bioimaging. *Spectrochimica Acta Part A: Molecular and Biomolecular Spectroscopy* **2019**, *216*, 61–68.

441. Wang, P.; Wu, J.; Liu, L.; Zhou, P.; Ge, Y.; Liu, D.; Liu, W.; Tang, Y. A peptide-based fluorescent chemosensor for measuring cadmium ions in aqueous solutions and live cells. *Dalton Trans*. **2015**, *44*, 18057–18064.

442. Neupane, L. N.; Park, J-Y.; Park, J. H.; Lee, K-H. Turn-on Fluorescent Chemosensor Based on an Amino Acid for Pb(II) and Hg(II) Ions in Aqueous Solutions and Role of Tryptophan for Sensing. *Org. Lett.* **2013**, *15*, 254–257.

443. Xia, N.; Shi, Y.; Zhang, R.; Zhao, F.; Liu, F.; Liu, L. Simple, rapid and label-free colorimetric assay for arsenic based on unmodified gold nanoparticles and a phytochelatin-like peptide. *Anal. Methods* **2012**, *4*, 3937–3941.

444. Hua, H-Y.; Chen, C-F. A new fluorescent chemosensor for anion based on an artificial cyclic tetrapeptide. *Tetrahedron Letters* **2006**, *47*, 175–179.

445. Lim, B.; Lee, J. A Peptoid-Based Fluorescent Sensor for Cyanide Detection. *Molecules* **2016**, *21*, 339.

446. Suzuki, M.; Owa, S.; Kimura, M.; Kurose, A.; Shirai, H.; Hanabusa, K. Supramolecular hydrogels and organogels based on novel L-valine and L-isoleucine amphiphiles. *Tetrahedron Letters* **2005**, *46*, 303-306.

447. Suzuki, M.; Sato, T.; Kurose, A.; Shirai, H.; Hanabusa, K. New low-molecular weight gelators based on L-valine and L-isoleucine with various terminal groups. *Tetrahedron Letters* **2005**, *46*, 2741-2745.

448. Mohmeyer, N.; Schmidt, H-W. A New Class of Low-Molecular-Weight Amphiphilic Gelators. *Chem. Eur. J.* **2005**, *11*, 863-872.

449. Suzuki, M.; Nanbu, M.; Yumoto, M.; Shiraib, H.; Hanabusa, K. Novel dumbbell-form low-molecular-weight gelators based on L-lysine: their hydrogelation and organogelation properties. *New. J. Chem.* **2005**, *29*, 1439-1444.

450. Suzuki, M.; Nigawara, T.; Yumoto, M.; Kimura, M.; Shirai, H.; Hanabusa, K. L-Lysine based gemini organogelators: their organogelation properties and thermally stable organogels. *Org. Biomol. Chem*. **2003**, *1*, 4124-4131.

451. Wang, C.; Zhang, D.; Zhu, D. A Chiral Low-Molecular-Weight Gelator Based on Binaphthalene with Two Urea Moieties: Modulation of the CD Spectrum after Gel Formation. *Langmuir* **2007**, *23*, 1478-1482.

452. Suzuki, M.; Sato, T.; Shirai, H.; Hanabusa, K. Powerful low-molecular-weight gelators based on L-valine and L-isoleucine with various terminal groups. *New J. Chem.* **2006**, *30*, 1184–1191.

453. de Jong, J. J. D.; Lucas, L. N.; Kellogg, R. M.; van Esch, J. H.; Feringa, B. L. Reversible Optical Transcription of Supramolecular Chirality into Molecular Chirality. *Science* **2004**, *304*, 278-281.

454. Xue, P.; Wu, H.; Wang, X.; He, T.; Shen, R.; Yue, F.; Wang, J.; Zhang, Y. Cation Tuning toward the Inference of the Gelation Behavior of Supramolecular Gels. *Scientific Reports* **2016**, *6:25390*, 1-6.

455. Liu, C-W.; Su, M.; Li, X-L.; Xue, T.; Liu, N.; Yin, J.; Zhu, Y-Y.; Wu, Z-Q. Multi-stimuli-responsive chiral organogels based on peptide derivatives. *Soft Matter* **2015**, *11*, 5727-5737.

456. Yan, X.; Cui, Y.; He, Q.; Wang, K.; Li, J. Organogels Based on Self-Assembly of Diphenylalanine Peptide and Their Application To Immobilize Quantum Dots. *Chem. Mater*. **2008**, *20*, 1522-1526.

457. Wang, J.; Liu, K.; Yan, L. Wang, A.; Bai, S.; Yan, X. Trace Solvent as a Predominant Factor To Tune Dipeptide Self-Assembly. *ACS Nano* **2016**, *10*, 2138–2143.

458. Terech, P.; Weiss, R. G. Low Molecular Mass Gelators of Organic Liquids and the Properties of Their Gels. *Chem. Rev*. **1997**, *97*, 3133-3159.

459. Fuhrhop, J-H. Fiuld and Solid Fibers Made of Lipid Molecular Bilayers. *Chem. Rev*. **1993**, *93*, 1585-1582.

460. Falconea, N.; Shao, T.; Xun, X.; Kraatz, H-B. Systematic Exploration of the pH-dependence of a peptide hydrogel. *Canadian Journal of Chemistry* **2019**, *97*, 430-434.

461. Motulsky, A.; Lafleur, M.; Couffin-Hoarau, A-C.; Hoarau, D.; Boury, F.; Benoit, J-P.; Leroux, J-C. Characterization and biocompatibility of organogels based on L-alanine for parenteral drug delivery implants. *Biomaterials* **2005**, *26*, 6242–6253.

462. Vintiloiu, A.; Leroux, J-C. Organogels and their use in drug delivery-A review. *Journal of Controlled Release* **2008**, *125*, 179-192.

463. Erdogan, H.; Sakalak, H.; Yavuz, M. S.; Demirel, G. Laser-Triggered Degelation Control of Gold Nanoparticle Embedded Peptide Organogels. *Langmuir* **2013**, *29*, 6975–6982.

464. Ray, S.; Das, A. K.; Banerjee, A. Smart oligopeptide gels: in situ formation and stabilization of gold and silver nanoparticles within supramolecular organogel networks. *Chem. Commun*. **2006**, 2816-2818.

465. Han, T. H.; Moon, H-S.; Hwang, J. O.; Seok, S.; Im, S. H.; Kim, S. O. Peptide-templating dye-sensitized solar cells. *Nanotechnology* **2010**, *21*, 1-6.

466. Han, T. H.; Oh, J. K.; Park, J. S.; Kwon, S-H.; Kim, S-W.; Kim, S-O. Highly entangled hollow TiO_2 nanoribbons templating diphenylalanine assembly. *J. Mater. Chem*. **2009**, *19*, 3512–3516.

467. Mohar, M.; Das, T. Phenylalanine-based low-molecular-weight gelator for the removal of metal ions and dyes from wastewater. *Soft Materials* **2019**, *17*, 328-341.

468. Debnath, S.; Shome, A.; Dutta, S.; Das, P. K. Dipeptide-Based Low-Molecular-Weight Efficient Organogelators and Their Application in Water Purification. *Chem. Eur. J*. **2008**, *14*, 6870-6881.

469. Guchhait, S.; Roy, S. Efficient peptide based gelators for aromatic organic solvents and vegetable oils: application in phase selective gelation and dye entrapment. *J. Sol-Gel Sci. Technol*. **2019**, *89*, 852-865.

470. Konda, M.; Maity, I.; Rasale, D. B.; Das, A. K. A New Class of Phase-Selective Synthetic β-Amino Acid Based Peptide Gelator: From Mechanistic Aspects to Oil Spill Recovery. *ChemPlusChem* **2014**, *79*, 1482-1488.

471. Lourenco, N. D.; Novais, J. M.; Pinheiro, H. M. Effect of some operational parameters on textile dye biodegradation in a sequential batch reactor. *Journal of Biotechnology* **2001**, *89*, 163–174.

472. Robinson, T.; McMullan, G.; Marchant, R.; Nigam, P. Remediation of dyes in textile effuent: a critical review on current treatment technologies with a proposed alternative. *Bioresource Technology* **2001**, *77*, 247-255.

473. Gemeay, A. H.; Mansour, I. K.; El-Sharkawy, R. G.; Zaki, A. B. Kinetics and mechanism of the heterogeneous catalysed oxidative degradation of indigo carmine. *Journal of Molecular Catalysis A: Chemical* **2003**, *193*, 109-120.

474. Daneshvar, N.; Ashassi-Sorkhabi, H.; Tizpar, A. Decolorization of orange II by electrocoagulation method. *Separation and Purification Technology* **2003**, *31*, 153-162.

475. Rinde, E.; Troll, W. Metabolic Reduction of Benzidine Azo Dyes to Benzidine in the Rhesus Monkey. *Journal of the National Cancer Institute* **1975**, *55*, 181-182.

476. Solpan, D.; Guven, O. Decoloration and degradation of some textile dyes by gamma irradiation. *Radiation Physics and Chemistry* **2002**, *65*, 549-558.

477. Yemashova, N.; Telegina, A.; Kotova, I.; Netrusov, A.; Kalyuzhnyi, S. Decolorization and Partial Degradation of Selected Azo Dyes by Methanogenic Sludge. *Applied Biochemistry and Biotechnology* **2004**, *119*, 31-40.

478. Hai, F. I.; Yamamoto, K.; Fukushi, K. Hybrid Treatment Systems for Dye Wastewater. *Critical Reviews in Environmental Science and Technology* **2007**, *37*, 315–377.

479. Liu, Y.; Wang, Y.; Jin, L.; Chen, T.; Yin, B. MPTTF-containing tripeptide-based organogels: receptor for 2, 4, 6-trinitrophenol and multiple stimuli-responsive properties. *Soft Matter* **2016**, *12*, 934-945.

480. Schrope, M. Deep Wounds. *Nature* **2011**, *472*, 152 -154.

481. de la Huz, R.; Lastra, M.; Lopez, J. Oil Spills. *Encyclopedia of Environmental Health* **2011**, 251-255.

482. Vibhute, A. M.; Muvvala, V.; Sureshan, K. M. A Sugar-Based Gelator for Marine Oil-Spill Recovery. *Angew. Chem. Int. Ed.* **2016**, *55*, 7782 –7785.

483. Okesola, B. O.; Smith, D. K. Applying low-molecular weight supramolecular gelators in an environmental setting -self-assembled gels as smart materials for pollutant removal. *Chem. Soc. Rev*. **2016**, *45*, 4226-4251.

484. Chen, J.; Boott, C. E.; Lewis, L.; Siu, A.; Al-Debasi, R.; Carta, V.; Fogh, A. A.; Kurek, D. Z.; Wang, L.; MacLachlan, M. J.; Hum, G. Amino Acid-Containing Phase-Selective Organogelators: A Water Based Delivery System for Oil Spill Treatment. *ACS Omega* **2020**, *5*, 18758−18765.

485. Li, J.; Huo, Y.; Zeng, H. Combinatorial identification of a highly soluble phase-selective organogelator with high gelling capacity for crude oil gelation. *J. Mater. Chem. A.* **2018**, *6*, 10196-10200.

486. Prathap, A.; Sureshan, K. M. A mannitol based phase selective supergelator offers a simple, viable and greener method to combat marine oil spills. *Chem. Commun*. **2012**, *48*, 5250–5252.

487. Sakamoto, K. Development of Gelling Agent for Spilled Oils. *Oil Spill Remediation*: *Colloid Chemistry-Based Principles and Solutions (eds P. Somasundaran, P. Patra, R.S. Farinato and K. Papadopoulos*) **2014**, 231-245.

488. Beer, P. D.; Gale, P. A.; Chen, G. Z. Mechanisms of electrochemical recognition of cations, anions and neutral guest species by redox-active receptor molecules. *Coordination Chemistry Reviews* **1999**, *185-186*, 3–36

489. Valeur, B.; Leray, I. Design principles of fluorescent molecular sensors for cation recognition. *Coordination Chemistry Reviews* **2000**, *205*, 3–40.

490. Beer, P. D.; Gale, P. A. Anion Recognition and Sensing: The State of the Art and Future Perspectives. *Angew. Chem. Int. Ed*. **2001**, *40*, 486-516.

491. Langton, M. J.; Serpell, C. J.; Beer, P. D. Anion Recognition in Water: Recent Advances from a Supramolecular and Macromolecular Perspective. *Angew. Chem. Int. Ed.* **2016**, *55*, 1974-1987.

492. Kubik, S. Anion recognition in water. *Chem. Soc. Rev*. **2010**, *39*, 3648–3663.

493. Kleerekoper, M. The Role Of Fluoride In The Prevention Of Osteoporosis. *Endocrinol. Metab. Clin. North Am*. **1998,** *27*, 441-452.

494. Zhang, S-W.; Swager, T. M. Fluorescent Detection of Chemical Warfare Agents: Functional Group Specific Ratiometric Chemosensors. *J. Am. Chem. Soc.* **2003**, *125*, 3420-3421.

495. Sohn, H.; Letant, S.; Sailor, M. J.; Trogler, W. C. Detection of Fluorophosphonate Chemical Warfare Agents by Catalytic Hydrolysis with a Porous Silicon Interferometer. *J. Am. Chem. Soc.* **2000**, *122*, 5399-5400.

496. Busschaert, N.; Caltagirone, C.; Rossom, W. V.; Gale, P. A. Applications of Supramolecular Anion Recognition. *Chem. Rev*. **2015**, *115*, 15, 8038–8155.

497. Zhou, Y.; Zhang, J. F.; Yoon, J. Fluorescence and Colorimetric Chemosensors for Fluoride-Ion Detection. *Chem. Rev.* **2014**, *114*, 5511-5571.

498. Moragues, M. E.; Martinez-Manez, R.; Sancenon, F. Chromogenic and fluorogenic chemosensors and reagents for anions. A comprehensive review of the year 2009. *Chem. Soc. Rev*. **2011**, *40*, 2593–2643.

499. de Silva, A. P.; Gunaratne, H. Q. N.; Gunnlaugsson, T.; Huxley, A. J. M.; McCoy, C. P.; Rademacher, J. T.; Rice, T. E. Signaling Recognition Events with Fluorescent Sensors and Switches. *Chem. Rev*. **1997**, *97*, 1515-1566.

500. Bregović, V. B.; Basarić, N.; Mlinarić-Majerski. K. Anion binding with urea and thiourea derivatives. *Coord. Chem. Rev*. **2015**, *295*, 80–124.

501. Cametti, M.; Rissanen, K. Recognition and sensing of fluoride anion. *Chem. Commun*. **2009**, 2809-2829.

502. Kim, W.; Sahoo, S. K.; Kim, G-D.; Choi, H-J. Novel C_{3V}-symmetric trindane based tripodal anion receptor with tris(coumarin-urea) extension for optical sensing of bioactive anions. *Tetrahedron* **2015**, *71*, 8111-8116.

503. Bregovic, V. B.; Halasz, I.; Basaric, N.; Mlinaric-Majerski, K. Anthracene adamantylbisurea receptors: switching of anion binding by photocyclization. *Tetrahedron* **2015**, *71*, 9321-9327.

504. Schiller, J.; Pérez-Ruiz, R.; Sampedro, D.; Marqués-López, E.; Herrera, R. P.; Díaz, D. D. Fluoride Anion Recognition by a Multifunctional Urea Derivative: An Experimental and Theoretical Study. *Sensors* **2016**, *16*, 658.

505. Muhammad, S.; Liu, C.; Zhao, L.; Wu, S.; Su, Z. A theoretical investigation of intermolecular interaction of a phthalimide based ‘‘on–off’’ sensor with different halide ions: tuning its efficiency and electro-optical properties. *Theor. Chem. Account* **2009**, *122*, 77–86.

506. Thongkum, D.; Tuntulani, T. Fluoride-induced intermolecular excimer formation of bispyrenyl thioureas linked by polyethylene glycol chains. *Tetrahedron* **2011**, *67*, 8102-8109.

507. Kumar, M.; Kumar, R.; Bhalla, V. F^- -Induced ‘turn-on’ fluorescent chemosensor based on 1, 3-*alt* thiacalix[4]arene. *Tetrahedron* **2009**, *65*, 4340–4344.

508. Lee, J.; Kwon, J. E.; You, Y.; Park, S. Y. Wholly π-Conjugated Low-Molecular-Weight Organogelator That Displays Triple-Channel Responses to Fluoride Ions. *Langmuir* **2014**, *30*, 2842−2851.

509. Rajamalli, P.; Prasad, E. Low Molecular Weight Fluorescent Organogel for Fluoride Ion Detection. *Org. Lett.* **2011**, *13*, 3714–3717.

510. Samai, S.; Dey, J.; Biradha, K. Amino acid based low-molecular-weight tris(bis-amido) organogelators. *Soft Matter* **2011**, *7*, 2121–2126

511. Coates, I. A.; Hirst, A. R.; Smith, D. K. Optimizing Biomimetic Gelators Constructed from Amino Acid Building Blocks. *J. Org. Chem*. **2007**, *72*, 3937-3940.

512. Basak, S.; Nanda, J.; Banerjee, A. A new aromatic amino acid based organogel for oil spill recovery. *J. Mater. Chem*. **2012**, *22*, 11658–11664.

513. Brar, S. K.; Singh, P.; Bajaj, M.; Deep, A.; Wangoo, N.; Sharma, R. K. Self assembly of a γ-amino butyric acid based derivative into tunable nano/micro structure. *Mater.Chem. Front*. **2017**, *1*, 449-454.

514. Frisch, M. J. *et.al*. Gaussian 09, Revision C.01; Gaussian, Inc.: Wallingford, CT, **2010**.

515. Tomasi, J.; Mennucci, B.; Cammi, R. Quantum Mechanical Continuum Solvation Models. *Chem. Rev.* **2005**, *105*, 2999–3094.

516. Reddy, N. S.; Rao, K. S. V. K. Polymeric Hydrogels: Recent Advances in Toxic Metal Ion Removal and Anticancer Drug Delivery Applications. *Indian Journal of Advances in Chemical Science* **2016**, *4*, 214-234.

517. Narayanaswamy, R.; Torchilin, V. P. Hydrogels and Their Applications in Targeted Drug Delivery. *Molecules* **2019**, *24*, 1-21.

518. Ahmed, E. M. Hydrogel: Preparation, characterization, and applications: A review. *Journal of Advanced Research* **2015**, *6*, 105–121.

519. Hoare, T. R.; Kohane, D. S. Hydrogels in drug delivery: Progress and challenges. *Polymer*, **2008**, *49*, 1993-2007.

520. Mondal, S.; Das, S.; Nandi, A. K. A Review on Recent Advances in Polymer and Peptide Hydrogels. *Soft Matter* **2020**, *16*, 1404-1454.

521. Li, J.; Xing, R.; Bai, S.; Yan, X. Recent advances of self-assembling peptide-based hydrogels for biomedical applications. *Soft Matter* **2019**, *15*, 1704-1715.

522. Kharkar, P. M.; Kiick, K. L.; Kloxin, A. M. Designing degradable hydrogels for orthogonal control of cell microenvironments. *Chem. Soc. Rev*. **2013**, *42*, 7335-7372.

523. Thiele, J.; Ma, Y.; Bruekers, S. M. C.; Ma, S.; Huck, W. T. S. 25th Anniversary Article: Designer Hydrogels for Cell Cultures: A Materials Selection Guide. *Adv. Mater.* **2014**, *26*, 125–148.

524. Bidarra, S. J.; Barrias, C. C.; Granja, P. L. Injectable alginate hydrogels for cell delivery in tissue engineering *Acta Biomaterialia* **2014**, *10*, 1646-1662.

525. Vashist, A.; Vashist, A.; Gupta, Y. K.; Ahmad, S. Recent advances in hydrogel based drug delivery systems for the human body. *J. Mater. Chem. B* **2014**, *2*, 147–166.

526. Sri. M, B.; Vadithya, A.; Chatterjee, A.; As A Review on Hydrogels as Drug Delivery in the Pharmaceutical Field. *International Journal of Pharmaceutical and Chemical Sciences* **2012**, *1*, 642-661.

527. Saul, J. M.; Williams, D. F. Hydrogels in Regenerative Medicine. *Handbook of Polymer Applications in Medicine and Medical Devices (Plastics Design Library)* **2011**, 279-302.

528. Hu, X-S.; Liang, R.; Sun, G. Superadsorbent hydrogel for removal of methylene blue dye from aqueous solution. *J. Mater. Chem. A* **2018**, *6*, 17612-17624.

529. Qi, X.; Wu, L.; Su, T.; Zhang, J.; Dong, W. Polysaccharide-based cationic hydrogels for dye adsorption. *Colloids and Surfaces B: Biointerfaces* **2018**, *170*, *1*, 364-372.

530. Paulino, A. T.; Guilherme, M. R.; Reis, A. V.; Campese, G. M.; Muniz, E. C.; Nozaki, J. Removal of methylene blue dye from an aqueous media using superabsorbent hydrogel supported on modified polysaccharide. *Journal of Colloid and Interface Science* **2006**, *301*, 55–62.

531. Raymond, D. M.; Nilsson, B. L. Multicomponent peptide assemblies. *Chem. Soc. Rev.* **2018**, *47*, 3659-3720.

532. Fichman, G.; Gazit, E. Self-assembly of short peptides to form hydrogels: Design of building blocks, physical properties and technological applications. *Acta Biomaterialia* **2014**, *10*, 1671-1682.

533. Aldilla, V. R.; Nizalapur, S.; Martin, A.; Marjo, C. E.; Rich, A.; Yee, E.; Suwannakot, P.; Black, D. S.; Thordarson, P.; Kumar, N. Design, synthesis, and characterisation of glyoxylamide-based short peptides as self-assembled gels. *New J. Chem*. **2017**, *41*, 13462-13471.

534. Petka, W. A.; Harden, J. L.; McCrath, K. P.; Wirtz, D.; Tirrell, D. A. Reversible Hydrogels from Self-Assembling Artificial Proteins. *Science* **1998**, *281*, 389-392.

535. O'Leary, L. E. R.; Fallas, J. A.; Bakota, E. L.; Kang, M. K.; Hartgerink, J. D. Multi-hierarchical self-assembly of a collagen mimetic peptide from triple helix to nanofibre and hydrogel. *Nature Chemistry* **2011**, *3*, 821-828.

536. Cardoso, A. Z.; Mears, L. L. E.; Cattoz, B. N.; Griffiths, P. C.; Schweins, R.; Adams, D. J. Linking micellar structures to hydrogelation for salt-triggered dipeptide gelators. *Soft Matter* **2016**, *12*, 3612-3621.

537. Aviño, F.; Matheson, A. B.; Adams, D. J.; Clegg, P. S. Stabilizing bubble and droplet interfaces using dipeptide hydrogels. *Org. Biomol. Chem*. **2017**, *15*, 6342–6348.

538. Yang, Z.; Liang, G.; Xu, B. Enzymatic Hydrogelation of Small Molecules. *Accounts of Chemical Research* **2008**, *41*, 315-326.

539. Adler-Abramovicha, L.; Gazit, E. The physical properties of supramolecular peptide assemblies: from building block association to technological applications. *Chem. Soc. Rev*. **2014**, *43*, 6881-6893.

540. Ni, R.; Chau, Y. Structural Mimics of Viruses Through Peptide/DNA Co-Assembly. *J. Am. Chem. Soc.* **2014**, *136*, 17902–17905.

541. Zou, Q.; Zhang, L.; Yan, X.; Wang, A.; Ma, G.; Li, J.; Mçhwald, H.; Mann S. Multifunctional Porous Microspheres Based on Peptide–Porphyrin Hierarchical Co-Assembly. *Angew. Chem. Int. Ed*. **2014**, *53*, 2366 –2370.

542. Inostroza-Brito, K.; Collin, E.; Siton-Mendelson, O. *et.al*. Co-assembly, spatiotemporal control and morphogenesis of a hybrid protein–peptide system. *Nat. Chem*. **2015**, *7*, 897–904.

543. Xu, X-D.; Chen, C-S.; Lu, B.; Cheng, S-X.; Zhang, X-Z.; Zhuo, R-X. Coassembly of Oppositely Charged Short Peptides into Well-Defined Supramolecular Hydrogels. *J. Phys. Chem. B* **2010**, *114*, 2365–2372.

544. Mei, L.; He, S.; Liu, Z.; Xu, K.; Zhong, W. Co-assembled supramolecular hydrogels of doxorubicin and indomethacin-derived peptide conjugates for synergistic inhibition of cancer cell growth. *Chem. Commun*. **2019**, *55*, 4411-4414.

545. Fleming, S.; Debnath, S.; Frederix, P. W. J. M.; Hunt, N. T.; Ulijn, R. V. Insights into the Coassembly of Hydrogelators and Surfactants Based on Aromatic Peptide Amphiphiles. *Biomacromolecules* **2014**, *15*, 1171-1184.

546. Makam, P.; Gazit, E. Minimalistic peptide supramolecular co-assembly: expanding the conformational space for nanotechnology. *Chem. Soc. Rev*. **2018**, *47*, 3406-3420.

547. Ryan, D. M.; Doran, T. M.; Nilsson B. L. Complementary π-π Interactions Induce Multicomponent Coassembly into Functional Fibrils. *Langmuir* **2011**, *27*, 11145–11156.

548. Hsu, S-M.; Wu, F-Y.; Lai, T-S.; Lin, Y-C. Lin, H-C. Self-assembly and hydrogelation from multicomponent coassembly of pentafluorobenzyl-phenylalanine and pentafluorobenzyl-diphenylalanine. *RSC Adv*. **2015**, *5*, 22943–22946.

549. Halperin-Sternfeld, M.; Ghosh, M.; Sevostianov, R.; Grigoriants, I.; Adler-Abramovich, L. Molecular Co-Assembly as a Strategy for Synergistic Improvement of the Mechanical Properties of Hydrogels. *Chem. Commun*. **2017**, *53*, 9586-9589.

550. Li, S.; Mehta, A. K.; Sidorov, A. N.; Orlando, T. M.; Jiang, Z.; Anthony, N. R.; Lynn. D. G. Design of Asymmetric Peptide Bilayer Membranes. *J. Am. Chem. Soc*. **2016**, *138*, 3579–3586.

551. Nagy, K. J.; Giano, M. C.; Jin, A.; Pochan, D. J.; Schneider, J. P. Enhanced Mechanical Rigidity of Hydrogels Formed From Enantiomeric Peptide Assemblies. *J. Am. Chem. Soc*. **2011**, *133*, 14975–14977.

552. Morris, K. L.; Chen, L.; Raeburn, J.; Sellick, O. R.; Cotanda, P.; Paul, A.; Griffiths, P.C.; King, S. M.; O'Reilly, R. K.; Serpell, L.C.; Adams, D. J. Chemically programmed self-sorting of gelator networks. *Nature Communications*, **2013**, *4:1480*, 1-6.

553. Raeburn, J.; Alston, B.; Kroeger, J.; McDonald, T. O.; Howse, J. R.; Cameronc, P. J.; Adams, D. J. Electrochemically-triggered spatially and temporally resolved multi-component gels. *Mater. Horiz*. **2014**, *1*, 241–246.

554. Abul-Haija, Y. M.; Scott, G. G.; Sahoo, J. K.; Tuttle, T.; Ulijn, R. V. Cooperative, ion-sensitive co-assembly of tripeptide hydrogels. *Chem. Commun*. **2017**, *53*, 9562-9565.

555. Adler-Abramovich, L.; Marco, P.; Arnon, Z. A.; Creasey, R. C. G.; Michaels, T. C. T.; Levin, A.; Scurr, D. J.; Roberts, C. J.; Knowles, T. P.J.; Tendler, S. J. B.; Gazit, E. Controlling the Physical Dimensions of Peptide Nanotubes by Supramolecular Polymer Coassembly. *ACS Nano* **2016**, *10*, 7436−7442.

556. Creasey, R. C. G.; Louzao, I.; Arnon, Z. A.; Marco, P.; Adler-Abramovich, L.; Roberts, C. J.; Gazit, E.; Tendler, S. J. B. Disruption of diphenylalanine assembly by a Boc-modified variant. *Soft Matter* **2016,** *12*, 9451-9457.

557. Maity, S.; Nir, S.; Reches, M. Co-assembly of aromatic dipeptides into spherical structures that are similar in morphology to red and white blood cells. *J. Mater. Chem. B* **2014**, *2*, 2583–2591.

558. Channon, K. J.; Devlin, G. L.; MacPhee, C. E. Efficient Energy Transfer within Self-Assembling Peptide Fibers: A Route to Light-Harvesting Nanomaterials. *J. Am. Chem. Soc.* **2009**, *131*, 12520–12521.

559. Khalily, M. A.; Bakan, G.; Kucukoz, B.; Topal, A. E.; Karatay, A.; Yaglioglu, H. G.; Dana, A.; Guler, M. O. Fabrication of Supramolecular n/p- Nanowires via Coassembly of Oppositely Charged Peptide-Chromophore Systems in Aqueous Media. *ACS Nano* **2017**, *11*, 6881–6892.

560. Huang, Z.; Guan, S.; Wang, Y.; Shi, G.; Cao, L.; Gao, Y.; Dong, Z.; Xu, J.; Luo, Q.; Liu, J. Self-assembly of amphiphilic peptides into biofunctionalized nanotubes: a novel hydrolase model. *J. Mater. Chem. B* **2013**, *1*, 2297–2304.

561. Li, Y.; Wang, L. Removing Organic Dyes by Using a Small Peptide Hydrogel. *Chem. Lett.* **2016**, *45*, 1253–1255.

562. Hussain, A.; Raveendran, V. A.; Kundu, S.; Samanta, T.; Shunmugam, R.; Pal, D.; Sarma, J. D. Mechanisms of Arsenic-Induced Toxicity with Special Emphasis on Arsenic-Binding Proteins. *Arsenic - Analytical and Toxicological Studies, Margarita Stoytcheva and Roumen Zlatev, IntechOpen* **2018**, 57-80.

563. Parker, K. J.; Kumar, S.; Pearce, D. A.; Sutherland, A. J. Design, synthesis and evaluation of a fluorescent peptidyl sensor for the selective recognition of arsenite. *Tetrahedron Letters* **2005**, *46*, 7043–7045.

564. Yang, T.; Zhang, X-X.; Yang, J-Y.; Wang, Y-T.; Chen, M-L. Screening arsenic(III)-binding peptide for colorimetric detection of arsenic(III) based on the peptide induced aggregation of gold nanoparticles. *Talanta* **2018**, *177*, 212-216.

565. Xie, H.; Qiao, Z.; Wang, H.; Duan, H.; Yang, Y.; Wang, C. Inhibition of β-amyloid peptide selfassembly and cytotoxicity by poly(LVFFco- β-amino ester). *J. Pept. Sci.* **2015**, *21*, 608-614.

566. Tjernberg, L. O.; Callaway, D. J. E.; Tjernberg, A.; Hahne, S.; Lilliehook, C.; Terenius, L.; Thyberg, J.; Nordstedt, C. A Molecular Model of Alzheimer Amyloid β-Peptide Fibril Formation. *The Journal of Biological Chemistry* **1999**, *274*, 12619–12625.

567. Li, Y.; Wang, F.; Cui, H. Peptide-based supramolecular hydrogels for delivery of biologics. *Bioengineering & Translational Medicine* **2016**, *1*, 306–322.

568. Altunbas, A.; Pochan, D. J. Peptide-Based and Polypeptide-Based Hydrogels for Drug Delivery and Tissue Engineering. *Top. Curr. Chem.* **2012**, *310*, 135–168.

569. Dimatteo, R. *et.al.* In situ Forming Injectable Hydrogels for Drug Delivery and Wound Repair. *Adv Drug Deliv Rev***. 2018**, *127*, 167–184.

570. Hu, B.; Owh, C.; Chee, P. L.; Leow, W. R.; Liu, X.; Wu, Y-L.; Guo, P.; Loh, X. J.; Chen, X. Supramolecular hydrogels for antimicrobial therapy. *Chem. Soc. Rev*. **2018**, *47*, 6917-6929.

571. Kumar, D.; Workman, V. L.; O'Brien, M.; McLaren, J.; White, L.; Ragunath, K.; Rose, F.; Saiani, A.; Gough, J. E. Peptide Hydrogels—A Tissue Engineering Strategy for the Prevention of Oesophageal Strictures. *Adv. Funct. Mater*. **2017**, *1702424*, 1-12.

572. DeForest, C. A.; Sims, E. A.; Anseth, K. S. Peptide-Functionalized Click Hydrogels with Independently Tunable Mechanics and Chemical Functionality for 3D Cell Culture. *Chem. Mater.* **2010**, *22*, 4783–4790.

573. Nandi, N.; Gayen, K.; Ghosh, S.; Bhunia, D.; Kirkham, S.; Sen, S. K.; Ghosh, S.; Hamley, I. W.; Banerjee, A. Amphiphilic Peptide-based Supramolecular, Non-Cytotoxic Stimuli-responsive Hydrogels with Antibacterial Activity. *Biomacromolecules* **2017**, *18*, 3621–3629.

574. Adak, A.; Ghosh, S.; Gupta, V.; Ghosh, S. Biocompatible Lipopeptide-Based Antibacterial Hydrogel. *Biomacromolecules* **2019**, *20*, 1889−1898.

575. Carrejo, N. C.; Moore, A. N.; Silva, T. L. L; Leach, D. G.; Li, I-C.; Walker, D. R.; Hartgerink, J. D. Multidomain Peptide Hydrogel Accelerates Healing of Full-Thickness Wounds in Diabetic Mice. *ACS Biomater. Sci. Eng*. **2018**, *4*, 1386–1396.

576. Sheikholeslam, M.; Wheeler, S. D.; Duke, K. G.; Marsden, M.; Pritzker, M.; Chen, P. Peptide and peptide-carbon nanotube hydrogels as scaffolds for tissue & 3D tumor engineering. *Acta Biomaterialia* **2018**, *69*, 107–119.

577. Du, X.; Zhou, J.; Shi, J.; Xu, B. Supramolecular Hydrogelators and Hydrogels: From Soft Matter to Molecular Biomaterials. *Chem. Rev.* **2015**, *115*, 13165–13307.

578. Rosen, H.; Abribat, T. The rise and rise of drug delivery. *Nat. Rev. Drug Discov*. **2005**, *4*, 381-385.

579. Wang, R.; Zhu, G.; Mei, L.; Xie, Y.; Ma, H.; Ye, M.; Qing, F-L. W. Tan, W. Automated Modular Synthesis of Aptamer−Drug Conjugates for Targeted Drug Delivery. *J. Am. Chem. Soc*. **2014**, *136*, 2731–2734.

580. Tan, W.; Wang, H.; Chen, Y.; Zhang, X.; Zhu, H.; Yang, C.; Yang, R.; Liu, C. Molecular aptamers for drug delivery. *Trends Biotechnol*. **2011**, *29*, 634–640.

581. Sun, H.; Zhu, X.; Lu, P.Y.; Rosato, R. R.; Tan, W.; Zu, Y. Oligonucleotide Aptamers: New Tools for Targeted Cancer Therapy. *Molecular Therapy-Nucleic Acids* **2014**, *3*, e182.

582. Tesauro, D.; Accardo, A.; Diaferia, C.; Milano, V.; Guillon, J.; Ronga, L.; Rossi, F. Peptide-Based Drug-Delivery Systems in Biotechnological Applications: Recent Advances and Perspectives. *Molecules* **2019**, *24*, 1-27.

583. Chen, C.; Zhang, Y.; Hou, Z.; Cui, X.; Zhao, Y.; Xu, H. Rational Design of Short Peptide-Based Hydrogels with MMP-2 Responsiveness for Controlled Anticancer Peptide Delivery. *Biomacromolecules*, **2017**, *18*, 3563-3571.

584. Jiang, T.; Wang, T.; Li, T.; Ma, Y.; Shen, S.; He, B.; Mo, R. Enhanced Transdermal Drug Delivery by Transfersome-Embedded Oligopeptide Hydrogel for Topical Chemotherapy of Melanoma. *ACS Nano* **2018**, *12*, 9693-9701.

585. Kurrikoff, K.; Langel, U. Recent CPP-based applications in medicine. *Expert Opinion on Drug Delivery* **2019**, *16*, 1183-1191.

586. Kratz, F.; Müller, I. A.; Ryppa, C.; Warnecke, A. Prodrug Strategies in Anticancer Chemotherapy. *ChemMedChem*. **2008**, *3*, 20–53.

587. Wang, Y.; Cheetham, A. G.; Angacian, G.; Su, H.; Xie, L.; Cui, H. Peptide–Drug Conjugates as Effective Prodrug Strategies for Targeted Delivery. *Adv. Drug. Deliv. Rev.* **2017**, *110-111*, 112–126.

588. Larson, N.; Ghandehari, H. Polymeric conjugates for drug delivery. *Chem. Mater*. **2012**, *24*, 840–853.

589. Navath, R. S.; Kurtoglu, Y. E.; Wang, B.; Kannan, S.; Romero, R.; Kannan, R. M. Dendrimers-drug conjugates for tailored intracellular drug release based on glutathione levels. *Bioconjugate Chem*. **2008**, *19*, 2446–2455.

590. Agasti, S. S.; Chompoosor, A.; You, C-C.; Ghosh, P.; Kim, C. K.; Rotello, V. M. Photoregulated Release of Caged Anticancer Drugs from Gold Nanoparticles. *J. Am. Chem. Soc*. **2009**, *131*, 5728–5729.

591. Lin, W.; Ma, G.; Yuan, Z.; Qian, H.; Xu, L.; Sidransky, E.; Chen, S. Development of Zwitterionic Polypeptide Nanoformulation with High Doxorubicin Loading Content for Targeted Drug Delivery. *Langmuir* **2019**, *35*, 1273-1283.

592. Moyer, T. J.; Chen, F.; Toft, D. J.; Ruff, Y.; Cryns, V. L.; Stupp, S. I. Self-Assembled Peptide Nanostructures Targeting Death Receptor 5 and Encapsulating Paclitaxel As a Multifunctional Cancer Therapy. *ACS Biomaterials Science & Engineering* **2019**, *5*, 6046-6053.

593. Pagels, R. F.; Prud'homme, R. K. Polymeric nanoparticles and microparticles for the delivery of peptides, biologics, and soluble therapeutics. *Journal of Controlled Release* **2015**, *219*, 519–535.

594. Carter, P. J. Introduction to current and future protein therapeutics: A protein engineering perspective. *Exp. Cell. Res*. **2011**, *317*, 1261–1269.

595. Frokjaer, S.; Otzen, D. E. Protein drug stability: a formulation challenge. *Nat. Rev. Drug. Discov*. **2005**, *4*, 298–306.

596. Koutsopoulos, S.; Zhang, S. Two-layered injectable self-assembling peptide scaffold hydrogels for long-term sustained release of human antibodies. *Journal of Controlled Release* **2012**, *160*, 451–458.

597. Davis, M.E.; Hsieh, P.C.H.; Takahashi, T.; Song, Q.; Zhang, S.; Kamm, R.D.; Grodzinsky, A.J.; Anversa, P.; Lee, R.T. Local myocardial insulin-like growth factor 1 (IGF-1) delivery with biotinylated peptide nanofibers improves cell therapy for myocardial infarction. *Proc. Nat.l Acad. Sci. USA*. **2006**, *103*, 8155–8160.

598. Gelain, F.; Unsworth, L. D.; Zhang, S. Slow and sustained release of active cytokines from self-assembling peptide scaffolds. *Journal of Controlled Release* **2010**, *145*, 231–239.

599. Nagy-Smith, K.; Yamada, Y.; Schneider, J. P. Protein release from highly charged peptide hydrogel networks. *J. Mater. Chem. B* **2016**, *4*, 1999–2007.

600. Lv, L.; Liu, H.; Chen, X.; Yang, Z. Glutathione-triggered formation of molecular hydrogels for 3D cell culture. *Colloids and Surf B: Biointerfaces* **2013**, *108*, 352–357.

601. Wang, H.; Wang, Y.; Zhang, X.; Yawen, H.; Xiaoyong, Y.; Linsha, M.; Zhou, H.; Long, J.; Liu, Q.; Yang, Z. Supramolecular nanofibers of self-assembling peptides and proteins for protein delivery. *Chem. Commun*. **2015**, *51*, 14239–14242.

602. Longley, D. B.; Harkin, D. P.; Johnston, P.G. 5-Fluorouracil: Mechanisms of Action and Clinical Strategies. *Nat. Rev. Cancer*. **2003**, *3*, 330–338.

603. Arias, J. L. Novel Strategies to Improve the Anticancer Action of 5-Fluorouracil by Using Drug Delivery Systems. *Molecules* **2008**, *13*, 2340–2369.

604. Diasio, R. B.; Harris, B. E. Clinical Pharmacology of 5-Fluorouracil. *Clin. Pharmacokinet*. **1989**, *16*, 215–237.

605. Price, C. I.; Horton, J. W.; Baxter, C. R. Topical liposomal delivery of antibiotics in soft tissue infection. *J. Surg. Res*. **1990**, *49*, 174–178.

606. Sahoo, J. K.; VandenBerg, M. A.; Bello, E. E. R.; Nazareth, C. D.; Webber, M. J. Electrostatic-driven self-sorting and nanostructure speciation in self-assembling tetrapeptides. *Nanoscale* **2019**, *11*, 16534-16543.

607. Liang, J. X.; Nguyen, Q. L.; Matsika, S. Exciplexes and conical intersections lead to fluorescence quenching in π-stacked dimers of 2-aminopurine with natural purine nucleobases. *Photochem. Photobiol. Sci*. **2013**, *12*, 1387-1400.

608. Ghosh, S.; Singh, S. K.; Verma, S. Self-assembly and potassium ion triggered disruption of peptide-based soft structures. *Chem. Commun*. **2007**, 2296–2298.

609. Ghosh, S.; Reches, M.; Gazit, E.; Verma, S. Bioinspired Design of Nanocages by Self-Assembling Triskelion Peptide Elements. *Angew. Chem. Int. Ed*. **2007**, *46*, 2002 – 2004.

610. Oniolo, C.; Alumbo, M. Solid-state Infrared Absorption Spectra and Chain Arrangement in Some Synthetic Homooligopeptides in the Intermolecularly Hydrogen-Bonded Pleated-Sheet β-Conformation. *Biopolymers* **1977**, *16*, 219-224.

611. Moretto, V.; Crisma, M.; Bonora, G. M.; Toniolo, C. Comparison of the Effect of Five Guest Residues on the β-Sheet Conformation of Host $(L\text{-Val})_n$ Oligopeptides. *Macromolecules* **1989**, *22*, 2939-2944.

612. Blondelle, S. E.; Forood, B.; Houghten, R. A.; Peraz-Paya, E. Polyalanine-Based Peptides as Models for Self-Associated β-Pleated-Sheet Complexes. *Biochemistry* **1997**, *36*, 8393–8400.

613. Dado, G. P.; Gellman, S. H. Intramolecular Hydrogen Bonding in Derivatives of β-Alanine and γ-Amino Butyric Acid; Model Studies for the Folding of Unnatural Polypeptide Backbones. *J. Am. Chem. Soc*.**1994**, *116*, 1054–1062.

614. Greenfield, N. J. Using circular dichroism spectra to estimate protein secondary structure. *Nat. Protoc*. **2006**, *1*, 2876–2890.

615. Toniolo, C.; Bonora, G. M. Linear Oligopeptides. XXVII. Contribution to the Circular Dichroism of Internal Peptide Chromophores. *Can. J. Chem*. **1976**, *54*, 70-76.

616. Toniolo, C.; Bonora, G. M.; Freer, R. J.; Kennedy, S. P.; Pittenger, K. L.; Becker, E. L. Synthetic Formyl-Methionyl Chemoattractants: A Conformation Activity Study of Oxidized Tripeptides. *Peptides* **1989**, *9*, 1195-1205.

617. Goodman, M.; Naider F.; Toniolo, C. Circular Dichroism Studies of Isoleucine Oligopeptides in Solution. *Biopolymers* **1971**, *10*, 1719-1730.

618. Cochran, A. G.; Skelton, N. J.; Starovasnik, M. A. Tryptophan Zippers: Stable, Monomeric β –Hairpins. *Proc. Natl. Acad. Sci*. **2001**, *98*, 5578-5583.

Appendix A

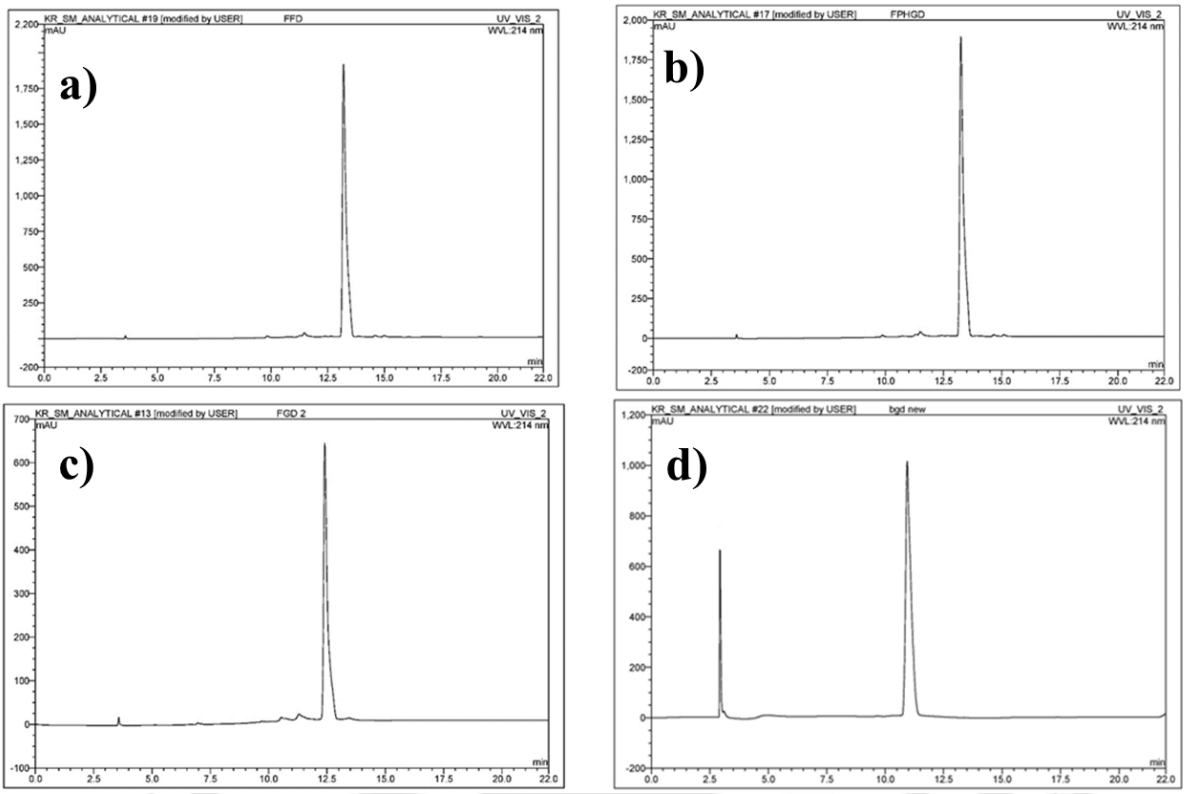

Figure A1: Analytical traces of a) M1, b) M2, c) M3 and d) M4 respectively.

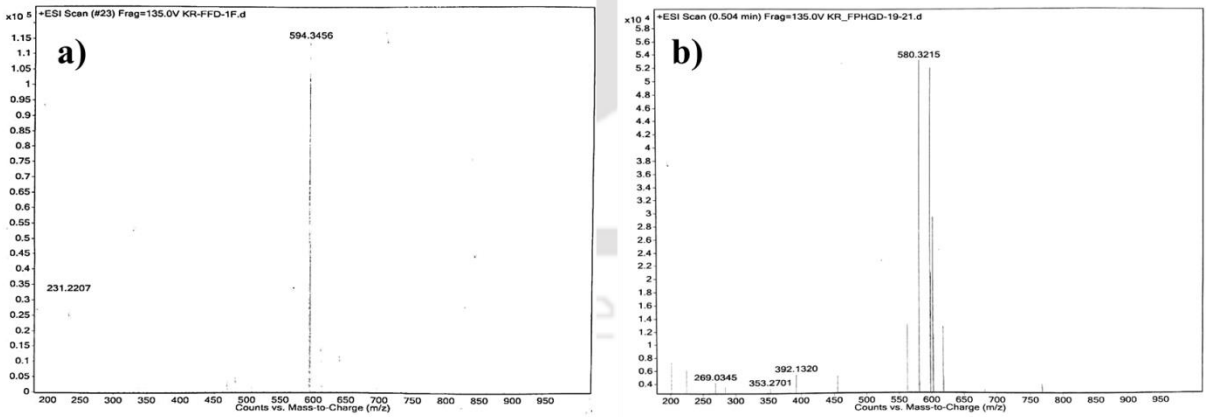

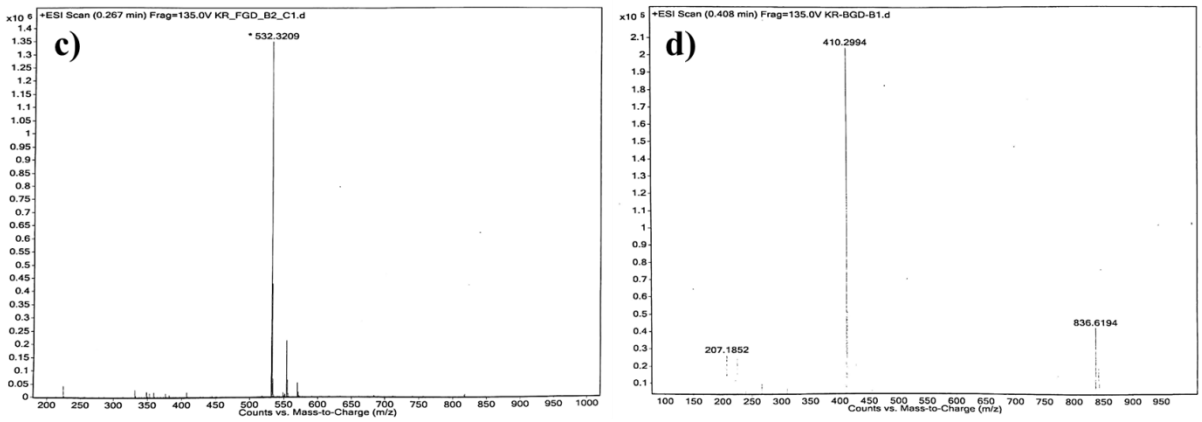

Figure A2: ESI-MS of M1-M4. a) Mass calc. for M1: $(M+H)^+$ =594.3287 Da; Mass Obs.: $(M+H)^+$=532. 3456 Da. b) Mass calc. for M2: $(M+H)^+$ =580.3131 Da; Mass obs.: $(M+H)^+$=580.3215 Da. c) Mass calc. for M3: $(M+H)^+$=532.3131 Da;Mass obs.: $(M+H)^+$=532. 3209 Da. d) Mass calc. for M4: $(M+H)^+$=410.2974 Da; Mass obs.:$(M+H)^+$=410.2994 Da.

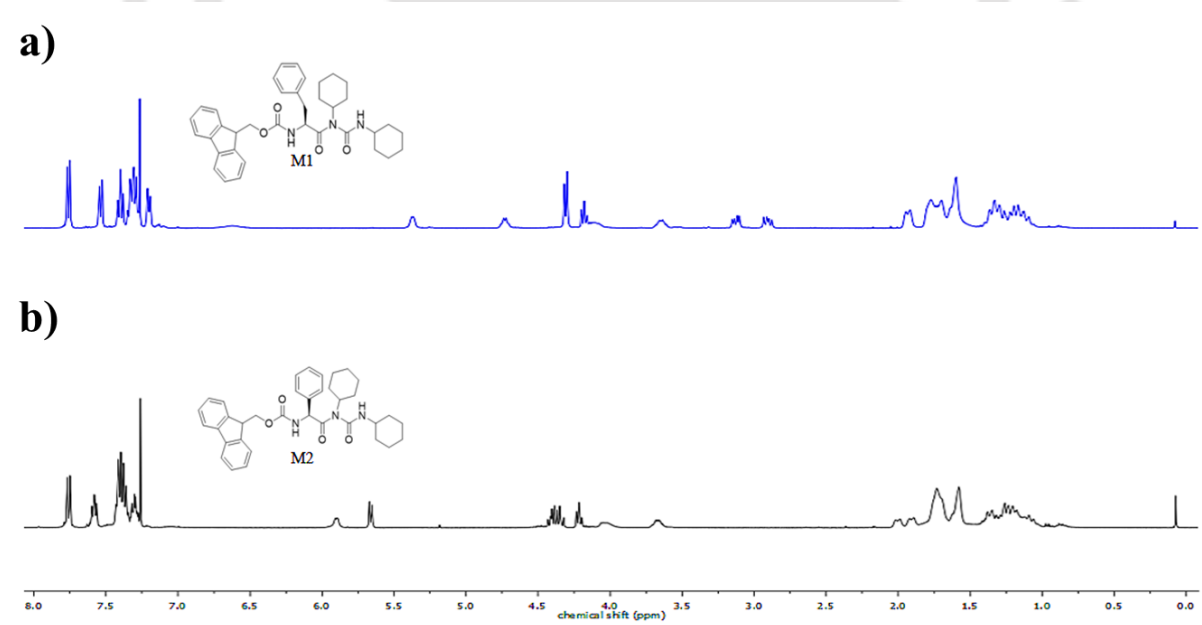

Figure A3: 400 MHz ^{1}H NMR spectra of a) M1 (5 mM) and b) M2 (5mM) in $CDCl_3$at 300K.

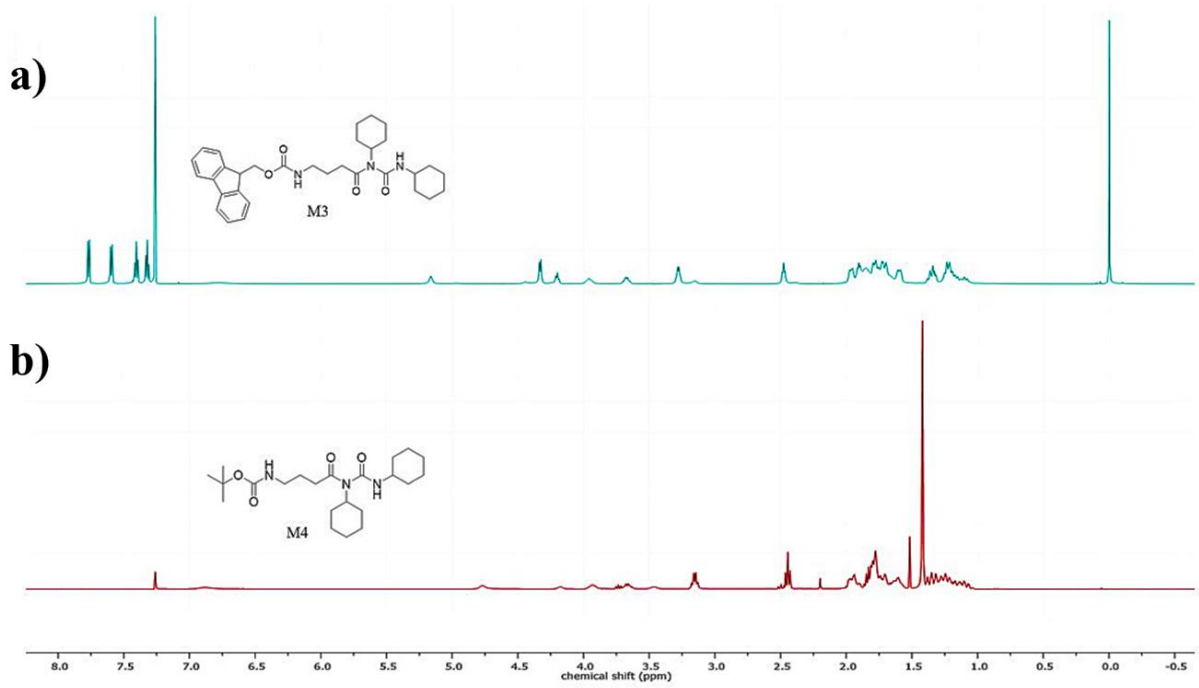

Figure A4: 400 MHz ^{1}H NMR spectra of a) M3 (5 mM) and b) M4 (5mM) in $CDCl_3$ at 300K.

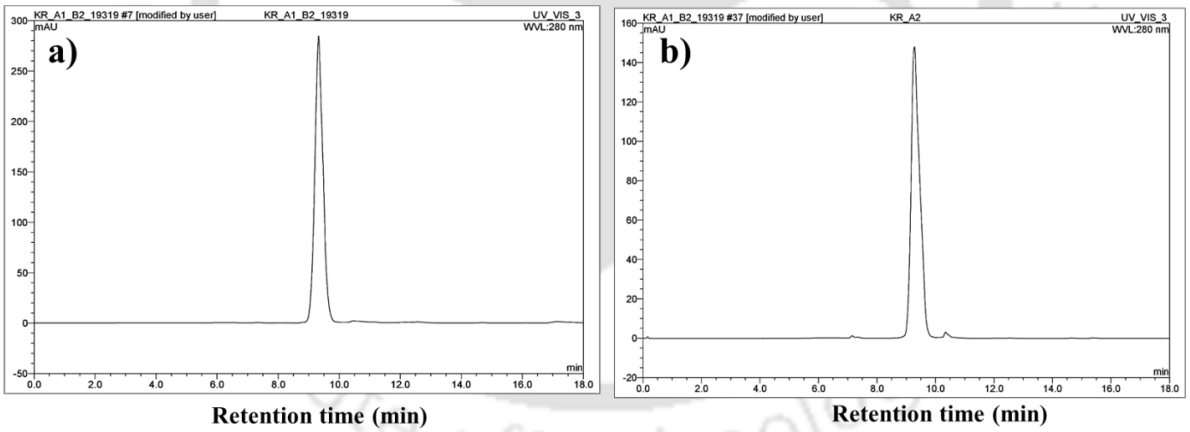

Figure A5: Analytical HPLC traces for (a) A1 and (b) A2

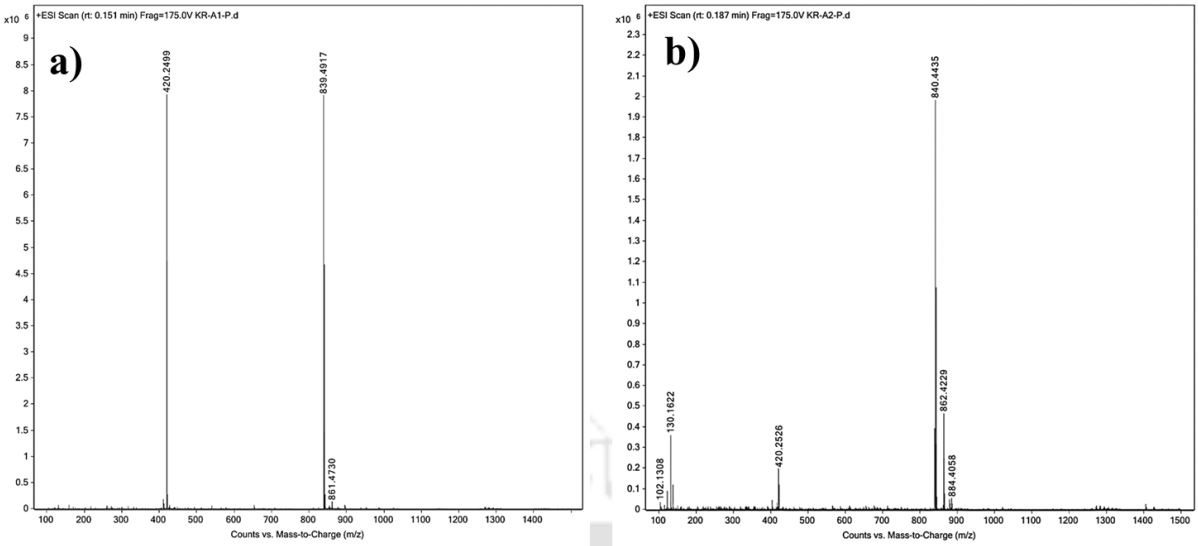

Figure A6: ESI-MS of a) A1 and b) A2.

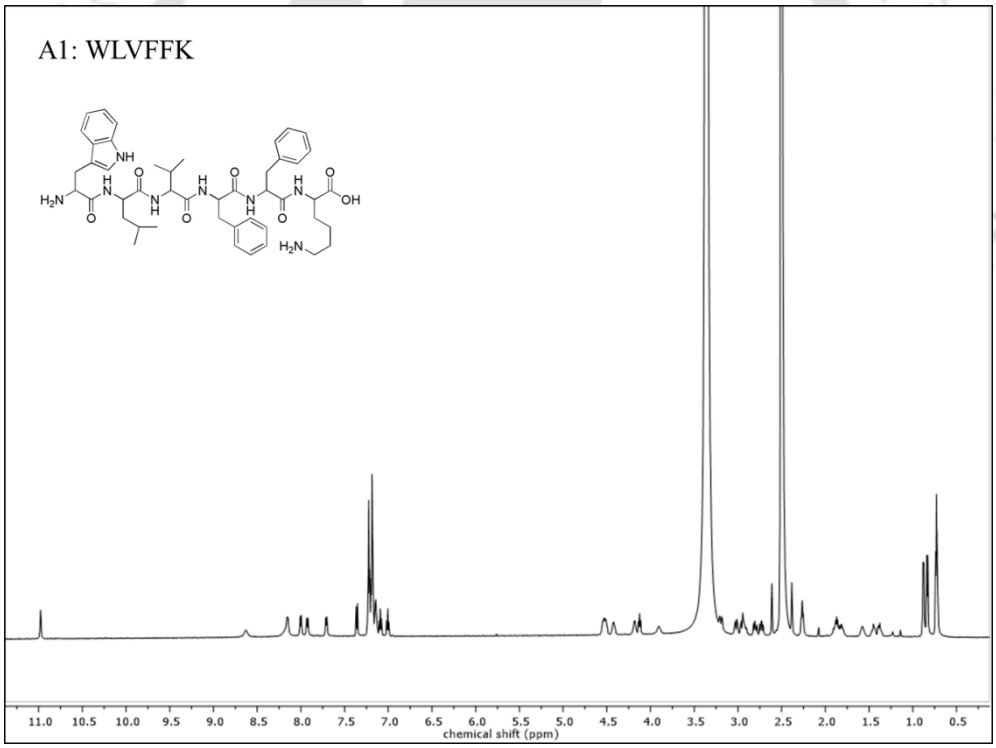

Figure A7: ^{1}H NMR (600 MHz) of A1 at in DMSO-d6 at 300K

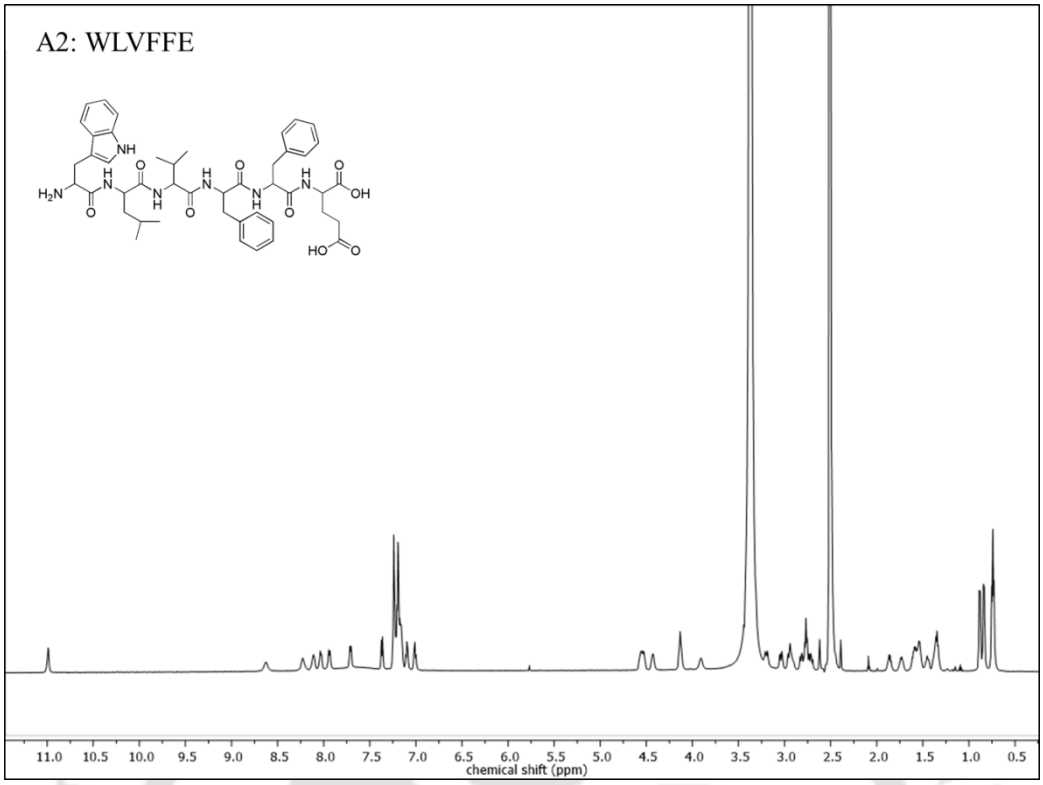

Figure A8: ^{1}H NMR (600 MHz) of A2 at in DMSO-d6 at 300K

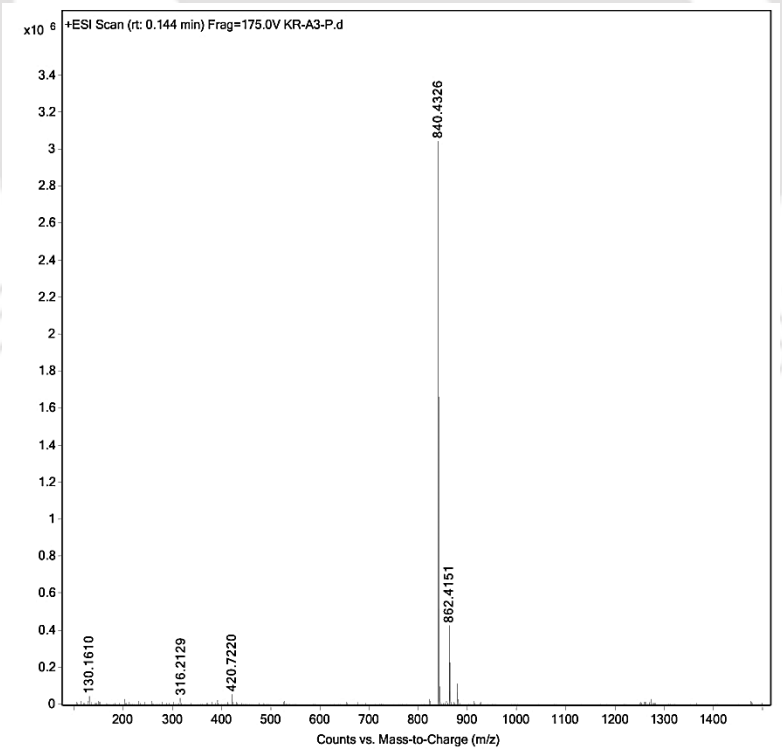

Figure A9: ESI-MS of A3

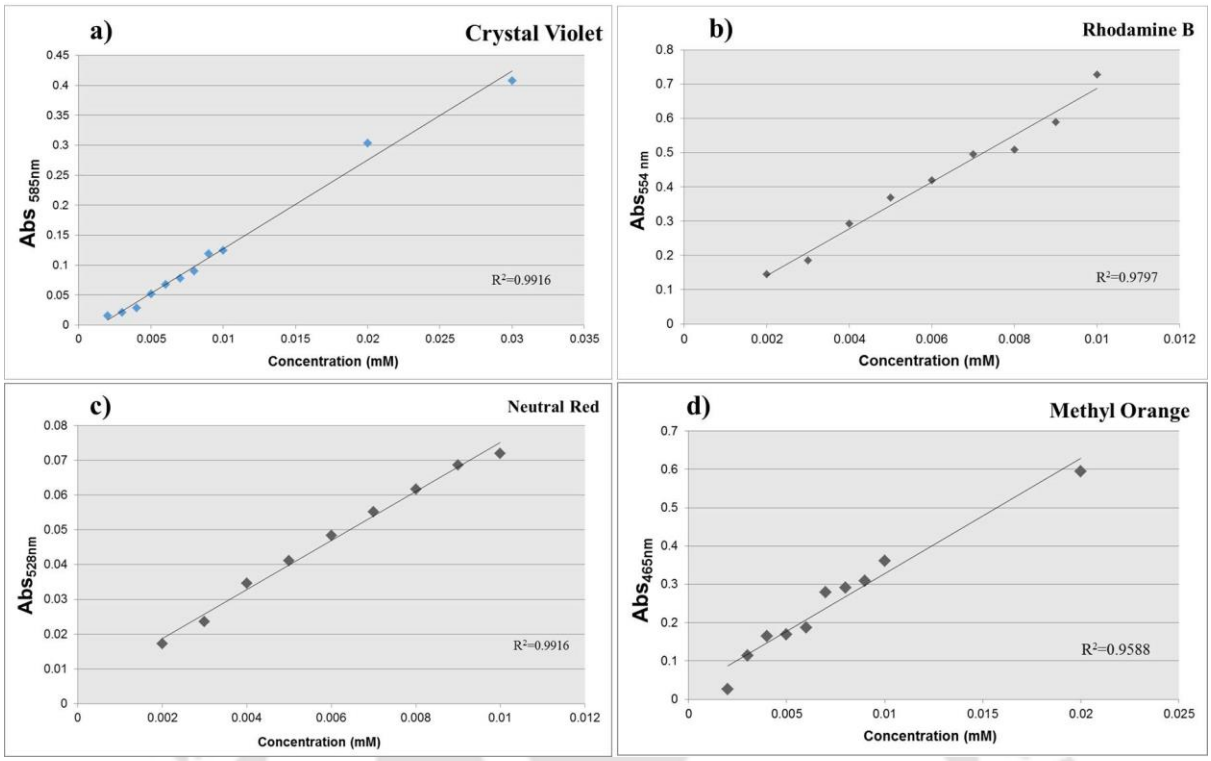

Figure A10: Calibration plots for a) CV, b) RB c) NR and d) MO.

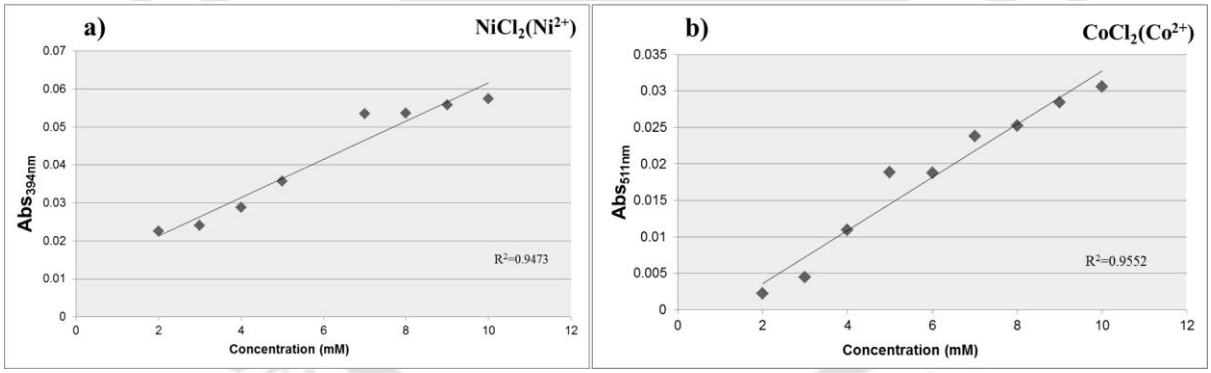

Figure A11: Calibration plots for a) Ni^{2+} and Co^{2+}

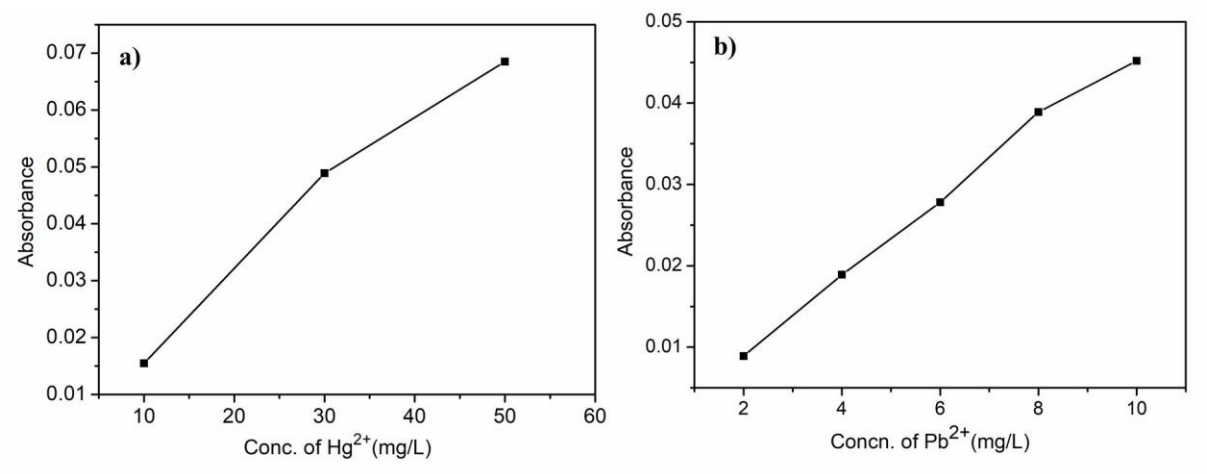

Figure A12: Calibration plots for a) Hg^{2+} and Pb^{2+} obtained from AAS experiment

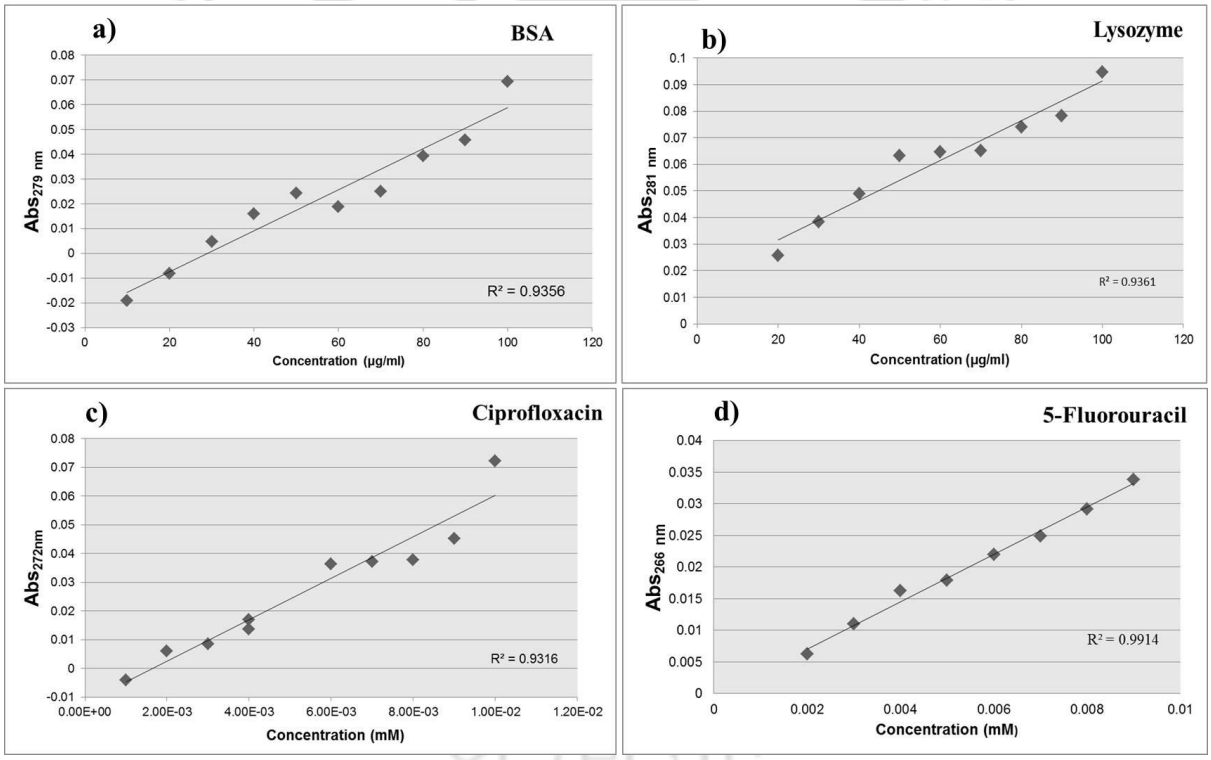

Figure A13: Calibration plots for a) BSA, b) lysozyme c) ciprofloxacin and d) 5-fluorouracil.

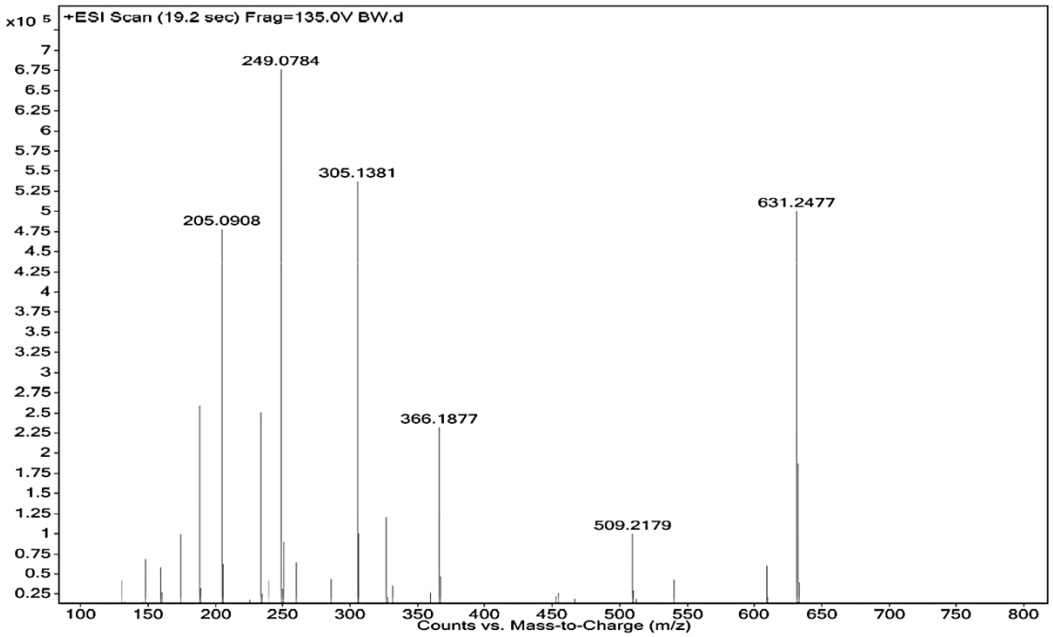

Figure A14: ESI-MS of Boc-W-OH

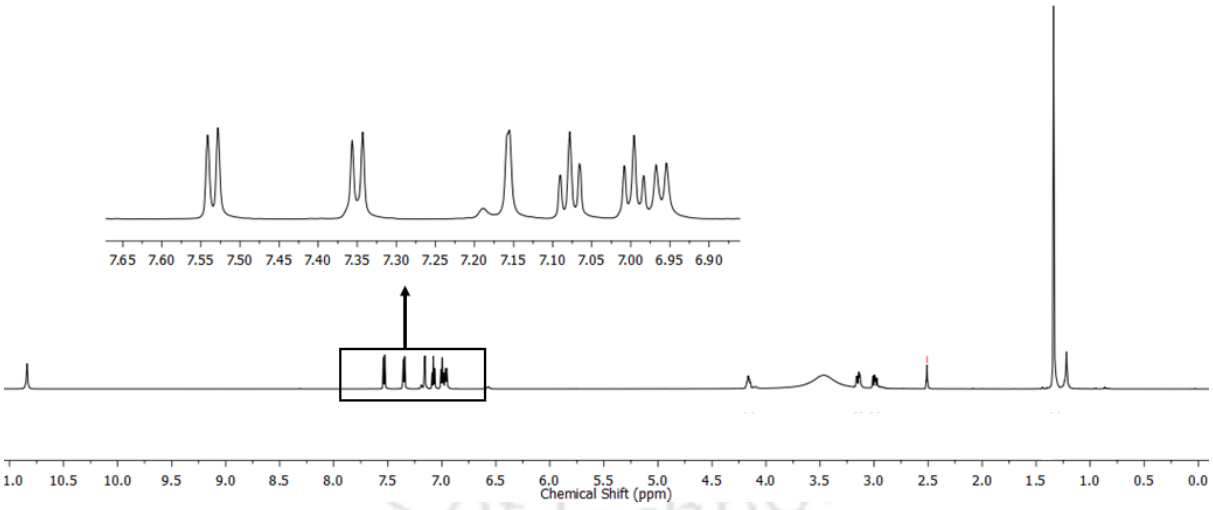

Figure A15: ^{1}H NMR (600 MHz) spectrum of Boc-W-OH in DMSO-d_6 at 300K.

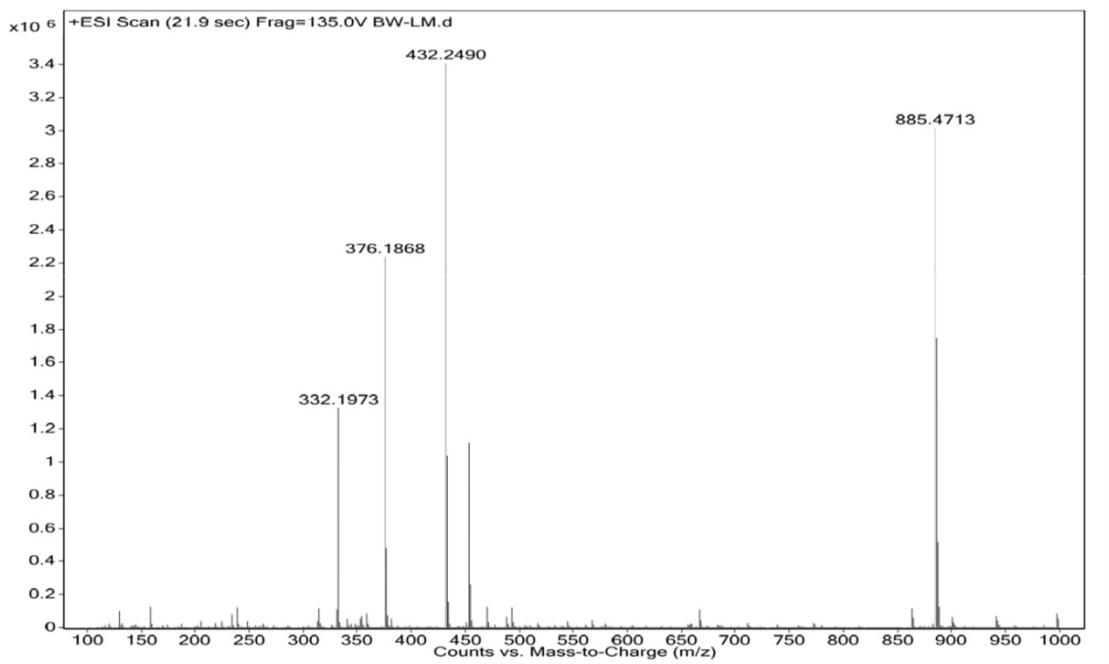

Figure A16: ESI-MS of Boc-WL-OMe

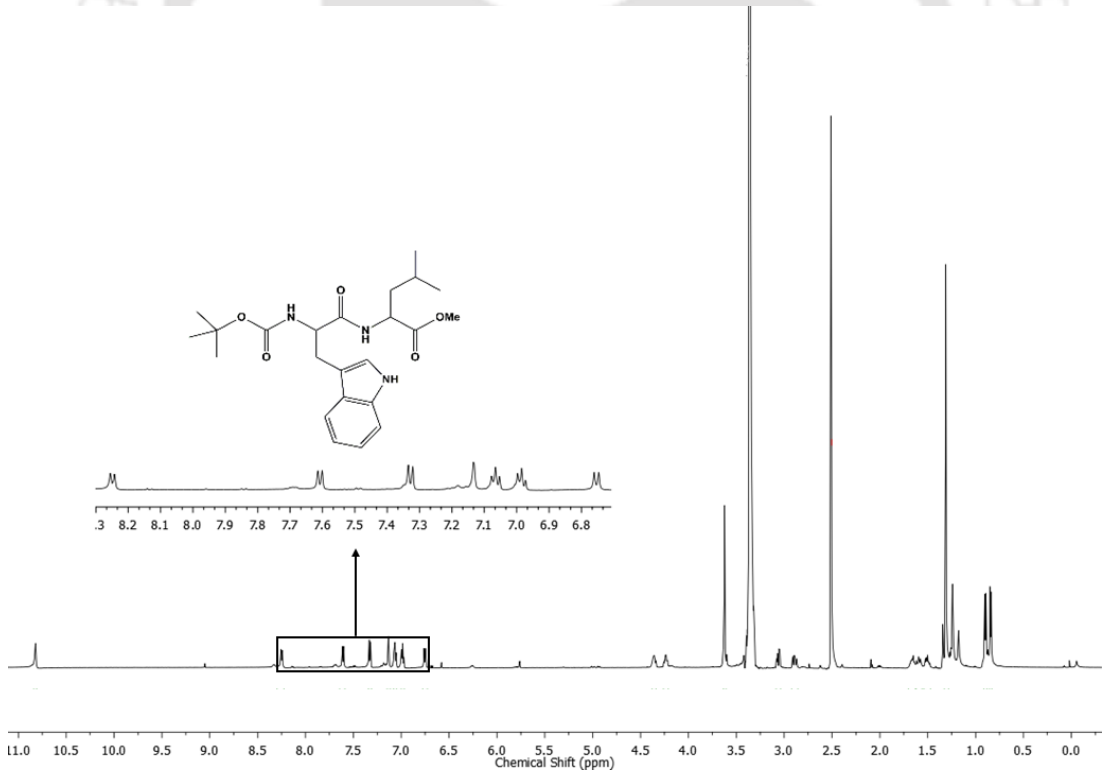

Figure A17: ^{1}H NMR (600 MHz) spectrum of Boc-WL-OMe in DMSO-d_6 at 300K.

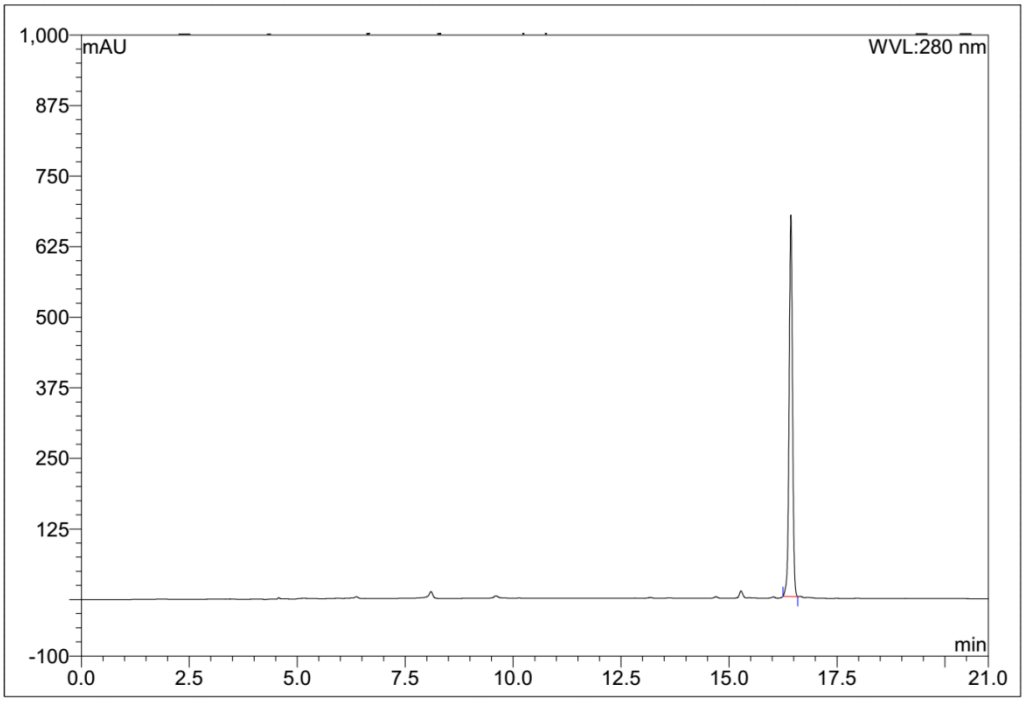

Figure A18: Analytical HPLC profile of P.

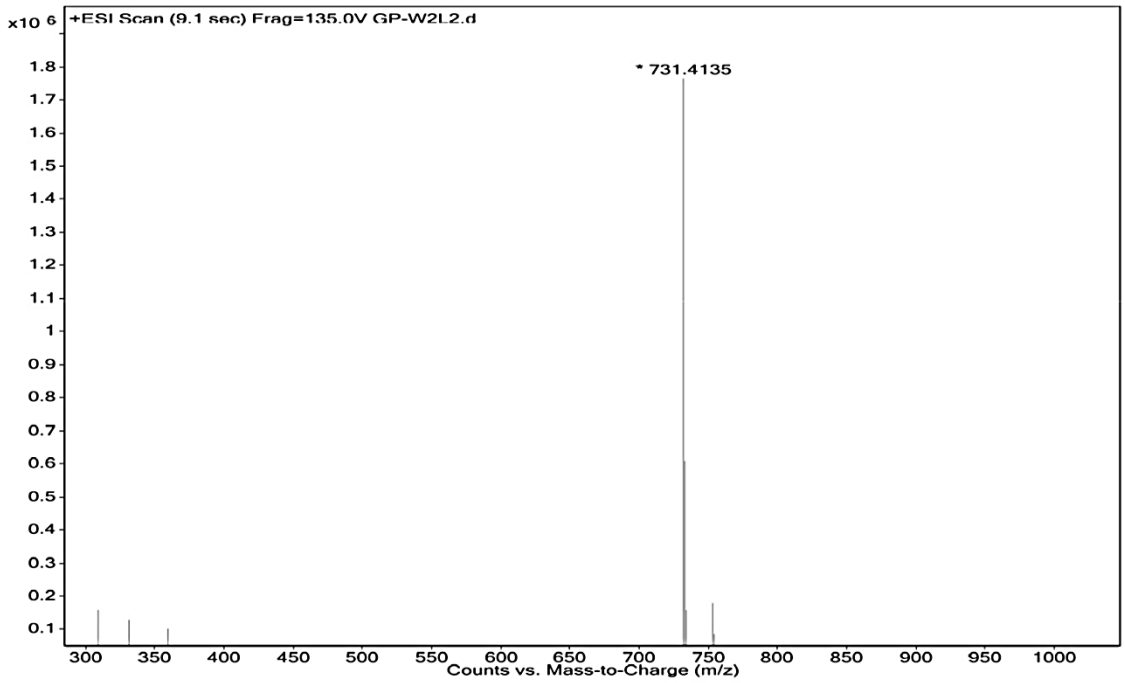

Figure A19: ESI-MS of Boc-WLWL-OMe (P)

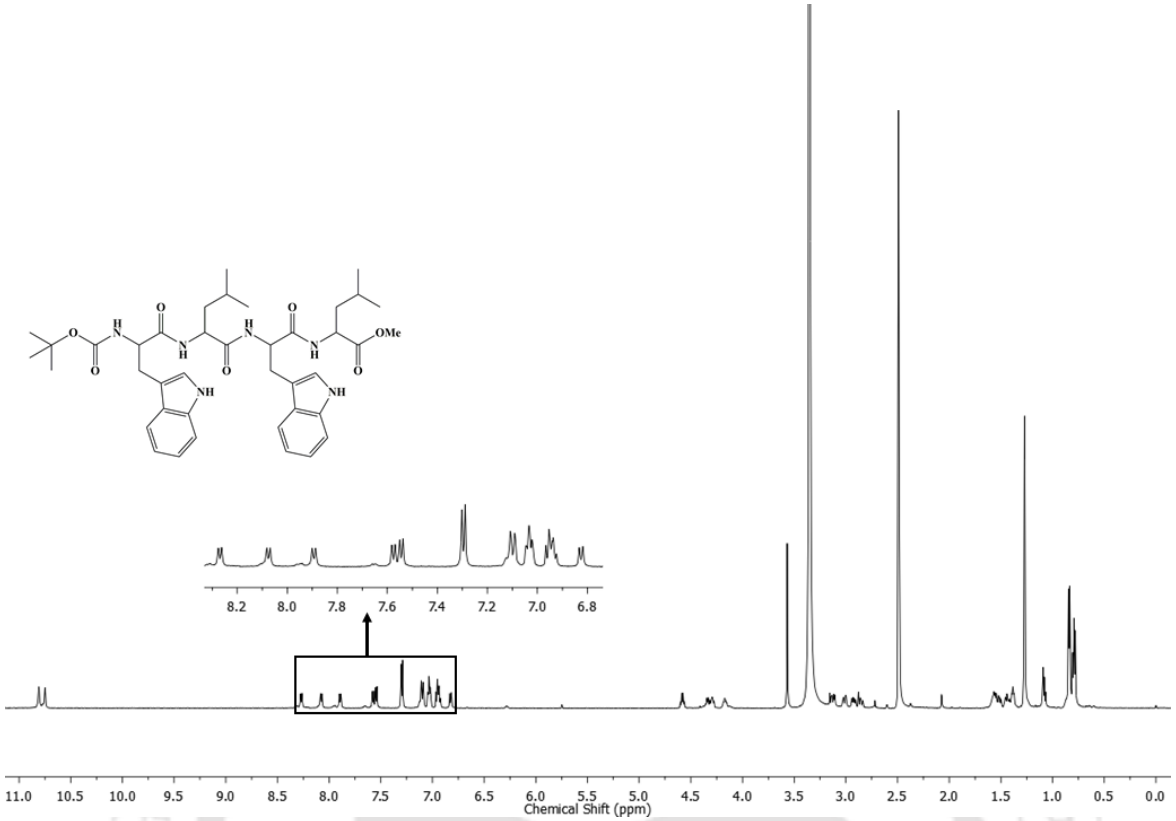

Figure A20: 1H NMR (600 MHz) spectrum of Boc-WLWL-OMe (P) in DMSO-d_6 at 300K.

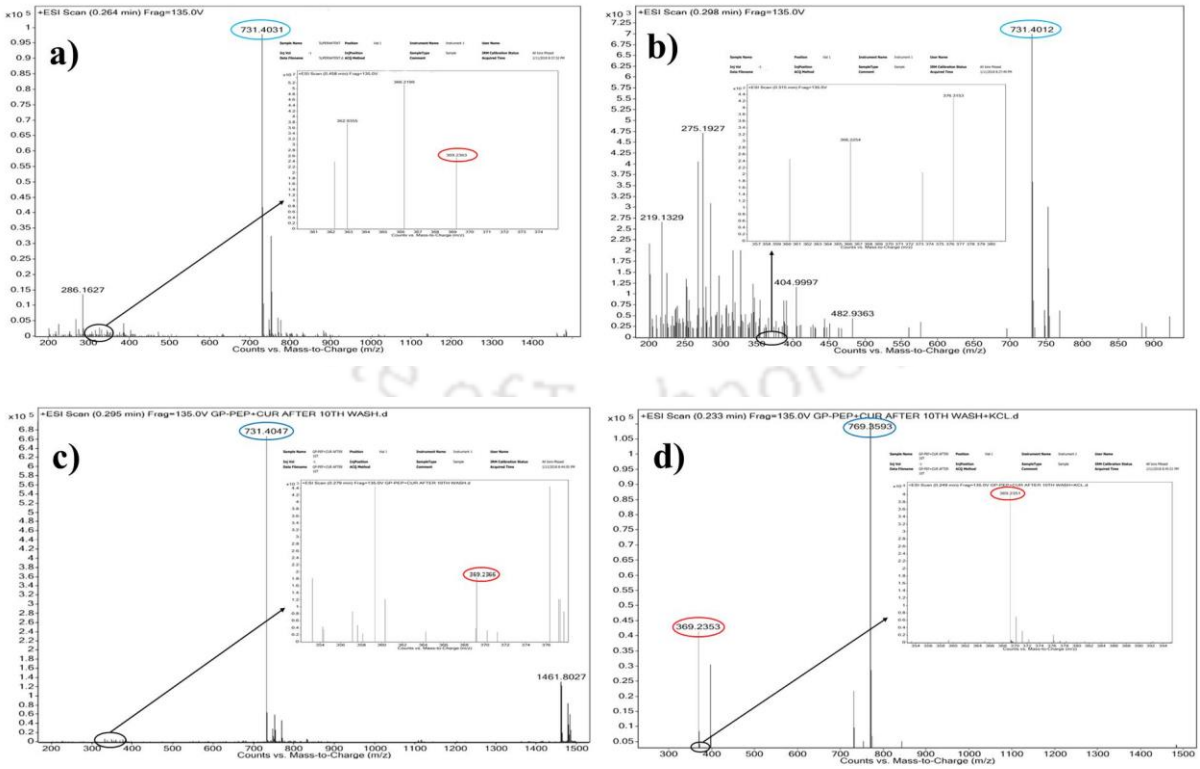

Figure A21: ESI-MS spectrum (a) of the supernatant after centrifuging the microspheres, when peptide was added to curcumin solution, (b) of the wash, (c) of the resuspension of lyophilized microphores in EtOH and (d) post addition of KCl to microspheres.

Appendix B

B1. Materials Purchased:

All amino acids used in solution phase synthesis, Dicyclohexylurea and all other organic solvents used in gelation, DMAP, DIC, DMF, DCM Piperidine, DIPEA, acetic anhydride, pyridine, TFA, tetrabutyl ammonium salts, metal salts were purchased from Spectrochem. All Fmoc protected amino acids, HOBt, PyBOP, Fmoc-OSu were purchased from G.L. Biochem.Ltd., sodium meta arsenite was purchased from Novabiochem, Arsenic solution was purchased from Sigma Aldrich.

B2. Instruments Used for Various Studies:

1. **NMR:** 400, 600 MHz Bruker NMR spectrometer
2. **FT-IR:** Spectrum Two Perkin Elmer FT-IR spectrometer
3. **FESEM:** FESEM Sigma 300 microscope, FESEM Sigma Zeiss Gemini microscope
4. **FETEM:** JEOL JEM (Model 2100F) at an operating voltage of 200 KV
5. **AFM** Agilent (5500 series).
6. **PXRD:** Bruker D2 Phaser X Ray diffractometer (Cu-Kα radiation, $\lambda = 1.5406$ Å)
7. **Rheology:** Anton Paar MCR102 Rheometer equipped with a 20 mm parallel-plate measuring system.
8. **Fluorescence:** Fluoromax-4 spectrophotometer.
9. **AAS:** AA240, Varian, Netherlands spectrophotometer.
10. **DLS:** Zetasizer Nano ZS90 from Malvern using a 632.8 nm He−Ne laser
11. **CD:** Jasco J-1500 spectropolarimeter.
12. **Fluorescence Microscopy:** Nikon eclipse Ts2R fluorescence microscope

List of Publications

1. Banerjee, R.; Deb, R.; **Roy, K**.; Chatterjee, S.; Nagotu, S. Uptake and intracellular fate of nona arginine peptide in yeast. *Pept. Sci.* **2018**, *e24101*, 1-11.
2. Pandit, G.; **Roy, K**.; Agarwal, U.; Chatterjee, S. Self-Assembly Mechanism of a Peptide-Based Drug Delivery Vehicle. *ACS Omega* **2018**, *3*, 3143−3155.
3. **Roy, K**.; Ghosh, S.; Chetia, M.; Satpati. P.; Chatterjee, S. Dicyclohexylurea derivatives of amino acids as dye absorbent organogels and anion sensors. *Org. Biomol. Chem*. **2019**, *17*, 3026-3039.
4. **Roy, K**; Pandit, G.; Chetia, M.; Sarkar, A. K.; Chowdhuri, S.; Bidkar, A. P.; Chatterjee, S. Peptide hydrogel as platform for sustained release of antimicrobial, antitumor drugs and proteins. *ACS Appl. Bio. Mater*. **2020**, *3*, 6251–6262.
5. **Roy, K**; Chetia, M.; Sarkar, A. K.; Chatterjee, S. Co-assembly of charge complementary peptides and their applications as organic dye/heavy metal ion (Pb^{2+}, Hg^{2+}) absorbents and arsenic (III/V) detectors**.** *RSC Adv.* **2020**, *10*, 42062-42075.